

VOLUME 76

MARCH 16, 1972

NUMBER 6

JPCA X

THE JOURNAL OF
PHYSICAL
CHEMISTRY

PUBLISHED BIWEEKLY BY THE AMERICAN CHEMICAL SOCIETY

THE JOURNAL OF PHYSICAL CHEMISTRY

BRYCE CRAWFORD, Jr., *Editor*
STEPHEN PRAGER, *Associate Editor*
ROBERT W. CARR, Jr., FREDERIC A. VAN-CATLEDGE, *Assistant Editors*

EDITORIAL BOARD: A. O. ALLEN (1970-1974), J. R. BOLTON (1971-1975),
F. S. DAINTON (1972-1976), M. FIXMAN (1970-1974),
H. S. FRANK (1970-1974), R. R. HENTZ (1972-1976), J. R. HUIZENGA (1969-1973),
W. J. KAUZMANN (1969-1973), R. L. KAY (1972-1976), W. R. KRIGBAUM (1969-1973),
R. A. MARCUS (1968-1972), W. J. MOORE (1969-1973), J. A. POPLER (1971-1975),
B. S. RABINOVITCH (1971-1975), H. REISS (1970-1974), S. A. RICE (1969-1975),
F. S. ROWLAND (1968-1972), R. L. SCOTT (1968-1972),
R. SEIFERT (1968-1972), W. A. ZISMAN (1972-1976)

CHARLES R. BERTSCH, *Manager, Editorial Production*

AMERICAN CHEMICAL SOCIETY, 1155 Sixteenth St., N.W., Washington, D. C. 20036
FREDERICK T. WALL, *Executive Director*

Books and Journals Division

JOHN K. CRUM, *Director*
JOSEPH H. KUNEY, *Head, Business Operations Department*
RUTH REYNARD, *Assistant to the Director*

©Copyright, 1972, by the American Chemical Society. Published biweekly by the American Chemical Society at 20th and Northampton Sts., Easton, Pa. 18042. Second-class postage paid at Washington, D. C., and at additional mailing offices.

All manuscripts should be sent to *The Journal of Physical Chemistry*, Department of Chemistry, University of Minnesota, Minneapolis, Minn. 55455.

Additions and Corrections are published once yearly in the final issue. See Volume 75, Number 26 for the proper form.

Extensive or unusual alterations in an article after it has been set in type are made at the author's expense, and it is understood that by requesting such alterations the author agrees to defray the cost thereof.

The American Chemical Society and the Editor of *The Journal of Physical Chemistry* assume no responsibility for the statements and opinions advanced by contributors.

Correspondence regarding accepted copy, proofs, and reprints should be directed to Editorial Production Office, American Chemical Society, 20th and Northampton Sts., Easton, Pa. 18042. Manager: CHARLES R. BERTSCH. Assistant Editor: EDWARD A. BORGER.

Advertising Office: Century Communications Corporation, 142 East Avenue, Norwalk, Conn. 06851.

Business and Subscription Information

Remittances and orders for subscriptions and for single copies,

notices of changes of address and new professional connections, and claims for missing numbers should be sent to the Subscription Service Department, American Chemical Society, 1155 Sixteenth St., N.W., Washington, D. C. 20036. Allow 4 weeks for changes of address. Please include an old address label with the notification.

Claims for missing numbers will not be allowed (1) if received more than sixty days from date of issue, (2) if loss was due to failure of notice of change of address to be received before the date specified in the preceding paragraph, or (3) if the reason for the claim is "missing from files."

Subscription rates (1972): members of the American Chemical Society, \$20.00 for 1 year; to nonmembers, \$60.00 for 1 year. Those interested in becoming members should write to the Admissions Department, American Chemical Society, 1155 Sixteenth St., N.W., Washington, D. C. 20036. Postage to Canada and countries in the Pan-American Union, \$5.00; all other countries, \$6.00. Single copies for current year: \$3.00. Rates for back issues from Volume 56 to date are available from the Special Issues Sales Department, 1155 Sixteenth St., N.W., Washington, D. C. 20036.

This publication and the other ACS periodical publications are now available on microfilm. For information write to: MICROFILM, Special Issues Sales Department, 1155 Sixteenth St., N.W., Washington, D. C. 20036.

THE JOURNAL OF
PHYSICAL CHEMISTRY

Volume 76, Number 6 March 16, 1972

JPCA_x 76(6) 805-946 (1972)

Hydrogen Chloride Chemical Laser from Hydrogen Atom-Chlorine Azide Reaction	W. W. Rice and R. J. Jensen*	805
Chemical Lasers Produced from O(¹ D) Atom Reactions. III. HCl Elimination Lasers from the O(¹ D) + CH _n Cl _{4-n} (n = 1, 2, and 3) Reactions	M. C. Lin	811
Quantum Yields for the Photooxidation of Sulfur Dioxide in the First Allowed Absorption Region	R. A. Cox	814
Solvent Effects on Acetophenone Photoreduction Studied by Laser Photolysis	Hanspeter Lutz, Marie-Christine Duval, Emilienne Bréhéret, and Lars Lindqvist*	821
Photochemistry of Trifluoromethylbenzenes. III. 1,4-Bis(trifluoromethyl)benzene	David Gray and David Phillips*	823
A Mechanism to Explain the CH Emission at 4330 Å in Oxygen Atom-Acetylene Systems	K. A. Quickert	825
Electroanalytical Measurements of Flash-Photolyzed Ferrioxalate	R. A. Jamieson and S. P. Perone*	830
Pulse Radiolysis Study of the Kinetics of Formation of Na ⁻ in Ethylenediamine by the Reaction of Solvated Electrons with Sodium Ions	James L. Dye, Marc G. DeBacker, John A. Eyre, and Leon M. Dorfman*	839
Electron Spin Resonance and Pulse Radiolysis Studies of the Reactions of OH and O ⁻ Radicals with Aromatic and Olefinic Compounds	P. Neta,* Morton Z. Hoffman, and M. Simic	847
Nuclear Magnetic Resonance Rate Studies of Hindered Rotation in Methyl N-Acetylsarcosinate	Alan L. Love, Terry D. Alger,* and Richard K. Olsen	853
Solvation and Self-Association of Water in Propylene Carbonate	David R. Cogley, Michael Falk, James N. Butler, and Ernest Grunwald*	855
A Low-Temperature Infrared Study of Sterically Hindered Associated Alcohols	C. Bourdéron, J.-J. Péron, and C. Sandorfy*	864
A Vibrational Overtone Study of Association in Liquid Methanol	C. Bourdéron, J.-J. Péron, and C. Sandorfy*	869
Hydrogen Bonding and Complex Formation of Dimethylamine. Infrared Investigations on the NH Stretching Vibration Bands	H. Wolff* and G. Gamer	871
The Role of the Diffuse Layer in Water-in-Oil Microemulsions	S. Levine* and K. Robinson	876
Relations between Crystal Structure, Molecular Electronic Polarizability, and Refractive Properties of Ice I	Allen P. Minton	886
Intermolecular Forces in Gases of Associating Substances	L. S. Moore and J. P. O'Connell*	890
The Volume Changes of Ionic Association Reactions	Paul Hemmes	895
Radioisotope Determination of the Surface Concentrations of Calcium and Phosphorus on Hydroxyapatite in Aqueous Solution	M. Kukura, L. C. Bell,* A. M. Posner, and J. P. Quirk	900
Effects of High-Pressure HCl on Transport Properties of the Molten 46 Mol % KCl-54 Mol % ZnCl ₂ Eutectic System	Billy R. Hubble and James L. Copeland*	904
The Physicochemical Properties of Aqueous Solutions of Fluorinated Surfactants	Kōzō Shinoda,* Masakatsu Hatō, and Takao Hayashi	909

Studies of the Vaporization Kinetics of Hydrogen-Bonded Liquids	F. R. McFeely and G. A. Somorjai*	914
A Comparison of Stabilization Energy and Resonance Energy as a Measure of the Delocalization Energy in Free Radicals	A. S. Rodgers,* M. C. R. Wu, and L. Kuitu	918
Thermodynamic Stability of Perylene-Iodine Charge-Transfer Complexes from Measurements of Iodine Vapor Absorption	S. Aronson,* B. Strumeyer, and R. Goodman	921
Phase Diagrams of Liquid Crystal Solvents Used in Nuclear Magnetic Resonance Studies	R. A. Bernheim* and T. A. Shuhler	925
An X-Ray Diffraction Investigation of the Vanadium-Deuterium System	Kenneth I. Hardcastle* and T. R. P. Gibb, Jr.	927
Radiation-Induced Polymerization of Pure Styrene at Low Temperature	Sueo Machi,* Joseph Silverman, and Donald J. Metz	930
Detection of the Triphenylmethyl Radical by Electron Spin Resonance in the Thermal Decomposition of Sodium Triphenylacetate	Edward G. Janzen* and Michael Buchheit	937
The Infrared Spectra of the Oxides and Carbonates of Silver	T. L. Slager,* B. J. Lindgren, A. James Mallmann, and Robert G. Greenler	940

COMMUNICATIONS TO THE EDITOR

Catalytic Hydrogenation of Propylene: Verification of Maximum Rate	Steven C. Weiner,* Reiji Mezaki, and Gary L. Haller	943
Free Ion Yields in γ -Irradiated Mixed Solvents	Gordon R. Freeman	944
Infrared Spectra of Nitrous Oxide Adsorbed on Sodium Type A Synthetic Zeolite	E. Cohen de Lara and J. Vincent-Geisse*	945

AUTHOR INDEX

Alger, T. D., 853	Duval, M.-C., 821	Hemmes, P., 895	Mallmann, A. J., 940	Rice, W. W., 805
Aronson, S., 921	Dye, J. L., 839	Hoffman, M. Z., 847	McFeely, F. R., 914	Robinson, K., 876
Bell, L. C., 900	Eyre, J. A., 839	Hubble, B. R., 904	Metz, D. J., 930	Rodgers, A. S., 918
Bernheim, R. A., 925	Falk, M., 855	Jamieson, R. A., 830	Mezaki, R., 943	Sandorfy, C., 864, 869
Bourdéron, C., 864, 869	Freeman, G. R., 944	Janzen, E. G., 937	Minton, A. P., 886	Shinoda, K., 909
Bréheret, E., 821	Gamer, G., 871	Jensen, R. J., 805	Moore, L. S., 890	Shuhler, T. A., 925
Buchheit, M., 937	Gibb, T. R. P., Jr., 927	Kuitu, L., 918	Neta, P., 847	Silverman, J., 930
Butler, J. N., 855	Goodman, R., 921	Kukura, M., 900	O'Connell, J. P., 890	Simic, M., 847
Cogley, D. R., 855	Gray, D., 823	Levine, S., 876	Olsen, R. K., 853	Slager, T. L., 940
Copeland, J. L., 904	Greenler, R. G., 940	Lin, M. C., 811	Péron, J.-J., 864, 869	Somorjai, G. A., 914
Cox, R. A., 814	Grunwald, E., 855	Lindgren, B. J., 940	Perone, S. P., 830	Strumeyer, B., 921
DeBacker, M. G., 839	Haller, G. L., 943	Lindqvist, L., 821	Phillips, D., 823	Vincent-Geisse, J., 945
de Lara, E. C., 945	Hardcastle, K. I., 927	Love, A. L., 853	Posner, A. M., 900	Weiner, S. C., 943
Dorfman, L. M., 839	Hatō, M., 909	Lutz, H., 821	Quickert, K. A., 825	Wolff, H., 871
	Hayashi, T., 909	Machi, S., 930	Quirk, J. P., 900	Wu, M. C. R., 918

In papers with more than one author the name of the author to whom inquiries about the paper should be addressed is marked with an asterisk in the by-line.

THE JOURNAL OF
PHYSICAL CHEMISTRY

Registered in U. S. Patent Office © Copyright, 1972, by the American Chemical Society

VOLUME 76, NUMBER 6 MARCH 16, 1972

Hydrogen Chloride Chemical Laser

from Hydrogen Atom-Chlorine Azide Reaction¹

by W. W. Rice and R. J. Jensen*

Los Alamos Scientific Laboratory, University of California, Los Alamos, New Mexico 87544 (Received July 29, 1971)

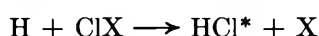
Publication costs assisted by the Los Alamos Scientific Laboratory, University of California

ClN_3 works as a chlorine source to produce HCl laser action from H_2 - ClN_3 gas mixtures containing less than 20 mol % ClN_3 . The sequence of reactions that lead to population inversion is as follows: $\text{ClN}_3 + h\nu \rightarrow \text{Cl} + \text{N}_3$ (I); $\text{Cl} + \text{H}_2 \rightarrow \text{HCl} + \text{H}$ (II); $\text{H} + \text{ClN}_3 \rightarrow \text{HCl}^* + \text{N}_3$ (III). Difficulties arise from the lack of an H_2 - ClN_3 chain reaction to propagate steps II and III, and from competing reactions that deplete the ClN_3 supply prior to step III. The effect of competing reactions becomes pronounced with increasing pressures, temperatures, and mole percentages of ClN_3 . Decomposition of ClN_3 into Cl_2 and N_2 occurs during storage. This decomposition noticeably affects the laser output by allowing the hydrogen atom-chlorine molecule reaction. When mixtures of ClN_3 - H_2 - $^{37}\text{Cl}_2$ were used, one could observe the two separate laser producing reactions in the same medium. The hydrogen atom-chlorine molecule reaction provides a population inversion over a much wider range of temperatures and pressures than the hydrogen atom-chlorine azide reaction. Corresponding $P_2(J)$ lines of $^1\text{H}^{35}\text{Cl}$ and $^1\text{H}^{37}\text{Cl}$ displayed equal power when a 1.2% $^{37}\text{Cl}_2$, 5.0% ClN_3 , 93.8% H_2 mixture was photolyzed. The laser power densities for these two isotopes of HCl were assumed to be equal, and a steady-state approximation was made for the time that the laser operated. Calculations based on these two assumptions give the ratio of the rate constants for the hydrogen atom-chlorine azide reaction to the hydrogen atom-chlorine molecule reaction, $(k_2/k_{11}) = (k_1/k_I) = 0.45 \pm 0.07$, where the Roman numeral subscripts refer to the reactions $\text{H} + \text{Cl}_2 \xrightarrow{k_N} \text{HCl}^*(v = N) + \text{Cl}$ and the Arabic numeral subscripts refer to the reactions $\text{H} + \text{ClN}_3 \xrightarrow{k_n} \text{HCl}^*(v = n) + \text{N}_3$.

Introduction

As early as 1961, Polanyi² suggested that the reaction of hydrogen atoms with chlorine molecules might produce HCl laser action from vibrational-rotational population inversion. The first HCl laser based on this reaction was obtained by Kasper and Pimentel³ from photolysis of a hydrogen-chlorine mixture. HCl laser action has also been observed from the reactions of hydrogen and other chlorine-containing compounds such as nitrosyl chloride⁴ and dichlorine monoxide.⁵

In each of these mixtures the upper laser levels were populated by an exothermic, pumping reaction



Assuming that hydrogen-chlorine azide mixtures can

undergo this same type of reaction, we would expect to observe laser action if the energy of reaction is deposited in vibration of the HCl molecule. The low Cl-N₃ bond energy and the high exothermicity of the proposed pumping reaction compare favorably with those of the chlorine sources that have been employed (see Table I).

In this article we report the characteristics of the HCl laser obtained from the photolysis of hydrogen-chlorine azide mixtures. Reaction mechanisms are suggested and operating conditions are described. The

- (1) Taken in part from the doctoral dissertation of W. W. Rice.
- (2) J. C. Polanyi, *J. Chem. Phys.*, **34**, 347 (1961).
- (3) J. V. V. Kasper and G. C. Pimentel, *Phys. Rev. Lett.*, **14**, 352 (1965).
- (4) A. Henry, F. Bourcin, I. Arditi, R. Charneau, and J. Menard, *C. R. Acad. Sci., Ser. B*, **267**, 616 (1968).
- (5) M. C. Lin, *Chem. Phys. Lett.*, **7**, 209 (1970).

Table I: Chlorine Sources for HCl Chemical Lasers

ClX Compound	Cl-X Bond Energy, ^a kcal mol ⁻¹	ΔH° of Pumping Reaction, ^a kcal mol ⁻¹	Reaction Initiation Methods ^b
Cl ₂	57.8	-45.2	fl, pe, rf
NOCl	37.9	-65.2	pe
Cl ₂ O	35.0	-68.1	pe
ClN ₃	37.2	-65.9	fl

^a Thermodynamic values calculated from data in "JANAF Thermochemical Tables," PB 168 370, CFSTI, Aug 1965; and T. C. Clark and M. A. A. Clyne, *Trans. Faraday Soc.*, **66**, 877 (1970). ^b fl = flash lamp, pe = pulsed electrical discharge, rf = radio frequency discharge.

relative rate constants for the hydrogen atom-chlorine azide reaction and the hydrogen atom-chlorine reaction are evaluated from the laser output of isotopically labeled gas mixtures.

Experimental Section

The chemical laser system and the detection and analysis instrumentation have been described elsewhere.⁶ The NaCl windows on the laser tube were replaced with more chemically resistant BaF₂ windows. The gas handling system was constructed and operated according to the guidelines we have given previously.⁷ Gas pressures in the laser tube and gas system were measured to within eight-thousandths Torr with a Texas Instruments Inc. model 145 quartz gauge.

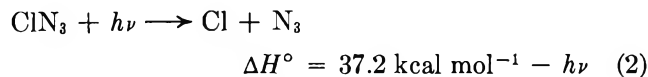
Chlorine azide was synthesized by the method of Raschig⁸ using Matheson Coleman and Bell practical grade NaN₃, Baker and Adamson USP grade H₃BO₃, and Baker and Adamson reagent grade NaOCl 5% solution. The ClN₃ was generated under vacuum, dried over P₂O₅, and stored in darkened bulbs where other gases were mixed with it. Great care was exercised during the preparation of ClN₃ gas mixtures to prevent stray light and mechanical shock from detonating the gas.

Chlorine gas enriched in chlorine-37 was prepared from Oak Ridge National Laboratory NaCl (the chloride was 3.95 atom% chlorine-35 and 96.05 atom% chlorine-37), J. T. Baker reagent grade AgNO₃, Allied Chemical reagent grade K₂Cr₂O₇, and Bio-Rad Laboratories 99.95 atom% D₂SO₄ (98% in D₂O). The chloride was converted to AgCl, washed in D₂O, dried in air, and treated under vacuum with D₂SO₄ and K₂Cr₂O₇ to generate chlorine. The D₂O and D₂SO₄ were used to prevent the formation of hydrogen chloride in the synthesis. The enriched chlorine, "³⁷Cl₂," was passed through a P₂O₅ drying coil, which was cooled in a Dry Ice-acetone bath, to remove any water vapor or SO₃ present.

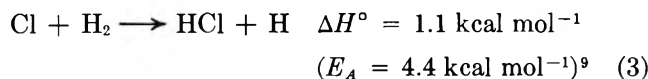
Results and Discussion

Mechanism. Photolysis of several mixtures of ClN₃ and H₂ resulted in HCl laser action. The laser action

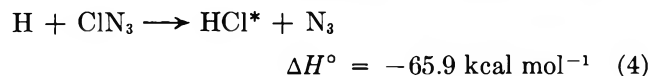
from this binary mixture suggests a sequence of reactions similar to that of the H₂-Cl₂ explosion laser: chlorine atoms from photodissociation of ClN₃



hydrogen atoms from chlorine atom attack on hydrogen

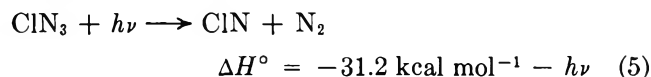


vibrationally excited HCl from pumping reaction



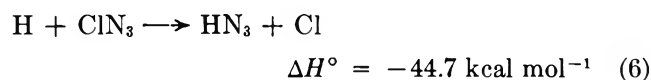
The population inversion must come from (4) since the HCl formed in (3) is produced in an endothermic reaction.

Competing Reactions. The H₂-ClN₃ reaction is complicated by competing reactions that do not lead to laser action. The photolysis step (2) may give other products

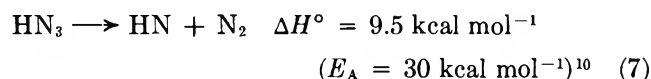


by taking this thermochemically favorable reaction path. Neither of these product molecules would proceed to (3) to free the needed hydrogen atoms.

The pumping reaction (4) could be further dissipated by the exothermic reaction

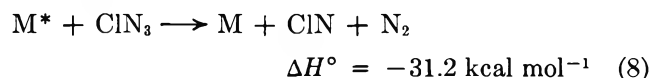


with the possibility of the hydrazoic acid decomposing on formation



The pumping reaction 1 in the H₂-Cl₂ explosion produces a chlorine atom that propagates the chain reaction; however, in the H₂-ClN₃ reaction an azide radical is produced that terminates the sequence. The reaction of an azide radical with a hydrogen molecule to produce atomic hydrogen would be endothermic and unlikely.

Collisions of the type



(6) R. J. Jensen and W. W. Rice, *Chem. Phys. Lett.*, **8**, 214 (1971).

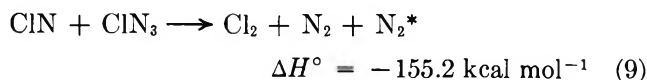
(7) W. W. Rice and R. J. Jensen, *J. Chem. Educ.*, **48**, 659 (1971).

(8) F. Raschig, *Chem. Ber.*, **41**, 4194 (1908).

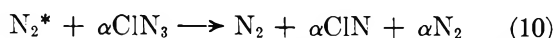
(9) P. H. Corneil and G. C. Pimentel, *J. Chem. Phys.*, **49**, 1379 (1968).

(10) I. Hajal and J. Combourieu, *J. Chim. Phys.*, **63**, 899 (1966).

become more effective as the temperature increases. If it is assumed that chlorine azide decomposition is similar to the hydrazoic acid branching chain,¹¹ then, as the temperature increases, the chain propagation step



followed by branching



could further consume chlorine azide without producing HCl laser emission.

Operating Conditions. As a consequence of these alternative reaction paths that thwart the pumping reaction, chlorine azide has proved to be a very poor source of chlorine for the HCl laser. Stimulated emission appears to be limited to those conditions where chlorine azide decomposition is dependent on photolysis and does not go to completion by thermal explosion. Both the pressure change after photolysis and the infrared absorption spectroscopy of reaction products indicate that a significant amount of chlorine azide remains unchanged after successful H₂-ClN₃ laser shots.

Gas mixtures ranging from 5.0 to 40.0 mol% chlorine azide in hydrogen were photolyzed over several pressures. No mixtures above 20.0% ClN₃ exhibited laser action at any pressure. Mixtures of 20.0% ClN₃ were marginal and worked only at pressures of a few Torr. The best results were obtained at 5.0%, 8.0%, and 10.0% ClN₃ and at pressures under 20.0 Torr.

The quenching of the laser output at high ClN₃ concentration is probably due to the increase in temperature and subsequent decomposition of ClN₃ by competing reaction paths. By comparing the change in pressure upon photolysis to the initial ClN₃ pressure, the degree of ClN₃ decomposition is determined. It was noted that the degree of ClN₃ consumption increased with increasing gas percentage of ClN₃.

The effect of pressure on laser output is depicted in Figure 1 for a typical working composition (8.0% ClN₃, 92.0% H₂). The mixture was photolyzed with a flash lamp input energy of 0.75 kJ (16.7 kV at 5.4 μF) and the resulting laser output was recorded with an oscillographic camera. The laser output consisted of a single narrow spike beginning about 8 μsec after flash lamp initiation and lasting 1.5–2.0 μsec. The relative peak power was obtained by measuring the height of the laser spike.

At low pressures the system fails to reach laser threshold because the number of excited HCl molecules formed is insufficient to overcome optical cavity losses. As the pressure is increased beyond the laser threshold, there is more ClN₃ photolyzed, more excited HCl formed, and greater intensity of stimulated emission. Laser power increases with pressure until the competing,

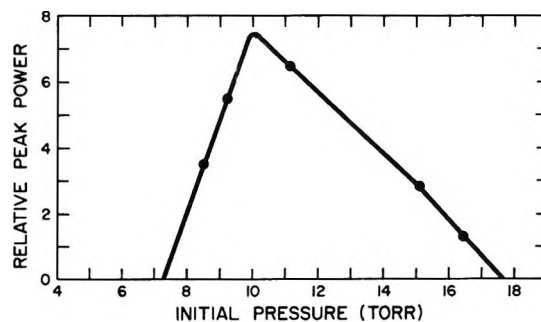
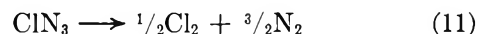


Figure 1. Effect of total pressure on laser output for 8.0% ClN₃, 92.0% H₂ laser mixture.

nonlaser producing reactions begin to deplete significantly the supply of ClN₃. As the pressure increases beyond this region an increasing amount of ClN₃ is removed before laser action can begin. A point below laser threshold is eventually reached where the amount of excited HCl formed is limited by lack of available ClN₃.

Effects of Chlorine. One noticeable feature of the H₂-ClN₃ laser mixtures is the increase in laser pulse duration as the gas mixtures are stored several days. This change arises from the slow decomposition of chlorine azide



As greater amounts of chlorine are formed, the contribution to the laser output from the H₂-Cl₂ chain reaction is seen.

This explanation is further substantiated by time resolved spectroscopy of both H₂-Cl₂ and H₂-Cl₂-ClN₃ mixtures. A 1.2% Cl₂, 98.8% H₂ mixture was photolyzed in 20–21 Torr shots with a 1.25 kJ (12.9 kV at 15.0 μF) flash lamp input energy. The laser onset was 15 μsec after flash lamp initiation and the duration of the pulse was approximately 50 μsec. Continued laser action after the flash lamp resulted from the H₂-Cl₂ chain reaction running its course. The transitions P₂(4) through P₂(9) were observed in sequence, the increasing temperature giving rise to higher J lines.¹²

In contrast, a 1.2% Cl₂, 10.0% ClN₃, 88.8% H₂ mixture under the same conditions gave a laser onset time 7.5 μsec after flash lamp initiation and lasted only 2 μsec. The faster onset and increased peak power indicated an increase in the number of reaction centers and an increase in reaction rates. A higher reaction temperature was indicated by higher J values in the emission spectrum, P₂(7) through P₂(12), and a v = 3 to v = 2 transition, P₃(7). The shortened pulse duration suggests that the chain reaction of the H₂-Cl₂ system is

(11) V. G. Voronkov and S. A. Rozenberg, *Dokl. Akad. Nauk SSSR*, **177**, 835 (1967).

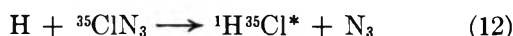
(12) The symbol P_v(J) represents a vibrational-rotational transition where P indicates ΔJ = -1 and Δv = 1, v is the vibrational quantum number of the upper laser level, and J is the rotational quantum number of the lower laser state.

quenched by the chlorine azide scavenging of hydrogen atoms.

Isotopic Labeling. To gain a better understanding of the contribution that each of these laser pumping reactions makes to the total output, special gas mixtures using the chlorine-37 isotope were made. $^{37}\text{Cl}_2$ containing 96.05% chlorine-37 and 3.95% chlorine-35 was produced by the synthesis outlined in the Experimental Section. The ClN_3 isotopes were in natural abundance, 75.53% chlorine-35 and 24.47% chlorine-37.

The only laser action obtained from test mixtures of hydrogen and the synthesized chlorine was on $^1\text{H}^{37}\text{Cl}$ transitions. Laser action in $\text{H}_2\text{-ClN}_3$ mixtures was observed from both $^1\text{H}^{35}\text{Cl}$ and $^1\text{H}^{37}\text{Cl}$, the $^1\text{H}^{35}\text{Cl}$ being more pronounced. The isotopic hydrogen chloride laser lines were compared for a 3.9% $^{37}\text{Cl}_2$, 10.0% ClN_3 , 86.1% H_2 mixture that was photolyzed with a 0.75 kJ (16.7 kV at 5.4 μF) input energy to the flash lamp.

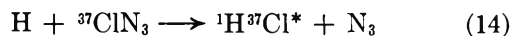
Since decomposition of ClN_3 has been shown to be negligible in the two hours mixing time, the $^1\text{H}^{35}\text{Cl}$ laser emission was attributed chiefly to the



reaction. On the other hand, the $^1\text{H}^{37}\text{Cl}$ laser emission was considered to be due to the



reaction with only a small contribution from the



reaction.

At a total pressure of 8.5 ± 0.5 Torr, laser oscillation began 6 μsec after flash lamp initiation and continued for 3.0–3.5 μsec . The $^1\text{H}^{35}\text{Cl}$ emission was relatively weaker than that of the $^1\text{H}^{37}\text{Cl}$ and the two lines that lased, $P_2(6)$ and $P_2(7)$, were delayed about 2 μsec from the corresponding $^1\text{H}^{37}\text{Cl}$ transitions.

The effect of pressure on $^1\text{H}^{35}\text{Cl}$ laser emission followed the same pattern shown earlier for ClN_3 . The emission increased with pressure to a maximum, then decreased on further pressure increase. The total laser output, largely from $^1\text{H}^{37}\text{Cl}$ laser action, increased with the pressure. This would be indicative of a slower rate of formation of excited hydrogen chloride from the hydrogen atom–chlorine azide reaction than from the hydrogen atom–chlorine reaction.

Relative Rate Constants. A series of laser shots with a 1.2% $^{37}\text{Cl}_2$, 5.0% ClN_3 , 93.8% H_2 gas mixture was photolyzed at 0.75 kJ. Unlike the previous gas mixtures, the laser outputs for both isotopic hydrogen chlorides were comparable (see Figure 2). The power of corresponding $^1\text{H}^{35}\text{Cl}$ and $^1\text{H}^{37}\text{Cl}$ lines appears to be nearly equal at both 10 Torr and 5 Torr. This equal-power condition can be expressed

$$P'(\nu') = P(\nu) \quad (15)$$

where $P(\nu)$ is the power density of frequency ν ; the

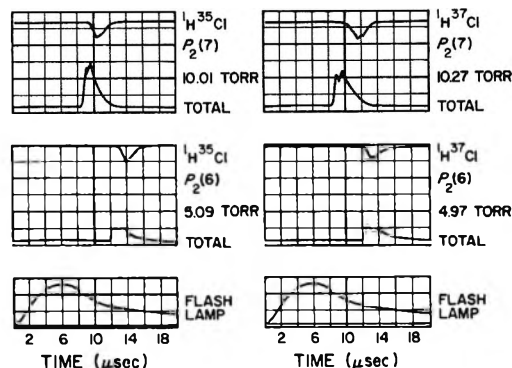


Figure 2. Equal power on corresponding $P_2(J)$ lines for 1.2% $^{37}\text{Cl}_2$, 5.0% ClN_3 , 93.8% H_2 laser mixtures. Arbitrary intensity scale.

primed ($'$) symbols refer to $^1\text{H}^{37}\text{Cl}$ and the unprimed symbols refer to $^1\text{H}^{35}\text{Cl}$. This equal-power expression may also be written

$$h\nu' \left[A'_{ij}N'_i + \left(\frac{N'_i}{g'_i} - \frac{N'_j}{g'_j} \right) g'_i B'_{ij} U'(\nu') \right] = h\nu \left[A_{ij}N_i + \left(\frac{N_i}{g_i} - \frac{N_j}{g_j} \right) g_i B_{ij} U(\nu) \right] \quad (16)$$

where the symbols are defined as follows: h = Planck's constant, ν = the frequency of the radiation for the transition from the i th to j th state, A_{ij} and B_{ij} = the respective Einstein coefficients for spontaneous and stimulated emission, N_i = population of the upper laser level, N_j = population of the lower laser level, g_i and g_j = the degeneracies of the respective i th and j th levels, and $U(\nu)$ = the energy density of frequency ν .

Inasmuch as spontaneous emission contributes little to the power of the laser output, the $A_{ij}N_i$ terms may be neglected. When comparing the power of corresponding $P_2(J)$ lines, the degeneracies of corresponding upper laser levels will be equal, $g'_i = g_i = 2J - 1$, and the degeneracies of like lower levels will be equal, $g'_j = g_j = 2J + 1$. Because the ratios of isotopic frequencies, Einstein coefficients, and energy densities are very close to unity for $^1\text{H}^{35}\text{Cl}$ and $^1\text{H}^{37}\text{Cl}$, a simplified equal power equation may be written

$$\left(\frac{N'_i}{g_i} - \frac{N'_j}{g_j} \right) = \left(\frac{N_i}{g_i} - \frac{N_j}{g_j} \right) \quad (17)$$

Since rotational equilibrium is obtained under conditions such as these,⁹ the populations of the rotational states may be expressed in terms of vibrational level populations using a Boltzmann distribution

$$\frac{N'(\prime)_i}{g_i} = \frac{B(\prime)_2 N(\prime)_2}{kT/hc} \exp - \frac{B(\prime)_2 J(J-1)}{kT/hc} \quad (\text{upper laser levels})$$

and

$$\frac{N(')_j}{g_j} = \frac{B(')_1 N(')_1}{kT/hc} \exp - \frac{B(')_1 J(J+1)}{kT/hc}$$

(lower laser levels) (18)

where B_2 and B_1 are rotational constants of the upper and lower vibrational states, J is the rotational quantum number of the lowest laser level, k is the Boltzmann constant, T is the absolute temperature, and c is the velocity of light. Because B'_2 and B_2 differ by only one part in a thousand and B'_1 and B_1 also differ by a like amount, the *average* of B'_2 and B_2 may be used in place of B'_2 and B_2 and the *average* of B'_1 and B_1 may be used for both B'_1 and B_1 . To simplify the Boltzmann expressions let

$$a_J = \frac{(B'_2 + B_2)/2}{kT/hc} \exp - \frac{J(J-1)(B'_2 + B_2)/2}{kT/hc}$$

and

$$b_J = \frac{(B'_1 + B_1)/2}{kT/hc} \exp - \frac{J(J+1)(B'_1 + B_1)/2}{kT/hc} \quad (19)$$

The equal-power equation 17 may now be written in terms of vibrational level populations

$$(a_J N'_2 - b_J N'_1) = (a_J N_2 - b_J N_1) \quad (20)$$

It should be noted that the above equation also holds for non-Boltzmann distributions of rotational states so long as a_J and b_J describe the distribution of energy in the respective rotational levels of both isotopic species.

The rates of formation of hydrogen chloride in the vibrational states of interest may be written

$$\begin{aligned} \frac{d[{}^1\text{H}^{37}\text{Cl}(v=2)]}{dt} &= 0.2447k'_2[\text{ClN}_3][\text{H}] + \\ &0.9605k'_{\text{II}}[{}^{37}\text{Cl}_2][\text{H}] - k'_{\text{D2}}[\text{M}][{}^1\text{H}^{37}\text{Cl}(v=2)] \\ \frac{d[{}^1\text{H}^{37}\text{Cl}(v=1)]}{dt} &= 0.2447k'_1[\text{ClN}_3][\text{H}] + \\ &0.9605k'_1[{}^{37}\text{Cl}_2][\text{H}] - k'_{\text{D1}}[\text{M}][{}^1\text{H}^{37}\text{Cl}(v=1)] \\ \frac{d[{}^1\text{H}^{35}\text{Cl}(v=2)]}{dt} &= 0.7553k_2[\text{ClN}_3][\text{H}] + \\ &0.0395k_{\text{II}}[{}^{37}\text{Cl}_2][\text{H}] - k_{\text{D2}}[\text{M}][{}^1\text{H}^{35}\text{Cl}(v=2)] \\ \frac{d[{}^1\text{H}^{35}\text{Cl}(v=1)]}{dt} &= 0.7553k_1[\text{ClN}_3][\text{H}] + \\ &0.0395k_1[{}^{37}\text{Cl}_2][\text{H}] - k_{\text{D1}}[{}^1\text{H}^{35}\text{Cl}(v=1)] \quad (21) \end{aligned}$$

The various terms in the rate equations are defined as follows: the numerical coefficients are isotopic abundances of chlorine, $k'_2 = k_2$ = rate constant for hydrogen atom-chlorine azide reaction that populates the upper laser level, $k'_1 = k_1$ = rate constant for hydrogen atom-chlorine azide reaction that populates the lower laser level, $k'_{\text{II}} = k_{\text{II}}$ = rate constant for hydrogen atom-chlorine reaction that populates the upper laser level, $k'_1 = k_1$ = rate constant for hydrogen atom-

chlorine reaction that populates the lower laser level, $k'_{\text{D2}} = k_{\text{D2}}$ = rate constant for overall deactivation of upper laser level, $k'_{\text{D1}} = k_{\text{D1}}$ = rate constant for overall deactivation of lower laser level, and M represents any deactivator, the ensemble average of which is presumed to be equal for each equation.

In the usual hydrogen-chlorine explosion about a fourth of the HCl formed is in the $v=2$ level and about a tenth is in the $v=1$ level.¹³ This infers that in these experiments *nanomoles* of excited HCl must be present during laser action; however, energy measurements show that only *picomoles* of HCl are involved in the laser function.

If one makes the assumption that the overall change in population from collisional deactivation and laser action is small during the brief period that the laser operates, then the usual steady-state approximation methods may be followed. Setting the rate equations equal to zero, one obtains expressions for N'_2 , N_2 , N'_1 , and N_1 that can be substituted into the equal-power equation (20). Rearrangement of this equation to separate the constants for the two pumping reactions results in the expression

$$1.804 \frac{[{}^{37}\text{Cl}_2]}{[\text{ClN}_3]} \left[\left(\frac{a_J}{k_{\text{D2}}} \right) k_{\text{II}} - \left(\frac{b_J}{k_{\text{D1}}} \right) k_1 \right] = \left[\left(\frac{a_J}{k_{\text{D2}}} \right) k_2 - \left(\frac{b_J}{k_{\text{D1}}} \right) k_1 \right] \quad (22)$$

This equation indicates that when equal power is observed for each set of corresponding transitions, the ratio of the relative rate constants may be determined from only a knowledge of the chlorine-chlorine azide ratio

$$\frac{k_2}{k_{\text{II}}} = \frac{k_1}{k_1} = 1.804 \frac{[{}^{37}\text{Cl}_2]}{[\text{ClN}_3]} \quad (23)$$

The concentrations of chlorine and chlorine azide at the time of laser operation must be determined indirectly. The concentration of chlorine azide at the time of peak power may be written

$$[\text{ClN}_3] = 1/RT [P^\circ_{\text{ClN}_3} - \Delta P(\Delta E/E_t)] \quad (24)$$

where R is the gas constant, $P^\circ_{\text{ClN}_3}$ = initial pressure of ClN_3 , ΔP = pressure change after photolysis = pressure of ClN_3 decomposed, $(\Delta E/E_t)$ = fraction of the total flash lamp energy emitted up to the time of peak power.

The chlorine concentration may be represented

$$[{}^{37}\text{Cl}_2] = 1/RT [P^\circ_{\text{Cl}_2} - \Delta P(\Delta E/E_t)(A_{\text{Cl}_2}/A_{\text{ClN}_3})] \quad (25)$$

where $P^\circ_{\text{Cl}_2}$ = initial pressure of ${}^{37}\text{Cl}_2$, and $(A_{\text{Cl}_2}/A_{\text{ClN}_3})$ = the ratio of flash lamp energy absorbed by chlorine to flash lamp energy absorbed by chlorine azide.

(13) K. G. Anlauf, P. J. Kuntz, D. H. Maylotte, P. D. Pacey, and J. C. Polanyi, *Disc. Faraday Soc.*, **44**, 183 (1967).

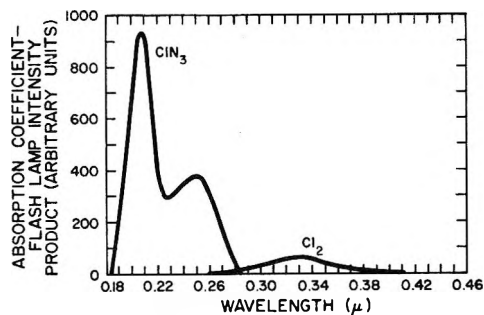


Figure 3. Comparison of flash lamp energy absorbed by Cl_2 and ClN_3 .

The initial pressures of chlorine and chlorine azide are the total initial pressures multiplied by the respective mole fractions: $P^\circ_{\text{Cl}_2} = (0.01193 \pm 0.00005) P^\circ_t$ and $P^\circ_{\text{ClN}_3} = (0.04999 \pm 0.00010) P^\circ_t$ where $P^\circ_t = 5.03 \pm 0.06$ Torr and 10.14 ± 0.13 Torr.

For the laser shots at $P^\circ_t = 5.03 \pm 0.06$ Torr the change in pressure, ΔP , was 0.022 ± 0.010 Torr; at $P^\circ_t = 10.14 \pm 0.13$ Torr the decrease in ClN_3 , ΔP , was 0.052 ± 0.012 Torr.

The fraction of the flash lamp energy deposited at the time of peak laser power, $(\Delta E/E_t)$, was measured from the flash lamp traces of Figure 2, which shows flash lamp power as a function of time. (The flash lamp output at the absorption frequencies of ClN_3 and Cl_2 had the same time profile as Figure 2 to within the accuracy of the experiment.) The area under the curve from flash lamp initiation to peak laser power is proportional to ΔE and the total area under the curve is proportional to E_t . The fraction of the energy deposited during the 5 Torr shots was 0.72 ± 0.02 and during the 10 Torr shots was 0.64 ± 0.02 .

The curves in Figure 3 were obtained by multiplying the chlorine¹⁴ and chlorine azide¹⁵ absorption coefficients at each wavelength by the relative flash lamp intensity at that wavelength. (It was assumed that the flash lamp was a 10^4 K blackbody.) The ratio of the areas under these curves is the fraction ($A_{\text{Cl}_2}/A_{\text{ClN}_3}$) and is equal to 0.110 ± 0.005 . This ratio is based on the assumptions that the quantum yield for

photolysis of chlorine is no better than that for the photolysis of chlorine azide and that the hydrogen-chlorine chain reaction has not had time to complete more than one or two cycles.

The ratio of the chlorine to chlorine azide concentration may be written

$$\frac{[^{37}\text{Cl}_2]}{[\text{ClN}_3]} = \frac{(0.01193 \pm 0.00005)P^\circ_t - \Delta P(\Delta E/E_t)(0.110 \pm 0.005)}{(0.04999 \pm 0.00010)P^\circ_t - \Delta P(\Delta E/E_t)} \quad (26)$$

For the laser shots where $P^\circ_t = 5.03 \pm 0.06$ Torr, $\Delta P = 0.022 \pm 0.010$ Torr, and $(\Delta E/E_t) = 0.72 \pm 0.02$, the concentration ratio was 0.247 ± 0.004 . Likewise at $P^\circ_t = 10.14 \pm 0.13$ Torr, $\Delta P = 0.052 \pm 0.012$ Torr, and $(\Delta E/E_t) = 0.64 \pm 0.02$, the concentration ratio was 0.247 ± 0.003 .

The largest uncertainty in the development above is the initial assumption that the power on all corresponding lines is equal. This uncertainty would affect the numerical coefficient in eq 23. If our equal power assumption is accurate to $\pm 10\%$, the ratio of the rate constants is

$$\frac{k_2}{k_{11}} = \frac{k_1}{k_1} = (1.8 \pm 0.3)(0.247 \pm 0.003) = 0.45 \pm 0.07 \quad (27)$$

The smaller rate constants for the hydrogen atom-chlorine azide reactions are probably due to the fact that one end of the ClN_3 molecule provides a chlorine atom while both ends of Cl_2 provide chlorine atoms.

Acknowledgments. We wish to thank the Associated Western Universities and the U. S. Atomic Energy Commission for fellowship support to W. W. Rice during this work.

(14) G. E. Gibson and N. S. Bayliss, *Phys. Rev.*, **44**, 188 (1933).

(15) T. C. Clark and M. A. A. Clyne, *Trans. Faraday Soc.*, **65**, 2994 (1969).

Chemical Lasers Produced from O(¹D) Atom Reactions. III. HClElimination Lasers from the O(¹D) + CH_nCl_{4-n} (n = 1, 2, and 3) Reactions¹

by M. C. Lin

*Physical Chemistry Branch, Naval Research Laboratory, Washington, D. C. 20390 (Received September 23, 1971)**Publication costs assisted by the Naval Research Laboratory*

Chemical HCl laser emissions were observed in the four-centered unimolecular elimination of HCl from vibrationally excited Cl₃COH, Cl₂HCOH, and ClH₂COH molecules in an optical cavity. The vibrationally excited methanol molecule, which possesses at least 130 kcal/mol of internal energy, was generated by insertion of an O(¹D) atom into a C-H bond of a chloromethane molecule. The O(¹D) atom was produced from the flash-photolytic decomposition of O₃. The vibration-rotation transitions of the laser emission were identified, and the initial populations ratios of the highest gain transitions have been estimated.

Introduction

We have recently reported the observation of HF laser emissions produced from the four-centered elimination reaction of chemically activated α -fluoromethanols.² The vibrationally excited methanol was generated by insertion of an O(¹D) atom into a C-H bond of a fluoromethane molecule. We have also observed HCl laser emissions in a similar study of the chloromethane analog. This is, to our knowledge, the first HCl elimination laser produced in a chemically activated system. Photochemical HCl elimination lasers, however, have been observed previously in the vacuum uv flash photolysis of chloroethylenes by Berry and Pimentel.³

Experimental and Results Section

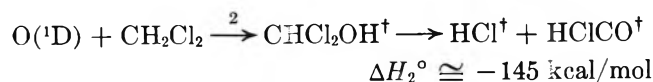
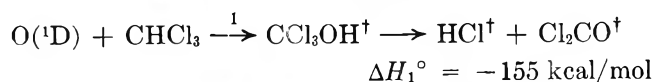
In the present work, the mixtures of O₃ and CH_nCl_{4-n} (n = 1, 2, and 3) were flash-photolyzed, in the presence of a diluent such as He or SF₆, in an optical cavity. The optical cavity and the detecting system have been described previously.⁴ HCl laser emissions were detected in all three chloromethane systems. The total emission traces are shown in Figure 1; in all cases, a total pressure of 30 Torr with SF₆ as a diluent and a constant energy of 1.5 kJ were employed. Figure 2 shows the total laser intensity as a function of the total pressure of the O₃-CH₂Cl₂ mixture, with either He or SF₆ as a diluent. The latter was found to be more efficient in enhancing the laser output, thanks probably to its small cross section for deactivation of the O(¹D) atom⁵ and its higher efficiency in lowering the rotational temperature of the lasing medium. At higher pressures (*i.e.*, $P > 40$ Torr), however, the SF₆ mixture shows a rapid decrease in the laser intensity; this may be due to the deactivation of HCl(v) by SF₆. Helium, on the other hand, exhibits a slower deactivation rate. Similar results were observed for the CHCl₃ and CH₃Cl systems.

The laser transitions were identified with a 50-cm Model 305 SMP03 monochromator, using 250- μ slits, which provided a resolution of about ± 0.5 cm⁻¹ in the spectral region of interest. The observed emissions were predominantly due to H³⁵Cl, despite the high isotope enrichment of H³⁷Cl. Only P₂₁(7) of the H³⁷Cl lines was detected in the highest gain CH₂Cl₂ system. On account of the lower gain of the H³⁷Cl line, it has a longer appearance time and weaker peak power than the H³⁵Cl counterpart, as shown in Figure 3.

Ozone was again found to be essential to the laser action. No laser oscillation was detected when chloromethane-SF₆ mixtures were flashed in the absence of O₃ under the same conditions. Mass spectrometric analysis of the condensable (at 77°K) fractions of the flashed samples indicate the presence of Cl₂CO, HClCO, and H₂CO, together with large amounts of CO₂, in the CHCl₃, CH₂Cl₂, and CH₃Cl systems, respectively. Large quantities of CO were detected in the noncondensable fractions of all three flashed samples.

Discussion

Similar to the fluoromethane systems (except CHF₃),² the presence of CO and CO₂ indicate that the vibrationally hot formaldehyde molecules formed in the following insertion-elimination reactions



(1) This work is partially supported by the Advanced Research Projects Agency under ARPA Order 660.

(2) M. C. Lin, *J. Phys. Chem.*, **75**, 3642 (1971).

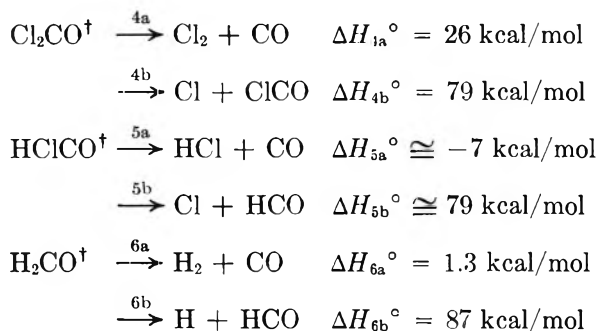
(3) M. J. Berry and G. C. Pimentel, *J. Chem. Phys.*, **51**, 2274 (1969); *ibid.*, **53**, 3453 (1970).

(4) L. E. Brus and M. C. Lin, *J. Phys. Chem.*, **75**, 2546 (1971).

(5) K. F. Preston and R. J. Cvetanović, *J. Chem. Phys.*, **45**, 2888 (1966).



may readily undergo further decomposition or elimination reactions, such as



For both Cl_2CO and H_2CO , the molecular elimination reactions are probably less likely, although these processes have been shown to occur in the photodecomposition reactions.^{6,7}

The energetics of the above reactions were calculated from the heats of formation of various species recommended in Benson's book.⁸ The heat of formation of HClCO , $\Delta H_f^\circ(298) (\text{HClCO}) = -40.7 \text{ kcal/mol}$, is the

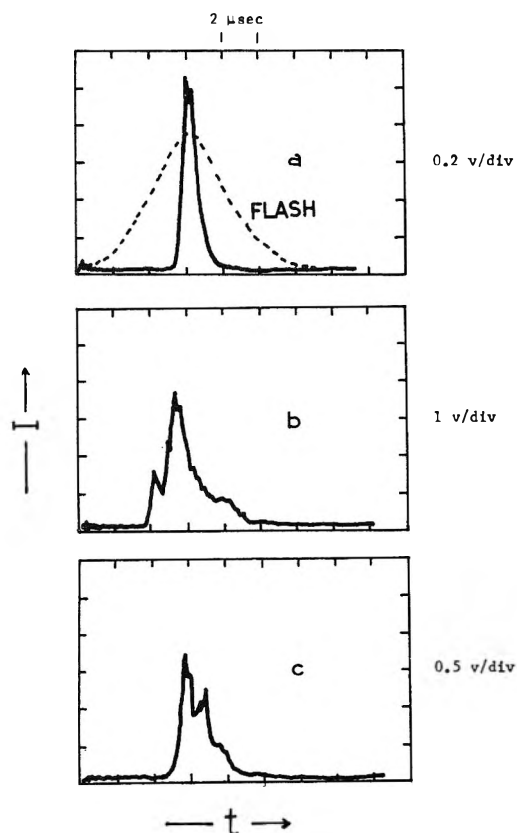


Figure 1. The total emission traces: (a) CHCl_3 mixture ($\text{O}_3:\text{CHCl}_3:\text{SF}_6 = 1:3:20$); (b) CH_2Cl_2 mixture ($\text{O}_3:\text{CH}_2\text{Cl}_2:\text{SF}_6 = 1:1.5:20$); (c) CH_3Cl mixture ($\text{O}_3:\text{CH}_3\text{Cl}:\text{SF}_6 = 1:1:20$). Solid curves, laser emissions; dotted curve, flash lamp output at 240 nm.

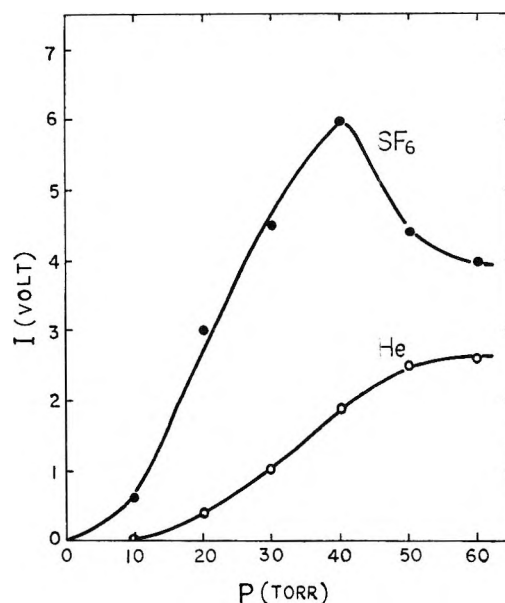


Figure 2. The effect of total pressure on the laser intensity of the CH_2Cl_2 system: $\text{O}_3:\text{CH}_2\text{Cl}_2:\text{He}(\text{SF}_6) = 1:1.5:20$; flash energy = 1.5 kJ.

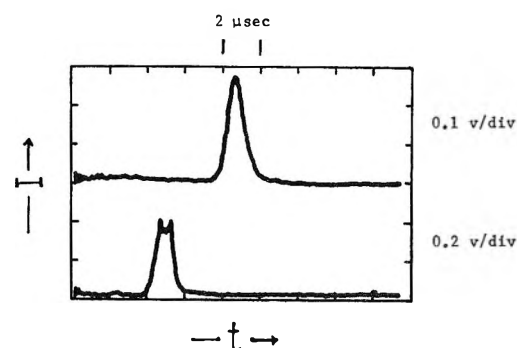


Figure 3. Emission traces of the $P_{21}(7)$ transition from the $\text{O}_3\text{-CH}_2\text{Cl}_2$ flashes: upper traces, H^{37}Cl ; lower trace, H^{35}Cl .

average of two values estimated by assuming $D(\text{HCO-Cl}) = 78.6$ and $D(\text{ClCO-H}) = 87.0 \text{ kcal/mol}$; both estimates agree within 4 kcal/mol. The energetics of the laser pumping reactions 1-3 are similar to those of the $\text{CH}_n\text{F}_{4-n}$ analog.² The presence of CO and CO_2 in the flashed CHCl_3 sample, in contrast to the CHF_3 system, is consistent with the fact that Cl_2CO decomposes more readily than F_2CO ; the first C-F bond dissociation energy of F_2CO is known to be about 137 kcal/mol.^{2,9} A more thorough kinetic study of these reactions using a conventional photolytic setup is certainly warranted, since neither the kinetics nor the mechanism of this type of insertion-elimination reaction has been investigated before.

(6) H. Okabe, A. H. Laufer, and J. J. Ball, *J. Chem. Phys.*, **55**, 373 (1971).

(7) J. G. Calvert and J. N. Pitts, Jr., "Photochemistry," Wiley, New York, N. Y., 1966.

(8) S. W. Benson, "Thermochemical Kinetics," Wiley, New York, N. Y., 1968.

(9) H. Henrici, M. C. Lin, and S. H. Bauer, *J. Chem. Phys.*, **52**, 5834 (1970).

Table I: Observed HCl Vibration-Rotation Transitions and Their Appearance Times in the CHCl₃, CH₂Cl₂, and CH₃Cl Systems^a

Transition	ν , cm ⁻¹	CHCl ₃	CH ₂ Cl ₂	CH ₃ Cl
$\Delta v = 2 \rightarrow 1$				
P(5)	2675.01 ^b		3.9	
P(6)	2651.82		3.5	
P(7)	2628.13		4.0	
P(8)	2604.09		4.6	
P(9)	2579.42		5.2	
P(10)	2554.34		6.2	
$\Delta v = 1 \rightarrow 0$				
P(7)	2727.78 ^c	5.2 ^d		4.4
P(8)	2703.01	4.8		5.2
P(9)	2677.73	5.6		6.2
P(10)	2651.97	6.6		7.0

^a Flash energy = 1.5 kJ, $P_{\text{total}} = 30$ Torr and O₃/CH_nCl_{4-n}/SF₆ = 1:3:20, 1:1.5:20, and 1:1:20 for $n = 1, 2$, and 3 , respectively.

^b Vacuum wavelengths observed by T. F. Deutsch, *IEEE J. Quantum Electron.*, **QE3**, 419 (1967). ^c Vacuum wavelengths observed by D. H. Rank, B. S. Rao, and T. A. Wiggins, *J. Mol. Spectrosc.*, **17**, 122 (1965). ^d Appearance time of the individual laser pulse in microseconds.

The results given in Table I allow us to estimate the initial relative population of HCl for the transition that has the highest gain. If we assume that the deactivation of HCl is negligible and that the rotational temper-

ature of HCl is about 300°K, then the observation that P₁₀(8) reaches threshold first in the CHCl₃ flashes, as shown in Table I, implies that $N_1/N_0 \approx 0.50 \pm 0.04$ for the HCl molecule produced in reaction 1 according to our gain calculations. Similar calculations lead to $N_2/N_1 \approx 0.75 \pm 0.10$ for the HCl molecule formed in reaction 2 and $N_1/N_0 \approx 0.61 \pm 0.05$ in reaction 3. The higher laser output observed for reaction 2 may be attributed to a higher HCl concentration resulting from the successive elimination reactions 2 and 5a. A similar result was also observed for the CH₂F₂ system.²

Conclusion

It is shown that the population ratios of the highest gain transitions in these three systems are all less than unity. This observation further supports the conclusion that the fraction of reaction energy that is distributed into the HX product of a unimolecular elimination reaction is usually relatively small,^{2,3,10-12} in contrast to the exothermic bimolecular abstraction reaction, $X + HY \rightarrow HX^\dagger + Y$ or $H + X_2 \rightarrow HX^\dagger + X$.^{12,13}

(10) P. N. Clough, J. C. Polanyi, and R. T. Taguchi, *Can. J. Chem.*, **48**, 2919 (1970).

(11) T. D. Padrick and G. C. Pimentel, *J. Chem. Phys.*, **54**, 720 (1971).

(12) H. W. Chang, D. W. Setser, and M. J. Perona, *J. Phys. Chem.*, **75**, 2070 (1971).

(13) P. D. Pacey and J. C. Polanyi, *Appl. Opt.*, **10**, 1725 (1971), and the references cited therein.

Quantum Yields for the Photooxidation of Sulfur Dioxide in the First Allowed Absorption Region

by R. A. Cox

Atomic Energy Research Establishment, Harwell, Didcot, Berkshire, U. K.

Publication costs borne completely by The Journal of Physical Chemistry

The quantum yield for sulfur trioxide production (ϕ_{SO_3}) was determined for the photolysis of SO_2 alone, $\text{SO}_2\text{-O}_2$ and $\text{SO}_2\text{-air}$ mixtures in the wavelength region 240–400 nm in a static system at room temperature. A method was developed in which the gaseous reaction products were extracted in aqueous solution and the sulfur trioxide determined as sulfate ion. At low concentrations of SO_2 relative to O_2 or air, ϕ_{SO_3} was 1×10^{-3} but increased with the initial concentration ratio $\text{SO}_2\text{-O}_2$ to a maximum of about 5×10^{-3} . In pure SO_2 , ϕ_{SO_3} was lower than when small amounts of O_2 were present. The quantum yields were considerably lower than the previously reported values for the photooxidation of SO_2 under similar conditions and there was some evidence that high values may result from a surface reaction. The results were reasonably consistent with current ideas on the mechanism of SO_2 photolysis and, by extrapolation from the results for $\text{SO}_2\text{-air}$ mixtures, an estimate of 0.3×10^{-3} has been made for the quantum yield for the photooxidation of SO_2 in the atmosphere by natural sunlight.

Introduction

Interest in the photochemical reactions of sulfur dioxide in the first allowed absorption region (260–330 nm) has been revived recently on account of the possible importance of these processes in the atmospheric chemistry of SO_2 . In particular the photooxidation of SO_2 has received considerable attention.

The formation of sulfur trioxide (SO_3) when sulfur dioxide (SO_2) and $\text{SO}_2\text{-oxygen}$ mixtures are exposed to uv radiation has been known for many years. Although there have been a number of investigations of the photooxidation of SO_2 in the 260–330-nm region the kinetics and mechanism of the reaction are still far from understood. Hall¹ reports a quantum yield (ϕ_{SO_3}) of 0.036 for SO_3 formation in the photooxidation of 12.7 mm SO_2 and 10.6 mm O_2 at 25° in a quartz reaction cell exposed to the 313 nm line from a mercury arc. In the same investigation, the rate of photooxidation of SO_2 (56–230 mm) with O_2 (50–200 mm) in sunlight was determined. The observed photolysis rate constant, k , was roughly independent of O_2 concentration and corresponds to a quantum yield of approximately 10^{-2} for SO_3 formation. Estimates of ϕ_{SO_3} from studies of the photooxidation of part per million concentrations of SO_2 in air at wavelengths $>290 \text{ nm}^2,^3$ have been made by Leighton.⁴ The estimates ranged from 3×10^{-3} to 0.3. Recent results of Urone, *et al.*,⁵ indicate that the lower value is more realistic for low concentrations of SO_2 .

Very recently two more reports of quantum yield determinations in the photooxidation of SO_2 at higher concentrations have appeared. Cadle, *et al.*,⁶ measured the quantum yields for the disappearance of SO_2 (ϕ_{SO_2}) using a photometric device to monitor the decline

in SO_2 concentration when mixtures of SO_2 (20–100 mm) and O_2 (50–390 mm) were exposed to an intense uv source. At 313 nm, ϕ_{SO_2} was 1.7×10^{-2} and over the integrated wavelength range 280–420 nm was 2×10^{-3} . There was no observed dependence of ϕ_{SO_2} on the initial O_2 and SO_2 concentration and the inert gases, N_2 and CO_2 , had no noticeable effect. Also Calvert, *et al.*,⁷ report a value of 0.08 ± 0.02 for ϕ_{SO_3} in the photolysis of pure SO_2 (760 mm) in the wavelength range 250–400 nm.

Since there is apparently no variation of ϕ_{SO_3} with O_2 or N_2 concentration, it is difficult to see why there should be such a large variation in the quantum yields determined for the different conditions. The present study was undertaken to obtain more information on this matter. The quantum yield for SO_3 formation has been determined in the photolysis at room temperature ($23 \pm 2^\circ$) of SO_2 alone, $\text{SO}_2\text{-oxygen}$, and $\text{SO}_2\text{-air}$ mixtures with a variety of reactant concentrations. In contrast to previous reports, ϕ_{SO_3} was found to be dependent on the concentration of O_2 . Considerable irreproducibility in the reaction rates was encountered,

(1) T. C. Hall, Jr., Ph. D. Thesis, University of California, Los Angeles, 1953.

(2) E. R. Gerhard and H. F. Johnstone, *Ind. Eng. Chem.*, **47**, 972 (1955).

(3) N. A. Renzetti and G. F. Doyle, *Int. J. Air Pollut.*, **2**, 327 (1960).

(4) P. A. Leighton, "Photochemistry of Air Pollution," Academic Press, New York, N. Y., 1961, p 234.

(5) P. Urone, H. Lutsep, C. M. Noyes, and J. F. Parcher, *Environ. Sci. Tech.*, **2**, 611 (1968).

(6) (a) D. S. Sethi, E. R. Allen, and R. D. Cadle, presented at 5th International Conference on Photochemistry, Yorktown Heights, N. Y.; (b) R. D. Cadle and E. R. Allen, *Science*, **167**, 243 (1970).

(7) S. Okuda, T. N. Rao, D. H. Slater, and J. G. Calvert, *J. Phys. Chem.*, **73**, 4412 (1969).

particularly at high SO_2 pressures. This may be due to a surface effect which would explain some of the differences observed previously. Extrapolation from the results with low pressures of SO_2 in air gave a value of $\phi_{\text{SO}_3} = 3 \times 10^{-4}$ for the photooxidation of SO_2 at part per million concentrations such as are found in the atmosphere.

Experimental Section

The photolyses were carried out in a cylindrical quartz cell, 10-cm length \times 5-cm diameter which was attached by a grease-free teflon stopcock to a conventional vacuum system for the handling of gas mixtures. SO_2 gas pressures were measured on an oil manometer containing dioctyl phthalate and a mercury manometer was used to measure air and oxygen. A trap cooled to -196° was placed between the mercury column and the remainder of the vacuum system to minimize contamination with mercury vapor.

Research grade sulfur dioxide (99.95%) was taken from a cylinder (Air Products Ltd.). The gas was passed through concentrated sulfuric acid and phosphorus pentoxide to remove traces of SO_3 and moisture, and was stored in the dark. To facilitate analyses (see later) a small amount of radioactive $^{35}\text{SO}_2$ (from U.K.A.E.A. Radiochemical Centre, Amersham, U. K.) was added to the pure SO_2 to give a specific activity of about 1.5×10^{-2} mc/mM. Air from a compressed air line was purified by passing it through columns of silica gel, activated charcoal, Molecular Sieve 13x and an absolute dust filter. Oxygen of spectroscopic grade (British Oxygen Ltd.) was used without further purification. Deionized distilled water was used to prepare aqueous solutions.

The light source was an UVS 500 medium pressure mercury arc (Englehard Hanovia Ltd.) placed 20 cm from the end window of the photolysis cell. An OX7 uv transmission glass filter (Chance-Pilkington) was used to isolate the spectral region 240–400 nm and a combination of an OX7 filter with a pyrex glass filter gave the 290–400-nm region. The 313-nm line from the arc was isolated using a chemical-glass filter system. The filter solutions (aqueous 0.18 M NiSO_4 (5 cm), 5×10^{-4} M K_2CrO_4 (5 cm), and 0.0245 M potassium bipthalate (1 cm)) and an OX7 filter were placed in this order between the lamp and the cell. A stop placed close to the cell window served to prevent the entry of extraneous radiation from the lamp and the whole optical system was shielded from room light with black photographic paper.

The light intensity transmitted through the reaction cell was monitored on a blue sensitive photodiode (Mullard 90CV) placed 5 cm behind the end window. The voltage drop resulting from passage of the photocurrent through a 2 k Ω resistor was fed directly to a 10 mV pen recorder. Absolute light intensities in the reaction cell were determined by ferrioxalate actinometry⁸ using the experimental procedure described by

Calvert and Pitts.⁹ A 5 cm \times 5 cm cylindrical pyrex cell with quartz end windows placed in the same position as the reaction cell was used for the actinometric measurements. The light flux in photons per second for the three wavelengths used were 1.0×10^{17} for the 240–400-nm region, 4.3×10^{16} for the 290–400-nm region and approximately 2.5×10^{15} for the 313-nm line. During the experiments with the glass filters the incident intensity was essentially constant with time. However there was a loss in the transmission of the chemical filters in the course of the experiments and the solutions were changed several times. In these experiments, the transmitted light intensity was monitored on the photodiode throughout each irradiation and a correction made for changes in the incident intensity. Several checks during the course of the experiments showed that the photometer calibration at 313 nm was reproducible.

The amount of light absorbed by SO_2 in the reaction cell was calculated from the extinction coefficients of SO_2 in the wavelength regions used. The extinction coefficient for SO_2 for the 313-nm line from the filter system was determined experimentally. The ratio I_o/I_{trans} was measured for different pressures of SO_2 in the cell and a Beer's Law plot gave a value of 47 l. mol $^{-1}$ cm $^{-1}$ for the extinction coefficient. This value is in agreement with that estimated for this wavelength from a published uv spectrum in ref 9. For the experiments in which a range of wavelengths were used, the incident intensity of the individual lines was estimated from the makers specified wavelength distribution from the arc and the transmission characteristics of the filters. The SO_2 extinction coefficients at each wavelength were estimated from the published absorption spectrum⁹ and were used to calculate the amount of each line absorbed. In the 240–400-nm region and at the highest SO_2 pressure used (700 Torr) 63% of the incident radiation was absorbed. The major absorbed lines (nm) were 334 (5.5% of absorbed light), 313 (34%), 302 (17%), 297 (8.7%), 289 (3.0%), 280 (5.8%), 265 (8.9%), 254 (4.8%), 248 (2.9%). In the 290–400-nm region 27% of the incident light was absorbed in the following lines (nm) 334 (16%), 313 (64.5%), 302 (16.1%), 297 (3.4%).

Before each photolysis the reaction cell was washed thoroughly with distilled water and then with methanol. After drying, the cell was attached to the vacuum system and pumped out at $<10^{-4}$ Torr for at least 1 hr. The required pressure of SO_2 was introduced to the cell and allowed to condense in a cold finger at -196° . Air or oxygen was admitted to a known pressure and the mixture was allowed to warm up and mix for at least 15 min before irradiation. The photodiode and re-

(8) C. G. Hatchard and C. A. Parker, *Proc. Roy. Soc., Ser. A*, **235**, 518 (1956).

(9) J. G. Calvert and J. N. Pitts, Jr., "Photochemistry," Wiley, New York, N. Y., 1966.

order were then switched on and the mixture was irradiated for the required period, usually overnight.

An analytical procedure was developed in which the SO_3 formed in the photolysis was dissolved in aqueous solution and determined as sulfate. After irradiation, 10 ml of a suitable aqueous solution (see below) was introduced into the cell from a pipette. The solution was shaken in the cell for several minutes and transferred to a small plastic bottle. At higher conversions a distinct white mist appeared in the cell when the aqueous solution was introduced but this disappeared quite rapidly on shaking. Since SO_2 is appreciably soluble in water at room temperature and would interfere with the analysis, pure N_2 was bubbled through the solution until all the dissolved SO_2 had been removed. The amount of sulfate present in the solution was then determined by radioactive assay or by a spectrophotometric method (see below). The most suitable solution found for the extraction of SO_3 was $1 \times 10^{-3} M$ hydrazine perchlorate with the pH adjusted to about 2 by addition of perchloric acid. The reducing properties of this solution served to prevent the oxidation of dissolved SO_2 to sulfate, which was found to occur to an appreciable extent when pure water was used. The low pH favored a more rapid removal of the SO_2 when N_2 was passed through the solution. It was necessary to use the perchlorate salt since other anions (e.g., Cl^- , NO_3^-) interfered with the subsequent spectrophotometric determination of sulfate.

Radioactive assay of the aqueous solution was made by liquid scintillation counting. Aliquots (0.5 ml) of the solution were dissolved in N.E. 220 scintillator solution (Nuclear Enterprises Ltd.) and counted on a Packard "Tri-Carb" liquid scintillation spectrometer. Determination of the total amount of sulfur present was based on the activity found when known amounts of radioactive sulfur dioxide were admitted to the reaction vessel and dissolved in aqueous 1 vol hydrogen peroxide solution. A correction was made for the radioactive decay of ^{35}S during the course of the experiments.

The removal of dissolved sulfur dioxide during the passage of nitrogen was followed by radioactive assay. The activity in successive 0.5 ml aliquots decreased rapidly when N_2 was bubbled through the solution until, after about 60 min, a constant count was obtained unaffected by further passage of N_2 . The final (constant) count was used to determine the sulfate ion concentration.

Spectrophotometric determination of sulfate was carried out using the barium perchlorate-thoranol method.¹⁰ An aliquot (usually 5 ml) of the solution containing sulfate ion was made up to 7 ml with water. Barium perchlorate (15 ml) solution (0.9 g $\text{Ba}(\text{ClO}_4)_2$ in 1 l. 0.1 M HClO_4 diluted 100-fold with AR dioxane) was added, followed by 3 ml aqueous thoranol (0.2 g/l.). The transmission of this solution was measured at 520

nm against a reagent blank. Calibration using aliquots of a standard potassium sulfate solution with 5 ml hydrazine perchlorate ($10^{-3} M$) showed Beer's Law to be obeyed only up to 25 μg sulfate in the sample. More concentrated sulfate solutions were diluted to come within the range of the analytical determination.

Preliminary studies on the removal of SO_2 from the hydrazine perchlorate solution indicated that some sulfate was produced during the process of washing out the reaction vessel and removal of SO_2 . Trial irradiations showed that only small conversions of SO_2 to SO_3 could be expected with the light intensity available and it was necessary to make blank determinations so that the SO_3 formed in the photolysis could be determined by difference.

A series of blank determinations were made in which the analytical procedure was carried out on SO_2 alone or SO_2 -air mixtures made up in the reaction vessel. Both radioactive assay and colorimetric analysis were used to determine the sulfate present in the extracts from the blank and the photolysis experiments and the results for the two methods agreed within $\pm 4\%$. The amount of sulfate formed in the blank experiments was between 0.06 and 0.11% of the initial SO_2 (the proportion increased with SO_2 concentration) and was quite reproducible for a given pressure of SO_2 . To determine the amount of SO_3 formed during the irradiation of a given pressure of SO_2 , the average value of the blank sulfate for that SO_2 pressure was subtracted from the total sulfate formed.

The main source of error in the quantum yield determinations in this work arises from the measurement of the SO_3 formed in the photolysis. The uncertainty associated with the determination of the total sulfate ion concentration (95% confidence limits) was estimated to be $\pm 8\%$ for a sulfate concentration of 3 $\mu\text{g}/\text{ml}$ in the sample. However, at the lowest SO_2 concentrations used and when the amount of sulfate from the photo-oxidation was less than the blank, the error in the SO_3 measurements was estimated to be as much as $\pm 50\%$.

Errors in the measurement of I_{abs} at 313 nm could arise from reflection at the rear cell window and from the divergence of the light beam. However these errors are not likely to amount to more than a few percent and are small compared with the error in the SO_3 determination. The possibility of a larger systematic error in the estimation of I_{abs} in the wide band irradiations cannot be dismissed. However the relatively good agreement that was found between the quantum yield determinations using 290–400-nm radiation and using 313-nm radiation, for otherwise similar conditions, suggests that a serious error was not present in the estimation of the absorbed intensity in the wide band irradiations.

(10) G. A. Persson, *Int. J. Air Water Pollut.*, 10, 845 (1966).

Results

(a) *Photolysis of SO₂-O₂ and SO₂-Air Mixtures at 290-400 nm.* Mixtures of SO₂ (29 mm) with different amounts of O₂ or air were photolyzed with 290-400-nm radiation and the yield of SO₃ determined. Photolysis times of about 17 hr were employed which gave conversions of between 0.5 and 1.8% based on the SO₃ yield. There was no noticeable fogging of the windows at these conversions. A constant initial pressure of SO₂ was used to ensure an essentially constant rate of light absorption and thus minimize any uncertainties arising from the estimation of the amount of light absorbed in each experiment. Table I shows the values of ϕ_{SO_3} , which ranged from 1.7×10^{-3} to 5.5×10^{-3} showing that the quantum efficiency for the photooxidation is low at the wavelengths and concentrations used. For pure SO₂, ϕ_{SO_3} was 3.4×10^{-3} which was lower than when small amounts of O₂ or air were present.

Table I: Quantum Yields for SO₃ Formation at 290-400 nm

Initial pressures, mm			Light absorbed, (photons) $\times 10^{20}$	Sulfate yield, ^a μmol	$10^3\phi_{\text{SO}_3}$
SO ₂	O ₂	N ₂			
28.6	5.51	3.10	3.4
28.6	15.6	...	5.49	3.92	4.3
29.4	5.4	...	5.63	4.68	5.0
28.9	148.5	526.5	5.51	1.52	1.7
28.9	65.5	232.5	5.68	2.45	2.6
29.1	25.5	90.5	5.50	3.57	3.9
28.8	9.1	31.9	5.32	3.82	4.3
29.2	3.3	11.9	5.38	4.90	5.5

^a Average of radioactive assay and spectrophotometric determination, with blank subtracted; blank sulfate at this pressure of SO₂ was 0.20 μmol .

(b) *Photolysis of SO₂-O₂ and SO₂-Air Mixtures with Monochromatic 313-nm Radiation.* Mixtures of SO₂ (2-70 mm) with air (60-450 mm) or O₂ (10-100 mm) were photolyzed with 313-nm radiation. Photolysis was normally for about 17 hr but for some experiments longer periods were necessary to obtain sufficient sulfate for measurement. The results are shown in Table II and are also plotted together with the results from Table I on Figure 1, as a function of the pressure of SO₂ relative to the sum of the partial pressures of SO₂ and O₂. As a result of the low quantum efficiencies, the total amount of SO₃ formed with the light intensity available at 313 nm was quite small. The sulfate yield was in some cases of the same magnitude as the blank and consequently the experimental error associated with the data in Table II is quite large as noted in the Experimental Section. Nevertheless the data for the monochromatic light plotted in Figure 1 shows good agreement with that obtained at larger conversion in the 290-400-nm photolyses.

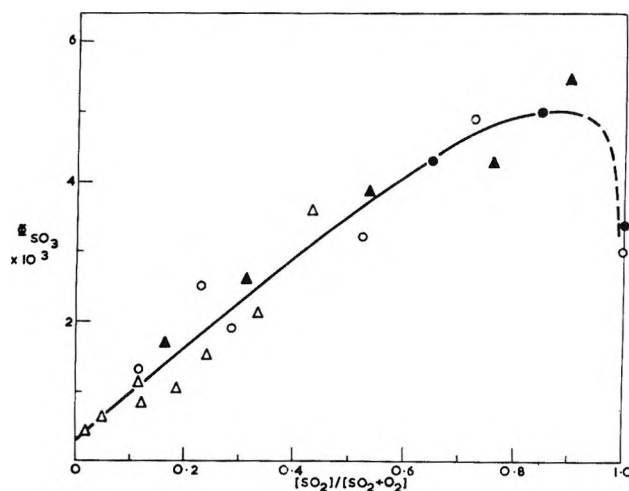


Figure 1. Variation of ϕ_{SO_3} with the concentration of SO₂ relative to the sum of the SO₂ and O₂ concentrations in the photolysis of SO₂-O₂ and SO₂-air mixtures. Key: Δ , SO₂ + air; \circ , SO₂ + O₂; open points, 313 nm; filled points, 290-400 nm with fixed pressure of SO₂ of 30 mm.

Table II: Quantum Yields for SO₃ Formation at 313 nm

Initial pressures, mm			Light absorbed (photons) $\times 10^{-20}$	Sulfate yield, ^a μmol	$10^3\phi_{\text{SO}_3}$
SO ₂	O ₂	N ₂			
28.4	0.20	0.10	3.0
12.1	106.3	...	1.14	0.25	1.3
29.8	99.8	...	0.33	0.14	2.5
29.9	75.4	...	1.77	0.56	1.9
29.5	27.0	...	1.15	0.61	3.2
29.1	10.6	...	1.26	1.02	4.9
2.0	92.1	326.9	0.45	0.03	0.4
4.5	91.7	325.3	0.39	0.04	0.6
11.8	90.6	321.4	1.52	0.26	1.1
29.4	93.0	329.5	1.46	0.37	1.5
69.7	91.7	325.3	4.45	2.70	3.6
12.0	52.8	74.0	0.92	0.16	1.0
11.5	23.0	81.5	1.04	0.37	2.1
10.8	98.0	350.0	0.047	0.22	28.0
29.3	97.8	349.2	0.078	0.15	11.5
43.8	98.0	347.0	0.20	0.20	6.0

^a Average sulfate yield from radioactive assay and spectrophotometric determination with blank subtracted.

Figure 1 shows that ϕ_{SO_3} increases with the concentration of SO₂ relative to O₂ in both SO₂-O₂ and SO₂-air mixtures. When the ratio $[\text{SO}_2]/[\text{SO}_2 + \text{O}_2]$ was >0.4 , the presence of N₂ (*i.e.*, when air was used instead of O₂) did not significantly affect ϕ_{SO_3} . For larger amounts of added O₂ or air ($[\text{SO}_2]/[\text{SO}_2 + \text{O}_2] < 0.2$), the quantum yields in the presence of air tended to be rather lower than with O₂, although the scatter on the points precludes any definite conclusion in this respect.

The final three rows on Table II show the results of the first three determinations in this investigation using 313-nm radiation. It is seen that ϕ_{SO_3} started at a

much higher value than any of the subsequent determinations and then decreased as the pressure of SO₂ was increased. This effect was attributed to surface conditioning. After several runs using 290–400-nm radiation the reaction rate became reproducible and the other results in Tables I and II were obtained in the "seasoned" vessel.

(c) *The Effect of Initial Pressure of SO₂*. The quantum yield for SO₃ formation was determined over an extended range of SO₂ initial pressures both in the presence and absence of O₂. In the first series of experiments SO₂-O₂ mixtures with an approximately 10-fold excess of SO₂, were photolyzed using 240–400 nm radiation. Irradiation times were varied from 2–17 hr giving up to 5% conversion. The initial pressure of SO₂ was varied between 30 and 700 mm and the results (Figure 2, open points) show a marked increase of ϕ_{SO_3} ,

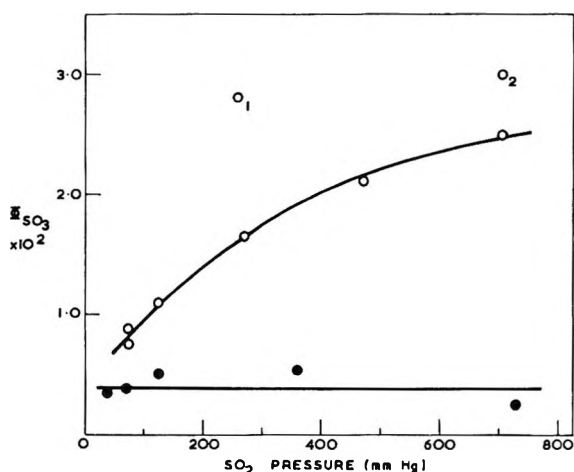


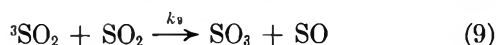
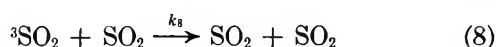
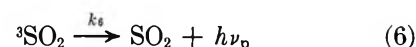
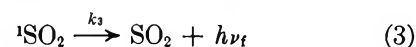
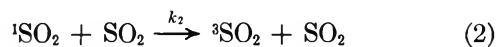
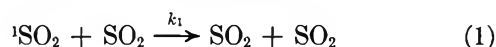
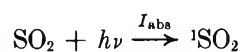
Figure 2. Effect of SO₂ pressure on ϕ_{SO_3} . Open circles, SO₂-O₂ mixtures (10:1), points marked 1,2 refer to the first two experiments in the series. Filled circles, SO₂ alone.

with the SO₂ pressure in this range. It will be noted again (Figure 2) that the first two experiments have unusually high reaction rates. These experiments were carried out after the reaction vessel had been pumped out for several weeks during which time it had not been used. Quantum yield determinations over an extended pressure range were then made using SO₂ alone and with 290–400-nm light. In the absence of O₂ some fogging of the cell windows was noticed. In this case there was no significant increase in ϕ_{SO_3} as the initial pressure of SO₂ was increased from 70 to 700 Torr. To within the experimental error (The error on the points at high SO₂ pressure is quite large since the sulfate blank increased with SO₂ concentration whereas with the irradiation times and light intensity used, the SO₃ yields in the second series of experiments were approximately constant.) the value was approximately 0.4×10^{-2} throughout the range. This result is puzzling as it seems unlikely from previous work that the presence of 10% O₂ or the use of radiation of wavelength

<290 nm could account for the difference between the two sets of results.

Discussion

In order to discuss the experimental results it is necessary to consider them in the light of current ideas on the photophysical processes involved in the photolysis of SO₂ in the first allowed absorption region. Observations of the fluorescence and phosphorescence emission have shown that absorption in this region leads to the formation of two upper states of SO₂, the first excited singlet ¹B₁ (¹SO₂) and the triplet ³B₁ (³SO₂). Initially ¹SO₂ is formed and this species is rapidly quenched by collisions with other molecules such as SO₂, O₂, and CO₂ at a rate close to the collision frequency.^{11,12} A fraction of these collisions results in intersystem crossing to ³SO₂. Calvert, *et al.*,⁷ have proposed the following scheme for the formation of SO₃ in the photolysis of pure SO₂



The rate constants for the unimolecular reactions 3–7 are too low for these reactions to compete with the bimolecular reactions at pressures above 1 Torr.¹¹ Only reactions 1, 2, 8, 9 need therefore to be considered in the present discussion. Evidence that triplet sulfur dioxide is the chemically active species which leads to sulfur trioxide production comes from the retarding effect of biacetyl on the rate of formation of SO₃ in SO₂ photolysis.⁷ Previously it has been shown that low pressures of biacetyl efficiently quench the excited ³SO₂ molecules by energy transfer.¹¹

Application of the steady state approximation to the concentrations of ¹SO₂ and ³SO₂ gives

$$\phi_{\text{SO}_3} = \frac{k_2}{k_1 + k_2} \frac{k_9}{k_8 + k_9} \quad (i)$$

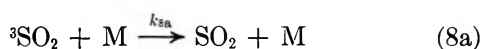
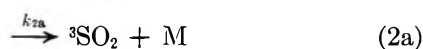
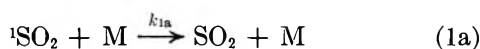
(11) (a) T. N. Rao, S. S. Collier, and J. G. Calvert, *J. Amer. Chem. Soc.*, **91**, 1609 (1969); (b) T. N. Rao, S. S. Collier, and J. G. Calvert, *ibid.*, **91**, 1616 (1969).

(12) T. N. Rao and J. G. Calvert, *J. Phys. Chem.*, **74**, 681 (1970).

Thus, in pure SO₂, ϕ_{SO_3} should be independent of the pressure of SO₂ in accord with the present results (Figure 2).

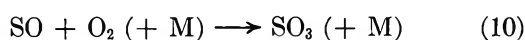
Rao, *et al.*,¹¹ have shown that with an excitation wavelength of 285 nm quenching collisions of ¹SO₂ with SO₂ result in spin inversion (reaction 2) about 8% of the time and 92% of the quenching collisions cause relaxation to the ground state (reaction 1), *i.e.*, $k_2/(k_1 + k_2) = 0.08$. This ratio is apparently only slightly dependent on wavelength, increasing to about 0.10 at 302 nm.¹² The present value of $\phi_{\text{SO}_3} = (0.38 \pm 0.10) \times 10^{-2}$ suggests, therefore, that reaction 9 is rather inefficient, only about 1 in 26 deactivating collisions of ³SO₂ with SO₂ resulting in chemical reaction at room temperature.

Emission studies^{11,13,14} have shown that both ¹SO₂ and ³SO₂ are quenched by other gases such as O₂, CO₂, N₂ at a rate comparable to quenching by SO₂



These studies give information only on the total quenching of the excited states and do not provide any distinction between physical quenching and chemical reaction.

The reaction of any added gases with SO radicals produced in reaction 9 must also be taken into account when quantum yield effects are considered. Previous workers^{1,15} have observed that elemental sulfur, which is produced in the photolysis of pure SO₂, is not formed in the presence of O₂. This has been attributed to the removal of SO radicals (which would otherwise lead to sulfur formation) in reaction 10 which may occur in the gas phase or at the surface



The present data obtained for the lower pressures of SO₂ with added O₂ or air (Figure 1) are qualitatively consistent with this model. Thus, in the presence of small amounts of O₂ or air, ϕ_{SO_3} increased almost two-fold over the O₂-free value. This would suggest that oxidation of SO radicals by reaction 10 approaches completion under these conditions. As the pressure of O₂ or air relative to SO₂ was further increased, ϕ_{SO_3} decreased. This can be attributed to competitive quenching of ³SO₂ by O₂ and N₂. An estimate of the expected quenching effect of O₂ and air was made using the relative quenching rate constants determined by Mettee¹³ for ¹SO₂ ($(k_{1a} + k_{2a})/(k_1 + k_2) = 0.32$: "a" refers to M = O₂; $(k_{1b} + k_{2b})/(k_1 + k_2) = 0.33$: "b" refers to M = N₂) and Calvert and his coworkers¹⁶ for ³SO₂ ($(k_{8a}/(k_8 + k_9) = 0.25$; $k_{8b}/(k_8 + k_9) = 0.18$). The calculated ratio $[\text{SO}_2]/([\text{SO}_2] + [\text{O}_2])$ required to reduce the quantum yield to its O₂ free value (assuming reaction¹⁰ to be 100% efficient) was 0.2 for additions of

pure O₂ and 0.5 for additions of air. It will be seen from Figure 1 that the O₂ free value of ϕ_{SO_3} was reached at $[\text{SO}_2]/([\text{SO}_2] + [\text{O}_2]) \simeq 0.5$ for additions of both O₂ and air. Although the observed quenching effect is of the expected order of magnitude, the expected difference between the quenching by pure O₂ and O₂ + N₂ mixtures (*i.e.*, air) was not observed.

In the presence of excess air such that the quenching of ¹SO₂ and ³SO₂ by O₂ and N₂ predominate over quenching by SO₂, the following expression can be derived

$$\phi_{\text{SO}_3} \approx \frac{[\text{SO}_2]}{[\text{O}_1]} \left\{ \frac{2k_{2a}k_9}{k_{8a}(k_{1a} + k_{2a})} \times \frac{\left(1 + \frac{k_{2b}[\text{N}_2]}{k_{2a}[\text{O}_2]}\right)}{\left(1 + \frac{k_{8b}[\text{N}_2]}{k_{8a}[\text{O}_2]}\right)\left(1 + \frac{k_{1b} + k_{2b}[\text{N}_2]}{k_{1a} + k_{2a}[\text{O}_2]}\right)} \right\} \quad (\text{ii})$$

Since $[\text{N}_2]/[\text{O}_2]$ is constant a plot of ϕ_{SO_3} against $[\text{SO}_2]/[\text{O}_2]$ for low concentrations of SO₂ in air should be linear and pass through the origin. The data from the present experiments for SO₂-air mixtures are plotted in this way in Figure 3. The best straight line through the points for $[\text{SO}_2]/[\text{O}_2] < 0.5$ has a slope of $(4.8 \pm 0.8) \times 10^{-3}$ and an intercept at $(0.35 \pm 0.18) \times 10^{-3}$ (95% confidence limits). This positive intercept would suggest that a small fraction of the collisions of O₂ with ¹SO₂ or ³SO₂ result in reaction giving SO₃. A process of this kind is consistent with the observed occurrence of a photooxidation reaction at part per million concentrations of SO₂ in air^{2,3} when reaction 9 would have no significance.

The quantum yields for SO₃ formation found in the present study are generally considerably lower than have been reported previously for SO₂ alone and SO₂-O₂ mixtures. The average value found for pure SO₂ was $(0.38 \pm 0.10) \times 10^{-2}$ in the pressure range 30-700 mm, *i.e.*, a factor of 20 lower than the previously reported value.⁷ Similarly for SO₂-O₂ mixtures with $P_{\text{SO}_2} \lesssim 70$ mm, ϕ_{SO_3} was always $< 10^{-2}$ which is low compared with previously reported values of 0.036¹ and 0.017.⁶ However, as the pressure of SO₂ was increased above about 70 Torr and in an unconditioned cell the quantum yields in the presence of O₂ increase with SO₂ pressure to a value of 0.03 at 740 mm SO₂. This effect was not expected on the basis of the mechanism involving the ¹B₁ and ³B₁ states of SO₂.

(13) H. D. Mettee, *J. Phys. Chem.*, **73**, 1071 (1969).

(14) (a) K. F. Greenough and A. B. F. Duncan, *J. Amer. Chem. Soc.*, **83**, 555 (1961); (b) R. B. Caton and A. B. F. Duncan, *J. Amer. Chem. Soc.*, **90**, 1945 (1968).

(15) J. N. Driscoll and P. Warneck, *J. Phys. Chem.*, **72**, 3736 (1968).

(16) H. Sidebottom, C. Badcock, G. E. Jackson, J. G. Calvert, G. Reinhardt, and E. Damon, *Environ. Sci. Tech.*, in the press.

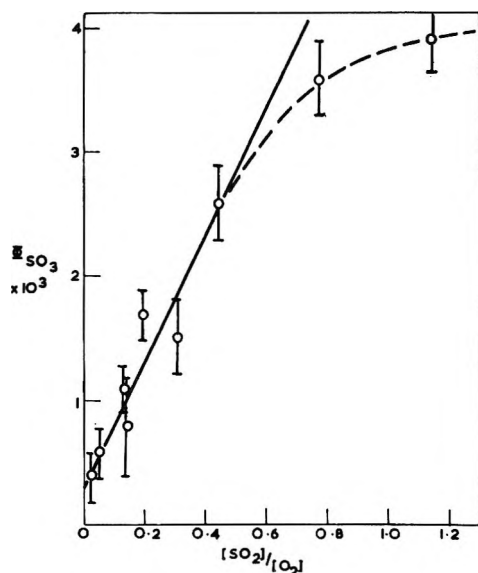


Figure 3. Plot of ϕ_{SO_3} against $[\text{SO}_2]/[\text{O}_2]$ for the photolysis of SO_2 -air mixtures.

A similar effect was found by Hall¹ who observed a linear increase in photolysis rate with SO_2 pressure in experiments with added O_2 and natural sunlight. The increase was ascribed to an increase in the rate of absorption of light by SO_2 , assuming the weak approximation to Beer's Law to hold. However, a consideration of the extinction coefficients of SO_2 in this wavelength region and the pressures of SO_2 used (50–200 mm), shows that the conditions for this approximation are only satisfied at unrealistically short path lengths. In fact the observed rates reflect an increase in ϕ_{SO_3} with the initial SO_2 pressure. No significant effect of O_2 pressure was noted although only a small range of pressure was used (50–200-mm O_2 with 100-mm SO_2). The quantum yields for SO_2 removal reported by Cadle, *et al.*,⁶ were also unaffected by O_2 pressure and also by additions of N_2 and CO_2 . These results are inconsistent with the observed kinetic behavior of the $^1\text{B}_1$ and $^3\text{B}_1$ states.

It is difficult to provide an adequate explanation of the differences between the results of these chemical studies and the predictions based on the emission studies of SO_2 photochemistry. The question arises as to whether an SO_3 formation reaction other than reaction 9 may occur in the photooxidation of SO_2 . The

high and irreproducible quantum yields found initially in the present study (Table II) and after evacuation of the reaction cell for an extended period (Figure 2) suggests that SO_3 may be formed in a photochemically induced heterogeneous reaction under some circumstances. Another possible source of complication may arise from the very nonuniform light absorption when high pressures of SO_2 are exposed to 260–330-nm radiation. For example, in the present experiments using the wide band (240–400 nm) irradiations and with 700 mm SO_2 , approximately 50% of the absorption occurred within 1 mm of the cell window. Under conditions of very nonuniform light absorption thermal oxidation of SO_2 either in the gas phase or at the wall, may occur as a result of the large local heat dissipation. A reaction of this type might be expected to become more important as the SO_2 pressure is raised (*i.e.*, as the light absorption becomes less uniform) and may explain the observed increase in ϕ_{SO_3} with SO_2 pressure. (A reviewer has suggested that singlet molecular oxygen might be involved in alternate oxidation paths. $\text{O}_2(^1\Delta_g)$ or $\text{O}_2(^1\Sigma_g^+)$ may be formed in the quenching reactions 2a and 8a ($M = \text{O}_2$). Furthermore, the lifetime of $\text{O}_2(^1\Delta_g)$ if formed, would be sufficiently long for it to reach the wall and react there.)

In the experiments at 290–400 nm and 313 nm, the light absorption in the cell was quite uniform, particularly at the lower pressure of SO_2 (<30 mm). Since there was reasonable agreement between the quantum yields determined at two widely differing light intensities, it is believed that a large contribution from thermal and/or heterogeneous reactions was not present in this case, and that the quantum yields are relevant to the gas phase reactions of excited triplet SO_2 .

The quantum yield given by the intercept in Figure 3 may be taken to approximate that for the photooxidation of atmospheric SO_2 in sunlight. The intercept value of $\phi_{\text{SO}_3} \approx 3 \times 10^{-4}$ gives a photooxidation rate which is a factor of approximately 5 less than the widely accepted value of 0.1–0.2% hr^{-1} in noonday sunlight. Recent work has shown that the rate in pure air containing small concentrations of SO_2 is considerably less than 0.1% hr^{-1} ¹⁷ and the present data seem to corroborate this.

(17) Personal communication of C. E. Junge (Mainz) to A. E. J. Eggleton of this group.

Solvent Effects on Acetophenone Photoreduction Studied by Laser Photolysis

by Hanspeter Lutz, Marie-Christine Duval, Emilienne Bréhéret, and Lars Lindqvist*

Laboratoire de Photophysique Moléculaire,¹ Université de Paris-Sud, Centre d'Orsay, 91-Orsay, France
(Received August 23, 1971)

Publication costs assisted by the Centre National de la Recherche Scientifique

The influence of the nature of the solvent on the rate constant of hydrogen abstraction, k_r , by acetophenone and benzophenone in the triplet state was studied by direct triplet lifetime measurements in mixed solvents using the 265- and 353-nm harmonics of a Q-switched Nd glass laser as excitation light source. A significant decrease in k_r with increasing solvent polarity was observed for acetophenone in 2-propanol-benzene and 2-propanol-water solutions; this effect was not shown by benzophenone. The results are discussed in terms of mixing of n, π^* and π, π^* triplet states.

An interesting feature in the photoreduction of acetophenone by 2-propanol is its reported dependence on the alcohol concentration. The photoreduction quantum yield of acetophenone in benzene increases with the concentration of added 2-propanol up to 1 *M* of alcohol and decreases at higher alcohol contents.² A similar effect has been observed for benzophenone.³ The concentration dependence has been related to the formation of an intermediate which may act as light filter or as quencher of triplet ketone.^{2,4-7} In a recent investigation of the acetophenone photoreduction, Lewis⁸ eliminated the influence of a possible intermediate by working at very low conversions and light intensities. The quantum yields were nevertheless low at high alcohol concentrations, and Lewis attributed this to the presence of a quenching impurity in commercial 2-propanol.

The primary process in these photoreductions is known to be the reaction of triplet ketone to form the ketyl radical. We have studied the influence of the nature of the solvent on this process by determining directly the lifetime of triplet acetophenone and benzophenone in mixed solvents using the laser photolysis technique and by relating this lifetime to the reactivity of the triplet state.

The sample to be studied, contained in a 1 cm square silica cell, was exposed to the third (353 nm) or fourth (265 nm) harmonic (pulse half-width, 30 nsec) of an Nd glass laser (Compagnie Générale d'Electricité). Transient optical densities were measured photoelectrically in a crossed-beam arrangement using a xenon flash lamp as monitoring light source. Acetophenone (Eastman) was purified by vacuum distillation. Benzophenone (Hopkins) was sublimed after recrystallization from ethanol-water. Benzene and 2-propanol (Merck) were spectroscopic grade. The solutions were degassed thoroughly.

On laser excitation at 353 nm of solutions containing acetophenone (0.1 *M*) or benzophenone (0.007 *M*) in 2-propanol-benzene, transient absorption due to triplet

formation was observed. A slowly disappearing residual absorption assigned to the ketyl radical remained at the end of the triplet decay. For acetophenone, the triplet decay was obtained from measurements at 380 nm, after correction for absorption due to radical formation during the triplet decay.⁹ This correction was based on the assumption that the residual absorption due to the ketyl radical is formed at the same rate as the triplet disappears. For benzophenone, two different monitoring wavelengths were chosen: 525 nm, the maximum of the triplet absorption, and 600 nm, a wavelength at which the ketyl absorption may be neglected compared to that of the triplet.¹⁰ In Figure 1 the overall decay rate constants, k , are plotted for acetophenone (curve a) and for benzophenone (curve b) as a function of the 2-propanol concentration in benzene. Acetophenone (0.0005–0.0015 *M*) was similarly studied in 2-propanol-water solution. The triplet, produced by excitation at 265 nm, was monitored at 350 nm. Curve c, Figure 1 shows the corresponding variations in the value of k .

The rate constants for hydrogen abstraction from 2-propanol, k_r , as represented in Figure 2, were obtained from the expression $k = k_d + k_r[\text{RH}]$ where RH represents 2-propanol and k_d is the rate constant of triplet decay including all decay processes except hydrogen

- (1) Groupe de recherche du C.N.R.S.
- (2) S. G. Cohen and B. Green, *J. Amer. Chem. Soc.*, **91**, 6824 (1969).
- (3) (a) S. G. Cohen, D. A. Laufer, and W. V. Sherman, *ibid.*, **86**, 3060 (1964); (b) S. G. Cohen and R. J. Baumgarten, *ibid.*, **89**, 3471 (1967).
- (4) J. N. Pitts, R. L. Letsinger, R. P. Taylor, J. M. Patterson, G. Recktenwald, and R. B. Martin, *ibid.*, **81**, 1068 (1959).
- (5) H. L. J. Bäckström, K. L. Appelgren, and R. J. V. Niklasson, *Acta Chem. Scand.*, **19**, 1555 (1965).
- (6) N. Filipescu and F. L. Minn, *J. Amer. Chem. Soc.*, **90**, 1544 (1968).
- (7) P. J. Wagner, *Mol. Photochem.*, **1**, 71 (1969).
- (8) F. D. Lewis, *J. Phys. Chem.*, **74**, 3332 (1970).
- (9) H. Lutz and L. Lindqvist, *Chem. Commun.*, 493 (1971).
- (10) H. Tsubomura, N. Yamamoto, and S. Tanaka, *Chem. Phys. Lett.*, **1**, 309 (1967).

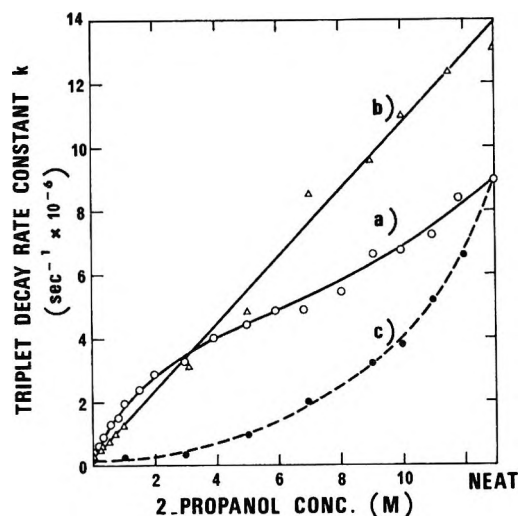


Figure 1. Triplet decay rate constant as a function of the concentration of 2-propanol added to: (a) acetophenone in benzene; (b) benzophenone in benzene; and (c) acetophenone in water.

abstraction from 2-propanol. The value of k_a was $3.3 \times 10^5 \text{ sec}^{-1}$ for acetophenone in benzene and $2.3 \times 10^5 \text{ sec}^{-1}$ in water; for benzophenone in benzene, k_a was $2.5 \times 10^5 \text{ sec}^{-1}$. The values of k_a may be slightly affected by a second-order triplet-triplet annihilation decay due to the high triplet concentration required to observe the triplet. In our calculation, k_a was assumed to be independent of $[\text{RH}]$.

The full line curves in Figure 2 show that k_r decreases with increasing alcohol concentration in the case of acetophenone but remains constant in the case of benzophenone. This difference in behavior may be due to variations in energy of the lowest-lying n, π^* and π, π^* triplet states. Lamola¹¹ showed in a phosphorescence study that acetophenone in a nonpolar medium exhibits a π, π^* triplet state situated only slightly above the n, π^* triplet state. In solutions of high alcohol content, the n electrons in the ground state become hydrogen bonded, and the energy of the n, π^* triplet state is raised with respect to the π, π^* triplet state. As the n, π^* triplet becomes more energetic, it assumes more π, π^* character, leading to decreased photochemical reactivity. This effect is expected to occur to a much higher extent in acetophenone than in benzophenone, due to the larger energy gap between the n, π^* and π, π^* triplets in the latter compound.¹² The influence of solvent polarity on the reactivity of acetophenone triplet is particularly evident in the photoreduction in 2-propanol-water solutions as shown by curves c in the Figures 1 and 2. In water solution containing 2 M 2-propanol k_r is only $0.5 \times 10^6 \text{ M}^{-1} \text{ sec}^{-1}$.

It has been postulated that the polar solvent effects may arise from solvation or hydrogen bonding with the ketone triplet.² The fact that the triplet reactivity of benzophenone is not altered in alcoholic solvents sug-

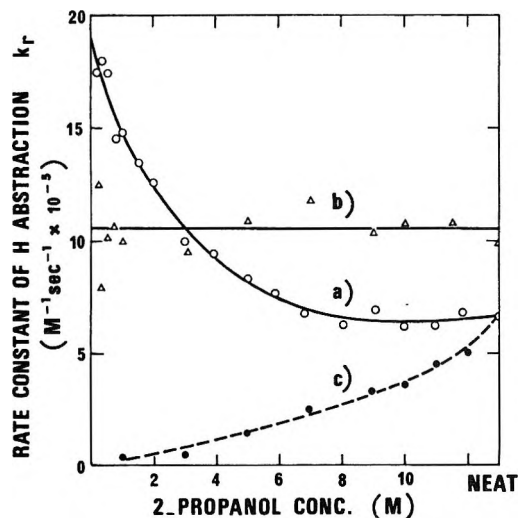


Figure 2. Rate constant of hydrogen abstraction as a function of the concentration of 2-propanol added to: (a) acetophenone in benzene; (b) benzophenone in benzene; and (c) acetophenone in water.

gests that hydrogen bonding does not exist or is very weak in the n, π^* triplet state. The same is, of course, expected to be true for acetophenone. Since the carbonyl oxygen becomes electron deficient in the n, π^* triplet state, the hydrogen-bonding interaction is supposed to be weak.

The values of the rate constants for hydrogen abstraction obtained by nanosecond laser photolysis may be compared with results from indirect measurements. For benzophenone, our value for k_r agrees reasonably well with the results of Beckett and Porter¹³ ($1.28 \times 10^6 \text{ M}^{-1} \text{ sec}^{-1}$) and those of Yang and Dusenbery¹⁴ ($1.25 \times 10^6 \text{ M}^{-1} \text{ sec}^{-1}$). For acetophenone however, the rate constants for hydrogen abstraction in benzene solutions containing 2 M 2-propanol reported by Yang and Dusenbery¹⁵ ($4.33 \times 10^5 \text{ M}^{-1} \text{ sec}^{-1}$) and Lewis⁸ ($7.5 \times 10^5 \text{ M}^{-1} \text{ sec}^{-1}$) are significantly lower than our value of $1.2 \times 10^6 \text{ M}^{-1} \text{ sec}^{-1}$ at the same alcohol concentration. It may be noted that the indirect methods include solvent effects on all secondary reactions involved in the photoreduction.

We conclude from the present study that a substantial part of the low efficiency of acetophenone photoreduction in polar solvents may be attributed to a decreased reactivity of the acetophenone triplet state. This reduced reactivity is supposed to be due to the higher π, π^* character of the acetophenone triplet in polar solvents.

(11) A. A. Lamola, *J. Chem. Phys.*, **47**, 4810 (1967).

(12) M. Batley and D. R. Kearns, *Chem. Phys. Lett.*, **2**, 423 (1968).

(13) A. Beckett and G. Porter, *Trans. Faraday Soc.*, **59**, 2038 (1963).

(14) N. C. Yang and R. L. Dusenbery, *Mol. Photochem.*, **1**, 159 (1969).

(15) N. C. Yang and R. L. Dusenbery, *J. Amer. Chem. Soc.*, **90**, 5899 (1968).

Photochemistry of Trifluoromethylbenzenes. III.

1,4-Bis(trifluoromethyl)benzene

by David Gray and David Phillips*

Department of Chemistry, The University, Southampton SO9 5NH, England (Received October 8, 1971)

Publication costs borne completely by The Journal of Physical Chemistry

Quantum yields of fluorescence, intersystem crossing to the triplet manifold and valence isomerization have been measured for 1,4-bis(trifluoromethyl)benzene vapor excited at 265.3, 253.7, and 248.2 nm. At the longest wavelength all excited molecules either fluoresce or intersystem cross. Valence isomerization as revealed by formation of the 1,3 isomer becomes important with increase in photon energy, but quantum yields are small, indicating further important decay processes under these conditions.

Introduction

This note is part III of a series of reports on the vapor phase photochemistry of trifluoromethyl substituted benzenes.¹⁻⁴ Parts I and II dealt with (trifluoromethyl)benzene¹ and 1,3-bis(trifluoromethyl)benzene.² We report here quantum yields of fluorescence, intersystem crossing and isomerization of 1,4-bis(trifluoromethyl)benzene.³

Experimental Section

Full details have been given in earlier reports.¹⁻³

Materials

1,4-Bis(trifluoromethyl)benzene was obtained from the Pierce Chemical Co. Inc. Gas-liquid chromatography on a β,β' -dipropionitrile column showed it to be better than 99.99% pure.

Results and Discussion

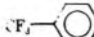
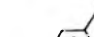

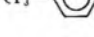
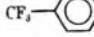
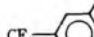



Absolute values of the quantum yield of fluorescence from 1,4-bis(trifluoromethyl)benzene excited at 265.3, 253.7, and 248.2 nm are shown in Figure 1, together with values before correction for the effect of the geometry of the fluorescence cell.⁴ Corrections were based upon extinction coefficients given by Berlman at the various wavelengths.⁵ It can be seen that the various trends with pressure resemble those for other members of this series of compounds, but in this case no study of the effect of added chemically inert gases has been carried out, and thus rate constants and cross-sections for vibrational relaxation processes are not given. Fluorescence yields extrapolated to zero pressure are shown in Table I to be similar to those obtained for the other CF₃ substituted benzenes.^{1,2} The radiative lifetime (τ_0) of 1,4-bis(trifluoromethyl)benzene has been given as 100 nsec based on measurement of the area under the absorption spectrum,⁵ which is rather shorter than those calculated for the 1,3 and monosubstituted derivatives of 239 and 198 nsec, respectively. This is in line with results on the fluorobenzenes⁶ for which the radiative

lifetimes of molecules belonging to the C_{2v} group were calculated to be longer than those from the D_{2h} group. However, it should be noted that for the fluorobenzenes values of τ_0 obtained from integrated absorption spectra are in serious disagreement with those obtained experimentally,⁷ and it would thus be advisable to measure fluorescence decay times for the CF₃ substituted benzenes in order to provide a better comparison. Berlman has given a decay time for 1,4-bis(trifluoromethyl)benzene in solution of 6.7 nsec,⁵ which combined with a fluorescence quantum yield measurement of 0.16⁵ indicates that the true radiative lifetime is 42 nsec.

Figure 2 shows the yield of phosphorescence from biacetyl sensitized by 1,4-bis(trifluoromethyl)benzene vapor at 25°. Quantum yields of intersystem crossing based on these values are given in Table I. It can be seen that as for other CF₃-substituted benzenes, fluorescence and intersystem crossing to the triplet manifold accounts for all of the molecules photoexcited at the longest wavelength used in the study, but at shorter wavelengths other processes become increasingly important. It was evident that photoisomerization may be important in such compounds since valence bond isomers of hexabis(trifluoromethyl)- and hexabis(pentafluoroethyl)benzenes have been reported to be formed upon photolysis of these compounds in solution.⁸ Furthermore it has been shown that the formation of the so-called benzvalene intermediate from the singlet manifold of a 1,4-disubstituted benzene can give

- (1) D. Gray and D. Phillips, Part I, *J. Chem. Phys.*, **55**, 5753 (1971).
- (2) D. Gray and D. Phillips, Part II, *J. Chem. Phys.*, in press.
- (3) D. Gray Ph.D. thesis, University of Southampton, 1970.
- (4) D. Phillips, D. Gray, and K. Al-Ani, *J. Chem. Soc. A*, 905 (1970).
- (5) I. Berlman, "Handbook of Fluorescence Spectra of Aromatic Molecules," Academic Press, New York, N. Y., 1965.
- (6) D. Phillips, *Chem. Soc., Spec. Publ., Photochem.*, **2**, 168, (1971).
- (7) E. K. C. Lee (private communication).
- (8) M. G. Barlow, R. N. Haszeldine, and R. Hubbard, *Chem. Commun.*, 202 (1969).

Table I: Quantum Yields of Photoprocesses in CF₃ Substituted Benzenes at 25°, Vapor Phase

Compound	Reference	Wavelength, nm	Φ_F^a	Φ_{ISC}^b	$\Phi_{1,3}^c$	Φ_{BV}^d	(1 - $\Sigma\Phi$) average
	1	265.3	0.20	(a) 0.73 (b) 0.75	0.07
	2	265.3	0.15	(a) 0.83 (b) 0.82	0.02
	This work	265.3	0.16	(a) 0.90	0	0	0
	1	253.7	0.08	(a) 0.41 (b) 0.41	0.51
	2	253.7	0.11	(a) 0.67 (b) 0.55	0.28
	This work	253.7	0.10	(a) 0.63	0.016	0.048	0.22
	1	248.2	0.04	(a) 0.14 (b) 0.19	0.80
	2	248.2	0.07	(a) 0.44 (b) 0.36	0.53
	This work	248.2	0.06	(a) 0.35	0.023	0.070	0.52

^a Φ_F = quantum yield of fluorescence, extrapolated to zero pressure. ^b Φ_{ISC} = quantum yield of intersystem crossing determined (a) by method of sensitization of phosphorescence of biacetyl and (b) by method of sensitization of cis-trans isomerization of but-2-ene. ^c $\Phi_{1,3}$ = quantum yields of formation of 1,3 isomer (from 1,4 only). ^d Φ_{BV} = estimated quantum yield of "benzvalene" intermediate.

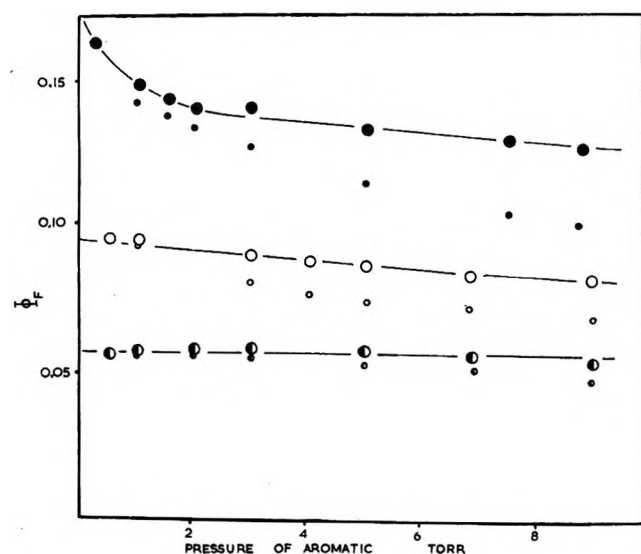
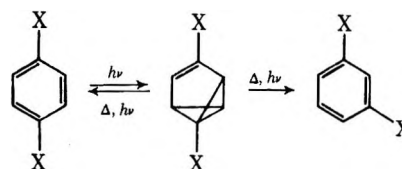


Figure 1. Quantum yield of fluorescence (Φ_F) of 1,4-bis(trifluoromethyl)benzene as a function of aromatic pressure. Key: Filled circles, 265.3 nm excitation; open circles, 253.7 nm excitation; half-circles, 248.2 nm excitation. Small points results before correction for geometry of viewing system.

rise to a 1,3 product isomer upon subsequent rearomatization of the benzvalene intermediate.^{9,10} Quantum yields of formation of the 1,3 isomer from the 1,4 upon excitation at 253.7 and 248.2 nm are given in Table I. It can be shown that provided all possible benzvalene



isomers are formed with equal probability, and that all such isomers revert quantitatively to the aromatic with

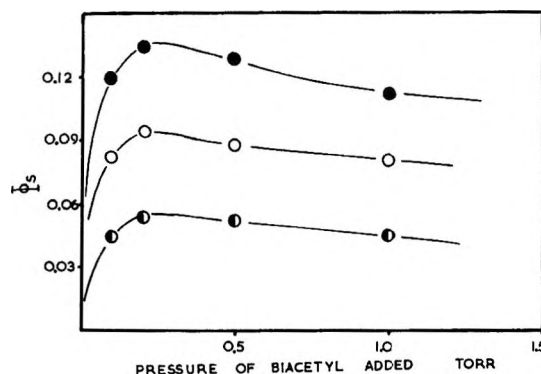


Figure 2. Quantum yield of emission of biacetyl sensitized by 2 Torr 1,4-bis(trifluoromethyl)benzene (Φ_a) as function of biacetyl pressure at 25°. Key: Filled circles, 265.3 nm excitation; open circles, 253.7 nm excitation; half-circles, 248.2 nm excitation.

(9) K. E. Wilzbach and L. Kaplan, *J. Amer. Chem. Soc.*, **86**, 2307 (1964).

(10) L. Kaplan, W. E. Wilzbach, W. G. Brown, and S. S. Young, *J. Amer. Chem. Soc.*, **87**, 675 (1965).

no preferred mode of bond breaking, then the total quantum yield of benzvalene formation will be three times that of the 1,3 isomer formation. These values are also shown in Table I from which it will be seen that benzvalene formation does not make up the deficit of molecules not undergoing fluorescence or intersystem crossing. It is evident, therefore, that if isomerization is playing a role in the deactivation of the excited singlet state of this compound, as has been suggested,¹¹ it

is the precursor of the benzvalene which provides the principal route to the ground state aromatic. This step can equally well be considered as a normal process of internal conversion.

(11) D. Phillips, J. Lemaire, C. S. Burton, and W. A. Noyes, Jr., "Advances in Photochemistry," Vol. 5, W. A. Noyes, Jr., J. N. Pitts, Jr., and G. Hammond, Ed., Wiley-Interscience, New York, N. Y., 1968, p 329.

A Mechanism to Explain the CH Emission at 4330 Å in Oxygen Atom-Acetylene Systems

by K. A. Quickert*

Institut für Physikalische Chemie der Universität Göttingen, 34 Göttingen, West Germany (Received July 22, 1971)

Publication costs assisted by the Institut für Physikalische Chemie der Universität Göttingen

A mechanism to account for the CH(²Δ) formation in oxygen atom-acetylene systems is proposed. The reaction leading to CH(²Δ) can be written, CH₂* + CH₂* → CH(²Δ) + CH₂, where CH₂* is formed in the initial step of the reaction and has an excitation energy of at least 30.5 kcal/mol. Recent results on the dependence of the emission intensity on a number of experimental parameters are shown to be consistent with the proposed mechanism.

Introduction

The chemiluminescence present in the room temperature reaction of oxygen atoms with acetylene has received considerable attention.¹⁻⁷ The most intense emission is in the blue part of the visible spectrum (4330 Å) and results from the CH ²Δ-²Π transition. Weaker emissions from CH(²Σ-²Π), C₂, OH, and CO are also observed.

Most workers have concentrated on the intense CH emission, often for the purpose of finding the mechanism of CH(²Δ) formation. These studies have provided a considerable amount of information on the dependence of the emission on a number of experimental parameters.^{1,5,7} No satisfactory mechanism has been found,^{1,5} however, even though extensive kinetic studies of the O + C₂H₂ reaction have also been carried out.⁸⁻¹¹

Until now, a number of reactions have been proposed to account for the CH(²Δ) formation in the O + C₂H₂ system, including among others, C₂H + O → CH + CO and C₂ + OH → CH + CO. The first reaction has received support from work on acetylene oxidation in shock waves¹² while the second is suggested mainly by acetylene flame work.^{13,14} It is possible

that these reactions account for the strong CH emission in these systems, but it is unlikely that they contribute significantly in the room temperature system.

* Address correspondence to the author at Chemistry Division, Environmental Health Center, Tunney's Pasture, Ottawa, K1A 0H3, Canada.

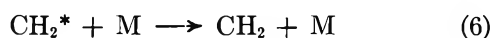
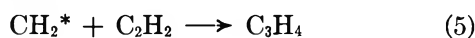
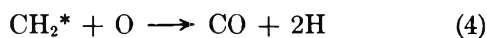
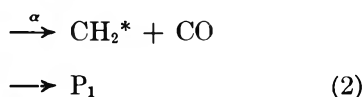
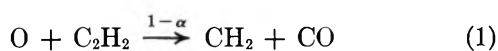
- (1) C. A. Arrington, W. Brennen, G. P. Glass, J. V. Michael, and H. Niki, *J. Chem. Phys.*, **43**, 1489 (1965).
- (2) A. Fontijn, W. J. Miller, and J. M. Hogan, Tenth Symposium (International) on Combustion, The Combustion Institute, 1965, p 545.
- (3) S. L. N. G. Krishnamachari and H. P. Broida, *J. Chem. Phys.*, **34**, 1709 (1961).
- (4) K. D. Bayes and R. E. W. Jansson, *Proc. Roy. Soc., Ser. A*, **282**, 275 (1964).
- (5) M. A. H. El-Dessouky, Ph.D. Thesis, Göttingen, 1970.
- (6) K. H. Becker and K. D. Bayes, *J. Chem. Phys.*, **48**, 653 (1968).
- (7) W. Brennen and T. Carrington, *ibid.*, **46**, 7 (1967).
- (8) A. A. Westenberg and N. de Haas, *J. Phys. Chem.*, **73**, 1181 (1969).
- (9) J. N. Bradley and R. S. Tse, *Trans. Faraday Soc.*, **65**, 2685 (1969).
- (10) K. Hoyermann, H. Gg. Wagner, and J. Wolfrum, *Z. Phys. Chem. (Frankfurt am Main)*, **63**, 193 (1969).
- (11) D. G. Williamson and K. D. Bayes, *J. Phys. Chem.*, **73**, 1232 (1969).
- (12) G. P. Glass, G. B. Kistiakowsky, J. V. Michael, and H. Niki, *J. Chem. Phys.*, **42**, 608 (1965).

This is shown by the analyses of Arrington, *et al.*,¹ and El-Dessouky,⁵ who have carried out detailed investigations of the CH emission.

The present paper proposes a mechanism for the CH(²Δ) formation in room temperature O + C₂H₂ systems, which is based on an electronically excited CH₂ radical. It is shown that the predicted dependence of the emission intensity on the O, C₂H₂, and O₂ concentrations agrees with that found experimentally. Also discussed are the temperature and pressure dependence of the intensity, as well as the magnitude of the absolute intensity.

Proposed Mechanism

The mechanism to account for the formation of CH(²Δ) (hereafter designated as CH*) can be written



The parameters α and β give the fraction of reactions 1 and 3 respectively, which lead to the products of interest (the magnitudes of α and β are discussed below). P₁ refers to other possible products of O + C₂H₂, namely HC₂O + H and C₂O + H₂. There is evidence that reaction 2 occurs to some extent,^{6,11} but it is assumed in this discussion that the contribution of (2) is small with respect to (1). This is based on the kinetic studies of low temperature O + C₂H₂ flow systems⁸⁻¹⁰ in which the formation of CH₂ can best explain the observed concentration profiles. The formation of C₃H₄¹⁰ in the system, as well as recent "crossed jet" experiments¹⁵ strengthen the case for CH₂ as the principal product.

CH₂* is assumed to be an electronically excited CH₂ molecule which lies at least 30.5 kcal/mol above the ground state and hence contains 60% of the exothermicity of reaction 1. The excitation value of CH₂* was obtained by setting the heat of reaction 3 to zero (the formation enthalpy of CH₂ was taken as 89 kcal/mol¹⁷). P₂ refers to other possible products of reaction 3 which do not include CH*. Reactions 4 and 5 are included to account for the removal of CH₂* by the species present in largest concentration, O and C₂H₂; M refers to a third body such as He or other added quenchers.

A steady-state assumption for CH₂* leads to

$$[\text{CH}_2^*] = \frac{\alpha k_1 O A}{k_4 O + k_5 A + k_6 [\text{M}]}$$

where O and A represent [O] and [C₂H₂], respectively. The term $k_3[\text{CH}_2^*]$ has been omitted in the denominator of the above expression since it is assumed small compared to the terms in O and A. The emission intensity, assuming negligible quenching of CH*, is then given by

$$I = \frac{R O^2 A^2}{(r O + A + k_6 [\text{M}]/k_5)^2} \quad (7)$$

where I is the intensity (photons/cm³ sec), $R = \beta \alpha^2 k_3 k_1^2 / k_5^2$ and $r = k_4 / k_5$. That CH* is negligibly quenched in most circumstances can be seen from the results of El-Dessouky,⁵ who found that the intensity was decreased by only about 10% for concentrations of an added quencher, CO₂, which were 10 times larger than the average O or C₂H₂ concentrations.

Experimental Correlation and Discussion

Expression 7 is the primary expression for the emission intensity and will be compared with the experimental work. The experimental data are mainly those of Arrington, *et al.*,¹ and El-Dessouky.⁵ The latter has measured I as a function of time and I integrated over time in a fast flow system for a large number of initial O and C₂H₂ concentrations. The system was held at room temperature and ~3 Torr, and linear flow rates of ~16 m/sec were used with the reagents very dilute in He. Under these conditions, diffusion effects are negligible and plug flow could be assumed.¹⁸

(a) *Pressure Dependence of I.* Both El-Dessouky⁵ and Arrington, *et al.*,¹ have varied the total pressure, by factors of 3 and 9, respectively, and have noted no significant change in the intensity. Expression 7 is essentially pressure independent if $k_6[\text{M}]/k_5$ is small with respect to $rO + A$, say 10% of the latter. This means that $k_5/k_6 > 3 \times 10^2$, since $O \approx A \approx 0.01[\text{M}]$ and $r = 2$ (see below). The magnitudes of k_5 and k_6 are not known, but it is quite possible that the inequality holds. Arrington, *et al.*,¹ have concluded that their pressure dependence of I makes it unlikely that the precursor to CH* is vibrationally excited (unless it is

(13) A. G. Gaydon, "The Spectroscopy of Flames," Chapman and Hall, London, 1957.

(14) E. M. Bulewicz, P. J. Padely, and R. E. Smith, *Proc. Roy. Soc., Ser. A*, **315**, 129 (1970).

(15) M. Gehring, K. Hoyermann, H. Gg. Wagner, and J. Wolfrum, (unpublished results). The initial products of the O + C₂H₂ reaction were determined using the apparatus described in ref 16. It was found that the mass peaks 28 and 14, corresponding to CO and CH₂, respectively, were the only ones to increase significantly with reaction.

(16) M. Gehring, K. Hoyermann, H. Gg. Wagner, and J. Wolfrum, *Z. Naturforsch. A*, **25**, 675 (1970).

(17) F. Zabel, Ph.D. Thesis, Göttingen, 1970.

(18) K. Hoyermann and H. Gg. Wagner, "Physical Chemistry, An Advanced Treatise," Vol. 6, W. Jost, Ed., Academic Press, New York, N. Y. (to be published).

diatomic). Electronic excitation often requires more collisions for deactivation, however, and hence this possibility cannot be eliminated. For the subsequent arguments it is assumed that the term in $[M]$ can be neglected, when M is an inert gas.

(b) *Concentration Dependence of I .* In order to compare expression 7 with the experimental results the value of r must be known; a knowledge of R is not needed since only relative intensities are generally measured. For the comparison given below it is assumed that $r = 2$. This value leads to good agreement between expression 7 and experiment, and is also not unreasonable in light of the fact that values of r of 2.6 ± 0.3^9 and 2.7 ± 1^{19} have been determined for ground state CH_2 . That CH_2 and CH_2^* react at different rates is to be expected, but the relative reaction rates of these molecules with O and C_2H_2 could still be similar. Expression 7 then takes on the simple form

$$I = RO^2A^2/(2O + A)^2 \quad (8)$$

(1) *Instantaneous Intensity.* It has been established^{1,5} that for the C_2H_2 concentration large and constant, the intensity of emission at time t varies as the square of the O atom concentration, i.e., $I(t) \simeq O^2(t)$ for A_0 large. For O_0 large and constant, it was found in a number of experiments⁵ that $I(t) \simeq A^2(t)$. This disagrees with ref 1 in which an $A^3(t)$ dependence was found. The $A^2(t)$ dependence is to be preferred, however, since in ref 1 a value of O_0/A_0 of only 3 was used (compared to ~ 5 in ref 5). Since the stoichiometry is two O to one C_2H_2 under these conditions,⁸⁻¹⁰ it can be shown that O was not constant but decreased by $\sim 35\%$ for the reaction time shown in Figure 2 of ref 1. Taking this into account results in an acetylene dependence of about 2 for the intensity.

An examination of expression 8 shows that $I(t) \simeq O^2(t)$ for A_0 large and constant and that $I(t) \simeq A^2(t)$ for O_0 large and constant. Hence expression 8 agrees with experiment for these two limiting cases.

Expression 8 can also be written explicitly as a function of time, applicable for any A_0 or O_0 . The stoichiometry of the overall reaction⁸⁻¹⁰ leads to the expressions for O and A

$$O = D/(2V \exp(Dk_1t) - 1)$$

$$A = (D + O)/2$$

where $D = 2A_0 - O_0$ and $V = A_0/O_0$. Substituting into (8) gives

$$I(t) = RD^2(3 + 2V \exp(Dk_1t) - 2V^{-1} \exp(-Dk_1t))^{-2} \quad D \neq 0 \quad (9a)$$

$$= 0.16RA_0^2(1 + 2k_1A_0t)^{-2} \quad D = 0 \quad (9b)$$

It is possible to test expression 9 by comparing it with some intensity profiles measured by El-Des-

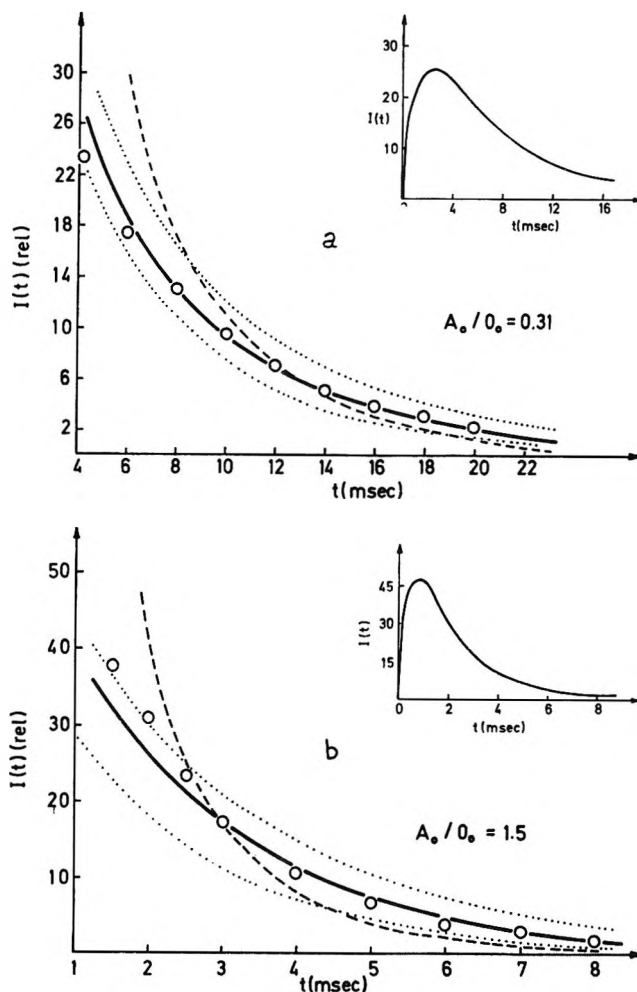


Figure 1. Comparison of the experimental intensity-time curve with those calculated theoretically. The circles represent the experimental points (ref 5), the solid curve was calculated using (9a), the upper dotted curve using (9a) and $Dk_1 - 15\%$, the lower dotted curve using (9a) and $Dk_1 + 15\%$, and the dashed curve using $I(t) \sim O^2(t)A^2(t)$. The inset shows the entire $I(t)$ vs. t curve.

souky.⁵ Figures 1a and 1b show two such comparisons, one on each side of the stoichiometric mixture (all intensities are relative). The solid line was obtained using expression (9a) and the circles represent the experimental points. The upper and lower dotted lines were calculated from (9a) but using a change in value of Dk_1 of -15% and $+15\%$, respectively; the $\pm 15\%$ error in Dk_1 includes errors in the concentrations and in the temperature of the system; k_1 was taken at $7.3 \times 10^{10} \text{ cm}^3/(\text{mol sec})$ and is the room temperature value given by ref 10. The dashed line is included to show the intensity profile for the case that $I(t) \simeq O^2(t)A^2(t)$. The inset shows the complete $I(t)$ vs. t curve and indicates that the measured curve first passes through a maximum, which is probably caused by initial mixing effects.

(19) J. M. Brown and B. A. Thrush, *Trans. Faraday Soc.*, **63**, 630 (1967).

It can be seen from Figure 1a and 1b that there is good agreement between the solid lines and the experimental points. The dashed line is too steep in each case and indicates that a pure $O^2(t)A^2(t)$ dependence is not correct. This shows the validity of expressions 9a and 8.

(2) *Integrated Intensity.* The integrated intensity I_g , $I_g = \int_0^\infty I(t)dt$, has also been measured.⁵ Integration of expressions 9a and 9b gives

$$I_g = \frac{RD}{25k_1} \left(0.6 \ln \frac{2V+4}{2V-1} + \frac{1}{2V-1} - \frac{2}{V+2} \right) \quad D > 0 \quad (10a)$$

$$= \frac{RD}{25k_1} \left(0.6 \ln \frac{V+2}{2-4V} + \frac{2V}{2V-1} + \frac{V}{V+2} \right) \quad D < 0 \quad (10b)$$

$$= 0.08RA_0/k_1 \quad D = 0 \quad (10c)$$

and allows a comparison with experimental findings. It has been found⁵ that $I_g \simeq O_0^2$ for A_0 large and constant, and $I_g \sim A_0^2$ for O_0 large and constant. Expressions 10a and 10b predict the same behavior. For V large, the log term in 10a can be expanded and it is found that $I_g \sim O_0^2/A_0$; similarly for V small, (10b) gives $I_g \sim A_0^2/O_0$. This agreement with experiment supports the conclusions reached in Section 1 above.

The validity of expression 10 can also be tested for the case when neither O nor A is in excess. Experimentally it is found that the ratio I_g/I_g^s has its maximum value at the stoichiometric point^{1,5} (I_g^s is the integrated intensity for the stoichiometric composition $D = 0$). Figure 2 shows a plot of I_g/I_g^s against $1/V$ using data obtained by El-Dessouky.⁵ The circles represent the experimental points and the curves were obtained by calculation. Curve 2 was obtained using expression 10 ($r = 2$), while 1 and 3 were calculated from analogous expressions in which r was taken as 1 and 3, respectively. It can be seen that experiment and theory agree quite well for the case $r = 2$, and it is for this reason that the value $r = 2$ was originally chosen. For r greater, the maximum deviates noticeably from the stoichiometric mixture and for r smaller, the agreement also becomes poorer.

The above analysis shows that expression 8 can adequately explain the O and A dependence of the intensity, measured either at time t or integrated over time. This functional form is further supported by the effect on the intensity of added O_2 .

(3) *Effect of Added O_2 .* The effect of O_2 as a quencher in the system has been studied by a number of workers.^{2,3,5,7} El-Dessouky⁵ and Brennen and Carington⁷ have obtained straight Stern-Volmer plots for not too large O_2 concentrations, but in each case it was observed that the calculated cross-section changed with O_0 and was very large. It was concluded that O_2 decreased the intensity by reacting with rad-

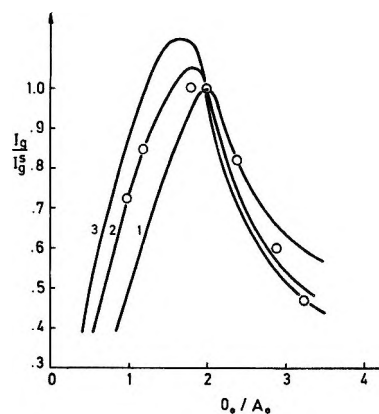


Figure 2. The integrated intensity ratio I_g/I_g^s (see text) plotted as a function of O_0/A_0 . Curves 1, 2, and 3 were calculated for values of the parameter r of 1, 2, and 3, respectively, and the experimental points are from ref 5.

ical precursors of CH^* . In one set of experiments⁵ ($A_0 = 9.75 \times 10^{14}$ molecules/cm³, $O_0 = 4 \times 10^{14}$ atoms/cm³), an addition of O_2 up to 10^{16} molecules/cm³ caused the integrated intensity to decrease by a factor of 7. The actual CH^* quenching by O_2 is expected to be small under these conditions since the addition of CO_2 in equal amounts⁵ decreased the intensity by only 30%.

According to the proposed mechanism one expects the following behavior. Since O_2 can react with CH_2^* , expression 7 becomes

$$I = CO^2A^2/(v(2O + A) + [O_2])^2 \quad (11)$$

where C is a constant, $v = k_6/k_{O_2}$, and k_{O_2} is the rate constant for $O_2 + CH_2^*$. It can be shown through calculation that $I(t=0) \simeq I_g$ for expression 11 when O_0 and A_0 are constant. By differentiating 11, one then obtains

$$d \ln(1/I_g) = 2d \ln (v(2O_0 + A_0) + [O_2]_0) \quad (12)$$

and hence a log-log plot as indicated by (12) should yield a straight line of slope 2 for the correct value of the parameter v . Figure 3 shows such a plot (using the data from ref 5) for v equals 2 and 3. It can be seen that a straight line with slope 2 results for $v = 3$, verifying expression 11. A value of 3 for v means that O removes CH_2^* six times faster than O_2 from the system.

(c) *Temperature Dependence of the Intensity.* Arrington, *et al.*,¹ have shown that the emission intensity is not strongly dependent on temperature, and have concluded that the activation energy for emission, E_a , should not be greater than one kcal/mol. According to the proposed mechanism the temperature dependence of the integrated intensity is given by $R/k_1 = k_3k_1/k_5^2$ (α and β are not expected to depend strongly on temperature). The activation energy for k_1 is close to 3 kcal/mol^{8,10} and hence for experiment and theory to agree, $2 < (2E_5 - E_3) < 3$, where E_3 and E_5 are the

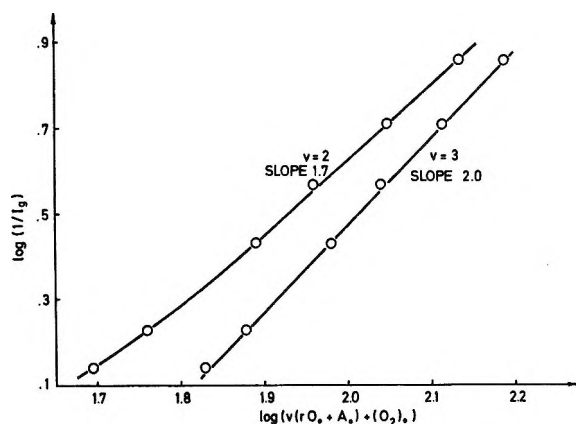


Figure 3. The effect of added O_2 on the intensity. Expression 12 is plotted using the results of ref 5.

activation energies of k_3 and k_5 , respectively, and $0 < E_6 < 1$. The values of E_5 and E_3 are not known, but if one assumes that $E_3 \approx 0$, *i.e.*, k_3 fast, then $E_5 \approx 1.3$. This is not an unreasonable value, which would indicate that the proposed mechanism is probably not inconsistent with the experimental results.

(d) *Absolute Emission Intensity.* An attempt should also be made to determine whether the absolute intensity predicted by the proposed mechanism is at all comparable to the intensity measured experimentally. Arrington, *et al.*,¹ have measured the absolute emission intensity and have shown that about one C_2H_2 in every 10^3 – 10^4 which reacts leads to CH^* . For a comparison with the experimental data,¹ an expression can be derived from 8, *i.e.*

$$\frac{I}{k_1 \bar{O} \bar{A}} = \frac{R}{k_1} \frac{\bar{O} \bar{A}}{(2\bar{O} + \bar{A})^2}$$

where \bar{O} and \bar{A} are average concentrations. This yields $\alpha^2 \beta k_3 k_1 / k_5^2 \approx 10^{-2}$. The ratio $k_3 k_1 / k_5^2$ was shown in (c) to be nearly temperature independent, and the assumption that the rate constants have similar frequency factors gives $k_3 k_1 / k_5^2 \approx 1$. Conjugate values of the constants α and β can then be calculated from $\alpha^2 \beta \approx 10^{-2}$: α ; 0.10, 0.14, 0.20; β , 1.0, 0.5, 0.25. This order of magnitude calculation indicates that $\sim 15\%$ of reaction 1 must give CH_2^* in order that the mechanism agree with experiment (if β is chosen not too small).

The experimental work of Poss²⁰ can be used to judge whether an α of $\sim 15\%$ is reasonable, or even possible. Poss²⁰ has measured the infrared chemiluminescence of CO in the $O + C_2H_2$ system and his results are consistent with vibrationally excited CO being produced by $O + C_2H_2$ and $O + CH_2$. The latter reaction produces vibrational excitation up to $v = 12$ and if CH_2^* is present in the system, an excitation up to $v = 18$ could be expected. The fact that the populations in the levels 18 and 12 are found²⁰ to be in the ratio 0.09/1 can be taken as evidence that CH_2^* could be present

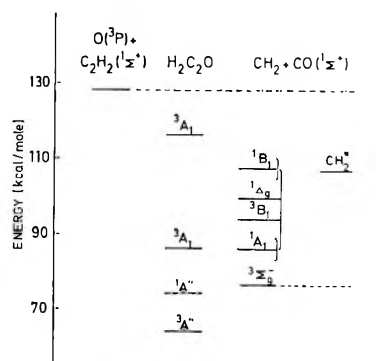


Figure 4. Energy levels in the $O + C_2H_2$ system.

and in concentrations sufficient for CH^* production, as discussed above. Thrush, *et al.*,²¹ have also mentioned the possibility of excited CH_2 in this system, although they favor other reactions, *i.e.*, $O + CH$, to account for the higher vibrational excitations of CO.

The question of which state of CH_2 is represented by CH_2^* is of interest and some clues may come from Figure 4, in which the energy levels of the various species in the system are depicted (relative to ground state ketene). The states of ketene were taken from those calculated from Dixon and Kirby,²² and although the exact energy of the levels is probably different there is little doubt that a number of triplet states exist below the $O + C_2H_2$ level. The CH_2 levels were taken from Herzberg.²³ The spread in the 1A_1 and 1B_1 levels reflects the uncertainty in the separation of the lowest singlet and triplet states of CH_2 .^{23,24} The positions of the $^1\Delta_g$ and 3B_1 states are uncertain, but they probably lie within the ranges shown.²⁵ A number of other states of CH_2 , both singlet and triplet, lie above those shown but their energies are generally unknown.²³

If the spin conservation rule holds in the reaction, one would expect triplet ketene as an intermediate (at high pressures, ground state ketene can be isolated^{26,27}). There is no reason to expect that all of the triplet ketene formed should be in the lowest $^3A_1'$ state, and some fraction could indeed be in the higher 3A_1 states. The rapid ketene decomposition from the higher states could then yield excited states of CH_2 , above the triplet ground state. For the states shown in Figure 4 only the 3B_1 state is a possibility for CH_2^* . If spin conservation does not hold in the reaction, then a number of the higher CH_2 singlet states are also possible.

(20) R. Poss, Ph.D. Thesis, Göttingen, 1971.

(21) P. N. Clough, S. E. Schwartz, and B. A. Thrush, *Proc. Roy. Soc., Ser. A*, **317**, 575 (1970).

(22) R. N. Dixon and G. H. Kirby, *Trans. Faraday Soc.*, **62**, 1406 (1966).

(23) G. Herzberg and J. W. C. Jones, *Proc. Roy. Soc., Ser. A*, **295**, 107 (1966).

(24) G. Duxburg, *J. Mol. Spectrosc.*, **25**, 1 (1968).

(25) P. C. H. Jordan and H. C. Longuet-Higgins, *Mol. Phys.*, **5**, 121 (1962).

(26) K. G. Seifert, thesis, Göttingen, 1969.

(27) K. Glaenger, thesis, Göttingen, 1971.

CH₂* can be singlet or triplet and yield two doublets in reaction 3.

(e) *Additional Considerations.* Another argument in favor of the proposed mechanism is that in the room temperature reaction of atomic oxygen with simple hydrocarbons, only O + C₂H₂ exhibits intense CH chemiluminescence. The reaction of O with CH₄, C₂H₄, C₂H₆, and C₃H₆ shows little or no chemiluminescence (it is about 3 orders of magnitude less with C₂H₄ compared to C₂H₂²), while the chemiluminescence in O + C₃H₄ (propyne) can be satisfactorily explained through the C₂H₂ formed.⁵ It is perhaps not insignificant then, that only in O + C₂H₂ can CH₂* be formed in the first step.

The reaction OH + C₂H₂ is also of interest since it is now known to give CH₃ + CO initially.¹⁶ No chemiluminescence was observed for this system,⁴ and according to the proposed mechanism one does not expect any formation of CH*. Other suggested mechanisms leading to CH* might be expected to take place in this system as readily as in O + C₂H₂, e.g., OH + C₂, especially since the reaction OH + C₂H₂ is more exothermic than O + C₂H₂.

Acknowledgments. The author wishes to thank the National Research Council of Canada for the award of a Post-doctoral Fellowship, and Professor H. Gg. Wagner for his interest and support for this work.

Electroanalytical Measurements of Flash-Photolyzed Ferrioxalate

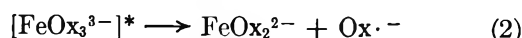
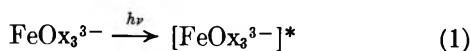
by R. A. Jamieson and S. P. Perone*

Department of Chemistry, Purdue University, Lafayette, Indiana 47907 (Received May 21, 1971)

Publication costs assisted by the U. S. Public Health Service

Electrochemical measurement techniques have been applied to the study of secondary photolytic processes in flash-irradiated ferrioxalate solutions. A current-voltage profile obtained immediately after irradiation qualitatively described the presence of a photolytic intermediate. The disappearance of this intermediate and product formation were followed using time-delay potentiostatic electrolysis. Comparison of time-delay kinetic data and digitally simulated data suggested a consecutive reaction scheme with a first-order process followed by a second-order process. The mechanism suggested envisions the absorption of light to cause a homolytic cleavage in the carbon-carbon bond of the oxalate ligand forming two radical ligands attached to a ferric dioxalate molecule. This oxidizable intermediate (A) is in rapid equilibrium with another intermediate (B) which is not oxidizable. The final step in the proposed mechanism is a mixed second-order reaction between A or B and ferrioxalate forming the product ferrous oxalate.

Detailed investigation of the photochemical activity of aqueous ferrioxalate solution was first carried out by Allmand and coworkers.¹⁻³ More recently, Parker⁴⁻⁶ and others⁷ have explored the ferrioxalate system for use as a sensitive chemical actinometer. The mechanism originally postulated for ferrioxalate photoreduction in solution involved the initial excitation followed by dissociation to give a ferrous oxalate molecule and oxalate radical anion. The oxalate radical would then react with another ferrioxalate ion.⁵ This scheme is shown below.



In 1959, Parker and Hatchard⁸ applied flash photol-

ysis with spectroscopic monitoring to the ferrioxalate system. They intended to measure the rate constant for the second-order reaction (eq 3) in the above scheme. The formation of Fe(II) in eq 2 was expected to give an instantaneous fall in absorbance of ferrioxalate followed by a slow fall in absorbance due to loss of Fe(III) in eq 3. These qualitative effects were observed at 313 nm and 366 nm, but the effect of concentration on the slow

- (1) A. J. Allmand and W. W. Webb, *J. Chem. Soc.*, 1518 (1929).
- (2) A. J. Allmand and W. W. Webb, *ibid.*, 1531 (1929).
- (3) A. J. Allmand and K. W. Young, *ibid.*, 3079 (1931).
- (4) C. A. Parker, *Proc. Roy. Soc., Ser. A*, 220, 104 (1953).
- (5) C. A. Parker, *Trans. Faraday Soc.*, 50, 1213 (1954).
- (6) C. G. Hatchard and C. A. Parker, *Proc. Roy. Soc., Ser. A*, 235, 518 (1956).
- (7) J. Lee and H. H. Seliger, *J. Chem. Phys.*, 40, 519 (1964).
- (8) C. A. Parker and C. G. Hatchard, *J. Phys. Chem.*, 63, 22 (1959).

reaction indicated that it was a first-order reaction rather than a second-order reaction. At long wavelengths, 405 nm and 436 nm, an intermediate was observed by a rise in absorbance on flashing. This indicated that the intermediate had an absorptivity larger than ferrioxalate.

With these observations, Parker and Hatchard⁸ proposed two intermediates, either of which would satisfy first-order kinetics with a predicted absorptivity larger than ferrioxalate. One of the proposed intermediates was a ferrous oxalate-oxalate radical while the other alternative was a ferrioxalate-oxalate radical. Parker and Hatchard also suggested the possibility of a direct reaction between a ferrous oxalate-oxalate radical and a ferrioxalate ion giving an intermediate dimer, the dissociation of which would give first-order kinetics. In all possibilities the reaction between oxalate radical (or possibly ferrous oxalate-oxalate radical) and ferrioxalate ion was assumed to be very fast compared to the first-order step.

Several other previous publications have considered various aspects of ferrioxalate photolysis in solution. Holden⁹ and Parker⁵ observed effects of oxalate concentration on quantum yield. Riggs¹⁰ attempted to relate observed temperature effects on quantum yield to the photolysis mechanism. The fractional primary quantum yield has been explained by rapid internal degradation of the excited state¹¹ and by the inefficiency of intersystem crossing.¹² Direct observation of radical intermediates (in frozen solution) has been reported.^{13,14} Taube¹⁵ has suggested that the reactive intermediate is $\text{CO}_2\cdot^-$ generated from the rapid dissociation of oxalate radical to give $\text{CO}_2\cdot^- + \text{CO}_2$.

There have been two reports which suggest that the initial step in the reduction of metal oxalate complexes is not the simultaneous formation of reduced metal ion and oxidized ligand (oxalate radical). Boldyrev, *et al.*,¹⁶ have proposed that the initial step in the thermal decomposition of all oxalates is the breaking of the C-C bond yielding two carbon dioxide radical ions. Duke¹⁷ has also suggested the initial step in decomposition of manganese oxalate is the breaking of the C-C bond yielding a diradical intermediate. He assumes that the C-C bond has been weakened by coordination to the metal ion.

Recent reviews^{12,18} and a monograph¹⁹ on photochemistry of coordination compounds appear to indicate an acceptance of Parker and Hatchard's⁸ revised mechanism for ferrioxalate photolysis. However, only Parker and Hatchard⁸ have applied a transient-sensitive technique to this system, and in their report three possible alternatives were suggested. Additional information obtained by an alternative transient-sensitive technique would appear very desirable to complement Parker and Hatchard's work. The information from both methods might then allow specification of a more definitive mechanism.

Previous experience with photoelectrochemistry²⁰⁻²² suggested the application of this technique to this system. Because of the sensitivity to electroactive species, it appeared possible to observe the decay of Fe(III) and gain in Fe(II) associated with either eq 3 of the originally postulated mechanism (second-order reaction), or the first-order process observed by Parker and Hatchard.⁸ In addition, the intermediate complexes proposed by Parker and Hatchard might also be electroactive.

Application of Potentiostatic Analysis to Photochemistry. Berg, *et al.*,²³⁻²⁵ and Perone and coworkers²⁰⁻²² have demonstrated the application of electroanalytical measurements to flash photolysis studies. It appears that the potentiostatic monitoring technique is particularly useful. Both qualitative and quantitative information can be obtained from this technique. The qualitative approach involves continuous measurement of current-time curves at various applied potentials, using one flash for each applied potential. The current at a specific time, t , is measured and plotted for each potential. This results in a point-by-point polarogram (current-voltage profile) which can qualitatively describe the species in solution at that time.

Time-delay analysis, developed by Perone and Birk,²⁰ employs fast electroanalytical sampling of the photolyzed solution at various time delays after the flash. One flash experiment is required for each data point. Electrolysis begins after a time-delay (τ); assuming no electrochemical complications, the concentration of an electroactive species at time τ can be calculated from the Cottrell equation, where the time (t) is measured from the start of electrolysis ($t \ll \tau$), and the potential has been chosen so that the current is diffusion limited.

(9) J. B. Holden, Ph.D. Thesis, Princeton University, 1961.

(10) W. M. Riggs, Ph.D. Thesis, University of Kansas, 1967.

(11) G. B. Porter, J. G. W. Doering, and S. Karanka, *J. Amer. Chem. Soc.*, **84**, 4027 (1962).

(12) E. L. Wehry, *Quart. Rev. Chem. Soc.*, **21**, 213 (1967).

(13) D. J. E. Ingram, W. G. Hodgson, C. A. Parker, and W. T. Rees, *Nature (London)*, **176**, 1227 (1955).

(14) G. A. Shagisultanova, L. N. Neokladnova, and A. L. Poznyak, *Dokl. Akad. Nauk SSSR, Engl. Trans., Phys. Chem. Sect.*, **162**, 491 (1965).

(15) H. Taube, *J. Amer. Chem. Soc.*, **70**, 1216 (1948).

(16) V. V. Boldyrev, I. S. Nev'yantsev, Yu I. Mikhailov, and E. F. Khairtdinov, *Kinet. Katal.*, **11**, 367 (1970).

(17) F. R. Duke, *J. Amer. Chem. Soc.*, **69**, 2885 (1947).

(18) A. W. Adamson, *et al.*, *Chem. Rev.*, **68**, 541 (1968).

(19) V. Balzani and V. Carassiti, "Photochemistry of Coordination Compounds," Academic Press, London, 1970.

(20) S. P. Perone and J. R. Birk, *Anal. Chem.*, **38**, 1589 (1966).

(21) J. R. Birk and S. P. Perone, *ibid.*, **40**, 496 (1968).

(22) H. E. Stapelfeldt and S. P. Perone, *ibid.*, **41**, 628 (1969).

(23) H. Berg and H. Schweiss, *Nature (London)*, **191**, 1270 (1961).

(24) H. Berg, *Z. Anal. Chem.*, **216**, 165 (1966).

(25) H. Berg, H. Schweiss, E. Stutter, and K. Weller, *J. Electroanal. Chem.*, **15**, 415 (1967).

$$C^* = i_d(\pi t^{1/2})/nFAD^{1/2} \quad (4)$$

where C^* is the bulk concentration of the electroactive species at time τ , i_d is the measured current at time, t , t is the electrolysis time, n is the number of electrons involved in the electrode reaction, F is the Faraday constant, A is the electrode area in cm^2 , and D is the diffusion coefficient of the electroactive species. By varying τ for several consecutive flash experiments, the time-dependent behavior of an electroactive species can be followed. Kinetic data and reaction order can then be obtained. The data can be treated by homogeneous kinetic equations.

Experimental Section

The apparatus for photoelectrochemical studies used in this work consists of three basic parts: (1) an external flash system, (2) a solid state potentiostat, and (3) a photolysis cell. A brief discussion of the apparatus is included below. A detailed discussion has been provided by Kirschner and Perone²⁶ and by Jamieson.²⁷

Flash Source, Optics, and Photolysis Cell. A sketch of the optics in the external flash system is shown in Figure 1. The relative distance of the lenses between both mirrors is adjusted for maximum demagnification without significant loss of light. The photolysis cell (Precision Cells, Inc., Hicksville, New York) is made of an optically flat uv quartz bottom (≈ 1 -in. diameter) fused to the Pyrex body.

In each photolysis experiment, either a Suntron 6A or Suntron 221 (Xenon Corp., Medford, Massachusetts) flash lamp was used. Flash energies could be provided in the range of 100–400 J, with a pulse half-width of about 6 μsec . The noise from the discharge of these flash lamps was minimized by isolation of the lamp within a shielded box (see Figure 1). About a $\pm 5\%$ fluctuation in intensity was observed in a series of flashes.

The high voltage power supply circuitry is essentially the same as reported earlier.²⁰ The capacitor bank was discharged through the flash lamp by initiating an external trigger pulse (Model C trigger module, Xenon Corp.).

Potentiostat. The potentiostatic circuitry employed

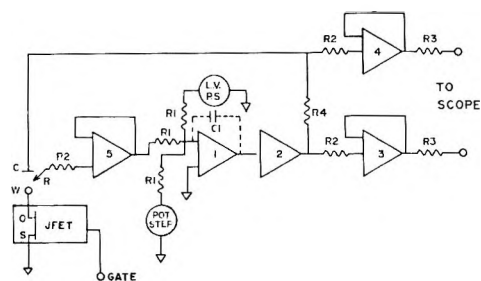


Figure 2. Schematic diagram of the potentiostat. The modules are: (1) controlling voltage adder, (2) current booster, (3, 4, and 5) voltage follower, JFET = low R_{ON} FET analog gate, L.V.P.S. = low voltage power supply, Pot. Step = potential-step unit. The component values are: $R_1 = 1000$ ohms, 1%; $R_2 = 1000$ ohms, 10%; $R_3 = 511$ ohms, 1%; $R_4 = 2000$ ohms, 1%; $C_1 = 82$ pF; C = counter electrode; R = reference electrode; and W = working electrode.

in this work is shown in Figure 2. Amplifiers 1, 3, 4, and 5 are Analog Devices Model 149B (Analog Devices, Cambridge, Mass.) chosen for their wide band pass, fast response, and high common mode rejection ratio. The booster amplifier (2) is an Analog Devices Model B100, which can supply up to 100 mA. The closed-loop unity gain crossover point for the potentiostat-cell system was 500 KHz, and the transient response time constant was 0.3 μsec .²⁸ The output signal is sampled by a Tektronix (Tektronix, Inc., Beaverton, Oregon) Model 536 oscilloscope with types D and T plug-ins and a Polaroid camera attachment.

Measurement Techniques. Data measurement is initiated by the output of a phototransistor, Fairchild FPT-100 (Fairchild Semiconductor, Mountain View, California), which senses the flash.

In the time-delay measurement technique, the working electrode (W_e) is connected to ground through an analog switch (see Figure 2). Prior to the flash, the switch is opened, disconnecting the W_e from ground and preventing electrolysis. The phototransistor output initiates the time-delay circuitry with the flash. After the set time-delay the switch is closed, grounding the W_e , and allowing electrolysis to occur.

A solid-state JFET analog switch, Crystallonics CAG-6 (Crystallonics, Cambridge, Massachusetts) was found to give microsecond switching times without significantly affecting the electrochemical response. The JFET is inserted between the working electrode and ground as shown in Figure 2. When the JFET is gated OFF, the drain-to-source (D-S) resistance is $\approx 10^9$ ohms. When the JFET is gated ON, the maximum (D-S) resistance is 6 ohms. The JFET can

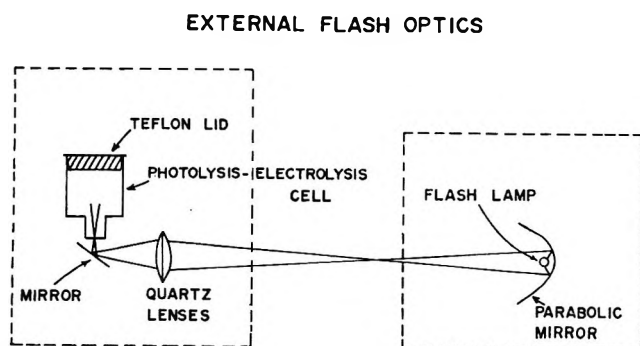


Figure 1. External flash optics.

(26) G. L. Kirschner and S. P. Perone, Symposium on Photochemical Methods, 9th National Meeting of the Society of Applied Spectroscopy, New Orleans, La., Oct 1970; *Anal. Chem.*, in press.

(27) R. A. Jamieson, Ph.D. Thesis, Purdue University, Lafayette, Ind., 1971.

(28) J. E. Mumby, Ph.D. Thesis, Purdue University, Lafayette, Ind., 1970.

change states in 700 nsec. The only observable electronic effect of the switch was the added uncompensated cell resistance. This slowed the overall response, but still allowed a minimum 200- μ sec sampling interval.

Upon initiation of the flash photolysis experiment, either a constant potential or potential-step electrolysis is performed. For constant potential electrolysis, the applied cell potential is held constant before and after the flash. For potential-step experiments, a digital logic device^{26,27} was constructed to provide a variable potential step triggered by the flash. In addition, this device provides for a variable time-delay period after the flash followed by a command pulse to gate the JFET switch closed.

Concentration Measurements of Photolytic Intermediates. The concentration of an intermediate can be estimated from time-delay potentiostatic current measurements by using the Cottrell equation (eq 4) assuming A and D are known. In this work, concentrations of photolytic intermediates have been estimated by comparing the potentiostatic current at a certain time (t) to the potentiostatic current at the same time (t) for a known unphotolyzed ferrioxalate solution. This assumes that the diffusion coefficients of the intermediates and ferrioxalate are similar. However, a more serious source of error must be considered. That is, due to the fact that irradiation of the electrode area is not 100% efficient, one must assume a smaller effective electrode area for current measurements of photolytic species compared to nonflash measurements. If completely parallel light entered the bottom of the photolysis cell, one could assume a 50% exposure of the spherical electrode area to photolyzed solution. However, the light is not parallel, but is focused above the HMDE. Therefore, the exposed electrode area lies somewhere between 50% and 100%. For convenience, it is assumed that 75% is a good estimate of effective electrode area for photolytic species. Thus, current measurements due to photolytic intermediates are corrected by a factor of 1.33 before comparison to the standard for concentration estimation. Birk and Perone²¹ considered several sources of analytical error, including the effects of nonhomogeneity of photolysis over the microelectrode surface as well as the uncertainty in the per cent effective electrode area. They concluded that the latter provided the main source of error for reported kinetic data. The error can be as great as $\pm 25\%$.

Time-Scale of Time-Delay Data. The time-delay measurements reported here represent at least an order of magnitude improvement in accessible time-scale using this technique compared to previous work.²² The time-delay potentiostatic current data are plotted at the value of the time-delay (τ) plus the potentiostatic sampling interval used (200 μ sec). The implicit assumption here is that the current level at the end of

the sampling interval is proportional to the bulk solution concentration at that point in time relative to the flash pulse. This assumption is consistent with the findings of Birk and Perone,²¹ who showed that for a potentiostatic measurement interval shorter than the half-life of the transient electroactive species, the current is directly proportional to the bulk concentration at all times.

Digital Simulation. Digital simulation experiments were performed on a Hewlett-Packard (Hewlett-Packard, Palo Alto, Calif.) 2116A computer equipped with 8K core memory, ASR-35 teletype, and high-speed paper tape reader. A Tektronix type 601 display oscilloscope was used to display the simulated data. Programming was performed using Hewlett-Packard BASIC.

Digital simulation of any given mechanism requires estimates of the initial reactant concentrations and rate constants. The initial concentrations in simulation studies here were estimated from current measurements which were corrected for effective electrode area as discussed earlier. One of two procedures was used to obtain these values. In one method the anodic current at long time ($\tau \simeq 1$ sec) was assumed to represent the final amount of ferrous oxalate generated by irradiation and secondary chemical reactions. From the stoichiometry of the simulated mechanisms, it was possible to represent the initial concentration of reactive intermediates.

The second method was an iterative procedure starting with preliminary simulated data obtained with a rough estimate of initial concentrations as obtained by method one. From the simulated fit to experimental data, a better estimate of the initial concentration is made by using the indicated rate constants and measured concentration values at short times. The procedure can be repeated until a consistent initial concentration is obtained.

Cell and Electrodes. The electrolysis-photolysis cell shown in Figure 1 has a capacity of about 200 ml. Solutions were deaerated for 30 min prior to analysis and between each experiment by oxygen-free nitrogen²⁹ dispersed in both the bottom and top regions of the cell. During each experiment, nitrogen was passed over the solution. Photolyzed solution was removed by a vibrostaltic pump (Chemical Rubber Co., Cleveland, Ohio) connected to a capillary extending to the bottom of the cell. Fresh deaerated solution could be introduced periodically from a reservoir through a hole in the Teflon lid covering the cell.

A hanging mercury drop electrode (HMDE) was used as a monitoring (working) electrode for all stationary electrode experiments. Reproducible drops were obtained by dialing the appropriate drop size with a microburet-type HMDE (Metrohm Ltd., Switzer-

(29) L. Meites, *Anal. Chim. Acta*, **18**, 364 (1958).

land). The electrode area was 2.22 mm². The reference electrode was a saturated calomel electrode with two compartments between the electrode and solution. The compartment closest to the reference electrode was filled with 1 M KCl, while the compartment closest to the solution was filled with the electrolyte of the solution investigated. Each compartment was isolated by a fine porosity sintered glass disk. A Luggin capillary reference probe was positioned as close as possible to the W_e to minimize uncompensated iR drop in the cell.³⁰ The counter electrode was a coiled 2-inch piece of No. 22 gauge platinum wire placed in the bottom portion of the cell at a convenient distance from the working electrode.

Near the completion of this work, the working electrode was placed in a support²⁸ which allowed easy position control along three coordinates. The x and y coordinates were adjusted roughly but the vertical coordinate z could be adjusted with an accuracy of ± 0.001 in. by means of a micrometer dial attached to the support.

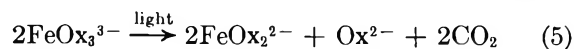
All experiments were carried out at ambient temperatures between 23° and 25°.

Reagents. All solutions were prepared from reagent grade chemicals without further purification. Distilled water was used after further purification by passage over a mixed cation-anion exchange bed (Amberlite MB-3).

Ferrioxalate solutions were prepared by diluting an appropriate amount of stock solution (0.1 M FeNH₄(SO₄)₂ in 0.1 M H₂SO₄) to 1 l., which contained ≈ 74 g of K₂C₂O₄·H₂O.³¹ The pH was adjusted to the desired value by addition of dilute H₂SO₄ or KOH. Except for those experiments investigating pH effects, all data reported here are for ferrioxalate solutions at pH 6.0, 0.4 M oxalate. No thermal decomposition of ferrioxalate was observed for solutions stored in the dark for up to one week.

Results and Discussion

The overall stoichiometry in the photoreduction of ferrioxalate is shown by equation 5. This indicates



that for every ferric ion lost, there is a corresponding gain of one ferrous ion. If a polarogram were recorded on a ferrioxalate solution before and after irradiation (>1 min), one would expect to observe the formation of oxidation current with a corresponding loss of reduction current. An example of this is shown in Figure 3. If, however, a polarogram could be obtained at very short times (<1.0 msec) after irradiation, the profile might be more complex due to the presence of distinct electroactive photolytic intermediates. By applying potentiostatic analysis to the ferrioxalate system simultaneous with flash irradiation, the point-by-point polarogram (current-voltage profile) shown

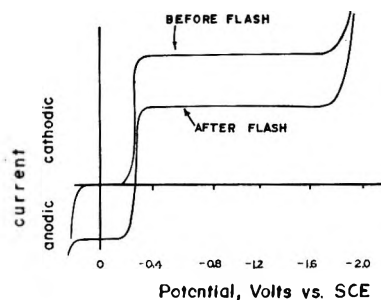


Figure 3. Predicted polarograms before and after irradiation.

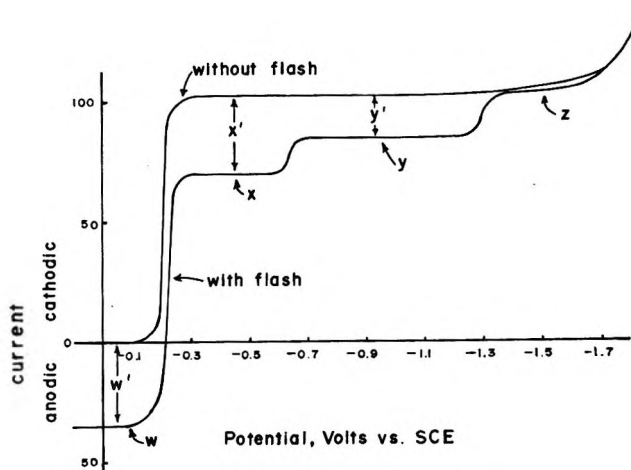


Figure 4. Current-voltage profile for 4.62×10^{-4} M FeOx₃³⁻, at 200 μ sec after irradiation. Current in μ A (128-J flash).

in Figure 4 was obtained. This profile provides a qualitative picture of the electroactive species in solution at 200 μ sec after irradiation and shows the *initial* effect of irradiation on the ferrioxalate system.

Figure 4 exhibits four current plateaus which, for simplicity of later discussions, have been labeled W , X , Y , and Z . Also, the loss or gain of current in each region resulting from the flash have been labeled w' , x' , y' , and z' , where z' is initially zero. It is interesting to note the simple initial relationship (1:1:1/2) between w' , x' , and y' , respectively. This relationship is an important consideration when describing the initial photolytic intermediates.

One might consider several possible combinations of oxidizable and reducible intermediates to explain the observed behavior. All reasonable combinations have been considered, only one of which fits all observable behavior. This involves the presence of either two oxidizable species or one species which can undergo two equivalent oxidizable processes. These oxidation steps occur in regions X and Y . (It should be noted here that these oxidation processes must proceed also in region W , and at all potentials positive of the $E_{1/2}$'s. Because unphotolyzed ferrioxalate is *reduced* in all

(30) S. P. Perone, *Anal. Chem.*, **38**, 1158 (1966).

(31) J. Baxendale and N. Bridge, *J. Phys. Chem.*, **59**, 783 (1955).

cathodic regions of the current-voltage profile, regions *X* and *Y* must be mixed current regions. In region *Z*, only ferrioxalate is electrolyzed. Because the current in this region is evidently unaffected initially by the flash, it is concluded that the ferrioxalate concentration is not diminished directly by the flash. This observation suggests that the initial oxidizable intermediate(s) cannot be ferrous molecules.

Thus, the ferrioxalate photolysis mechanism proposed by Parker and Hatchard⁸ cannot fit our observations. They have postulated the instantaneous formation of FeOx_2^{-2} and $\text{Ox}\cdot^-$ or $[\text{FeOx}_2^{-2}-\text{Ox}\cdot^-]$ as initial photolytic intermediates. Neither of these possibilities is consistent with our observation that ferrioxalate is not diminished initially by the flash. Thus, it is concluded that the initial intermediate must be a ferric diradical species which contains both oxidizable and reducible groups in the same molecule. Such an intermediate has been postulated for thermal decomposition of metal oxalates.^{16,17}

The following sections present the experimental data which substantiate the proposed explanation of the photoelectrochemical behavior and lead to an explicit photochemical mechanism.

Time-Delay Studies. The assignment of particular electroactive species to explain the current-voltage (*i-E*) profile in Figure 4 was complicated by the possibility of mixed currents in all regions. Additional information needed to make these assignments has come from time-delay studies. (From this point on, when "time" refers to τ in a time-delay experiment, the term "time (τ)" will be used.)

Time-delay potentiostatic analysis has revealed that, initially, plateau *W* decreases and plateaus *X* and *Y* increase with time (τ) (see Figure 5a); *i.e.*, there is a loss of net oxidation current in region *W* and a corresponding increase in net reduction current in regions *X* and *Y*. It was also observed that the rate of change of w' and x' is initially greater than y' . During these initial changes of *W*, *X*, and *Y*, region *Z* decreases. Eventually, at a time τ_{min} regions *X*, *Y*, and *Z* merge forming one plateau (Figure 5b). At this time, the amount of oxidation current equals approximately the amount of lost reduction current.

After τ_{min} , the reduction region (now one plateau) decreases as time (τ) increases. During this decrease, region *W* undergoes a simultaneous increase in oxidation current. At long time delays ($\tau \approx 1$ sec), the plateau reduction current (*X-Y-Z*) becomes approximately equal to the initial level of plateau *X* and the increase in region *W* has also reached the initial level of plateau *W*. (See Figure 5c.)

A plot of current vs. time (τ) for region *W* is shown in Figure 6. Not only does this plot summarize the qualitative observations described above, but it also illustrates an important fact for mechanistic suggestions. This fact is: the net oxidation current in

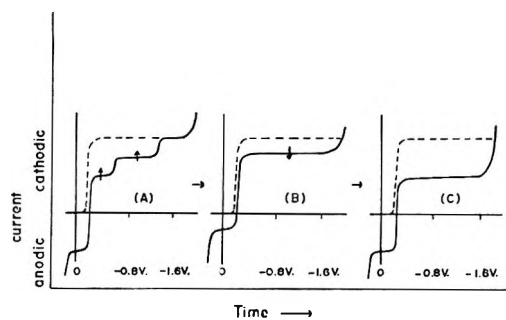


Figure 5. Effect of time on current-voltage profile. A, initial profile; B, profile at τ -min; C, profile at long time (>1 sec).

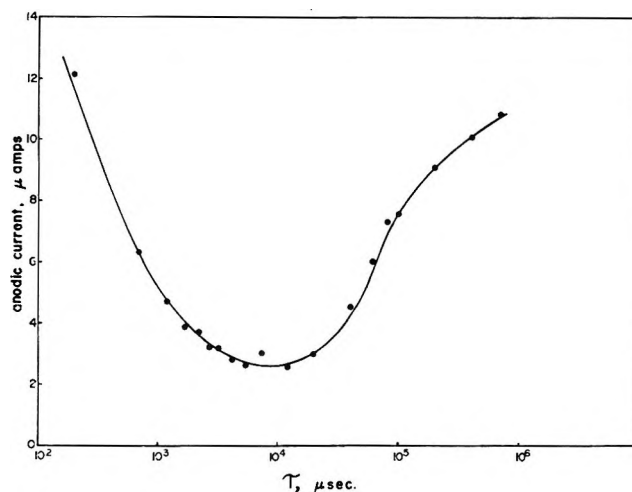


Figure 6. Current vs. $\log(\tau)$ after flash for $1.84 \times 10^{-4} M$ FeOx_3^{3-} . $E_{\text{applied}} = -0.100$ V vs. sce (128-J flash).

region *W* can reach a minimum value which is definitely less than 50% of the "final" level of oxidation current.

If, as suggested in eq 2, FeOx_2^{-2} and $\text{Ox}\cdot^-$ were the first detectable species, both oxidizable in region *W*, then one-half of the final level of FeOx_2^{-2} would be generated immediately. One would, therefore, predict that the oxidation current in region *W* would never decrease below 50% of the final level. Figure 6 illustrates that it does go below 50%, ruling out this possibility.

The intimate relationship among all four regions can be observed by a plot of w' , x' , y' , or z' vs. time (τ). This is shown in Figures 7 and 8. Note the nearly identical behavior of w' and x' . Also, Figure 7 shows that τ_{min} is common to all regions. From Figure 8, it appears that one curve can show the change in current for all regions after τ_{min} . These observations are all consistent with the postulated singular ferric diradical intermediate.

Current-voltage profiles obtained before and after τ_{min} have not indicated the formation of any other intermediate electroactive species. The possibility of the formation of an oxidizable intermediate species

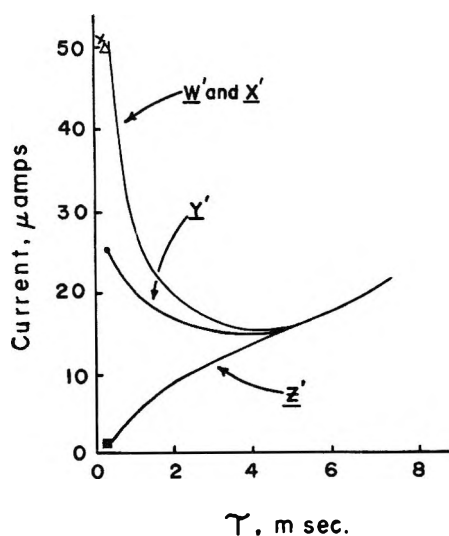


Figure 7. Current vs. τ ($\tau < 10$ msec) after flash for w' , x' , y' , and z' (155-J flash).

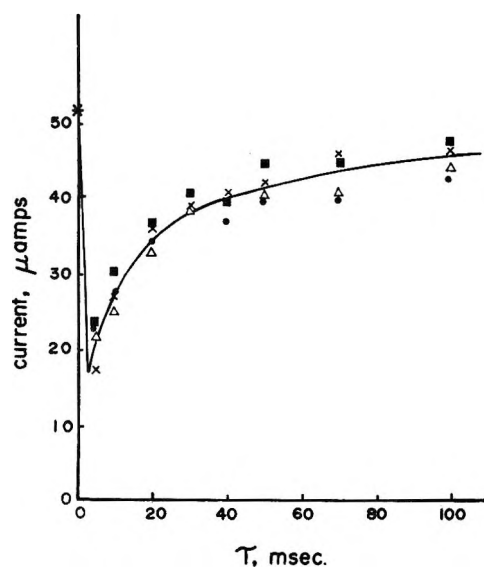


Figure 8. Current vs. τ ($\tau > 10$ msec) after flash for $4.62 \times 10^{-4} M$ FeOx_3^{3-} (155-J flash). Key: ●, w' ; x , z' ; Δ , y' ; Δ , x' . Current vs. $\log(\tau)$ after flash for $1.84 \times 10^{-4} M$ FeOx_3^{3-} . $E_{\text{applied}} = -0.100$ V vs. sce (128-J flash).

with and $E_{1/2}$ so anodic as to be undetectable was discounted because thermodynamically it could not reduce ferrioxalate. The formation of an intermediate reducible species with a half-wave potential anodic of the Hg oxidation background was discounted because the conversion of it to product, FeOx_2^{2-} would cause the net change in current in region W to be inconsistent with other regions, contrary to what is observed.

One final observation obtained from time-delay potentiostatic analysis is that w'_{initial} and w'_{final} are approximately equal. (The same is true for x'_{initial} and x'_{final} .) Also, from the above discussions, it is obvious that the data in region W reflect the total mechanistic picture. Therefore, subsequent kinetic studies have

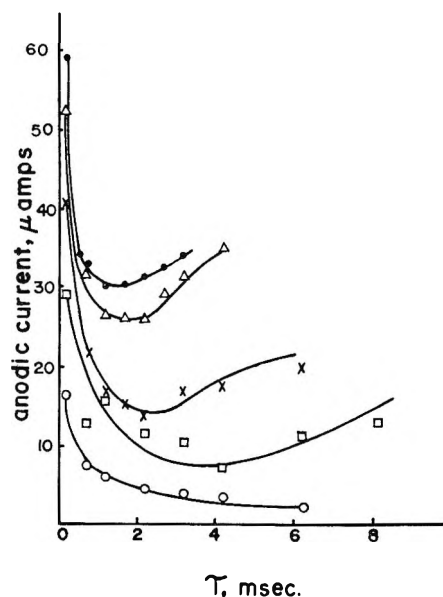


Figure 9. Current vs. τ ($\tau < 10$ msec) after flash at various concentrations of ferrioxalate. ($E_{\text{applied}} = -0.100$ V vs. sce) (128-J flash). Key: ●, $9.24 \times 10^{-4} M$ FeOx_3^{3-} ; Δ , $7.39 \times 10^{-4} M$ FeOx_3^{3-} ; \times , $5.55 \times 10^{-4} M$ FeOx_3^{3-} ; \square , $3.69 \times 10^{-4} M$ FeOx_3^{3-} ; \circ , $1.84 \times 10^{-4} M$ FeOx_3^{3-} .

focused on this region, as it is free of mixed currents. That is, time-delay kinetic data in region W can be interpreted as following the disappearance of the initial diradical intermediate and subsequent formation of FeOx_2^{2-} .

Concentration and pH Effects on Time-Delay Kinetic Data. Variation of the initial ferrioxalate concentration produced a noticeable effect upon current-time (τ) plots obtained in region W . Figure 9 summarizes these results. As the initial concentration of ferrioxalate decreases, the minimum shifts to a later time (τ) and the ratio of $w'_{\tau_{\text{min}}}/w'_{\text{initial}}$ decreases. These observations were used to distinguish between the various specific mechanisms which were investigated by digital simulation, as described below.

The pH range of the ferrioxalate solution was varied from pH 4.5 to 6.5. A close look at the electrode processes at -0.6 V and -1.35 V, showed that the pH had little effect on the $E_{1/2}$ of the first wave while there was a slight cathodic shift in the latter wave as the pH increased (25 mV). Time-delay kinetic data were observed to be unaffected within this pH range.

Mechanistic Studies

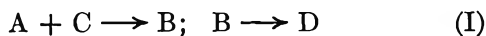
Digital Simulation. The technique of digital simulation was used to distinguish between the various mechanistic possibilities. Quantitative details of the methods used are given in the experimental section.

The time-delay currents measured in region W (Figure 6) represent the summation of oxidation currents due to the initial diradical species and final product FeOx_2^{2-} . The simplest mechanistic explanation of the kinetic data displayed in Figure 6 is a two-step process

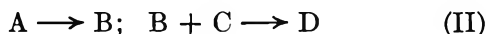
in which the initial oxidizable diradical species is converted to a nonoxidizable intermediate which subsequently leads to the formation of oxidizable product (FeOx_2^{2-}).

The specific criteria employed in simulation studies to differentiate between acceptable and nonacceptable mechanisms were the effects of the initial concentration on τ_{min} . (It was reported above that the minimum in the experimentally observed kinetic plot decreased relative to the initial value and shifted to later times as the initial concentration decreased (see Figure 9)). Thus, mechanisms involving consecutive reversible and irreversible first-order processes were rejected because simulation for different initial concentrations showed that the minimum did not vary in time or in magnitude *relative* to the initial value.

More important than consecutive first-order processes are those involving a mixed second-order process which could be either preceded or followed by a first-order reaction. These processes represent the possibilities which have been suggested by Parker and Hatchard.⁸ The basic skeletons for these alternatives are shown below as cases I and II.

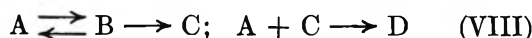
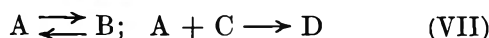
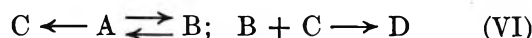
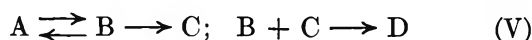
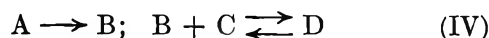
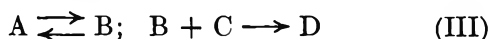


or



In both cases C represents ferrioxalate, D ferrooxalate, A the intermediate initially formed as a result of irradiation, and B the nonoxidizable intermediate suggested earlier. Simulation of cases I and II with decreasing initial concentration revealed that the minimum shifted to a later time for both cases, but only in case II did the minimum decrease relative to the initial measurement. Therefore, case II is consistent with the observed behavior for this system, and it provides a very probable mechanistic pathway.

Within the type of reaction scheme of case II, various alternatives were found which qualitatively fit the data. These are shown below.



Mechanisms similar to IV have been eliminated because no reasonable equilibrium between the stable product, FeOx_2^{2-} , and a nonoxidizable species (B) could be conceived.

To distinguish between the remaining choices, rate constants were varied to observe the effect upon the

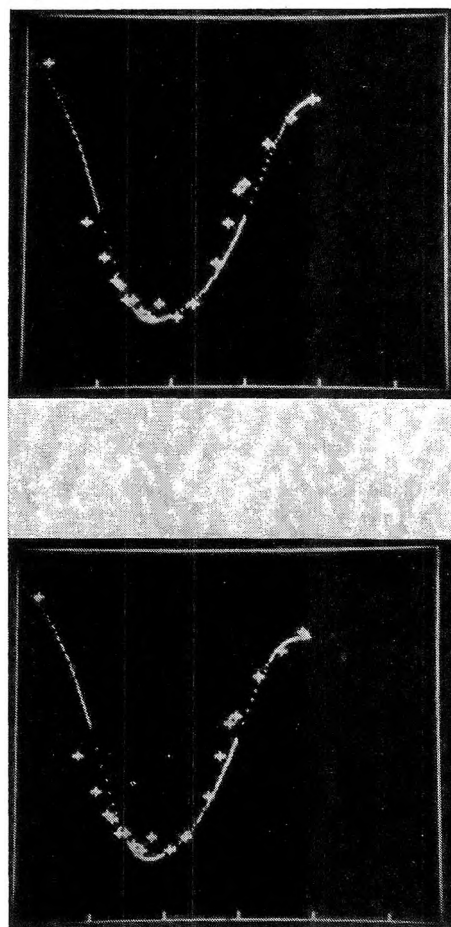


Figure 10. Digital simulation of concentration *vs.* $\log(\tau)$ after flash for two mechanisms. Upper photo: simulation of case VIII. Rate constants: $k_1 = 800 \text{ sec}^{-1}$, $k_2 = 100 \text{ sec}^{-1}$, $k_4 = 1.5 \text{ sec}^{-1}$, and $k_3 = 3.3 \times 10^{+6} \text{ l./m sec}$. Initial concn: $[A] = 4.22 \times 10^{-6} \text{ M}$, $[C] = 1.42 \times 10^{-4} \text{ M}$. Lower photo: simulation of case V. Rate constants: $k_1 = 675 \text{ sec}^{-1}$, $k_2 = 100 \text{ sec}^{-1}$, $k_4 = 2 \text{ sec}^{-1}$, $k_3 = 5 \times 10^{+4} \text{ l./m sec}$. Initial concn same as above; discrete points represent real data taken from Figure 8.

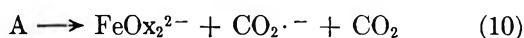
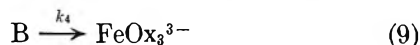
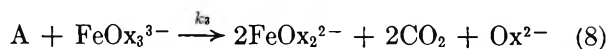
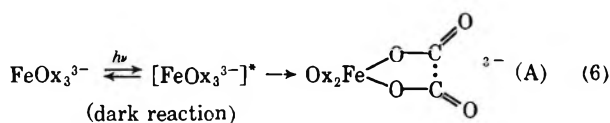
simulated data, and the rate constants were adjusted to give the closest fit of the simulated data to the real data. Figure 10 shows the fit obtained between the simulated data and real data of region W over four decades in time (100 μsec to 1 sec) for cases V and VIII. (Similar fits were obtained for regions X, Y, and Z.) Unfortunately, all of the mechanisms (II–VIII) were found to fit the real data equally well. Thus, differentiation between these possible mechanisms was done by considering plausible intermediates which fit not only the mechanism suggested by digital simulation but also the electrochemical observations described earlier.

Mechanism. The conclusions derived from the current–voltage profile, current–time data, and digital simulation can be summarized as criteria for any postulated mechanism. These criteria are the following.

(1) The basic skeleton for the mechanism should be a first-order process followed by a second-order process

(2) The first intermediate (A) must be oxidizable in region *W* but it cannot be a ferrous molecule. (3) Intermediate B must not be oxidizable in region *W*. (4) Intermediate B must also reach a significant concentration to explain the observation that the minimum current in region *W* (Figure 6) can be lower than 50% of the final oxidation current during the reaction. (5) A fifth criterion, not obtained from this work, is that excited state intermediates cannot be detected directly at a metal electrode.³² The theory behind this statement suggests that an excited state species will transfer its excess energy to a metal electrode before it can get close enough to the electrode for electron transfer.

The most plausible mechanism that the authors can propose is shown below



The first three equations represent the major pathways. The initial step, after excitation, would be the breaking of the C–C bond in the oxalate ligand to form species A, followed by equilibration with an unoxidizable species B (eq 7) or reaction with a ferrioxalate molecule (eq 8). The best fit of this simulated mechanism suggests that $k_1 = 800 \text{ sec}^{-1}$, $k_2 = 100 \text{ sec}^{-1}$, $k_3 = 3 \times 10^5 \text{ l./m sec}$, and $k_4 = 1.5 \text{ sec}^{-1}$ (see Figure 10).

An intermediate species analogous to A has been suggested by Duke¹⁷ as an intermediate in the catalytic oxidation of glycols by manganese dioxalate. He proposes that the initial step in the decomposition of MnOx_2 is also the breaking of the C–C bond which has been weakened by coordination to the metal ion. Boldyrev, *et al.*,¹⁶ also suggest that the initial step in the thermal decomposition of all oxalates is the cleavage of the C–C bond. Therefore, there appears to be some precedent for proposing the initial step of the mechanism suggested here.

Intermediate A is the species detected initially in regions X and Y. It has the characteristics to allow concurrent 2-electron oxidation and 1-electron reduction steps to occur which are necessary to explain the current–voltage profile at short times (see Figure 4). The presence of these characteristics in one species also explains the coincidental current–time behavior in regions *W*, X, and Y. In this molecule, the reduction of

the ferric atom would occur at or very near the same reduction potential of ferrioxalate. Thus, it contributes to the reduction current in regions X, Y, and Z. The oxidation processes would involve the stepwise oxidation of the radical ligands. The oxidation of the first radical makes it more difficult to oxidize the second radical ligand, giving rise to the two distinct oxidation steps forming regions X and Y. Concurrent electrode processes in one species are not common, but intermediate A is an unstable species which could undergo intramolecular oxidation and reduction. The chemical identity of B is unknown, but its presence in the reaction scheme is necessary. Although the mechanism shown indicates that the initial intermediate A reacts with the second molecule of ferrioxalate, it is also plausible that B could react in an analogous manner. In either case, any postulate of B must satisfy criteria 3 and 4 to be acceptable.

One possible structure for intermediate B would result from the reformation of the C–C bond creating a metastable species. A similar process of net bond formation has been used to explain the natural chemiluminescence of lophine.³³ In the excited state, the molecule would not be electrochemically detected as such, but would be reducible as normal ferrioxalate after it transferred its excess energy to the electrode. In this way, there would be no apparent loss of Fe^{3+} molecules, but there would be a loss of oxidizable radical ligands.

There is, however, one very important point which diminishes the possibility that B is a metastable species, *i.e.*, the lifetime of species B. To fit this mechanism, B must have a half-life in the milliseconds range which is two or three orders of magnitude longer than might be predicted in fluid solutions.³⁴ Therefore, if intermediate B is a metastable species, it is exceptionally long-lived. Without further experimental evidence, B cannot be designated as an excited species with any degree of certainty.

The loss of B in eq 9 has been included to allow for the deactivation of B to normal ferrioxalate if B were a metastable species. Equations 10 and 11 were included only to show possible alternatives to eq 8, which must be the major pathway by which ferrous oxalate is formed.

Parker and Hatchard⁸ have calculated first-order and second-order rate constants for the single reaction observed after irradiation to see which order fit the data best. The values reported were $\approx 250 \text{ sec}^{-1}$ and $\approx 1.2 \times 10^{+6} \text{ l./m sec}$ which are in the same range as reported here. A direct correlation of this mechanism

(32) H. Bucher, K. H. Drexhage, M. Fleck, H. Kuhn, O. Mobius, F. P. Schafer, J. Sondermann, W. Sperling, P. Tillman, and J. Wiegand, *Mol. Cryst.*, **2**, 199 (1967).

(33) E. H. White and M. J. C. Harding, *J. Amer. Chem. Soc.*, **86**, 5686 (1964).

(34) F. Lytle, personal communication.

to their observations is difficult since the oxalate-to-ferric ratio was greater in this work. However, since excess oxalate is known to retard product formation, then it is possible that eq 8 of this mechanism is the chemical reaction observed by Parker and Hatchard. Perhaps the excess oxalate has slowed the second reaction to a point where it is the rate-determining step in this work.

The instantaneous drop in absorbance by ferrioxalate after irradiation observed by Parker and Hatchard⁸ can only be explained by this mechanism if intermediate A has a significantly different absorption spectrum compared to ferrioxalate. If this were true, then intermediate A might also be the intermediate observed by Parker and Hatchard which absorbs more strongly than ferrioxalate at 405 and 436 nm.

The initial objective of this work was to complement the investigations initiated by Parker and Hatchard⁸ by applying photoelectrochemical measurements. It

has been shown here that the observations of this work are not consistent with the standard mechanistic framework. However, the new mechanism suggested here is consistent with Parker and Hatchard's experimental observations as well as the photoelectrochemical data, although it suffers from the inability to assign chemical significance to species B. Additional studies using concurrent spectroscopic and electrochemical measurement techniques are under development in this laboratory and should allow more definitive characterization of species B.

Acknowledgment. The authors wish to acknowledge the work performed by Dr. H. D. Drew in initiating this project and also the assistance in instrumentation design received from G. L. Kirschner, J. I. H. Patterson, and D. O. Jones. This work supported by Public Health Service Grant No. CA-07773 from the National Cancer Institute.

Pulse Radiolysis Study of the Kinetics of Formation of Na^- in Ethylenediamine by the Reaction of Solvated Electrons with Sodium Ions¹

by James L. Dye, Marc G. DeBacker,

Department of Chemistry, Michigan State University, East Lansing, Michigan 48823

John A. Eyre, and Leon M. Dorfman*

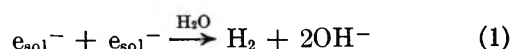
Department of Chemistry, The Ohio State University, Columbus, Ohio 43210 (Received October 12, 1971)

Publication costs assisted by the U. S. Atomic Energy Commission

Fast reaction studies of the formation of Na^- in ethylenediamine from e_{sol}^- and sodium ion were carried out by the pulse radiolysis method. The decay of the absorbance of e_{sol}^- and the growth of that of Na^- were both second order with similar rate constants which were independent of the concentration of sodium ion above about $10^{-2} M$ but decreased with a decrease in the concentration of Na^+ below this value. The presence of Cs^+ had no effect upon the rate. At low concentrations of Na^+ , excess K^+ caused the reaction to reach equilibrium rather than to proceed to completion. The results show that the formation of species containing two electrons (which may be coupled with metal cation) precedes the reaction in which Na^- is formed. Quantitative kinetic tests of the mechanism are presented.

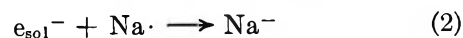
Introduction

Bimolecular reactions of the solvated electron with another single-electron species have now been observed by a variety of methods in a number of solvents. The reaction in water



has been established by isotopic² and by kinetic stud-

ies.^{2,3} Reaction of the solvated electron with a metal atom (or monomer or ion pair) according to

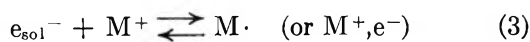


(1) This work was supported by the U. S. Atomic Energy Commission and was initiated while J. L. D. was a visiting scientist on sabbatical leave at The Ohio State University in 1969.

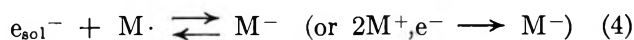
(2) L. M. Dorfman and I. A. Taub, *J. Amer. Chem. Soc.*, **85**, 2370 (1963).

(3) M. S. Matheson and J. Rabani, *J. Phys. Chem.*, **69**, 1324 (1965).

has been proposed to explain the flash⁴ or laser⁵ photolysis of alkali metal-amine solutions. The reactions



and



where $M\cdot$ is the alkali metal atom or monomer and M^+, e^- is the ion pair, have been invoked in esr kinetic studies⁶ and optical studies⁷ of flash photolyzed metal-ether solutions. Recently, reaction 3 has been proposed to explain some of the absorbance changes which follow the photolysis of dilute solutions of pyrenide ion in tetrahydrofuran.⁸ The detailed role of the alkali metal species in the kinetics remains somewhat obscure, and the identity of individual elementary reactions uncertain. The present pulse radiolysis study of the solvated electron in ethylenediamine solutions in the presence of sodium ions, with and without potassium or cesium ions, was undertaken in an attempt to sort out the roles of the various metal ions and to further relate the decay of the electron absorbance to the growth of the V band, attributed to Na^- .^{9,10}

Solutions of alkali metals in ammonia and in amines have been studied for a number of years. However, in spite of these efforts, even the stoichiometry of the species present in solution has not been unequivocally determined. Electrochemical, thermodynamic, and magnetic resonance studies of metal-ammonia solutions give evidence for the existence of species with the stoichiometry M , M^- , and possibly M_2 .¹¹⁻¹⁴ The absence of definitive changes in the spectroscopic properties of metal-ammonia solutions with concentration has led to the proposal that the metal-containing species and also the spin-paired species are formed by relatively weak interaction among solvated electrons and alkali metal cations.^{14,15}

In contrast to the behavior of metal-ammonia solutions, metal solutions in some amines and ethers show new optical bands¹⁶ and esr absorptions¹⁷ which are characteristic of metal-containing species. The esr results show unequivocally that at least one species of stoichiometry M is present as a minor constituent. However, the stoichiometry of the species responsible for the metal-dependent optical absorption has been the subject of speculation for some time. With the demonstration by Hurley, Tuttle, and Golden¹⁸ that metal-amine solutions could release significant amounts of sodium from Pyrex, some of the confusion in the field was removed. The similarity of the solvent and temperature dependence of the position of the optical band with these properties of the charge-transfer-to-solvent band of iodide ion, led Matalon, Golden, and Ottolenghi⁹ to propose the stoichiometry M^- . This stoichiometry was also used to explain the kinetics of recombination of species produced by flash photolysis of metal-amine^{4,5} and metal-ether^{6,7} solutions.

It has recently been shown¹⁰ that the major absorption in solutions of sodium in ethylenediamine (maximum at 650 nm) originates from a species of stoichiometry Na^- . The absorption of e_{sol}^- is small even in dilute solutions.¹⁶ At the other extreme, dilute cesium solutions in this solvent show only the infrared absorption of the solvated electron.^{19,20} Solutions of potassium and rubidium and concentrated solutions of cesium in ethylenediamine show both the solvated electron absorption and a metal-dependent band, presumably from M^- . In less strongly solvating media such as in ethylamine and the higher monoamines and in ethers the solvated electron absorption becomes less pronounced and the spectrum is dominated by the absorption of M^- . The equilibrium



lies so far to the right in ethylenediamine that the addition of a sodium salt to a solution of cesium in this solvent yields only the band of Na^- when stoichiometric amounts of salt are used.¹⁰

Several investigators have shown^{4-7,21,22} that metal solutions in amines and in ethers yield the solvated electron upon photolysis. The rate of formation of Na^- ^{4,5} and of intermediates⁷ after a dissociating flash have been studied. Huppert and Bar-Eli⁵ studied this process as a function of temperature and ionic strength in 1,2-propanediamine and in ethylenediamine. They found the growth of the Na^- absorption to be a second-order process with a rate which was independent of

(4) A. Gaathon and M. Ottolenghi, *Israel J. Chem.*, **8**, 165 (1970).

(5) D. Huppert and K. H. Bar-Eli, *J. Phys. Chem.*, **74**, 3285 (1970).

(6) S. H. Glarum and J. H. Marshall, *J. Chem. Phys.*, **52**, 6251 (1970).

(7) J. G. Kloosterboer, L. J. Giling, R. P. H. Rettschnick, and J. D. W. VanVoorst, *Chem. Phys. Lett.*, **8**, 462 (1971).

(8) M. Fisher, G. Ramme, S. Claesson, and M. Szwarc, *ibid.*, **9**, 309 (1971).

(9) S. Matalon, S. Golden, and M. Ottolenghi, *J. Phys. Chem.*, **73**, 3098 (1969).

(10) M. G. DeBacker and J. L. Dye, *ibid.*, **75**, 3092 (1971).

(11) E. Becker, R. H. Lindquist, and B. J. Alder, *J. Chem. Phys.*, **25**, 971 (1956).

(12) E. Arnold and A. Patterson, Jr., *ibid.*, **41**, 3089, 3098 (1964).

(13) S. Golden, C. Guttman, and T. R. Tuttle, Jr., *ibid.*, **44**, 3791 (1966).

(14) For a review of models and additional references see J. L. Dye, *Pure Appl. Chem.*, **1** (1970).

(15) M. Gold, W. L. Jolly, and K. S. Pitzer, *J. Amer. Chem. Soc.*, **84**, 2264 (1962).

(16) For references to optical properties of metal solutions see I. Hurley, T. R. Tuttle, Jr., and S. Golden in ref 14, p 449.

(17) For references to esr studies of metal solutions see R. Catterall, ref 14, p 105.

(18) I. Hurley, T. R. Tuttle, Jr., and S. Golden, *J. Chem. Phys.*, **48**, 2818 (1968).

(19) R. R. Dewald and J. L. Dye, *J. Phys. Chem.*, **68**, 121 (1964).

(20) J. L. Dye, M. G. DeBacker, and L. M. Dorfman, *J. Chem. Phys.*, **52**, 6251 (1970).

(21) J. Eloranta and H. Linschitz, *ibid.*, **38**, 2214 (1963).

(22) M. Ottolenghi, K. Bar-Eli, and H. Linschitz, *ibid.*, **43**, 206 (1965).

added Na^+ . Several years ago it was reported²³ that reaction 5 could be studied in ethylenediamine by using pulse radiolysis to produce the solvated electron. Both the decay of the absorption of e^- and the growth of the absorption of Na^- followed second-order kinetics. The present paper describes the kinetics of this reaction including the effect of concentration of sodium ion and of other salts.

Experimental Section

The techniques of pulse radiolysis²⁴⁻²⁶ used in this laboratory²⁷ have been described in detail. A Varian V-7715A electron linear accelerator was used as a pulse source of 3-4-MeV electrons, generally at a pulse current of about 350 mA. The pulse width was varied from 100 to 500 nsec. A 100-nsec pulse delivers a dose of about 6×10^{16} eV/g to water.

The transient optical absorption was simultaneously observed with two separate photodetectors. Either an RCA 7102 or 7200 photomultiplier was used below about 1000 nm and for all kinetic studies. To study absorption spectra into the infrared, a liquid nitrogen cooled indium antimonide detector, Model A10X, obtained from Barnes Engineering, Inc., was used. This detector, which has been used²⁸ out to 2250 nm, has a rise-time (10 to 90%) of about 80 nsec with the circuitry which has been described.²⁸ The linearity of the detector was tested with a chopped light signal superimposed on a steady signal. No deviation from linearity could be detected within a sensitivity of 1%. A flashed 500-W Osram xenon lamp, Type X BO 450 W, was used as light source. Bausch and Lomb grating monochromators, Type 33-86-25, $f/3.5$, were used with appropriate cutoff filters.

Reaction cells with high purity silica optical windows, of a geometry previously described,²⁰ were used. With runs containing sodium and potassium, the procedures previously described²⁰ were used with the modification that ethylenediamine was either poured or distilled from a storage bulb under vacuum into the reaction cell. For runs with cesium, a waste storage bulb was added to the cell configuration to permit prior rinsing of the cell with ethylenediamine. A side arm permitted cesium-containing capillaries to be broken under vacuum. Alkali metal salts were added in small, thin-walled bulbs which were broken *in situ* as required.

Ethylenediamine, obtained as a gift from Dow Chemical Co., had a stated purity of 99%. It was freeze-purified as recommended,^{10,29} and then was distilled onto a potassium mirror to form a stable blue solution. After a 24-hr storage over potassium, the solvent was distilled into an evacuated storage bulb. Sodium and potassium, with nominal purities of 99.99%, were obtained from J. T. Baker Co. Cesium was obtained as a gift from Dow Chemical Co. The metals were triply distilled by using a cool flame and stored in short lengths of 2-mm i.d. capillary tubing.

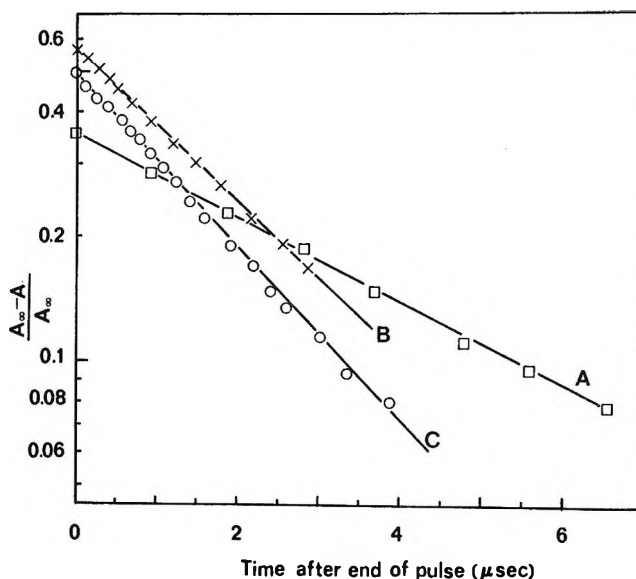


Figure 1. First-order growth of e_{solv}^- in basic ethylenediamine after the end of the pulse. Absorbance measured at 1000 nm. A, Dilute KNHR ($\approx 10^{-3} M$) with $\approx 10^{-2} M$ KI present; B, $4 \times 10^{-3} M$ KNHR; C, $4 \times 10^{-3} M$ KNHR + $3 \times 10^{-3} M$ NaBr.

Results and Discussion

The formation of solvated electrons in pure ethylenediamine and in basic ethylenediamine (containing $\approx 5 \times 10^{-3} M$ potassium ethylenediamide, KNHR) has been described previously.²⁰ The lifetime of e_{solv}^- in the irradiated pure solvent is only a few microseconds, being limited by reaction with the counterion. However, in basic ethylenediamine, the solvated electron is stable for at least several seconds after the pulse. By contrast, in basic ammonia, the lifetime is only about a microsecond unless a radical scavenger such as ethanol is present.²⁰ There is another significant difference between the behavior with ammonia and that with ethylenediamine. In basic ammonia which contains ethanol ($\gtrsim 10^{-2} M$) the absorbance of the electron grows only during the pulse, while in basic ethylenediamine (made basic with decomposed sodium, potassium, or cesium solutions) there is an additional substantial growth of the absorbance after the pulse. The growth of absorbance is first order in all cases. As shown in Figure 1, the final value of the absorbance can be nearly three times that at the end of the pulse. Within a given run

(23) J. L. Dye, ref 14, p 483.

(24) M. S. Matheson and L. M. Dorfman, *J. Chem. Phys.*, **32**, 1870 (1960).

(25) L. M. Dorfman and M. S. Matheson, *Progr. React. Kinet.*, **3**, 237 (1965).

(26) M. S. Matheson and L. M. Dorfman, "Pulse Radiolysis," M.I.T. Press, Cambridge, Mass., 1969.

(27) W. D. Felix, B. L. Gall, and L. M. Dorfman, *J. Phys. Chem.*, **71**, 384 (1967).

(28) L. M. Dorfman, F. Y. Jou, and R. Wageman, *Ber. Bunsenges. Phys. Chem.*, **75**, 681 (1971).

(29) L. H. Feldman, R. R. Dewald, and J. L. Dye, *Advan. Chem. Ser.*, No. 50, 163 (1964).

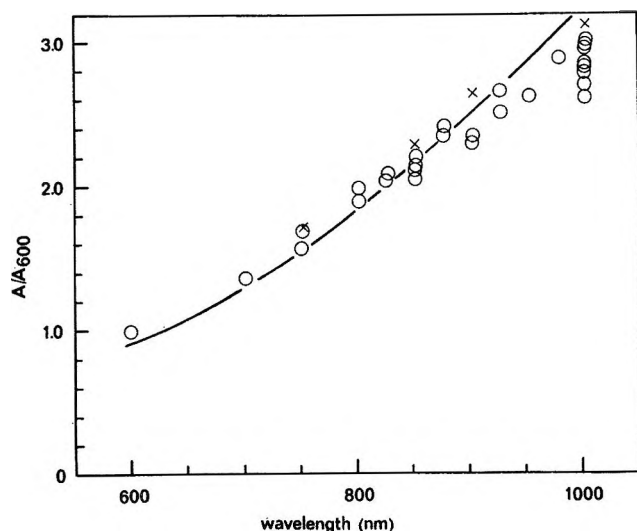
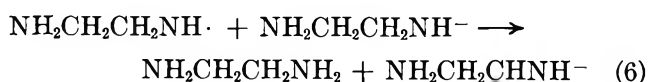


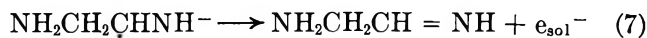
Figure 2. Absorbance after growth of e_{sol}^- in basic ethylenediamine in the presence of K^+ . The pulse radiolysis results have been normalized to 600 nm: O, run of 4/2/69; X, run of 6/7/69; —, spectrum of Cs and e_{sol}^- in ethylenediamine.^{19, 20}

(fixed basicity) both the rate constant for this formation and the relative increase in absorbance were independent of total radiation dose, salt concentration, and (above 700 nm) wavelength. For example, 22 growth curves in a solution which was $4 \times 10^{-3} M$ in KNHR (and for some of the pulses also $3 \times 10^{-3} M$ in NaBr) were examined over the wavelength range from 700 to 1000 nm. Analysis of these data yielded $A_{\infty}/A_0 = 2.62 \pm 0.28$ and $k = 5.22 \pm 0.89 \times 10^5 \text{ sec}^{-1}$. [All uncertainties given in this paper represent statistical estimates of the standard deviation obtained by a least-squares analysis of the data.] At shorter wavelengths (650–375 nm) the value of A_{∞}/A_0 remained constant, but the first-order rate constant for the growth of absorbance increased progressively by a factor of 2–3. The spectrum is unchanged during the growth (checked over the complete wavelength range of 600 to 1600 nm only with solutions made basic with potassium). Even when the concentration of KI was as high as 0.27 M there was not more than 10% contribution from the R band of K^- . This is illustrated by Figure 2 in which the wavelength dependence of the absorbance (relative to that at the reference wavelength of 600 nm) is compared with that of the solvated electron in ethylenediamine.

The independence of the growth rate with metal, salt, and pulse length suggests the decomposition of an intermediate species to produce the solvated electron. One possible reaction scheme consists of the scavenging reaction



followed by a rearrangement and electron detachment



Reaction 6 represents the abstraction of an α -hydrogen in basic solutions. The first-order formation of the solvated electron could then presumably result from reactions 6 and 7.

Whenever sodium ions were present in the solution, the growth of absorbance of e_{sol}^- was followed by its decay and the simultaneous growth of the absorbance of Na^- . The spectrum at times long enough to reach equilibrium is compared in Figure 3 with that of a solution of sodium in ethylenediamine.¹⁹ If the stoichiometry of the conversion is given by eq 5, then we may relate the absorbances A_1 and A_2 at two different wavelengths to the corresponding extinction coefficients by

$$A_1 - A_1^\circ = \frac{1\epsilon_{\text{Na}^-} - 2^1\epsilon_e^-}{2\epsilon_{\text{Na}^-} - 2^2\epsilon_e^-} (A_2 - A_2^\circ) \quad (8)$$

in which A_1° and A_2° represent the absorbance at the time of maximum e_{sol}^- absorbance. The absorbance at 600 nm proved to be a linear function of that at 1000 nm during the entire reaction. The slope was independent of the nature and concentration of the cation and of pulse duration. Data obtained from 19 sets of traces yielded

$$\frac{\epsilon_{\text{Na}^-}^{600} - 2\epsilon_e^{600}}{2\epsilon_e^{1000} - \epsilon_{\text{Na}^-}^{1000}} = 1.77 \pm 0.19$$

The band shapes are known from studies of metal solutions.¹⁹ These can be used with the present result to determine the ratio of the extinction coefficients at the respective band maxima. By using the known extinction coefficient of Na^- , $\epsilon_{\text{Na}^-} = 8.2 \times 10^4 M^{-1} \text{ cm}^{-1}$ at 650 nm, we obtain $\epsilon_e = 2.0 \pm 0.3 \times 10^4 M^{-1} \text{ cm}^{-1}$ for the solvated electron at 1280 nm at 25°. This gives an oscillator strength of 0.88 ± 0.12 .¹⁰

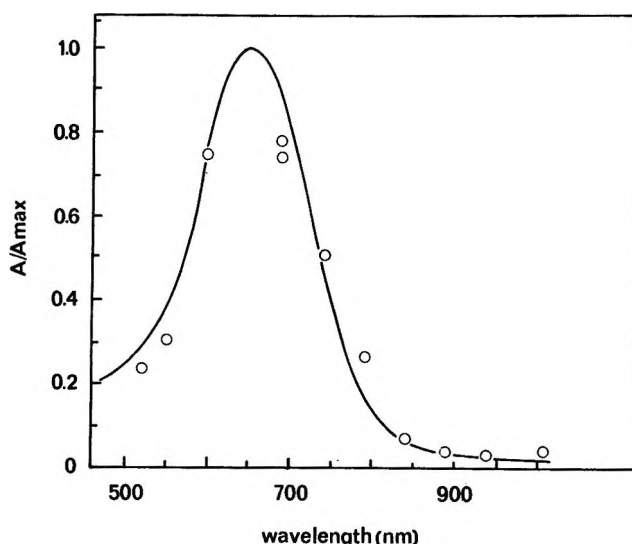


Figure 3. Absorbance (normalized to 650 nm) at long times after the reaction $2e^- + \text{Na}^+ \rightarrow \text{Na}^-$: O, pulse radiolysis results; —, spectrum of Na in ethylenediamine.¹⁹

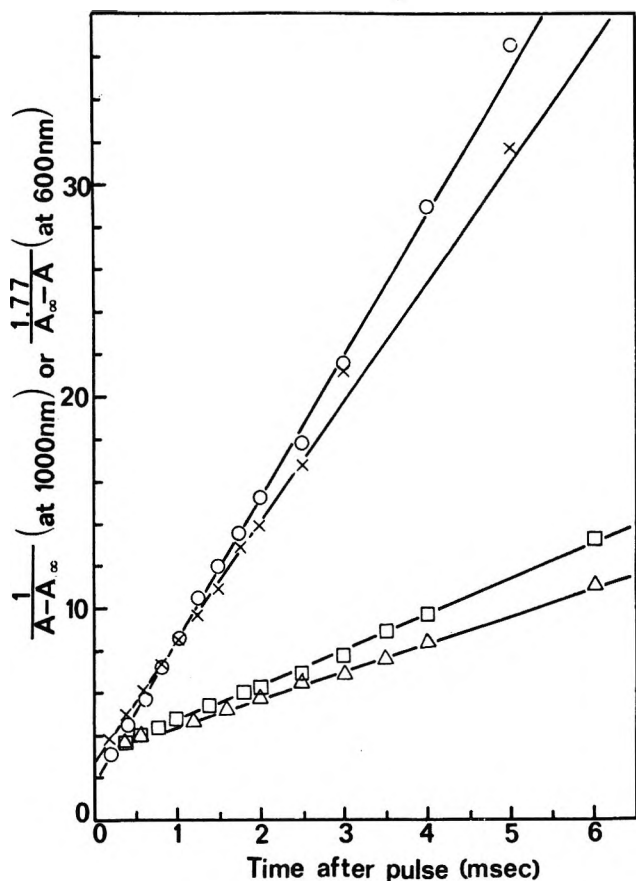


Figure 4. Representative second-order decay of the absorbance of e_{soi}^- and growth of that of Na^- in ethylenediamine. The conversion factor of 1.77 is obtained from the extinction coefficients. The slopes for decay and growth are equal within the uncertainty of the conversion factor: \square , decay; \triangle , growth for $1.6 \times 10^{-3} M$ NaBr and $9 \times 10^{-3} M$ CsNHR; \circ , decay; \times , growth for $0.038 M$ NaBr and $\approx 3 \times 10^{-3} M$ NaNHR.

Reaction 5 is essentially complete at the concentrations of e_{soi}^- and Na^+ used in these experiments (with or without added Cs^+ ; however, see later for the effect of K^+). From the extinction coefficients and the equilibrium absorbances at 600 and 1000 nm, we obtain $K_5 \geq 10^{10} M^{-2}$ at ambient temperatures.

Both the decay of absorbance of e_{soi}^- and the growth of that of Na^- followed second-order kinetics. Figure 4 shows second-order plots of the decay of absorbance at 1000 nm and growth at 600 nm for two different sets of conditions. About half of the data were treated by a simultaneous fit of second-order kinetics to both growth and decay with a nonlinear least-squares program.³⁰ For the rest of the data, the growth and the decay were separately fit to second-order expressions. The results are summarized in Table I. A plot of the average second-order rate constant *vs.* the total concentration of added sodium (metal plus salt) is given in Figure 5. The rate constant refers to the rate law

$$-d[e^-]/dt = 2d[\text{Na}^-]/dt = 2k[e^-]^2$$

Most of the individual points in this figure represent the average value of from 4 to 15 determinations of the rate constant. Some of the data were obtained with low concentrations of sodium ions and higher concentrations of potassium ions. As will be shown later, under these conditions reaction 5 is not complete. For such cases, the rate constants shown in Figure 5 refer to the forward reaction.

Table I: Summary of Pseudo-Second-Order Rate Constants for the Reaction of e_{soi}^- with Na^+ in Ethylenediamine

$10^3 [\text{Na}^+]$ (total molarity)	No. of replications	$k \times 10^{-9}$, $M^{-1} \text{sec}^{-1}$	Stand. dev $\times 10^{-9}$	Comments
0.7	3	0.132	0.015	a, b
0.9	2	0.10	0.03	d, f
1.6	3	0.38	0.06	a, b
1.8	3	0.21	0.04	d, f
2.6	3	0.70	0.11	d, f, h
2.7	3	0.64	0.06	d, f
2.8	5	1.61	0.15	d, e
3	5	0.63	0.13	a, c
3.3	8	1.18	0.08	d, e
3.5	3	1.04	0.19	a, b
5.6	1	0.82	0.17	d, f, h
6.3	3	1.20	0.17	a, b
7.5	7	1.51	0.26	a, d
7.5	7	1.78	0.28	d, f, g
10	3	1.33	0.15	a, c
18	8	1.79	0.33	d, e
22	4	1.58	0.12	d, e
40	4	1.54	0.20	a, c
65	4	1.74	0.31	d, e
86	5	1.76	0.25	d, e
121	5	1.27	0.10	d, e
160	3	1.42	0.27	a, c
542	15	1.48	0.15	d, e

^a Average rate constant obtained by fitting growth and decay separately. ^b Solution made basic by decomposition of $9 \times 10^{-3} M$ Cs. ^c Solution made basic by decomposition of saturated solution of Na ($\approx 3 \times 10^{-3} M$). No K^+ or Cs^+ added. Na^+ added as NaBr. ^d Solution made basic by decomposition of K. Values from 2 to $6 \times 10^{-3} M$ depending on the run. ^e Simultaneous fit of decay and growth of absorbance. ^f $[\text{K}^+] > [\text{Na}^+]$; reaction goes to equilibrium. Decay and growth of absorbance fitted simultaneously to obtain both forward and backward rate constant. ^g KI added in amounts from 2.7×10^{-3} to $0.17 M$. ^h For this run, the coefficient in eq 8 was too small by about 20%. The origin of this discrepancy is not known.

It can be seen from Figure 5 that the second-order rate constant is essentially independent of sodium ion concentration above $0.01 M$. However, between 0.01 and $0.001 M$, the rate constant decreases by an order of magnitude. These results provide a basis for discussion of several possible mechanisms. It should be noted at the outset that the results of conductance

(30) J. L. Dye and V. A. Nicely, *J. Chem. Educ.*, **48**, 443 (1971).

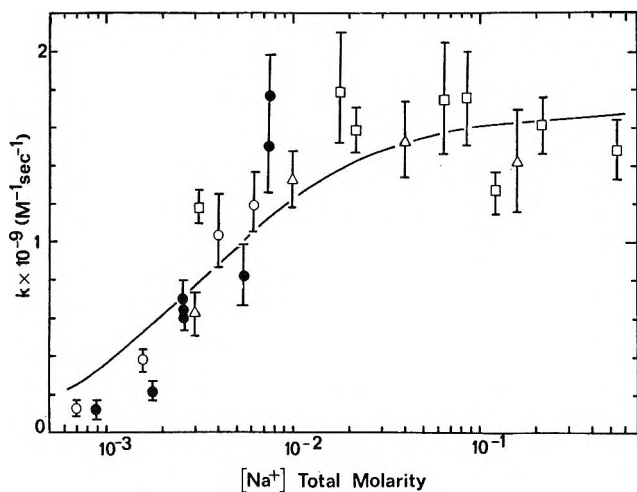
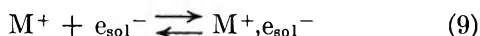


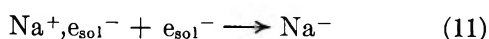
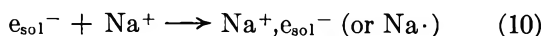
Figure 5. Pseudo-second-order rate constant for the reaction of e_{sol}^- with Na^+ in ethylenediamine. The solid line was obtained by least-squares fit of eq 15. Na^+ was added as NaBr : \circ , $\text{CsNHR} = 9 \times 10^{-3} M$; \triangle , no Cs or K^+ , $\text{NaNHR} \approx 3 \times 10^{-3} M$; \square , KNHR varied from ≈ 2 to $5 \times 10^{-3} M$; \bullet , forward rate constant; KNHR varied from ≈ 2 to $6 \times 10^{-3} M$; for some cases KI was also added. Reaction proceeds to equilibrium.

studies of metal solutions³¹ in ethylenediamine seem to demand that solvated electrons form ion pairs with added cations in ethylenediamine just as do ordinary salts and that the formation constants are not strongly dependent on the cation. Even for the most dilute solutions used in this study, the reaction

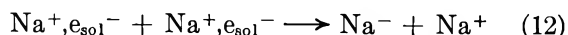


is more than 90% complete at equilibrium. Furthermore, we would expect "loose" ion-pair formation to occur by diffusion control. Therefore, on the time scale used for the study of the kinetics of formation of Na^- , reaction 9 should be at equilibrium. The invariance of the spectral shape of dilute cesium-ethylenediamine solutions with concentration¹⁹ and the similarity with the spectrum of e_{sol}^- in this solvent²⁰ indicate that the optical properties of the solvated electron are not altered significantly by such ion-pair formation. This is also the case for metal-ammonia solutions.¹⁴

A plausible reaction mechanism for the formation of Na^- seemed, on the basis of the results for solutions containing only sodium ions, to be that previously proposed⁶ as a result of esr studies



with the modification that reaction 12 be written as equivalent to reaction 11



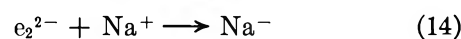
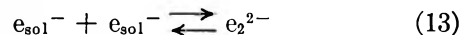
This would simply require that the equilibrium for reaction 10 lie far to the right and be reached within a

few microseconds at the appropriate concentration of sodium ion. The rate need then not depend on the concentration of sodium ions when other cations are not present at appreciable concentrations. If, however, another cation is present in excess, the pseudo-second-order rate constant would decrease by the factor

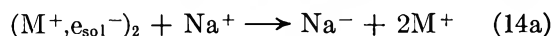
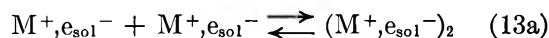
$$\frac{K_5^{\text{Na}}[\text{Na}^+]}{K_5^{\text{M}}[\text{M}^+]}$$

in which K_5^{Na} and K_5^{M} are the appropriate equilibrium constants for reaction 5. The data, however, show that the rate is independent of the presence of other cations, even when they are in excess concentration. This mechanism (reactions 10 and 12) appears, therefore, to be ruled out. Only if the equilibrium constant for the formation of a species of stoichiometry Na were much greater than the corresponding reaction to form Cs or K and if the spectrum of Na were nearly the same as that of e_{sol}^- could the data be compatible with this mechanism.

Since the results with mixed metal cations rule out the foregoing mechanism, we are forced to conclude that the formation of a species containing *two* electrons occurs prior to the step in which Na^- is formed. One such mechanism is



It should be noted that the following two reactions, in which the solvated electron and the dielectron species might be associated with metal cations, are considered equivalent forms of reactions 13 and 14, respectively.



By using the steady-state approximation for the concentration of the dielectron species the rate law gives

$$k = \frac{k_{13f}}{1 + k_{13r}/(k_{14}[\text{Na}^+])} \quad (15)$$

in which k is the pseudo-second-order rate constant. The solid line in Figure 5 was obtained by an appropriately weighted least-squares fit of all of the data to eq 15. This yields $k_{13f} = 1.66 \pm 0.12 \times 10^9 M^{-1} \text{sec}^{-1}$ and $k_{13r}/k_{14} = 3.5 \pm 0.8 \times 10^{-3} M$. Although the fit to this mechanism is not very good, complications caused by ion-pair dissociation at low concentrations and by ionic strength effects at high concentrations would be expected and are not included in the data treatment. The approximate value of k_{13f} may be compared with the value^{2,3} $k_1 = 5 \times 10^9 M^{-1} \text{sec}^{-1}$ for the analogous reaction in water.

It has recently been noted¹⁰ that potassium salts can apparently reverse reaction 5. To study this effect,

(31) R. R. Dewald and J. L. Dye, *J. Phys. Chem.*, **68**, 128 (1964).

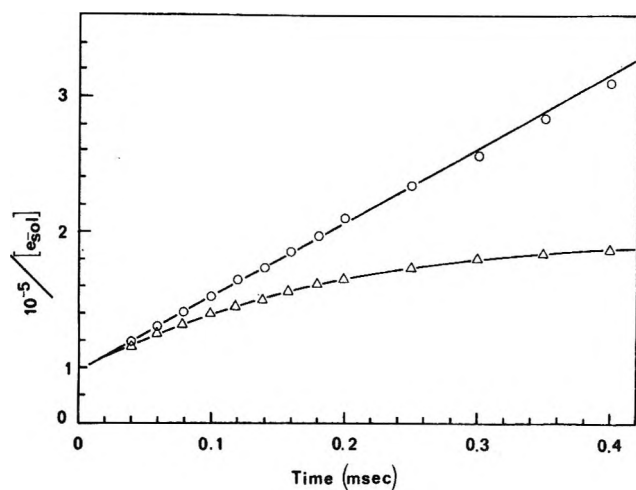


Figure 6. Effect of K⁺ on reaction of e_{soi}⁻ with Na⁺ in ethylenediamine: O, [NaBr] = 1.6 × 10⁻³ M; [CsNHR] = 9 × 10⁻³ M; Δ, [NaBr] = 1.8 × 10⁻³ M, [KNHR] = 5 × 10⁻³ M.

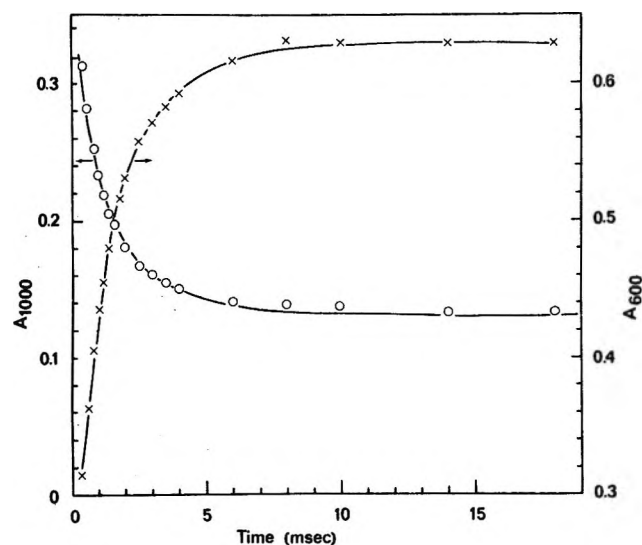
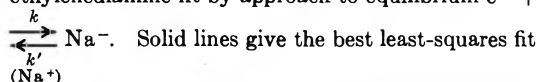


Figure 7. Decay of e_{soi}⁻ and growth of Na⁻ in ethylenediamine fit by approach to equilibrium e⁻ + e⁻



(Na⁺)
to both growth and decay simultaneously with adjustment of initial absorbances and *k*. Reverse rate constant calculated from final absorbances and *k*: O, decay at 1000 nm; X, growth at 600 nm.

solutions containing both Na⁺ and K⁺ with the latter in excess were studied by pulse radiolysis. In these cases, the reaction proceeded to an equilibrium in which appreciable absorbance remained at 1000 nm. Figure 6 compares the rate of decay of the absorbance at 1000 nm for a solution which contains Cs⁺ and one which contains about the same concentration of K⁺. Both solutions have about the same concentration of Na⁺. For reactions which did not go to completion, the decay of absorbance at 1000 nm and the growth at 600 nm were fit simultaneously by the rate law

$$\frac{d[\text{Na}^-]}{dt} = -\frac{1}{2} \frac{d[e_{\text{soi}}^-]}{dt} = k[e_{\text{soi}}^-]^2 - k'[\text{Na}^-] \quad (16)$$

The concentrations of e_{soi}⁻ and of Na⁻ were calculated from the absorbance values at the two wavelengths by using the extinction coefficients previously obtained. A typical fit of the data is shown in Figure 7 which gives the calculated and observed absorbances at the two wavelengths as a function of time. As shown in Figure 8, the values of the equilibrium "constant" *K*₅ calculated from the rate data as *k*'/*k* and also from the absorbances at equilibrium are nearly the same. The data are summarized in Table II.

Table II: Kinetic and Equilibrium Data for the Reaction of e_{soi}⁻ with Na⁺ in Ethylenediamine in the Presence of an Excess of K⁺ ^a

10 ³ · [Na ⁺], ^b M	10 ² [K ⁺], ^b M	10 ⁻³ <i>k</i> ', ^c sec ⁻¹	10 ⁻⁶ <i>k</i> / <i>k</i> ', M ⁻¹	10 ³ · [Na ⁻] [∞] , M	10 ⁶ [e ⁻] [∞] , M	10 ⁻⁶ <i>K</i> ₅ , ^d M ⁻¹
0.9	2	3.8	0.30	0.25	0.81	0.38
0.9	2	5.0	0.18	0.43	1.12	0.34
1.8	5	2.1	0.91	0.26	0.50	1.02
1.8	5	1.6	1.75	0.19	0.39	1.23
1.8	5	3.1	0.51	0.21	0.56	0.68
2.7	5	0.77	7.1	0.25	0.18	8.0
2.7	5	0.74	6.3	0.37	0.23	7.2
2.7	5	0.68	12.1	0.21	0.21	4.7
7.5	11	<i>e</i>	...	0.50	0.11	39
7.5	81	<i>e</i>	...	0.50	0.15	23
7.5	81	2.4	6.6	0.42	0.22	8.8
7.5	81	1.6	10.6	0.41	0.18	12.7
7.5	170	0.64	2.8	0.46	0.28	5.9
7.5	170	1.67	11.5	0.25	0.21	5.9
7.5	170	1.86	6.8	0.35	0.29	4.2

^a The run described in footnote *h* of Table I is not included.

^b Total molarity. The solution was made basic by decomposition of K metal solution. K⁺ added as KI, Na⁺ added as NaBr.

^c See eq 16. *k* and *k*' obtained by simultaneous least-squares fit of decay of absorbance at 1000 nm and growth at 600 nm. ^d Calculated as 10⁻⁶[Na⁻][∞]/([e⁻][∞])². ^e *k*' = 0 within uncertainty.

Figure 5 shows that the forward rate constant, *k*, has about the same dependence on the total sodium ion concentration as in the absence of potassium ions. The data are not extensive enough to permit a quantitative determination of the dependence of the rate constants and the equilibrium constant on the concentration of potassium and sodium ions. The value of *K*₅ decreases with decreasing [Na⁺] and with increasing [K⁺] as expected for the formation of a species such as K⁺,e⁻ from Na⁻ and K⁺. (These spectra and those obtained when KI was added to solutions of sodium in ethylenediamine¹⁰ show no evidence of the formation of the band of K⁻ at 850 nm.) However, attempts to fit the data with several simple equilibrium schemes failed, largely because they predicted a much larger effect at high concentrations of K⁺ than was observed. Both these data

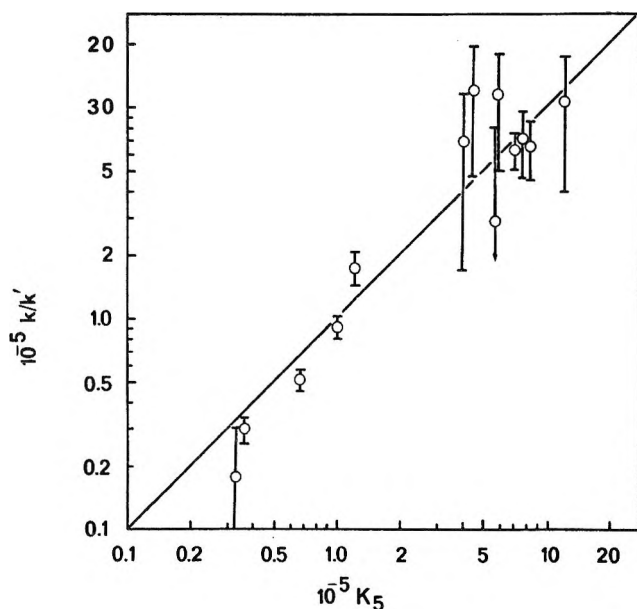


Figure 8. k/k' obtained from least-squares fit of kinetic data compared with the equilibrium constant, K_5 , obtained from absorbances at the end of reaction. Error bars calculated from ± 1 standard deviation on k' .

and those obtained previously¹⁰ show that the potassium ion has a significantly greater affinity for the electron than does cesium ion.

Conclusions

Recent kinetic studies of the formation of M^{-4-7} in amines and ethers have been interpreted in terms of an

intermediate of stoichiometry M to which a second electron adds in a subsequent step. Indeed, consideration of coulombic interactions leads us to expect the diffusion-controlled formation of ion pairs. However, the present studies indicate that the formation of Na^- in ethylenediamine occurs by reaction of Na^+ with a species which already contains two electrons.

The conclusions from this work may be compared with other recent studies⁴⁻⁷ in which different experimental methods have been used. The experimental results from the photochemical studies of Gaathon and Ottolenghi⁴ and of Huppert and Bar-Eli⁵ are similar to ours. The absence of an ionic strength effect would be expected if most of the electrons formed ion pairs. The equation used by Glarum and Marshall⁶ to fit their data (their eq 4a) has the same dependence on the cation concentration as that given by eq 15, derived from our proposed mechanism. The high value of the preexponential noted by Glarum and Marshall⁶ does not rule out the present mechanism because the observed second-order rate constant is a combination of rate constants and concentrations. The results of Kloosterboer, *et al.*,⁷ indicate that in the ethers which they used (diglyme, DME, tetraglyme), a new species of stoichiometry Na is formed. Its absorption at 830 nm is so far removed from that of their stated absorption maximum for the solvated electron (≈ 1500 nm) that it cannot be merely a "loose" ion pair Na^+, e^- . Since no similar transient was observed in the present work in ethylenediamine, no direct comparison with the kinetics in these ethers can be made.

Electron Spin Resonance and Pulse Radiolysis Studies of the Reactions of OH and O⁻ Radicals with Aromatic and Olefinic Compounds¹

by P. Neta,^{*2} Morton Z. Hoffman,³ and M. Simic⁴

Radiation Research Laboratories and Center for Special Studies, Mellon Institute of Science, Carnegie-Mellon University Pittsburgh, Pennsylvania 15213,
Department of Chemistry, Boston University, Boston, Massachusetts 02215,
Department of Zoology, University of Texas, Austin, Texas 78712, and
Pioneering Research Laboratory, U. S. Army Natick Laboratories, Natick, Massachusetts 01760
(Received October 6, 1971)

Publication costs assisted by Carnegie-Mellon University and the U. S. Atomic Energy Commission

The reactions of OH and O⁻ radicals with several aromatic or unsaturated organic compounds in irradiated aqueous solutions have been studied using both electron spin resonance and pulse radiolysis techniques. Each compound examined could react with the radical by addition to a double bond or aromatic ring or by hydrogen abstraction from an aliphatic chain. The relative yields of the radicals produced by the two possible mechanisms were compared at different pH values where either OH ($pK_a = 11.9$) or O⁻ is the main reacting radical. The results indicate that the rate of addition of O⁻ to an aromatic ring or to a double bond is much lower than that of OH, whereas the rates of hydrogen abstraction are comparable. For example, phenylacetic acid undergoes addition of OH to the ring but its reaction with O⁻ involves H abstraction from the CH₂ group. Similar results were obtained with diphenylacetic acid, *o*-, *m*-, and *p*-methylbenzoic acids, *p*-methoxybenzoic acid, benzyl alcohol, *p*-benzenedimethanol, *p*-phenylenediacetic acid, thymine, and crotonic acid. These findings also suggest the use of O⁻ for the production of radicals containing a double bond or an aromatic ring which cannot be produced by the reactions of OH or H since these latter radicals add to the unsaturated site in preference to abstraction.

Introduction

Differences between the reactivities of the neutral and the dissociated forms of the hydroxyl radical (OH \rightleftharpoons O⁻, $pK = 11.9$,⁵ 11.8⁶) have been demonstrated in several systems. Whereas most inorganic anions examined have been found to react with O⁻ much more slowly than with OH,⁷⁻⁹ cations react more rapidly,⁷ and oxygen reacts only with O⁻ and with a very high rate constant.¹⁰ Studies on organic compounds are scarce, but generally O⁻ has been found to react more slowly than OH. The difference in reactivity is small (less than a factor of 2) in case of hydrogen abstraction from aliphatic alcohols,^{7-9,11} but much larger (perhaps more than two orders of magnitude) in case of addition to benzoate ion.¹¹

It appeared to us that observation of the radicals formed by the reactions of OH and O⁻ both by esr and by pulse radiolysis could throw some light on the relative importance of the two reactions. We have chosen to compare the reactivities of OH and O⁻ with organic compounds that can undergo reaction by two modes: addition to an aromatic or olefinic system and hydrogen abstraction. By using esr and optical absorption techniques, the specificity of the reaction of OH and O⁻ could be discerned and the rate constants evaluated.

Experimental Section

The organic compounds studied were phenylacetic acid (Eastman Organic Chemical), diphenylacetic acid

(Eastman Organic Chemical), benzyl alcohol (Baker Analyzed Reagent), *o*-, *m*-, and *p*-methylbenzoic acid (Matheson Coleman and Bell and Aldrich), *p*-methoxybenzoic acid (K & K Laboratories), *p*-benzenedimethanol (Aldrich), *p*-phenylenediacetic acid (Aldrich), thymine (Cyclo Chemical), and crotonic acid (Matheson Coleman and Bell). Solutions for the pulse radiolysis experiments were prepared in triply distilled water and for the esr experiments in doubly distilled water. The pH of solutions was adjusted using Baker Analyzed potassium hydroxide. At pH < 11 solutions were buffered using Baker Analyzed sodium phosphates or sodium tetraborate. All solutions were saturated with N₂O which converts e_{aq}⁻ into OH or O⁻.

The esr experiments were performed at the Mellon

(1) Supported in part by the U. S. Atomic Energy Commission, by NSF Grant GP 11213, and by NIH Grant GM-13557.

(2) Carnegie-Mellon University.

(3) Boston University.

(4) University of Texas.

(5) J. Rabani and M. S. Matheson, *J. Phys. Chem.*, **70**, 761 (1966).

(6) J. L. Weeks and J. Rabani, *ibid.*, **70**, 2100 (1966).

(7) D. Zehavi and J. Rabani, *ibid.*, **75**, 1738 (1971).

(8) G. V. Buxton, *Trans. Faraday Soc.*, **65**, 2150 (1969); **66**, 1656 (1970).

(9) G. Hughes and H. A. Makada, *ibid.*, **64**, 3276 (1968).

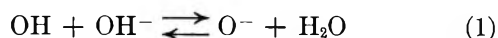
(10) G. E. Adams, J. W. Boag, and B. D. Michael, *Nature* (London), **205**, 898 (1965); *Proc. Roy. Soc., Ser. A*, **289**, 321 (1966).

(11) B. L. Gall and L. M. Dorfman, *J. Amer. Chem. Soc.*, **91**, 2199 (1969).

Institute by the steady-state *in situ* radiolysis-esr technique recently described.¹² The esr spectra were recorded while the solution was flowing through a flat silica cell located in the esr cavity and was being irradiated with 2.8-MeV electrons from a Van de Graaff accelerator. The pulse radiolysis experiments were performed at the U. S. Army Natick Laboratories using the kinetic spectrophotometry technique previously reported.¹³ Here the radiation source was a Febetron 705 instrument which provided 30-nsec pulses of 2.3-MeV electrons.

Results and Discussion

The radiolysis of neutral and mildly alkaline aqueous solutions generates e_{aq}^- , OH, and H with *G* values of approximately 2.8, 2.8, and 0.6, respectively.¹⁴ In the presence of N_2O , e_{aq}^- is virtually completely converted to O^- , which is in rapid equilibrium with OH ($k_1 = 1.2 \times 10^{10} M^{-1} sec^{-1}$, $k_{-1} = 9.2 \times 10^7 sec^{-1}$)³



Thus the form of the species reacting with the organic solute is controlled by the pH of the system. Under these conditions the contribution from the reaction of the H atoms does not exceed 12% and at high pH H reacts with OH^- to form e_{aq}^- which in turn is converted to O^- by reaction with N_2O . In all experiments carried out in the present study the concentrations of the organic solutes were $\sim 10^{-3} M$, ensuring quantitative scavenging of the OH radicals in mildly alkaline solutions since the rate constants for the reaction of OH with these compounds are close to $10^{10} M^{-1} sec^{-1}$. In strongly alkaline solutions equilibrium 1 will be achieved before reaction of OH or O^- with the solute occurs. Under equilibrium conditions the apparent rate constant for the reaction of a solute S with OH and O^- to form a transient with a rate constant of formation k_{obsd} is

$$k_{obsd} = k_{OH+S} \left(\frac{[H^+]}{[H^+] + K_{OH}} \right) + k_{O^-+S} \left(1 - \frac{[H^+]}{[H^+] + K_{OH}} \right) \quad (I)$$

where $K_{OH} = 1.26 \times 10^{-12}$. Determination of k_{obsd} at different pH values can yield both k_{O^-+S} and k_{OH+S} if both O^- and OH lead to the formation of the same transient. However, if two different radicals are formed by the reactions of O^- and OH the relative extinction coefficients of the two transients at the monitoring wavelength must be taken into account. If the rate of formation of a transient can be measured under such conditions that the transient of interest is predominantly formed and is the only absorbing species at the monitoring wavelength, the rate constant for the formation of this transient can be directly determined. It is, therefore, necessary to determine the transient ab-

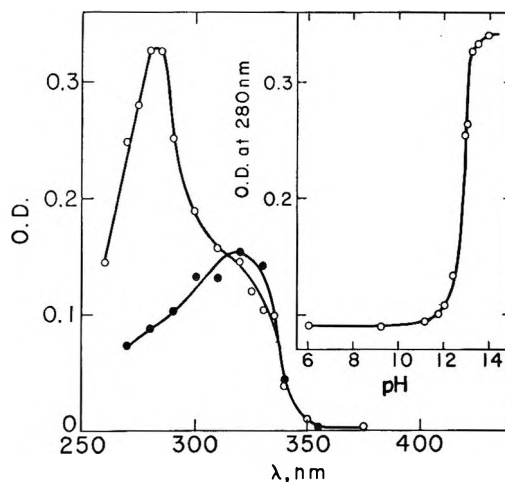


Figure 1. Transient absorption spectra resulting from the reactions of OH and O^- radicals with phenylacetic acid. Solutions containing $2 \times 10^{-3} M$ phenylacetic acid and saturated with N_2O were irradiated at pH 9.3 (●) and at pH 13.6 (○). The insert shows the effect of pH on the initial optical density at 280 nm. The irradiation dose was 2 krad/pulse.

sorption spectra as a function of pH in order to make a judicious choice of conditions. A change in transient absorption spectrum and k_{obsd} with change in pH serves as an indication of the difference in the mode of attack of OH and O^- . The esr spectra recorded with irradiated solutions at different pH values will identify the main radicals formed and indicate any change in site of attack.

Pulse Radiolysis Experiments

The transient absorption spectra observed from irradiated aqueous solutions of phenylacetic acid saturated with N_2O at pH 9.3 and pH 13.6 are shown in Figure 1. The optical density was measured less than 1 μsec after the 30-nsec Febetron pulse, after the formation of the transient was complete and before any appreciable decay took place. The spectrum observed at pH 9.3 is very similar to that reported previously¹⁵ and can be assigned to the radical formed by OH addition to the aromatic ring. All of the three possible isomers are expected to be formed simultaneously as has been recently demonstrated by esr for the case of benzoic acid.¹² Hydrogen abstraction by OH from the aliphatic side chain should take place at a rate which is comparable to that for aliphatic acids, for example propionic acid.¹⁶ At this pH abstraction is expected to account for less than 10% of the OH reactions.¹⁵

(12) K. Eiben and R. W. Fessenden, *J. Phys. Chem.*, **75**, 1186 (1971).

(13) M. Simic, P. Neta, and E. Hayon, *ibid.*, **73**, 3794 (1969).

(14) See, e.g., M. Anbar in "Fundamental Processes in Radiation Chemistry," P. Ausloos, Ed., Interscience, New York, 1968, p 651.

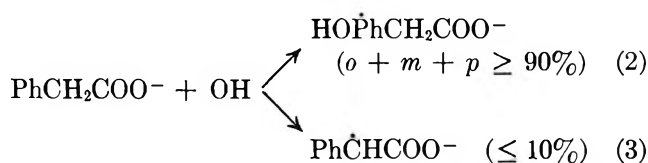
(15) P. Neta and L. M. Dorfman, *Advan. Chem. Ser.*, **81**, 222 (1968).

(16) M. Anbar and P. Neta, *Int. J. Appl. Radiation Isotopes*, **18**, 493 (1967).

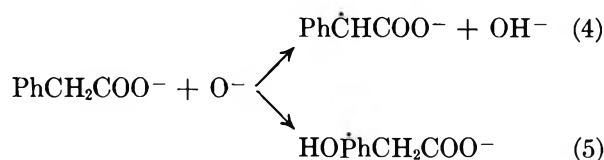
Table I: Rate Constants and Transient Absorptions in the Reactions of OH and O⁻ with Some Aromatic Compounds

Compound	pH 9			pH 14		
	$k_{\text{OH}+\text{S}}, M^{-1} \text{ sec}^{-1}$	$\lambda_{\text{max}}, \text{ nm}$	$\epsilon \text{ (at } \lambda_{\text{max}}), M^{-1} \text{ cm}^{-1}$	$k_{\text{O}^{-}+\text{S}}, M^{-1} \text{ sec}^{-1}$	$\lambda_{\text{max}}, \text{ nm}$	$\epsilon \text{ (at } \lambda_{\text{max}}), M^{-1} \text{ cm}^{-1}$
Benzoic acid	6.0×10^9 ^a	350 ^b 330 ^c	3,800 ^b 3,600 ^c	4×10^7 ^b	350 ^b	3,800 ^b
Phenylacetic acid	7.9×10^9 ^a	320	5,400	2×10^8	282	$\geq 11,000$
Diphenylacetic acid	4×10^9	320	5,250	6×10^7	340	$\geq 9,000$
<i>p</i> -Methylbenzoic acid	8×10^9	340	3,550	5×10^8	280	$\geq 27,000$
Thymine	5.5×10^9	375	...	4×10^8	<330	...

^a From ref 10. ^b From ref 12. ^c From ref 13.



The spectrum recorded at pH 13.6 indicates some contribution by the OH adduct at 320 nm but the main absorption at 280 nm must be due to the presence of a completely different radical. Since the rate of O⁻ addition to the ring is much slower than that of OH, whereas the rate of abstraction does not change significantly, it must be concluded that the contribution by the abstraction reaction would be greater than addition to the ring at pH 13.6. The main radical formed at this pH is, therefore, Ph $\dot{\text{C}}\text{HCOO}^-$ with an absorption maximum at 282 nm.



Reaction 5 represents the addition of O⁻ to the aromatic ring; the species produced is written in its protonated form equivalent to the OH adduct. O⁻ radical addition to the aromatic ring in benzoate at pH 14 generates a transient species,¹⁷ the absorption spectrum of which is identical with that of the OH adduct^{17,18} indicating that deprotonation of the OH group probably does not take place at pH ≤ 14 . This finding is consistent with the previous observation¹³ that an unpaired electron at position β to a hydroxyl group does not decrease the pK of this group and therefore dissociation can be expected to take place at pH > 14 as in cyclohexanol.

Comparison of the spectra at pH 9.3 and 13.6 would allow estimation of the relative yields of the different radicals at the different pH values. It can be estimated that the contribution of reaction 3 at pH 9.3 does not exceed 10% and that of reaction 5 at pH 13.6 does not exceed 30%. The extinction coefficients for the HO $\dot{\text{P}}\text{hCH}_2\text{COO}^-$ and Ph $\dot{\text{C}}\text{HCOO}^-$ radicals were calculated by a comparison with the formation of (CNS)₂⁻ (using $\epsilon_{(\text{CNS}_2^-)}^{500} = 7600$ ¹⁹) and were found to be 5400

and $\geq 11,000 M^{-1} \text{ cm}^{-1}$ at their respective maxima (Table I).

The effect of pH on the initial optical density at 280 nm is shown in the insert of Figure 1. The inflection point of this curve should be higher than the pK for OH by the ratio of the rate constants of OH and O⁻ and is only slightly less than expected.

The weighted average rate constant for the net reaction of OH and O⁻ with phenylacetic acid at pH 14 was measured from the rate of formation of the transient at 290 nm and found to be $k_{\text{obsd}} = 2.2 \times 10^8 M^{-1} \text{ sec}^{-1}$. From the known rate constant for the OH radical addition to phenylacetic acid, $7.9 \times 10^9 M^{-1} \text{ sec}^{-1}$,¹⁵ the partial contribution of k_{OH} at pH 14 is calculated from eq I to be $6.2 \times 10^7 M^{-1} \text{ sec}^{-1}$. The rate constant for the reaction of O⁻ is, therefore, $2 \times 10^8 M^{-1} \text{ sec}^{-1}$. This value is accurate only to about $\pm 30\%$ since no correction can be made for the different yields and extinction coefficients of the radicals formed. A similar experiment with benzoate,¹⁷ where only addition to the ring can take place, gave $k_{\text{obsd}} = 8.5 \times 10^7 M^{-1} \text{ sec}^{-1}$ at pH 14. The contribution of OH from eq I, taking $k_{\text{OH}} = 6.0 \times 10^9 M^{-1} \text{ sec}^{-1}$,¹⁵ is $4.7 \times 10^7 M^{-1} \text{ sec}^{-1}$, which leaves about $4 \times 10^7 M^{-1} \text{ sec}^{-1}$ for $k_{\text{O}^{-}+\text{benzoate}}$. This value is almost an order of magnitude higher than the previously given upper limit¹¹ obtained indirectly from competition kinetics. Both results indicate, however, that the addition of O⁻ to an aromatic ring is at least two orders of magnitude slower than the addition of OH. A comparison of these results with the above value obtained for phenylacetic acid supports the conclusion arrived at on the basis of the spectra that the majority of O⁻ radicals reacting with this latter compound abstract hydrogen from the CH₂ group and do not add to the aromatic ring.

Diphenylacetic acid was similarly studied and some of the results are shown in Figure 2. The difference between the spectra at pH 9.3 and pH 14 again suggests that O⁻ forms a radical different from that formed by

(17) M. Simic and M. Z. Hoffman, *J. Phys. Chem.*, in press.

(18) R. Wander, P. Neta, and L. M. Dorfman, *J. Phys. Chem.*, **72**, 2946 (1968).

(19) J. H. Baxendale, P. L. T. Bevan, and D. A. Stott, *Trans. Faraday Soc.*, **64**, 2389 (1968).

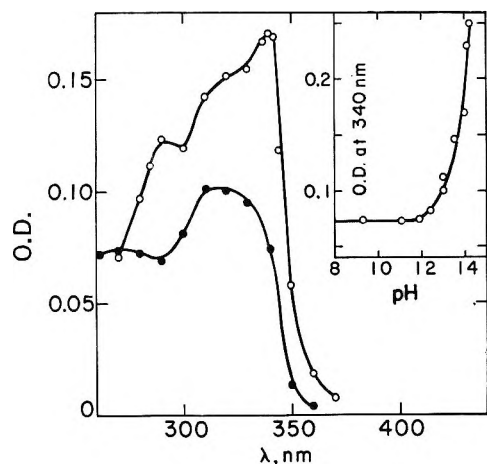


Figure 2. Transient absorption spectra resulting from the reactions of OH and O^- radicals with diphenylacetic acid. Solutions containing $1 \times 10^{-3} M$ diphenylacetic acid and saturated with N_2O were irradiated at pH 9.3 (●) and at pH 14 (○). The insert shows the effect of pH on the initial optical density at 340 nm.

OH. The radical formed by the reaction of O^- is most probably $Ph_2\dot{C}COO^-$ resulting from H abstraction. The transient absorption maxima and extinction coefficients are given in Table I. The rate constants for the formation of the transient absorption at 340 nm were measured at different pH values and were found to be the following: pH 9.1: 4×10^9 , pH 12.4: 5×10^8 , pH 13.0: 2.0×10^8 , pH 13.5: 1.5×10^8 , pH 13.8: 1.1×10^8 , and pH 14.0: $9 \times 10^7 M^{-1} sec^{-1}$. Using the value found at pH 9.1 as the rate constant for the reaction of OH with diphenylacetic acid the values of k_{obsd} measured at pH 12.4 and 13 are in reasonable agreement with eq I. From the three values of k_{obsd} at pH 13.5–14.0 a rate constant of $6 \times 10^7 M^{-1} sec^{-1}$ can be calculated for the reaction of O^- with diphenylacetic acid to form the $Ph_2\dot{C}COO^-$ radical.

The transient absorption spectra obtained with irradiated solutions of *p*-methylbenzoic acid are presented in Figure 3. The hydroxycyclohexadienyl radical formed at pH 9.1 shows absorption characteristic of this type of radical¹⁵ with maximum at 340 nm and $\epsilon = 3550 M^{-1} cm^{-1}$. Another weak band of absorption is observed around 280 nm. The radical formed at pH 14 shows little absorption at 340 nm but a very strong band at 280 nm with $\epsilon \geq 27,000$. This radical is assigned as the *p*-carboxybenzyl radical formed by hydrogen abstraction from the methyl group. The spectrum observed for this radical is different from that reported for the benzyl radical which has absorption bands at 305 and 317 nm.^{20, 21} The position of the carboxyl group profoundly alters the absorption spectrum of the benzyl radical; in the case of *o*- and *m*-methylbenzoic acids at pH 14 the extremely strong absorption band of the *p*-carboxybenzyl radical at 280 nm is not present.

The rate constant for the reaction of O^- with *p*-

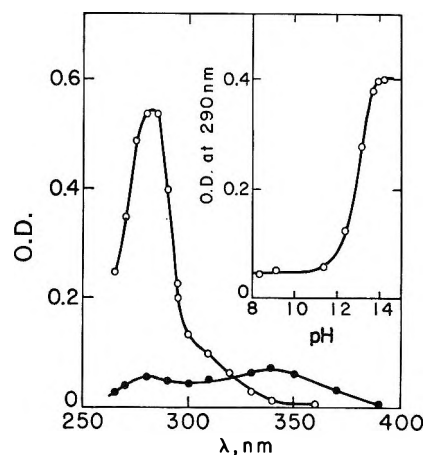


Figure 3. Transient absorption spectra resulting from the reactions of OH and O^- radicals with *p*-methylbenzoic acid. Solutions containing $1 \times 10^{-3} M$ *p*-methylbenzoic acid and saturated with N_2O were irradiated at pH 9.1 (●) and at pH 14 (○). The insert shows the effect of pH on the initial optical density at 290 nm.

p-methylbenzoic acid at pH 14 was measured by following the formation of the transient absorption at 280 nm and k_{obsd} was found to be $5 \times 10^8 M^{-1} sec^{-1}$. The rate constant for the OH reaction was not measured but can be estimated as $8 \times 10^9 M^{-1} sec^{-1}$, comparable to that for phenylacetic acid.¹⁵ The contribution of k_{OH} at pH 14 would be about $5 \times 10^7 M^{-1} sec^{-1}$, or only about 10% that of O^- . Since the absorption of the OH adduct at 280 nm is <10% that of the radical formed by O^- reaction (Figure 3) the rate constant of $5 \times 10^8 M^{-1} sec^{-1}$ can be practically attributed completely to the reaction of O^- with *p*-methylbenzoic acid. This number is reasonable when compared to other rate constants^{7-9, 11} for hydrogen abstraction by O^- (methanol for example), since the hydrogen atoms at position α to the aromatic ring are expected to be easily abstractable. The rate constants for H abstraction by O^- from *p*-methylbenzoic acid, phenylacetic acid, and diphenylacetic acid decrease in that order with the decrease in the number of H atoms available at the α position, although substituent effects also contribute to these changes.


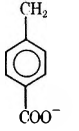
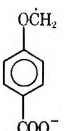
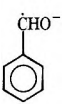
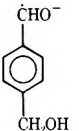
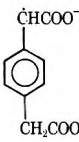
Similar results have been obtained with thymine. The addition of OH to thymine generates a radical which shows λ_{max} 375 nm. At high pH an additional strong absorption band appears at $\lambda < 330$ nm which is attributed to the radical formed by hydrogen abstraction from the methyl group of thymine. Because of the high extinction coefficient of thymine the maximum of the transient absorption could not be determined. In a previous radiolysis study of thymine²² it

(20) H. T. J. Chilton and G. Porter, *J. Phys. Chem.*, **63**, 904 (1959).

(21) R. J. Hagemann and H. A. Schwarz, *ibid.*, **71**, 2694 (1967).

(22) L. S. Myers, Jr., M. L. Hollis, L. M. Theard, F. C. Peterson, and A. Warnick, *J. Amer. Chem. Soc.*, **92**, 2875 (1970).

Table II: ESR Parameters for Organic Radicals Produced by Reactions of O⁻ in Irradiated Aqueous Solutions at pH 14

Compound	Suggested Radical	<i>g</i> factor ^a	Hyperfine Constants ^b
Phenylacetic acid		2.00298	$a_{\alpha}^H = 15.04$ $a_o^H = 4.67$ (2) $a_m^H = 1.58$ (2) $a_p^H = 5.51$
<i>p</i> -Methylbenzoic acid		2.00273	$a_{\alpha}^H = 15.76$ (2) $a_o^H = 5.07$ (2) $a_m^H = 1.77$ (2)
<i>p</i> -Methoxybenzoic acid		2.00300	$a_{\alpha}^H = 17.74$ (2) $a_o^H = 0.52$ (2) $a_m^H = 0.26$ (2)
Benzyl alcohol		2.00333	$a_{\alpha}^H = 12.60$ $a_o^H = 5.01; 4.18$ $a_m^H = 1.56; 1.27$ $a_p^H = 6.17$
<i>p</i> -Benzenedimethanol		2.00319	$a_{\alpha}^H = 12.23$ $a_o^H = 5.07; 4.19$ $a_m^H = 1.60; 1.23$ $a_{CH_2}^H = 3.34$ (2)
<i>p</i> -Phenylenedi-acetic acid		2.00299	$a_{\alpha}^H = 14.84$ $a_o^H = 4.61; 4.56$ $a_m^H = 1.53$ (2) $a_{CH_2}^H = 4.04$ (2)
Crotonic acid	$CH_2 \cdots \dot{C}H \cdots CH - COO^-$	2.00298	$a_{\alpha}^H = 12.76$ $a_{\beta}^H = 3.92$ $a_{\gamma}^H = 13.40; 13.69$

^a The *g* factors are measured relative to the peak from the silica cell and are accurate to ± 0.00005 . Second-order corrections have been made [R. W. Fessenden, *J. Chem. Phys.*, **37**, 747 (1962)]. ^b Hyperfine constants are given in gauss and are accurate to ± 0.03 G. Where two protons are equivalent this is indicated parenthetically.

was suggested that the reaction of O⁻ with this compound involves hydrogen abstraction from the CH₂ group in contrast to the reaction of OH which adds to the 5,6-double bond of thymine. These suggestions are further confirmed by the observation of the esr spectra of the radicals formed in irradiated aqueous solutions of thymine at different pH values.²³ At pH < 13 only the OH adduct radical was observed whereas at pH > 13 the main radical formed was that obtained by abstraction.

Electron Spin Resonance Experiments

In these experiments esr spectra were recorded with *in situ* irradiated solutions at different pH values. The spectrum observed with phenylacetic acid at pH 12 consisted of a large number of lines of relatively low intensity. They could be accounted for by at least two, and possibly three, radicals but they could not be fully analyzed because too many lines overlapped and the low field lines were partly within the noise level. Most probably all three isomers of the hydroxycyclo-

hexadienyl radical are formed, as in the case of benzoic acid.¹² Because of the CH₂ group in phenylacetic acid there are 3 times as many lines but of lower intensity, making analysis very difficult. At pH 14 the intensity of these lines was much lower and only the most intense were observed. However, a new spectrum appeared which was absent at pH 12. The lines were sufficiently intense to allow full observation of the whole spectrum. A complete analysis was made and the parameters are summarized in Table II. The radical formed from phenylacetic acid at pH 14 shows a 15 G doublet with additional splittings by two sets of two equivalent hydrogen atoms and another single hydrogen. The coupling constants are very similar to those reported for the benzyl radical.²⁴⁻²⁶ The 15-G doublet can only be assigned to the alpha hydrogen in the radical Ph $\dot{C}H$ -

(23) P. Neta, *Radiation Res.*, in press.

(24) W. T. Dixon and R. O. C. Norman, *J. Chem. Soc.*, 4857 (1964).

(25) H. Fischer, *Z. Naturforsch. A*, **20**, 488 (1965).

(26) A. Carrington and I. C. P. Smith, *Mol. Phys.*, **9**, 137 (1965).

COO⁻ as indicated in Table II. The 5.5-G doublet can be assigned to the hydrogen at the para position and the triplet splittings are assigned to the ortho and meta positions similarly to the case of the radical from benzyl alcohol.^{25,27} The *g* factor is very different from the value of 2.0022 expected for hydroxycyclohexadienyl radicals.¹² It is, therefore, concluded that the reaction of O⁻ with phenylacetic acid yields the Ph \dot{C} HCOO⁻ radical. In this radical, as in other benzyl radicals, the conjugation of the unpaired electron on the α carbon with the aromatic π system does not allow free rotation around the Ph-C bond. When the radical is asymmetric around this bond all the hydrogens on the ring are expected to have different hyperfine constants. This was confirmed for the Ph \dot{C} HOH radical^{25,27} and for Ph \dot{C} HO⁻ (see below). For the Ph \dot{C} HCOO⁻ radical, however, the two ortho hydrogens show the same splitting (4.67 G) and appear to be equivalent (to within 0.1 G). The reason for this apparent difference is not clear. The fact that the meta hydrogens appear to be equivalent is not important because the difference between two very small splittings could be unobservable.

Similar experiments were carried out with *p*-methylbenzoic acid, *p*-methoxybenzoic acid, and benzyl alcohol, but in these cases the line intensities found at pH 10-12 were too low for analysis and the radicals formed by OH addition to the ring could not be identified. However, higher intensity lines were observed at pH 13.5-14 and are assigned as summarized in Table II. In all cases the main spectrum recorded at pH 14 was practically absent (<10%) at pH 12.

The parameters calculated for the *p*-carboxybenzyl radical (Table II) are similar to those reported for benzyl radical.²⁴⁻²⁶ The hyperfine splitting constant by the CH₂ group is slightly smaller for *p*-carboxybenzyl than the value of 16.4 G observed for benzyl, most probably because of the electron withdrawing effect of the carboxyl group. The *g* factor for the benzyl radical is also lower (2.00260)²⁸ than that for the *p*-carboxybenzyl radical.

The irradiation of *p*-methoxybenzoic acid at pH 13.8 led to the formation of the $\dot{C}H_2OPhCOO^-$ radical by hydrogen abstraction and again this radical was not detected at pH 11.7 and 8.5. The *g* factor and the α -proton splitting for this radical (Table II) resemble those for the $\dot{C}H_2OH$ radical.¹² Very little spin density is transmitted to the ring as is exemplified by the hyperfine constants for the ortho and meta hydrogen atoms which are an order of magnitude smaller than those in the benzyl-type radicals. Both of these facts are consistent with the structure given in Table II in which the unpaired electron is localized on the CH₂ group.

The spectrum recorded with an irradiated solution of benzyl alcohol at pH 14 consisted of 64 lines of equal intensities. Since the spectrum of Ph \dot{C} HOH obtained by photolysis of benzyl alcohol + hydrogen peroxide contained twice as many lines²⁷ it is concluded that the

radical observed at pH 14 must exist in the dissociated form Ph \dot{C} HO⁻. This is expected, since a *pK* = 8.4 for the Ph \dot{C} HOH radical has been determined by pulse radiolysis.²⁹ The α -hydroxybenzyl radical could also be produced at lower pH values by the partial (< 20%) reaction of OH, but its steady-state concentration must be very low and it was not detected at pH 9.5. The five hydrogen atoms on the ring of Ph \dot{C} HO⁻ all have different hyperfine constants (Table II) as was found²⁷ for Ph \dot{C} HOH. The values for the two radicals are comparable and the inequivalence is slightly more pronounced in the dissociated radical. The *g* factor is higher and the alpha proton splitting is lower for Ph \dot{C} HO⁻ as compared to Ph \dot{C} HOH, in agreement with similar findings of the effect of proton dissociation on esr parameters for other radicals (see, *e.g.*, ref 12).

A spectrum was observed with an irradiated solution of diphenylacetic acid at pH 14 which was not present at pH 12. All the splittings are small and the total spread of the spectrum was only about half that of Ph \dot{C} HCOO⁻. Complete analysis was not possible because a large portion of the lines was masked by the signal from the silica cell. However, the radical formed is probably Ph₂ $\dot{C}COO^-$, as it does not show any large splitting and the *g* factor is approximately 2.0028.

Solutions of *p*-benzenedimethanol and *p*-phenylenediacetic acid were also studied at pH 11.5 and pH 14. It was hoped that under mildly alkaline conditions OH addition to the ring would produce only one isomer with an analyzable spectrum, but unfortunately, the lines were not sufficiently intense. This fact could be due to the increase in the number of lines or in the portion of OH reacting with the side chains. The spectra observed at pH 14 were much more intense than those at pH 11.5 and were analyzed in terms of the parameters and structures given in Table II. It is clear that O⁻ reacts with the aliphatic side chain to abstract a hydrogen atom. The parameters found for the radical obtained from benzenedimethanol are similar to those for the radical from benzyl alcohol except for the para hydrogen splitting of 6.2 G which is replaced by a 3.3 G triplet splitting by the CH₂ group. For phenylenediacetic acid the hyperfine constants are similar to those for the radical obtained from phenylacetic acid, with the obvious change in the para position, but the non-equivalence of the ortho hydrogens could be detected.

In all the compounds studied so far a comparison was made between OH addition to the aromatic ring and hydrogen abstraction by O⁻ from an aliphatic side chain. In order to compare the rates for the addition of OH and O⁻ to an aliphatic double bond, crotonic acid was examined at pH 11 and 14. With solutions

(27) R. Livingston and H. Zeldes, *J. Chem. Phys.*, **44**, 1245 (1966).

(28) P. Neta and R. H. Schuler, to be published.

(29) J. Lilie and A. Henglein, *Ber. Bunsenges. Phys. Chem.*, **73**, 170 (1969).

irradiated at the lower pH value in the presence of N_2O two radicals were detected, both formed by addition of OH to the double bond. The radical $CH_3\dot{C}HOH\dot{C}HCOO^-$ has a g factor of 2.00301 and the hyperfine constants are $a_{\alpha}^H = 20.41$ G, $a_{\beta}^H = 15.70$ G, $a_{CH_3}^H = 1.44$ G, and $a_{OH}^H = 0.35$ G. The second radical observed at pH 11 was identified as $CH_3\dot{C}HCHOH\dot{C}OO^-$ by the following parameters: $g = 2.00257$, $a_{CH_3}^H = 25.45$ G, $a_{\alpha}^H = 21.65$ G, $a_{\beta}^H = 15.58$ G. The values of the hyperfine constants for these two radicals are similar to those reported by Fischer³⁰ for the corresponding undissociated radicals. It is estimated that OH radicals add to the double bond of crotonic acid to form the two possible radicals at comparable rates. At pH 14, however, none of these adducts is observed and instead a different radical is formed with hyperfine constants characteristic of an allyl-type^{27,31} radical: 13.69, 13.40, 12.76, and 3.92 G. This radical must have the structure $CH_2\dot{C}H\dot{C}H-COO^-$ as formed by hydrogen abstraction from the methyl group with the assignment of the splittings as given in Table II. This again demonstrates that the rate constant for addition of O^- is very low compared to the addition of OH and the abstraction of hydrogen by O^- .

Conclusion

The results presented clearly show that the main course of reaction of the hydroxyl radical with aromatic and olefinic organic compounds is different for OH and O^- . The rate of addition of OH to the double bond or to an aromatic ring is in most cases about an order of magnitude higher than the rate of abstraction. With O^- the situation is reversed. This difference can be utilized for the production of two radicals under different conditions. At pH < 12 radicals will be produced mainly by addition of OH and at pH > 13 radicals will be produced mainly by abstraction of hydrogen by O^- . This hydrogen abstraction process is particularly important because it appears to be unique to O^- in contrast to most other radicals which add to aromatic and olefinic compounds.

Acknowledgment. We thank Dr. E. Hayon of the U. S. Army Natick Laboratories for the use of the pulse radiolysis apparatus and his interest in this work.

(30) H. Fischer, *Z. Naturforsch. A*, **19**, 866 (1964).

(31) R. W. Fessenden and R. H. Schuler, *J. Chem. Phys.*, **39**, 2147 (1963).

Nuclear Magnetic Resonance Rate Studies of Hindered Rotation in

Methyl *N*-Acetylsarcosinate

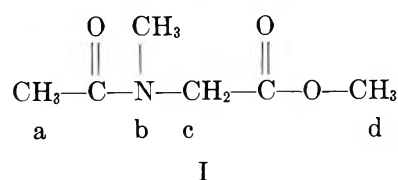
by Alan L. Love,¹ Terry D. Alger,* and Richard K. Olsen

Department of Chemistry, Utah State University, Logan, Utah 84321 (Received September 8, 1971)

Publication costs assisted by the National Institutes of Health

A rate study from about 40 to 80° was performed on the hindered rotation in methyl *N*-acetylsarcosinate. No evidence was observed at any temperature to indicate that any proton signals were split into anything more than a doublet, indicating a simple two-site problem. In addition, the rate parameters were in agreement for all signals, indicating that a single rate process controlled the reaction. The single rate process is most likely the hindered internal rotation due to the partial double bond character of the C-N amide bond. The rate parameters at about 62° for this process are $k \approx 7.2 \text{ sec}^{-1}$, $E_a = 17.7 \text{ kcal/mol}$, $\Delta F^\ddagger = 18.9 \text{ kcal/mol}$, $\Delta H^\ddagger = 16.9 \text{ kcal/mol}$, and $\Delta S^\ddagger = -4.5 \text{ eu}$.

Hindered internal rotation in amides, attributed to partial double-bond character in the C-N amide bond, has been extensively studied by nmr techniques.²⁻⁴ It is not surprising, therefore, that the *N*-methyl (b) and *N*-methylene (c) protons of methyl *N*-acetylsarcosinate (I) exhibit doublet splittings from the cis-trans isomerism possible from this type of restricted motion.⁵



It is unusual, however, that the acetyl methyl (a) and

methyl ester (d) protons should also be split into doublets since Gutowsky and Holm⁶ reported the signals due to the acetyl groups in the *N*-methyl- and *N,N*-dimethylacetamides to be singlets. As there are structural similarities in the latter compounds and I, there exists the possibility that the splittings of the a and d protons of I may not be due to hindered rotation about the amide bond, but rather may be due to an alternate source such as the exchange between folded and extended conformers as described for various dipeptides⁷ or alanylalanine⁸ derivatives. A rate study of the two groups of protons may resolve the question of the origin of the splittings. Protons a and d are considered one group which possibly exhibit folded-extended isomerism, while protons b and c are the other group exhibiting cis-trans isomerism. If the origin of the doublet spectra of the b and c protons is in fact different from that of the splittings in the a and d protons, the rates of exchange between their two-site environments would not be expected to be the same for the two cases of isomerism. On the other hand, if all protons are split by the same effect, the rates of exchange should be equal. Since each of the proton signals of I is only a doublet,⁵ discussions of multisite analysis beyond the two site case have been avoided. Any residual multisite effect should be evident in variations of the rate parameters for the various protons. It should be noted that while Bovey, Ryan, and Hood⁵ interpreted all doublets in I as arising from cis-trans isomerism, they performed no rate study to confirm this assumption. The present authors, however, have used all the proton assignments made in Bovey's paper.⁵

This article concentrates on a rate study of the a and b protons of methyl *N*-acetylsarcosinate (I). These protons were chosen since they possessed larger chemical shift differences under slow-exchange conditions for their respective groups. Compound I was prepared by the method of Olsen⁹ and sealed neat after repeated freeze-thaw degassing. All data were taken on a Varian A-60 spectrometer equipped with a variable temperature controller. Exchange rates were obtained by curve fitting experimental proton spectra with computer-calculated spectra for several trial exchange rates. The complete line-shape computer program was based on Kubo's method for many-site exchange.¹⁰ Measurements of parameters needed for rate calculations were made over a range of -25 to 80° in an attempt to minimize errors in the parameters. The plots for the log of the width of the signals at half-intensity ($W_{1/2}$) vs. $1/T$ gave straight lines in the regions of no exchange which were easily extrapolated into the exchange region to obtain the natural line widths. Plots of the logs of the populations (P) vs. $1/T$, and of the chemical shift (ω) vs. T also gave straight lines, which were extrapolated into the exchange region. None of the proton signals ever separated into more than a doublet nor

Table I: Rate Constants for the cis to trans Exchange of I

$t, ^\circ\text{C}$	$k_a, \text{sec}^{-1}{}^a$	$k_b, \text{sec}^{-1}{}^b$
38.6	...	1.2
45.1	...	1.5
45.9	0.95	...
51.3	1.2	2.9
52.9	...	4.8
55.0	5.5	6.3
57.6	...	4.5
59.6	5.1	6.7
61.6	7.2	9.4
61.8	7.1	7.4
66.4	7.8	11.0
71.4	9.5	15.0
76.5	13.5	...
80.2	16.0	...

^a Errors are approximately $\pm 30\%$. ^b Errors are approximately $\pm 20\%$.

Table II: Activation Parameters for the cis to trans Transition of I

	acetyl (a)	<i>N</i> -methyl (b)
$E_A, \text{kcal/mol}$	17.7 ± 3.3	17.8 ± 1.2
$\Delta H^\ddagger, \text{kcal/mol}$	16.9 ± 3.2	17.0 ± 1.1
$\Delta F^\ddagger, \text{kcal/mol}$	18.2 ± 0.28	18.8 ± 0.1
$\Delta S^\ddagger, \text{kcal/mol}$	-4.9 ± 11.4	-4.1 ± 3.8
$k (61.8^\circ), \text{sec}^{-1}$	5.2 ± 2.3	8.1 ± 1.2

gave any evidence that the exchange processes were multirate determined.

The rates for the exchange from the cis to the trans isomer (using the notation of proton signals for I from Bovey, *et al.*⁵) are reported in Table I from ca. 40 to 80° for protons a and b. The results are equal for both protons within experimental error. The results of the analysis of activation parameters are reported in Table II; these are also equal for protons a and b within ex-

(1) This article is based upon part of a thesis submitted by A. L. Love as partial fulfillment of requirements for a Ph.D. degree.

(2) (a) H. S. Gutowsky, D. W. McCall, and C. P. Slichter, *J. Chem. Phys.*, **21**, 279 (1953); (b) J. A. Pople, W. G. Schneider, and H. J. Bernstein, "High Resolution NMR," McGraw-Hill, New York, N. Y., 1959.

(3) J. W. Emsley, J. Feeny, and L. H. Sutcliffe, "High Resolution Nuclear Magnetic Resonance Spectroscopy," Vol. II, Pergamon Press, New York, N. Y., 1969.

(4) T. H. Siddall, W. E. Stewart, and F. D. Knight, *J. Phys. Chem.*, **74**, 3580 (1970).

(5) F. A. Bovey, J. J. Ryan, and F. C. Hood, *Macromolecules*, **1**, 305 (1968).

(6) H. S. Gutowsky and C. S. Holm, *J. Chem. Phys.*, **25**, 1228 (1956).

(7) M. Marraud, J. Neel, M. Avignon, and P. V. Huong, *J. Chim. Phys. Physicochim. Biol., Phys.*, **67**, 959 (1970).

(8) V. F. Bystrov, S. L. Portnova, V. Q. Tsetlin, V. T. Ivanov, and Yu. A. Ovchinnikov, *Tetrahedron*, **25**, 493 (1969).

(9) R. K. Olsen, *J. Org. Chem.*, **35**, 1912 (1970).

(10) This program was graciously supplied by Dr. M. Saunders of Yale University.

perimental error.¹¹ The only conclusion that can be drawn, therefore, is that the splittings observed in protons and of methyl *N*-acetylsarcosinate (I) are all due to cis-trans isomerism resulting from restricted rotation about the carbonyl-nitrogen amide bond. Any possible folded-extended isomerism motion is, therefore, too rapid (or too slow) on an nmr time scale to affect the spectra.

Acknowledgments. This work was supported by grants from the National Institutes of Health (CA 10653) and the National Science Foundation (GP 18436).

(11) The experimental error ($\pm 25\%$ average) is somewhat larger than in other nmr rate studies due to the relatively large viscosity of the solutions at the lower temperatures and due to the relatively small chemical shift differences between the cis and trans isomers.

Solvation and Self-Association of Water in Propylene Carbonate¹

by David R. Cogley,^{2,3} Michael Falk,⁴ James N. Butler,^{2,5} and Ernest Grunwald*³

Corporate Research Division, Tyco Laboratories, Inc., Waltham, Massachusetts 02154
Atlantic Regional Laboratory, National Research Council of Canada, Halifax, Nova Scotia, Canada,
Division of Engineering and Applied Physics, Pierce Hall, Harvard University, Cambridge, Massachusetts 02138
Department of Chemistry, Brandeis University, Waltham, Massachusetts 02154 (Received August 18, 1971)

Publication costs assisted by Brandeis University, Harvard University, and the Petroleum Research Fund

Nuclear magnetic resonance (chemical shift) and infrared spectroscopic measurements of water in propylene carbonate have been made at water concentrations up to 3.5 *m*. The nmr measurements covered the temperature range from -57 to $+93^\circ$. Both the nmr and infrared spectra of water show hydrogen-bonded association with propylene carbonate, with an average enthalpy of about -1.2 kcal/mol. The solvation of water by propylene carbonate is such that the infrared spectra of H₂O and D₂O retain the simplicity characteristic of effective *C*_{2v} symmetry. Dependence of the nmr and infrared spectra on water concentration is most consistent with a chemical model in which water monomers and dimers are the principal species; the dimer formation constant is 0.18 ± 0.03 kg/mol at 25° and the molal enthalpy of dimerization is -1.4 kcal. Cyclic trimers of water are not a major species in propylene carbonate.

Introduction

Studies of the chemical interactions of water in relatively inert organic solvents can provide valuable information about the structure of water itself, particularly its hydrogen bonds. In discussing solvent-solute interactions, two kinds of models are generally employed: (1) the solvent is regarded as a continuum within which the individual solute molecules are contained; and (2) specific chemical association complexes between solute and solvent are recognized.⁶ In the treatment of hydrogen bonding in inert organic solvents, the specific chemical association model has commonly been used.⁷

In simple hydrocarbon solvents such as benzene, cyclohexane, and toluene, water is predominantly unassociated^{8,9} (partly because of its low solubility), but in chlorinated hydrocarbon solvents, it is almost certainly associated with itself. The principal species is apparently either a dimer or a trimer, but this is in dispute. For example, in dichloroethane, some solubility and vapor pressure studies have indicated that water trimers or tetramers^{8,10} are predominant, whereas other

vapor pressure and solvent extraction studies⁹ have indicated that dimers are more probable. Nmr^{10,11} and infrared^{12,13} studies have been similarly ambiguous in their interpretation. In other solvents which are hydrogen-bond acceptors (amines, ketones, etc.) the

- (1) Issued as NRCC No. 12250.
- (2) Tyco Laboratories, Inc.
- (3) Brandeis University.
- (4) Atlantic Regional Laboratory.
- (5) Harvard University.
- (6) J. F. Coetzee and C. D. Ritchie, "Solute-Solvent Interactions," Marcel Dekker, New York, N. Y., 1969.
- (7) G. C. Pimentel and A. L. McClellan, "The Hydrogen Bond," W. H. Freeman, San Francisco, Calif., 1960.
- (8) (a) S. D. Christian, H. E. Affsprung, and J. R. Johnson, *J. Chem. Soc.*, 1896 (1963); (b) J. R. Johnson, S. D. Christian, and H. E. Affsprung, *ibid.*, A, 77 (1966).
- (9) W. L. Masterton and M. C. Gendrano, *J. Phys. Chem.*, **70**, 2895 (1966).
- (10) T. F. Lin, S. D. Christian, and H. E. Affsprung, *J. Phys. Chem.*, **69**, 2980 (1965).
- (11) L. Ödberg and E. Högfeldt, *Acta Chem. Scand.*, **23**, 1330 (1969).
- (12) L. B. Magnusson, *J. Phys. Chem.*, **74**, 4221 (1970).
- (13) C. Jolicœur and A. Cabana, *Can. J. Chem.*, **46**, 567 (1968).

trimer has been proposed¹⁴ as the principal associated water species. This model seems to be based primarily on some early nmr work with alcohols¹⁵ in which the concentration dependence of methanol proton chemical shift in chloroform was interpreted as strong evidence for cyclic trimers.

Direct association of water with solvent molecules and other solutes to form simple species has also been invoked. For example, 1:1 water-acetone complexes were identified in dichloroethane solvent;¹⁰ several cyclopentanone-water complexes were identified in carbon tetrachloride;¹⁶ a 1:1 pyridine-water complex was identified by infrared studies in pyridine itself;¹⁷ and 1:1 water complexes with a number of amines have been studied by solubility methods in benzene, cyclohexane, and toluene.¹⁸

In describing the structure of liquid water, models have been used which contain elements of specific, as well as continuum, association. All the models emphasize hydrogen bonded structure.^{19,20} The "cluster model"^{21,22} visualizes larger aggregates, the "continuum model"²³⁻²⁸ visualizes structures with a range of properties, and the "two-state" model²⁹ distinguishes between hydrogen-bonded water and nonhydrogen-bonded water as the primary structural elements of the liquid. Considerable controversy³⁰ still exists as to which is the best description of liquid water. We hope that the studies of dilute water in propylene carbonate reported here may illuminate this problem from a different viewpoint.

Propylene carbonate [4-methyl-1,3-dioxolan-2-one, PC] is one of a class of dipolar, aprotic solvents of high dielectric constant which have been studied recently.³¹ It has been suggested that it is a close approximation to an "ideal structureless dielectric" solvent for studies of electrolytes.³² The dielectric constant of PC is 65.0 at 25°;³³ the dipole moment is 4.94 D.³⁴ Unlike water, PC does not exhibit any self-association, as evidenced by a Kirkwood *g* factor value of unity (1.02 at -60°).³³ Thus, structural effects in the solvent are minimal, and the main intermolecular forces which operate are strong but nonspecific dipole-dipole and London dispersion interactions. PC also has a wide liquid range (-49.2-247.1° at 1 atm)³⁵ which allows temperature effects to be studied easily.

We report here the results of studies of water in propylene carbonate over a wide range of temperature and concentration using nmr and infrared methods. Neither of these methods alone gives decisive information, but together they give a fairly clear picture of the water interactions. Our data show that the interaction of water solute with PC solvent is best described by a continuum model: the water molecules form hydrogen bonds to solvent molecules, yet retain an effective C_{2v} symmetry. If the solvation were such as to produce a mixture of discrete chemical species (HOH, HOH·PC, PC·HOH·PC), the infrared spectra would

have shown it. On the other hand, the self-association of water in PC is best described by a chemical model in which there are two distinct solvated species: a monomer and a dimer.

Experimental Section

Nuclear Magnetic Resonance. The PC was prepared according to standard methods³⁶ which have consistently yielded solvent of high purity. Typical concentrations of impurities after distillation from an adiabatic Podbielniak vacuum still were 10 ppm (parts per million) propylene oxide, 2 ppm allyl alcohol, 20 ppm propylene glycol, and less than 2 ppm water.

The water used for preparing the solutions was doubly distilled and CO₂-free. All solutions were prepared and stored in a Vacuum Atmospheres drybox in an atmosphere of high purity argon, in which the water and oxygen levels were maintained at less than 1 ppm by use of a recirculating purification train. The master sample of water-PC containing 3.473 *m* water was prepared by quantitative addition of water to PC. The water was exposed to the drybox atmosphere for less than 1 sec during this operation. Other solutions of known water concentration were then prepared by quantitative dilution of the master sample with PC. Nmr sample tubes containing the known solutions were sealed with the aid of a resistance-heated tungsten coil by fusing the top of the nmr tube. The sealing process took about 30 sec.

The water concentrations calculated from the weights

- (14) J. R. Johnson, S. D. Christian, and H. E. Affsprung, *J. Chem. Soc. A*, 1924 (1967).
- (15) A. D. Cohen and C. Reid, *J. Chem. Phys.*, **25**, 790 (1956).
- (16) R. L. Lynch, S. D. Christian, and H. E. Affsprung, *J. Phys. Chem.*, **73**, 3273 (1969).
- (17) W. K. Thompson, *J. Chem. Soc.*, 4028 (1964).
- (18) M. D. Gregory, S. D. Christian, and H. E. Affsprung, *J. Phys. Chem.*, **71**, 2283 (1967).
- (19) H. S. Frank, *Science*, **169**, 635 (1970).
- (20) F. H. Stillinger, Jr., *J. Phys. Chem.*, **74**, 3677 (1970).
- (21) H. S. Frank and M. J. Evans, *J. Chem. Phys.*, **13**, 507 (1945).
- (22) G. Nemethy and H. A. Scheraga, *ibid.*, **36**, 3382 (1962); **41**, 680 (1964).
- (23) T. T. Wall and D. F. Hornig, *ibid.*, **43**, 2079 (1965).
- (24) V. Vand and W. A. Senior, *ibid.*, **43**, 1869, 1873, 1878 (1965).
- (25) M. Falk and T. A. Ford, *Can. J. Chem.*, **44**, 1699 (1966).
- (26) J. Schiffer and D. F. Hornig, *J. Chem. Phys.*, **49**, 4150 (1968).
- (27) T. A. Ford and M. Falk, *Can. J. Chem.*, **46**, 3579 (1968).
- (28) W. A. P. Luck and W. Ditter, *J. Phys. Chem.*, **74**, 3687 (1970).
- (29) G. E. Walrafen, *J. Chem. Phys.*, **48**, 244 (1968); **50**, 560 (1969).
- (30) J. Schiffer, *J. Chem. Phys.*, **50**, 566 (1969); G. E. Walrafen, *J. Chem. Phys.*, **50**, 567 (1969).
- (31) D. R. Cogley, J. N. Butler, and E. Grunwald, *J. Phys. Chem.*, **75**, 1477 (1971); R. J. Jasinski, *Adv. Electrochem. Electrochem. Eng.*, **8**, 253 (1971).
- (32) H. L. Friedman, *J. Phys. Chem.*, **71**, 1723 (1967).
- (33) L. Simeral and R. L. Amey, *ibid.*, **74**, 1443 (1970).
- (34) R. Kempa and W. H. Lee, *J. Chem. Soc.*, 1936 (1958).
- (35) Propylene Carbonate Technical Bulletin, Jefferson Chemical Company, Inc., P. O. Box 53300, Houston, Texas 77052 (ca. 1962).
- (36) R. J. Jasinski and S. Kirkland, *Anal. Chem.*, **39**, 1663 (1967).

of the components were compared with the water concentrations calculated from nmr water peak areas and solution density values. The concentrations agreed within experimental error, which was about 5% for the nmr peak areas and much less for the solution weighings.

A Varian HR-60 nmr spectrometer which operated at 56.4 MHz was used in this study. It was possible to obtain chemical shift values with a precision of 0.2 Hz in most cases by bracketing the water resonance with a sideband of the PC methyl doublet generated with a sine wave generator. The frequency of the sidebands was measured accurately with a Hewlett-Packard Model 522B frequency counter. Each reported chemical shift is the average of at least five determinations. In a separate experiment using Wilmad Type 517 coaxial nmr tubes, the chemical shift of the PC methyl doublet in pure PC was compared with that in various water-PC solutions at 36.4°. After correction for differences in magnetic susceptibility,³⁷ the chemical shift of the PC methyl doublet was found to be independent of the water concentration, within ± 0.2 Hz. The chemical shift of the methyl doublet with respect to an external standard, as the temperature was changed, was not determined.

The nmr probe temperature was controlled by a preheated flow of nitrogen boiled from a Dewar vessel, and the available temperature range was approximately -100 to $+100^\circ$. The temperature was controlled by a thermocouple just below the sample, but was measured by inserting a thermocouple into the sample well at the height of the receiver coil. The precision of the temperature control was better than 0.1° , and the accuracy of the temperature varied from 0.1° near room temperature to approximately 0.4° at the high and low extremes of probe temperature.

The magnetic field was optimized at each temperature using cyclopentane fast sweep ringing. The limit of detection, where the water resonance began to merge with the base line noise, was approximately $0.05 m$ H₂O in PC solution.

Infrared Spectroscopy. Propylene carbonate used in the infrared measurements (Matheson Coleman and Bell) was dried thoroughly over Molecular Sieves (Linde, Type 5A, $1/16$ -in. pellets) and was used without further purification. Solutions of H₂O, D₂O, and their mixtures in propylene carbonate were prepared volumetrically, with care taken to avoid subsequent loss, gain, or exchange of water.

Spectra were recorded on a Perkin-Elmer Model 521 spectrophotometer. Cells with calcium fluoride windows and optical paths between 30 and 90 μ were used. Compensation for solvent absorption was achieved using pure solvent in the reference beam in a cell whose optical path was 1 or 2 μ shorter than that used in the sample beam. A thermostated cell holder was used to control temperature.³⁸

Results

Nuclear Magnetic Resonance. The chemical shifts (ν) of the water proton resonance with respect to the center of the methyl doublet of PC are given in Table I. The proton resonances were sharp, except at the lowest temperatures where there was slight broadening. This broadening could easily be attributed to the high viscosity (60 centistokes at -50°)³⁵ of PC at low temperatures.

Table I: Interpretation of Water Proton Chemical Shifts in Propylene Carbonate

Temp, °C	ν_0 , ppm ^a	a , $2K_2'$ · $(\nu_2 - \nu_0)^b$	b , ppm · m^{-2}	K_2' , m^{-1}
-57.2	1.38	0.982	-0.089	0.42
-47.2	1.287	0.792	-0.078	0.34
-28.2	1.205	0.638	-0.055	0.29
-13.7	1.138	0.526	-0.043	0.24
0.9	1.058	0.448	-0.028	0.21
25.1	0.945	0.362	-0.037	0.18
28	(0.933)	(0.353)	(-0.036)	0.18 ^c
48.5	0.846	0.291	-0.030	0.15
71.9	0.750	0.218	-0.012	0.12
93.5	0.665	0.183	-0.009	0.105 ^d

^a Referenced to center of methyl proton resonance doublet of PC; $\nu_0 = 1.075 - 0.00455 (t^\circ \text{C})$; $\nu(g) = -1.28$ ppm (Table II). $\beta = (d\nu_0/dT)/(\nu_0 - \nu_g) = -2.04 \times 10^{-3} \text{ deg}^{-1}$ at 25° .

^b In ppm · m^{-1} ; eq 5. ^c Based on infrared measurements. Nmr data at 28° interpolated. ^d In $K_2' = -4.108 + 698/T$; $\Delta H^\circ = -1.39$ kcal, $\Delta S^\circ = -8.2$ e.u.; correlation coefficient 0.993; standard error of fit of K_2' , $\pm 4\%$.

The chemical shifts are plotted vs. the molal concentration of water (m) in Figure 1. It is clear that the plots of ν vs. m at each temperature are nearly linear, with nonzero slopes, and the intercepts (ν_0) are well defined. The data at each temperature are represented satisfactorily by an empirical equation, $\nu = \nu_0 + am + bm^2$. Values of ν_0 , a and b were calculated by the method of least squares and are listed in Table I; the constants a and b will be discussed later.

For comparison, we also measured the chemical shift of water in liquid water containing 0.5 M PC as a function of temperature. These results are listed in Table II, together with values for water vapor.³⁷

Infrared Spectra. Infrared spectra of H₂O in PC were recorded at seven concentrations between 0.083 and 1.68 mol/l. at temperatures of 28 and 73° . Spectra of D₂O and D₂O-H₂O mixtures in PC were also obtained. Typical spectra in the region of H₂O stretching, D₂O stretching, and H₂O bending fundamentals at 28° are shown in Figure 2. Because of high solvent

(37) J. A. Pople, S. G. Schneider, and H. J. Bernstein, "High-Resolution Nuclear Magnetic Resonance," McGraw-Hill, New York, N. Y., 1959.

(38) T. A. Ford, P. F. Seto, and M. Falk, *Spectrochim. Acta, Part A*, 25, 1650 (1969).

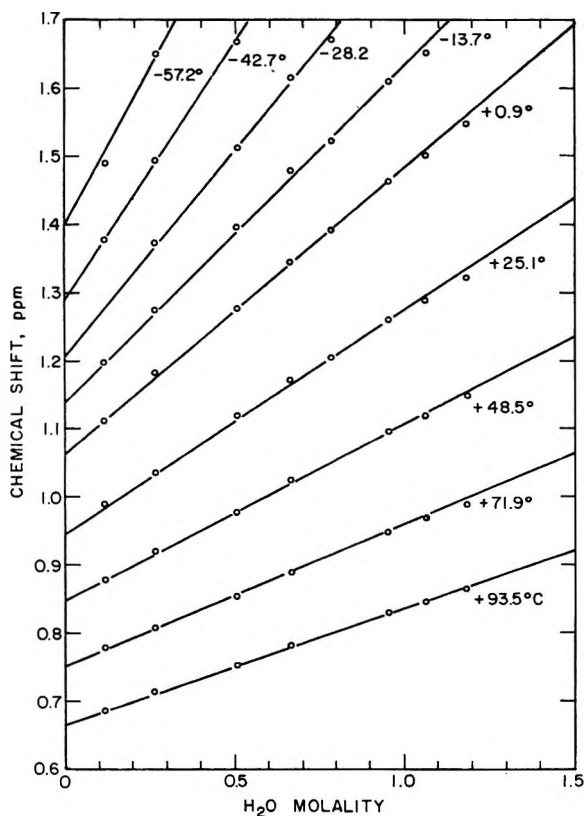


Figure 1. Nmr chemical shift of water in propylene carbonate as a function of water concentration at different temperatures. Lines are straight. The chemical shifts are in ppm, downfield of center of methyl proton resonance doublet of PC, and are precise to 0.002–0.007 ppm.

Table II: Nmr Chemical Shift of Water Protons in Water Containing 0.5 M Propylene Carbonate

Temp, °C	$\nu(l)$, ppm ^a
1.3	3.553
25.2	3.296
37.2	3.183
48.8	3.061 ^c
gas ^b	-1.28

^a Downfield of center of methyl proton resonance doublet of PC. Mean deviations are about ± 0.007 . ^b Chemical shift of water vapor relative to liquid water at 25° is -4.58 ppm.³⁷ ^c $\nu(l) = 3.564 - 0.0103t$ °C; $\beta = (d\nu(l)/dT)/(\nu(l) - \nu(g)) = -2.25 \times 10^{-3}$ at 25°.

absorptivity, the HOD and D₂O bending regions could not be investigated.

The solid curves in Figure 2 represent essentially the spectrum in the limit of zero water concentration and may be assigned to the solvated water monomer. For H₂O, the two principal peaks in the OH stretching region (Figure 2A) correspond approximately to the two stretching fundamentals of water vapor,³⁹ symmetric $\bar{\nu}_1$ at lower frequency and antisymmetric $\bar{\nu}_3$ at higher frequency. There are no other bands assignable to the

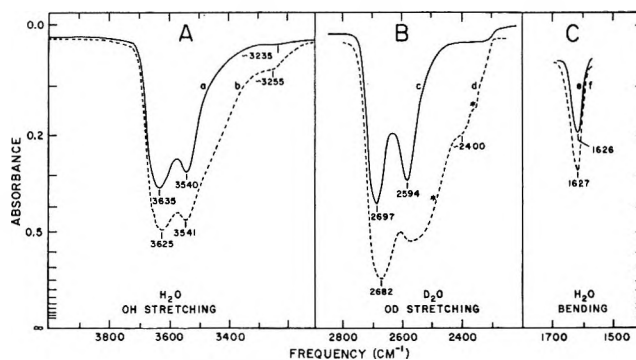


Figure 2. Infrared spectra of H₂O and D₂O in PC at two concentrations. Solvent absorption compensated by a reference cell. Asterisk in D₂O spectrum marks an incompletely compensated solvent band. The optical path is 85.5 μ m in a and e, 31.8 μ m in b and f, 103 μ m in c and 29.0 μ m in d. The concentration of H₂O or D₂O in formula weights per liter is 0.35 in a and e, 1.68 in b and f, 0.48 in c and 1.70 in d. Spectra obtained at other concentrations (1.40, 1.09, 0.936, 0.602) were intermediate.

solvated HOH monomer in the OH stretching region, except for a barely perceptible band at 3235 cm^{-1} that may be assigned to the first overtone, $2\bar{\nu}_2$, of the H₂O bending vibration. The H₂O bending fundamental $\bar{\nu}_2$ (Figure 2C) gives rise to a single band at 1626 cm^{-1} , essentially independent of H₂O concentration.

For D₂O, the spectrum of the solvated monomer in the OD stretching region (solid curve, Figure 2B) is analogous to that of HOH monomer in the OH stretching region. It shows two peaks, one at 2697 cm^{-1} , the other (of slightly lower intensity) at 2594 cm^{-1} .

For HOD, the spectrum of the solvated monomer shows two bands that are assignable to stretching vibrations. There is one band for the OD stretching fundamental with a peak at 2624 cm^{-1} and a half-width of 90 cm^{-1} , and one for the OH stretching fundamental with a peak at about 3590 cm^{-1} and a half-width of about 140 cm^{-1} (the band profile of the latter is somewhat uncertain because of an intense solvent absorption—the first overtone of the carbonyl stretching vibration—which occurs in this region and which is difficult to compensate perfectly). The OD stretching fundamental at 2624 cm^{-1} is quite close to the mean (2642 cm^{-1}) of the two OD stretching peaks of D₂O. Similarly, the OH stretching fundamental at 3590 cm^{-1} is quite close to the mean (3588 cm^{-1}) of the two OH stretching peaks of H₂O.

At higher water concentrations, an additional broad absorption appears in the OH and OD stretching regions, as shown by the dotted curves in Figure 2. These changes in the infrared spectrum will be interpreted later in terms of water association.

The temperature effect on the OH stretching peaks of H₂O in the limit of low water concentrations in PC is

(39) P. Saumagne and M. L. Josien, *Bull. Soc. Chim. Fr.*, 813 (1958).

summarized in Table III. Increasing temperature causes an overall decrease of band intensity and a shift of both $\bar{\nu}_1$ and $\bar{\nu}_3$ to higher frequency. The broad band at 3400 to 3500 cm^{-1} , which appears at high concentrations, becomes even less intense at higher temperature than do the principal bands.

Table III: Temperature Shifts of OH Stretching Band Maxima of H_2O in Propylene Carbonate^a

Temp. °C	cm ⁻¹			$\Delta\bar{\nu}_{\text{aver.}}/\Delta T$, cm ⁻¹ /deg
	$\bar{\nu}_1$	$\bar{\nu}_3$	$\bar{\nu}_{\text{aver.}}$	
28	3540 ± 2	3635 ± 2	3587.5 ± 3	0.28 ± 0.10 ^b
73	3549 ± 2	3652 ± 2	3600.5 ± 3	
gas ^c	3657	3756	3707	

^a 0.3 *m* solution. Association of water is negligible under these conditions. ^b $\beta = (\Delta\bar{\nu}_{\text{aver.}}/\Delta T)/(\bar{\nu}_{\text{aver.}} - \bar{\nu}_{\text{gas}}) = (2.3 \pm 0.8) \times 10^{-3} \text{ deg}^{-1}$. ^c W. S. Benedict, N. Gailar, and E. K. Plyler, *J. Chem. Phys.*, **24**, 1139 (1956); frequencies independent of temperature. For liquid water²⁵ $\beta = (\Delta\bar{\nu}/\Delta T)/(\bar{\nu} - \bar{\nu}_{\text{gas}}) = (2.1 \pm 0.2) \times 10^{-3} \text{ deg}^{-1}$.

The fundamental carbonyl stretching band of PC (at 1791 ± 1 cm^{-1} in dry PC) was examined for evidence of C=O...HOH bonding. In PC saturated with D_2O , which contained about 12 mol % D_2O , this band shifted to 1788 ± 1 cm^{-1} . (This small downward frequency shift was confirmed by the corresponding shift of the first overtone of this band from 3572 ± 1.5 cm^{-1} in dry PC to 3568 ± 1.5 cm^{-1} in PC saturated with D_2O .) In a dilute solution of PC in D_2O the carbonyl stretching fundamental was further lowered to 1778 ± 2 cm^{-1} , corresponding to a shift of -13.0 ± 2.3 cm^{-1} . This may be compared to the corresponding shift of -21 ± 2 cm^{-1} which has been observed for acetone⁴⁰ which offers no other hydrogen-bond acceptor sites than the carbonyl oxygens.

The strong bands in the 1000–1200- cm^{-1} region have been examined for evidence of involvement of the ester oxygens in hydrogen bonding. Several of these bands undergo frequency shifts from dry to aqueous PC. Vibrations involving motion of ester oxygens are known to occur in this frequency region, but since detailed vibrational assignments are lacking, our spectra do not provide clear information on the occurrence of hydrogen bonding to the ester oxygens.

Discussion

I. Water Monomer-Solvent Interaction. In this section we wish to interpret the nmr and infrared spectra observed in the limit of low water concentration, which may be assigned to solvated water monomer. Four points will be made. (1) The solvated water monomer molecules have effective C_{2v} symmetry. (2) The solvation of the water molecules includes hydrogen bonding. (3) The solvated-water-monomer species is *not* a mixture of discrete hydrogen-bonded solvation

complexes. (4) The solvent medium acts in effect as a hydrogen bonding continuum.

1. Effective C_{2v} Symmetry. Although the nmr spectrum of water in PC shows only a single HOH proton resonance, consistent with C_{2v} symmetry, that evidence by itself is not sufficient. Our conclusions are based largely on the characteristic simplicity of the infrared spectrum at low water concentrations in the OH and OD stretching regions.

The infrared spectra of HOH and DOD in the OH and OD stretching regions for water at low concentrations in PC are markedly similar to those for water in the gas phase. In each case there are two absorption maxima, spaced about 95 cm^{-1} apart, and the higher-frequency peak is the more intense. The similarity of the solution and vapor spectra suggests that the water molecules in solutions are not greatly distorted from the C_{2v} symmetry of the vapor molecules. If this be granted, then the higher frequency peaks in PC correspond effectively to the antisymmetric stretching vibration $\bar{\nu}_3$, and the lower frequency peaks to the symmetric stretching vibration $\bar{\nu}_1$. If the two frequencies corresponded to two kinds of OH bonds (or OD bonds) differing substantially in the strength of their hydrogen bonds to the solvent, then the lower frequency band, corresponding to the stretching vibration of the more strongly bonded OH (or OD) group, would be the more intense.⁷

The spectrum of HOD in PC confirms this analysis. There is just one peak in the OH stretching region and one peak in the OD stretching region. If the water monomer existed as several distinct species, corresponding to distinct modes of attachment to the solvent, then several HOD bands would be expected in the OH stretching region, with analogous bands in the OD stretching region. Moreover, the frequencies of the observed stretching peaks for HOD practically coincide with the mean of $\bar{\nu}_1$ and $\bar{\nu}_3$ for H_2O and D_2O , respectively.

The shape of the broad band of HOD in PC resembles that of HOD in liquid water and, as in the case of water, it is best interpreted in terms of a distribution of rapidly interconverting water-solvent bonds.

This type of observation is not unique to propylene carbonate, and similar phenomena have been observed in other solvents. Some typical OH stretching frequencies are given in Table IV.⁴¹ Note that although the absolute values of the frequencies shift by more than 300 cm^{-1} in this series, the relative positions of the bands—their separation, and the position of the HDO with respect to the two modes of H_2O and D_2O —are qualitatively the same for dilute water in all solvents. The frequency shifts are, of course, a result of the familiar shift of hydrogen bond strength with basicity

(40) M. Falk and P. F. Seto, unpublished results.

(41) A. J. Tursi and E. R. Nixon, *J. Chem. Phys.*, **52**, 1521 (1970).

Table IV: Comparison of OH Stretching Frequencies (in cm^{-1}) of Monomeric H_2O and HDO in Propylene Carbonate with Those in Other Media^a

Medium	$\bar{\nu}_3$	$\bar{\nu}_1$	$\bar{\nu}_{\text{aver}}$	$\bar{\nu}_{\text{HOD}}$	$\bar{\nu}_1 - \bar{\nu}_3$
Vapor ^b	3756	3657	3707	3707	99
Nitrogen, 20°K ^c	3726	3632	3679	3680	94
Carbon tetrachloride ^d	3705	3613	3659	3662	92
Benzene ^f	3682	3596	3639	3639	86
<i>p</i> -Xylene ^f	3680	3592	3636	3634	88
1,2-Dichloroethane ^g	3678	3595	3637	3635	83
Acetonitrile ^h	3640	3548	3594	3586	92
Propylene carbonate	3635	3540	3587	3587	95
Acetone ^e	3615	3535	3575	3575	80
Tetrahydrofuran ^d	3572	3499	3536	3524	73
Hexamethylphosphorotriamide ^h	3500	3452	3476	3470	48
Triethylamine ^d	3410(?)	3368(?)	3389	3374	42

^a Except where indicated, the spectra were recorded at room temperature. Where several determinations were available, the most recent has been tabulated. ^b W. S. Benedict, N. Gailar, and E. K. Plyler, *J. Chem. Phys.*, **24**, 1139 (1956). ^c Reference 41. ^d D. N. Glew and N. S. Rath, *Can. J. Chem.*, **49**, 837 (1971). ^e Reference 39. ^f E. Gentric, A. LeNarvor, and P. Saumagne, *C. R. Acad. Sci. Ser. C*, **270**, 1053 (1970). ^g Reference 13. ^h A. LeNarvor, E. Gentric, and P. Saumagne, *Can. J. Chem.*, **49**, 1933 (1971).

of the hydrogen band acceptor.^{42,43} By this criterion, PC falls between acetonitrile and acetone in its basicity.

2. Hydrogen Bonding. Both nmr chemical shifts (Tables I and II) and infrared OH stretching frequencies (Table III) for water in PC fall between the values for water vapor and liquid water. As the temperature increases, they shift toward the values for water vapor. Such behavior is typical of hydrogen bonding.

There is a strong analogy between the temperature coefficients $\beta = (d\nu/dT)/(\nu - \nu_g)$ for water in PC and liquid water. For the nmr chemical shift of water at infinite dilution in PC, $\beta = 2.04 \times 10^{-3} \text{ deg}^{-1}$ (Table I); the corresponding temperature coefficient for liquid water is $2.25 \times 10^{-3} \text{ deg}^{-1}$ (Table II). Within experimental error, these values are equal.

For the mean of the infrared stretching frequencies $\bar{\nu}_1$ and $\bar{\nu}_3$, $\beta = 2.3 \times 10^{-3} \text{ deg}^{-1}$ for water in PC and $2.1 \times 10^{-3} \text{ deg}^{-1}$ for liquid water (Table III). Within experimental error these values are the same as those for the nmr data. This supports the hypothesis that the solvation of water by PC includes hydrogen bonding.

The frequency shifts of the carbonyl stretching fundamental and overtone bands show that the carbonyl group is a site of interaction between water and PC. The smaller magnitude of the shift for PC compared with that for acetone may indicate that for PC it is not the exclusive site. The infrared spectra do not provide any clear indication of interaction of ester oxygens with water, but neither can such interactions be eliminated as a possibility on these grounds.

We now wish to estimate the contribution from hydrogen bonding to the solvation energy of water in PC. In first approximation, this energy may be estimated from the shift, $(\bar{\nu} - \bar{\nu}_g)$ of the OH stretching frequency from that of the gas phase. Part of this shift is due to solvation other than hydrogen bonding; for solvents where no hydrogen bonding is expected with water (*e.g.*, CCl_4 , CS_2), we find that $(\bar{\nu} - \bar{\nu}_g) \approx 120(n^2 - 1)/(2n^2 + 1)$, where n is the refractive index, and the variable $(n^2 - 1)/(2n^2 + 1)$ is suggested by the Kirkwood-Bauer-Magat relation.⁴⁴ On this basis, we predict that the average OH stretching frequency for water in PC would be 3666 cm^{-1} if there were no hydrogen bonding. The difference between the measured and the predicted value (-78 cm^{-1}) is a measure of the hydrogen bond energy. If we assume that differences in stretching frequency are in direct proportion to hydrogen bond energy,^{7,43} we can convert this to kilocalories by comparison with ice, where the enthalpy of formation per hydrogen bond⁷ is known to be approximately -6 kcal/mol . Since the difference in OH stretching frequency between water vapor and ice at 0° is $3305 - 3707 = -402 \text{ cm}^{-1}$, this gives $(-6 \text{ kcal/mol})/(-402 \text{ cm}^{-1}) = -1.2 \text{ kcal/mol}$ for the enthalpy of formation of the water-PC hydrogen bond.

3. Nature of Solvated Species. We now wish to consider the possible species that could be formed by hydrogen bonding between water and PC. Since the average enthalpy of hydrogen-bond formation is only -1.2 kcal , we expect there could be a number of H_2O -PC species. For example, if ΔS° for the process $\text{HOH} + \text{PC} \rightarrow \text{HOH} \cdot \text{PC}$ were equal to that for the dimerization of water in PC (see next section), the equilibrium constant would be 0.11 l./mol . For the addition of a second PC molecule, this equilibrium constant would be multiplied by a statistical factor of one-half. Such a model leads to a distribution of 36% HOH, 43% HOH·PC, and 21% PC·HOH·PC. The number of species present at significant concentrations could be even greater because the acceptor site of PC could be either the carbonyl oxygen or an ester oxygen (Figure 3).

If all these species gave discrete vibrational spectra, we would expect to see a very complex band structure. Since we do *not* in fact observe such complexities, we may infer that the interactions between water and PC are too variable or short-lived to give rise to discrete chemical species.

4. The Solvent as a Hydrogen Bonding Continuum. Thus the interactions between monomer water and solvent molecules seem to give rise to many rapidly interconverting configurations that are too ill defined or

(42) W. Gordy, *J. Chem. Phys.*, **9**, 215 (1941).

(43) K. F. Purcell and R. S. Drago, *J. Amer. Chem. Soc.*, **90**, 3886 (1968); R. S. Drago, N. O'Brien, and G. C. Vogel, *J. Amer. Chem. Soc.*, **92**, 3924 (1970).

(44) E. Bauer and M. Magat, *J. Phys. Radium*, **9**, 319 (1938).

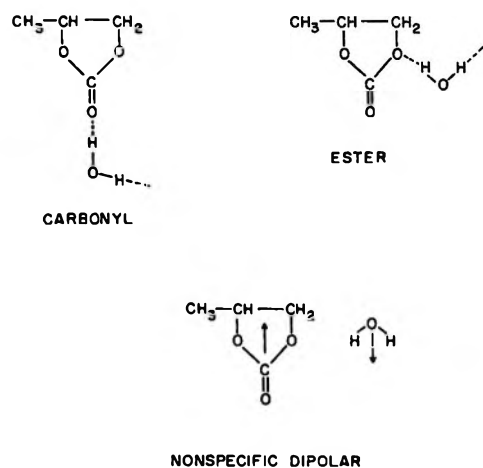


Figure 3. Several configurations for interactions between water and PC.

short-lived to be amenable to treatment as discrete chemical species. This model is similar in its essentials to the "continuum model" of liquid water, which postulates a continuous range of hydrogen bonded structures.²³⁻²⁸

II. Nature of Associated Species. Interpretation of Infrared Data. To examine more closely the structure of the additional infrared stretching bands that appear at high water concentration, we subtracted the absorptivities obtained at low concentration (for the monomer water, Figure 4A) from the observed absorptivities at the higher concentrations and obtained a spectrum for the associated species which varied with the concentration, and with the fraction of monomer assumed. Although the assumed monomer fraction strongly affects the spectrum in the range from 3500 to 3700 cm^{-1} , in the range from 3200 to 3400 cm^{-1} (where the monomer absorptivity is low) the spectrum of associated water species is essentially independent of this assumption. The shape (not the magnitude) of the 3200–3400- cm^{-1} spectrum is to a good approximation independent of the formal water concentration, which implies strongly that there is only one species responsible for these bands.

Studies of water association in other solvents have indicated that solvents which have two or more basic sites dissolve water primarily as monomer and dimer units, whereas solvents having only one basic site dissolve water primarily as trimers or more associated units.¹⁴ We therefore tested two hypotheses: that the associated water species in PC is a dimer and that it is a cyclic trimer.

For the dimer assumption, the usual equilibrium and mass-balance considerations lead to the following expressions

$$\epsilon_2 = [\epsilon - (1 - \alpha_2)\epsilon_1]/\alpha_2 \quad (1)$$

$$\alpha_2 = 1 - [(\sqrt{1 + 8K_2C} - 1)/4K_2C] \quad (2)$$

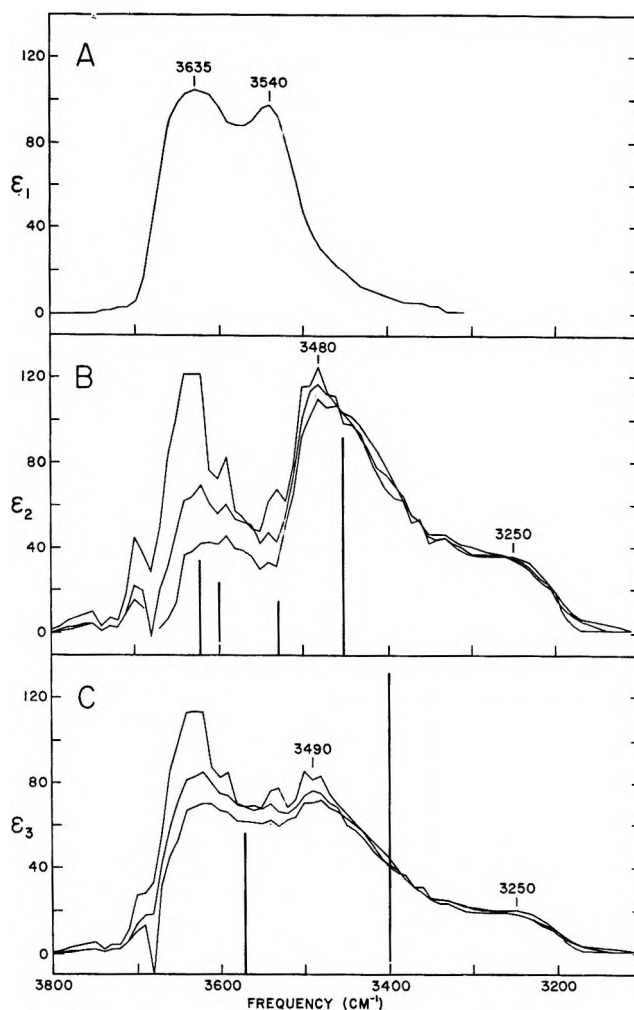


Figure 4. Absorptivity of water species in propylene carbonate in the OH stretching region plotted at 10- cm^{-1} intervals. (A) H_2O monomer absorptivity calculated from absorbance data for 0.3 mol $\text{H}_2\text{O}/\text{l}$.; (B) H_2O dimer absorptivity calculated from absorbance data at H_2O concentrations of 0.60, 1.09, and 1.68 mol/l.; (C) H_2O trimer spectrum calculated from the same absorbance data. The predicted frequencies and intensities (very approximate) for an open dimer and a cyclic trimer are shown as vertical lines in (B) and (C).

In these equations ϵ_2 is the absorptivity for 18 g of the dimer, ϵ is the observed absorptivity for 18 g of solute, ϵ_1 is the absorptivity at infinite dilution (monomer only), α_2 is the mole fraction of the dimer, C is the formal concentration of water (formula weights per liter), and K_2 is the association constant in liters per mole. The consistency of the model requires that the calculated absorptivity of the dimer, ϵ_2 , be independent of concentration within the experimental error. This is true for only a narrow range of K_2 values. Figure 4B shows the calculated values of ϵ_2 for three values of C for $K_2 = 0.15$ l./mol, computed from experimental values of ϵ and ϵ_1 at 10- cm^{-1} intervals throughout the OH stretching region. In the range from 3200 to 3500 cm^{-1} , the dimer absorptivities are in agreement within the apparent experimental error. The curves cross

each other in a random manner, indicating that there is no need to invoke any additional equilibria to explain the observations. In the range from 3500 to 3700 cm^{-1} the data are quite inaccurate because ϵ_1 is large and the calculated ϵ_2 values are the result of differences between two large and nearly equal numbers. Nevertheless, there seems to be significant structure in this region: a peak at 3650 cm^{-1} and perhaps two other peaks. Thus the associated species has absorption bands in the same region as does the monomer, even though we cannot establish their shape in accurate detail. The optimum fit is obtained with $K_2 = 0.15 \pm 0.03$ l./mol (0.18 kg/mol). The statistical limits of error on this constant are difficult to establish unambiguously, since the frequency range of data chosen affects both the K_2 for minimum variance and the standard deviation of this constant.

As suggested by several authors,^{8b,10} a plausible major species is the cyclic trimer of water, and we tested a model in which only monomers and trimers were considered as species. The equilibrium and mass-balance considerations yield the following expressions for trimer absorptivity (for 18 g), ϵ_3 , and mole fraction, α_3

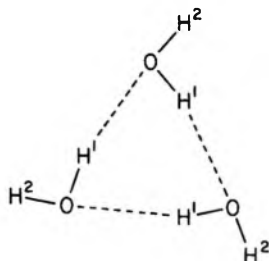
$$\epsilon_3 = [\epsilon - (1 - \alpha_3)\epsilon_1]/\alpha_3 \quad (3)$$

$$\alpha_3 = 1 - \left\{ \frac{C/6K_3 + \sqrt{(C/6K_3)^2 + (1/9K_3)^3}}{C/6K_3 - \sqrt{(C/6K_3)^2 + (1/9K_3)^3}} \right\}^{1/3} / C \quad (4)$$

In these equations K_3 is the formation constant of the trimer from three monomer molecules and all other notation is the same as above. This model fits the data about as well as the dimer model, the optimum K_3 value being 0.5 ± 0.1 l.²/mol². The calculated trimer absorptivities are shown in Figure 4C.

Even though the cyclic trimer model appears to be consistent with the infrared data, we can eliminate it as a possibility on two different grounds.

First, let us consider whether the spectrum of the hypothetical trimer generated by means of eq 3 agrees with the frequencies and intensities expected of a cyclic trimer. The most likely configuration of such a trimer is the following



with either the planar structure (C_{3h} symmetry) or the more likely nonplanar structure (C_3 or C_1 symmetry).⁴⁵

The three H^2 protons, which are not involved in the water-water hydrogen bonds, would form slightly stronger bonds to the solvent than those of the H_2O

monomers, because the water oxygens act as acceptors of $\text{OH}^1 \cdots \text{O}$ bonds of considerable strength. Neglecting the coupling of motions of the H^2 protons, unlikely to be appreciable because these protons are far apart, one would expect the three fundamental stretching vibrations of the OH^2 groups to give rise to a single band. We estimate that the frequency of this band would be some 10 cm^{-1} below the mean of ν_1 and ν_3 of H_2O monomers, about 3577 cm^{-1} . Its integrated intensity would be roughly half of the mean intensity of $\bar{\nu}_1$ and $\bar{\nu}_3$ of the monomers, as only half of the protons of the trimer are H^2 .

The three protons H^1 participate in hydrogen bonds which can be expected to be comparable in strength to the average bond in liquid water, since each of the oxygen atoms in the ring acts as an acceptor and donor of hydrogen bonds. This is known to increase considerably the strength of hydrogen bonds⁴⁵ and would lead to an average stretching frequency of about 3400 cm^{-1} , that of liquid water at room temperature. If the trimer had C_{3h} symmetry, the coupling of the three OH^1 stretching vibrations would lead to a fully symmetric A_1' stretching mode at a frequency somewhat below 3400 cm^{-1} , infrared inactive, and a doubly degenerate E' stretching mode at a frequency somewhat above 3400 cm^{-1} in which the whole infrared intensity would reside. If the trimer had C_3 symmetry, the fully symmetric mode would become infrared active, but not very intense; under C_1 symmetry, the degeneracy of the E mode would be lifted and three closely spaced bands might be observed. In any event, the band or bands due to OH^1 stretching would be centered at about 3400 cm^{-1} .⁴⁶ They would be several times as intense as those due to OH^2 stretching because there are equal numbers of H^1 and H^2 protons, and the formation of a strong hydrogen bond leads to a manifold increase in the infrared intensity of the fundamental OH stretching band.⁷

The above frequencies and intensities predicted for a cyclic trimer have been indicated as vertical lines in Figure 4C. The predictions are in clear disagreement with the spectrum derived from the experimental data by means of eq 2.

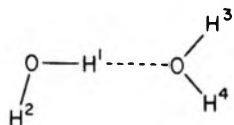
The trimers can also be eliminated as a major contributor on the basis of the nmr chemical shift data at low water concentrations (Figure 1). An excellent fit to the concentration dependence of chemical shift at all temperatures was obtained with a nearly linear empirical function having very little curvature. No evi-

(45) J. Del Bene and J. A. Pople, *J. Chem. Phys.*, **52**, 4858 (1970).

(46) An alternate estimate of this stretching frequency can be derived from the OH stretching frequencies of H_2O polymers in solid nitrogen matrix.⁴¹ These "polymers," which may actually include a cyclic trimer, or other small oligomer species of similar hydrogen bond strength, give rise to the following frequencies in the OH stretching region; 3688, 3510, 3435, 3355, 3320, and 3220 cm^{-1} . The highest of these frequencies almost certainly arises from "non-hydrogen-bonded" OH groups, akin to OH^2 of the cyclic trimer; the average of the remaining five frequencies is 3368 cm^{-1} .

dence was found for zero slope at zero water concentration or for inflection points of the type found for methanol protons by Cohen and Reid.¹⁵

Returning to the dimer model, we can predict qualitatively the hydrogen stretching spectrum of the dimer as follows. The dimer may be expected to have the "open" structure^{45,47}



The fundamental stretching vibration of the hydrogen bonded proton H¹ will be essentially decoupled from other vibrations and should yield an intense absorption band at the lowest frequency. This frequency is 3547.5 cm⁻¹ for H₂O dimer in a solid nitrogen matrix at 20°K, 131.6 cm⁻¹ below the mean of $\bar{\nu}_1$ and $\bar{\nu}_3$ frequencies of the H₂O monomer in the same medium.⁴¹ Assuming the same frequency shift for H₂O in PC, the expected stretching frequency of H¹ is 3456 cm⁻¹, in reasonable agreement with the observed strong band at about 3480 cm⁻¹. Protons H³ and H⁴ have effective C_{2v} symmetry and would be expected to give rise to a symmetric and antisymmetric stretching frequency with about the same separation, 95 cm⁻¹, and the same relative intensities as for $\bar{\nu}_1$ and $\bar{\nu}_3$ of the monomer H₂O. The effect of the hydrogen bond to the oxygen would be to lower the OH³ and OH⁴ frequencies by about 10 cm⁻¹ from the monomer values, hence we predict a band at 3530 cm⁻¹ and a slightly more intense band at 3625 cm⁻¹. Proton H², because its mate is hydrogen bonded to another water molecule and vibrates at a much lower frequency, would be expected to have a decoupled stretching vibration at a frequency some 10 cm⁻¹ higher than the mean of $\bar{\nu}_1$ and $\bar{\nu}_3$ of the monomer H₂O, *i.e.*, about 3600 cm⁻¹. These predicted frequencies, together with the expected intensities, relative to those of the monomer, are indicated as vertical lines in Figure 4B. The predicted spectrum is fully consistent with that derived from the experimental data, within their experimental uncertainty. We must note that the broad band near 3250 cm⁻¹ is not a fundamental of the dimer, but rather seems to be the first overtone of the bending vibration (2 ν_2) of the dimer, greatly intensified by Fermi resonance with the broad absorption centered at 3480 cm⁻¹. This assignment is confirmed by the spectrum of D₂O in PC which shows an analogous shoulder near 2400 cm⁻¹, intensifying at higher D₂O concentrations (Figure 2).

In conclusion, the infrared spectra indicate a single associated species of consequence. The data are inconsistent with a cyclic trimer, and fully consistent with an open dimer. The half-width of the 3480-cm⁻¹ band of the dimer is about 140 cm⁻¹, comparable with that of the monomer bands, and pointing to a distribution of water-water interactions. This distribution is less

wide than that in liquid water, which has an OH stretching half-width of about 260 cm⁻¹ for HDO at room temperature.²⁵

Interpretation of Nmr Data. The dimer model yields⁴⁸ a simple expression for the chemical shift ν at low water concentrations

$$\nu = \nu_0 + 2K_2'(\nu_2 - \nu_0)m(1 - 4K_2'm) \quad (5)$$

where ν_0 is the chemical shift of the monomer protons (Table I) and ν_1 is the hypothetical mean chemical shift of the dimer protons. For the nmr work, the water concentration (m) is expressed in moles/kg solvent; this makes K_2' in molal units larger by a factor of 1.20 (density of PC) than the molar K_2 obtained in the infrared experiments.

Because of the very small curvature of the plots in Figure 1 we cannot evaluate K_2' and $(\nu_2 - \nu_0)$ independently, but can obtain an accurate value for their product. The results of the least squares fit of the data to the function $\nu = \nu_0 + am + bm^2$ have been given in Table I. The term in m^2 is small and b is too inaccurate to be treated further. On the other hand, a is obtained with good precision and may be identified with $2K_2'(\nu_2 - \nu_0)$ in (5). From the infrared data at 28°, we obtained $K_2 = 0.15$ l./mol and hence $K_2' = 0.18$ kg/mol. Thus at 28°, where $a = 0.353$ ppm mol/kg, we obtain $\nu_2 - \nu_0 = 0.999$ ppm.

To obtain the temperature coefficient of K_2' we need to know the temperature coefficient of $\nu_2 - \nu_0$. From Table I we know that the temperature coefficient of ν_0 is 0.00455 ppm/deg. We also found empirically that for both liquid water and water in PC, the temperature coefficient of ν was 0.2% of $\nu - \nu_g$. If we assume a similar relationship for ν_2 , we obtain a temperature coefficient of $(\nu_2 - \nu_0)$ which is 0.2% of 0.999 ppm or approximately 0.002 ppm/deg. Using this value of the temperature coefficient we have obtained values of K_2' which are listed in Table I.

A plot of $\log K_2'$ vs. $1/T$ gives an enthalpy for the formation of the water dimer of -1.39 kcal/mol. From the frequency shifts of the average OH stretching vibrations of the dimer compared to the monomer, we estimate in the same way we did above an enthalpy of formation of $(-6 \text{ kcal/mol}) (-107 \text{ cm}^{-1})/(-402 \text{ cm}^{-1}) = -1.6 \text{ kcal/mol}$, in satisfactory agreement.

In the preceding section it was estimated that ΔH for the hydrogen bonded solvation of water monomer in PC is -1.2 kcal/mol. To obtain the analogous enthalpy of hydrogen bonding of the water dimer, the enthalpy change for dimerization must be added to that for the solvation of 2 mol of monomer. The result is -3.8 kcal/mol of dimer, or -1.9 kcal/formula weight

(47) K. Morokuma and L. Pedersen, *J. Chem. Phys.*, **48**, 3275 (1968).

(48) D. R. Cogley, Ph.D. Thesis, Brandeis University (1970); In deriving eq 5, the exact expression for $[\text{H}_2\text{O}]/m$ was expanded in power series, and terms of order m^3 and higher were neglected.

of H₂O—substantially more negative than ΔH for the solvation of water monomer.

Concluding Remarks

An important point to be made from this study is that to describe hydrogen bonding between water and the propylene carbonate solvent, we have had to use a continuum model, whereas for the hydrogen bonding between water molecules in dilute solution, we have had to use a specific chemical association model. The combined infrared and nmr data conclusively eliminate cyclic trimer and suggest that an open dimer is the only

associated species of importance in the concentration range investigated.

Acknowledgments. This research was supported by the Petroleum Research Fund of the American Chemical Society, the National Research Council of Canada, and the U. S. Air Force Cambridge Research Laboratories, Office of Aerospace Research, but does not necessarily constitute the opinion of any of these agencies. The authors thank Dr. George Brink and Mr. Ping F. Seto for recording the infrared spectra and help with computations.

A Low-Temperature Infrared Study of Sterically Hindered Associated Alcohols

by C. Bourdéron, J.-J. Péron, and C. Sandorfy*

Département de Chimie, Université de Montréal, Montréal, Québec, Canada (Received September 27, 1971)

Publication cost assisted by Université de Montréal

The infrared spectra of sterically hindered alcohols were measured in solution at temperatures ranging from 20° to -190°. As the temperature is lowered several different hydrogen bonded species appear. It is shown that certain oligomers subsist even at -190°. The evolution of molecular association upon lowering the temperature was followed by the OH stretching fundamental as well as its first overtone. The relative intensity of monomer and oligomer bands with respect to the polymer band is greater for the overtones making it easier to ascertain the presence of the former.

Introduction

The existence of monomers, dimers, oligomers, and polymers in solutions of self-associated alcohols is a well known fact, and numerous attempts have been made to use infrared spectroscopy for the identification of the various hydrogen bonded (HB) species, and to study the equilibria between them. We cite only the fundamental work of Smith and Creitz,¹ the contributions of Coburn and Grunwald,² and Bellamy and Pace.³

In 1957, Van Thiel, Becker, and Pimentel⁴ used the matrix isolation method (N₂ at 20°K) in order to distinguish between monomers, cyclic dimers and trimers, linear tetramers and polymers in the case of methanol. It was not until 1970 that Barnes and Hallam^{5,6} took up and extended this work using argon matrices to study methanol and ethanol. They found a greater number of bands, and modified some of the previous assignments.

Whereas matrix isolation methods allow the identification of bands due to dimers, oligomers, and polymers, they do not inform us on the conditions of their existence in random media, such as solutions. The present work was undertaken in order to gain information on

association in dissolved alcohols. Infrared spectra were taken, using solvents which become rigid glasses at liquid nitrogen temperature. As the temperature is gradually lowered we observe the gradual appearance and disappearance of various associated species. We measured the OH stretching fundamentals and their first overtones, which yield much useful information.

One alcohol and two phenols, affected by steric hindrance to a different extent, were chosen because of the relatively slow changes in their association pattern when the temperature is lowered. Results obtained on an unhindered alcohol are communicated in the following paper.

The alcohol and phenols we examined were, in order

(1) F. A. Smith and E. C. Creitz, *J. Res. Nat. Bur. Stand.*, **46**, 145 (1951).

(2) W. C. Coburn, Jr., and E. Grunwald, *J. Amer. Chem. Soc.*, **80**, 1318 (1958).

(3) L. J. Bellamy and R. J. Pace, *Spectrochim. Acta*, **22**, 525 (1966).

(4) M. Van Thiel, E. D. Becker, and G. C. Pimentel, *J. Chem. Phys.*, **27**, 95 (1957).

(5) A. J. Barnes and H. E. Hallam, *Trans. Faraday, Soc.*, **66**, 1920 (1970).

(6) A. J. Barnes and H. E. Hallam, *ibid.*, **66**, 1932 (1970).

of decreasing steric hindrance: 2,6-diisopropylphenol (DIPP); 2,6-dimethylphenol (DMP); 2,2,4-trimethyl-3-pentanol (TMP).

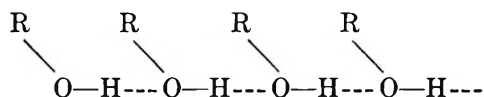
It is perhaps useful to describe the aggregates which we hope to distinguish.

(a) Molecules not engaged in HB, with OH stretching frequencies higher than 3600 cm^{-1} . We shall refer to these as monomers, and to the corresponding bands as "free bands."

(b) Open-chain aggregates where the end group oxygen atom is engaged in HB as a proton acceptor but not as a proton donor. The OH stretching frequencies are still above 3600 cm^{-1} . Since there is little hope of distinguishing a from b in solution spectra, we shall call both a and b type bands "free bands." Their near coincidence may cause some band broadening and asymmetry, but we shall not be concerned with this.

(c) "Oligomers;" aggregates containing two, three, or four OH groups. Thus, "oligomer" will be considered as a generic term for dimers, trimers, and tetramers. There can be open-chain or cyclic species for each of these, the former having a "free" OH end group, the latter having none. These species have characteristic OH stretching frequencies which under favorable experimental conditions are distinguishable in infrared solution spectra.

In open-chain trimers and tetramers, and in long chains like



the first OH group (which is a proton donor but not a proton acceptor) is expected to have an OH stretching frequency close to that of the bonded OH group of a dimer, and in all probability will not be distinguishable from it.

Oligomers are expected to have bands in the $3500\text{--}3380\text{ cm}^{-1}$ region. This is assumed even if (as in cyclic trimers or tetramers) all the oxygen atoms act as proton donors as well as acceptors, since the nonlinearity of their HB would make them weaker than in polymers.

(d) "Polymers;" aggregates containing more than four OH groups, either open-chain or cyclic. By "polymer bands," we mean bands due to those OH groups of these species, which act both as proton donors and proton acceptors. We do not make any distinction as to the length of the polymer chain. The polymer bands are assumed to be the usually broad bands in the 3300 cm^{-1} region. The bands due to the central OH groups of open-chain trimers and tetramers are unlikely to be distinguishable from these. Only those of cyclic trimers and tetramers are expected to be so, since they differ significantly from polymers by structural characteristics such as bond angles.

Thus, we hope to find distinct bands for "free" OH

groups, dimers, cyclic trimers, cyclic tetramers, and polymers.

We believe that the above definitions and assumptions are in agreement with general knowledge on HB and we shall not discuss them at this point. We would like to point out, however, that our assignments are in perfect agreement with the order of increasing stability of the species (free, open dimer, cyclic trimer, cyclic tetramer, polymer) which Del Bene and Pople obtained in their recent *ab initio* calculations on self-associated water molecules.⁷

Experimental Section

The solvents used were 1:1 mixtures of (a) CCl_3F (Freon-11) and $\text{CF}_2\text{Br-CF}_2\text{Br}$ (Freon 114-B2) and (b) CCl_3F and methylcyclohexane. We shall abbreviate these as FR and FM. In certain cases we used 2:1 mixtures of the alcohol studied and CCl_3F . The compounds were purified by conventional methods. The spectra were measured on a Perkin-Elmer Model 621 instrument and, in the overtone region, a Cary model 17 spectrometer. For details we refer to previous publications from this laboratory.⁸⁻¹⁰

The Low Intensity of the Polymer Overtones

The relative intensities of the OH stretching bands of the free and the differently associated species are very different at the level of the fundamentals and at the level of the overtones (*cf.* Luck and Ditter¹¹). At concentrations and temperatures where no free bands are detectable in the fundamental region these bands still appear strongly in the overtone region.

Since the mechanical anharmonicity of the polymer OH stretching vibration has been shown to *increase*^{9,12} with respect to that of the free OH vibration, this drop in intensity of the polymer overtones could be due to the decreased electric anharmonicity of the latter.

This observation applies mainly to the relative intensities of the monomers and the polymers but, to a lesser extent, it is also verified for oligomers and polymers in cases where the oligomers (like cyclic trimers) have structures very different from the polymers.

This fact is important since monomers, and certain oligomers, whose bands cannot be seen in the fundamental region because of their low intensity, stand a good chance of being detected in the overtone region.

Interpretation of the Spectra

A. 2,6-Dimethylphenol (Figures 1 and 2). At a concentration of 0.095 M only the free OH band appears at room temperature in FR. When the temperature is

(7) J. Del Bene and J. A. Pople, *J. Chem. Phys.*, **52**, 4858 (1970).

(8) G. Durocher and C. Sandorfy, *J. Mol. Spectrosc.*, **22**, 347 (1967).

(9) G. Durocher and C. Sandorfy, *ibid.*, **15**, 22 (1965).

(10) M. Asselin and C. Sandorfy, *J. Chem. Phys.*, **52**, 6130 (1970).

(11) W. A. P. Luck and W. Ditter, *J. Mol. Struct.*, **1**, 261 (1967).

(12) M. Asselin and C. Sandorfy, *ibid.*, **8**, 145 (1971).

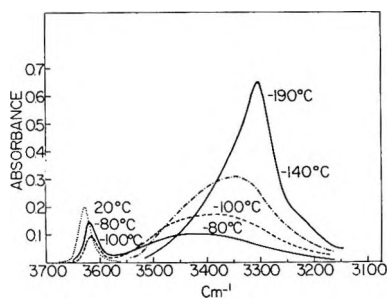


Figure 1. The OH stretching fundamental of 2,6-dimethylphenol at different temperatures. Concentration at 20°: 0.095 M in FR; cell length: 0.183 mm.

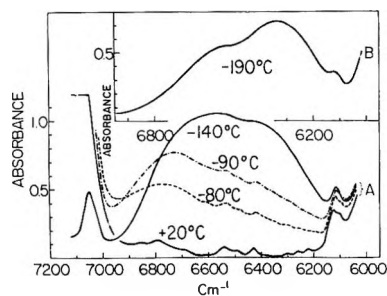


Figure 2. The first overtones of the OH stretching vibration of 2,6-dimethylphenol at different temperatures. Concentration at 20°: 0.102 M in FR; cell length: 10 cm. Scale expansion: A, 5X; B, 2 X.

lowered, the broad associated band appears. A peak, shifting toward 3300 cm^{-1} , becomes gradually preponderant. This peak is undoubtedly due to the polymer. However, even at the lowest temperature, we see a strong shoulder, centered at about 3380 cm^{-1} . This must be due to oligomers which survived because of the steric shielding of the OH group. The free band has disappeared well before -140° and the maximum is at the polymer frequency.

Now, if we turn our attention to the region of the first overtone, we find a different picture. The free band is still present at -140° and the oligomer band is still prominent. We cannot explain this merely by changed overlap conditions. The curves corresponding to -80° and -95° , which clearly show the presence of oligomers and the presence of the strong free band, eliminate this possibility (Figure 2). Only at the lowest temperature (-190°) does the polymer band become preponderant. We clearly have oligomers, even at the lowest temperature.

This example is an illustration of the fact that the intensity ratio monomer:oligomer:polymer has been significantly modified in favor of the less associated species. The same alcohol in FM yields similar spectra, except that the polymer band is less developed.

B. 2,6-Diisopropylphenol. In the case of DMP we were not able to distinguish between the various possible oligomers. In order to do this for at least one alcohol, we turned to a sterically more strongly hin-

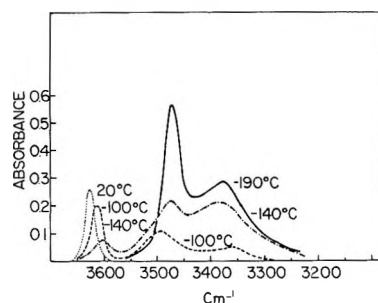


Figure 3. The OH stretching fundamental of 2,6-diisopropylphenol at different temperatures. Concentration at 20°: 0.118 M in FR; cell length: 0.183 mm.

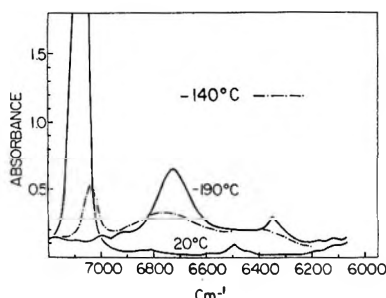


Figure 4. The first overtone of the OH stretching vibration of 2,6-diisopropylphenol at 20 and -190° . Concentration at 20°: 0.117 M in FR; cell length: 10 cm.

dered one. For DIPP we found an interesting difference between the spectra taken in the two solvents. In FR (Figures 3 and 4) two bands appear when temperature is decreased. The one at higher frequency (3474 cm^{-1}) is relatively sharp (its half-width is equal to about 35 cm^{-1}); the other, at 3376 , is broader but nearly symmetrical.

In FM (Figure 5) we find a band at lower frequencies (3325 cm^{-1}) while the intensity of the band at 3474 has considerably decreased. The 3325-cm^{-1} band must belong to the polymer. One may be tempted to assign the 3474 band found in FR to an OH---Br type hydrogen bond. Its frequency seems to be much too low, however, and it was shown previously that no such hydrogen bonds occur between CF_3Br_2 and alcohols or phenols.¹³ Also, the band is still present in FM which does not contain Br atoms. Another possibility for this band would be an OH--- π type hydrogen bond. Actually, a band was found at 3575 cm^{-1} in the spectrum of liquid DIPP at room temperature.¹⁴ One might be tempted to argue that it shifted to 3474 cm^{-1} upon cooling to -190° . In order to check this assumption, we prepared a solution of DIPP in a 1:1 mixture of CCl_3F and 1,2,4-trimethylbenzene which is useable down to -100° . The OH--- π band only shifts

(13) M. C. Bernard-Houplain, C. Bourdérion, J.-J. Péron, and C. Sandorfy, *Chem. Phys. Lett.*, **11**, 149 (1971).

(14) K. Szczepaniak and M. Falk, *Spectrochim. Acta, Part A*, **26**, 883 (1970).

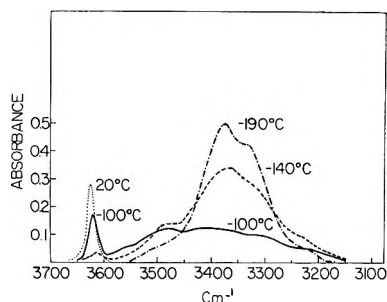


Figure 5. The OH stretching fundamental of 2,6-diisopropylphenol at different temperatures. Concentration at 20°: 0.104 *M* in FM; cell length: 0.183 mm.

from 3576 cm^{-1} at 20° to 3558 cm^{-1} at -100°. If we suppose that the shifting remains linear up to -190° in conformity with previous observations,¹² we would expect a frequency of 3545 at -190°, not 3474.

We have to conclude, therefore, that the 3474- cm^{-1} band is an OH---OH band. The absence of a free OH band contradicts an assignment to an open-chain oligomer (or dimer) present in appreciable quantities. (This argument assumes that "free" OH bands due to end groups have intensities not very different from the intensities of the monomer bands. This important assumption is very difficult to prove, but Bellamy and Pace³ have shown that for mixed dimers, the end groups do cause free bands in the infrared spectrum. (There is, indeed, no reason to believe that free bands due to end groups are weaker than the monomer bands. The end group oxygens donate electronic charge to the HB so they should attract more charge from their hydrogen, and this should make the O-H bond which they form more polar, and the band more intense.) A cyclic dimer is unlikely on theoretical grounds.^{7,15} A cyclic tetramer is unlikely to have a frequency about 150 cm^{-1} higher than the polymer band. Thus we suggest that, very probably, the 3474- cm^{-1} band belongs to the cyclic trimer. The band observed in both solvents at about 3370 cm^{-1} might then well be due to a cyclic tetramer (although our evidence for this is only indirect).

The weakness of the 3474- cm^{-1} band in FM indicates that the Br atoms in FR make the concentration of the cyclic trimer and/or the intensity of the 3474 band increase. This is undoubtedly linked to a donor-acceptor interaction in which the oxygen lone-pair is attracted by a bromine atom.^{13,16}

More important than the assignment of the bands to individual species is the fact that the existence of cyclic oligomers is substantiated, even at liquid nitrogen temperatures.

In the region of the first overtone at -190° in FR (Figure 4) a strong band appears at 6725 cm^{-1} . This is likely to belong to the trimer, since if it belonged to the tetramer, it would have zero or negative anharmonicity. This would contradict a long series of observations made on the mechanical anharmonicity of free

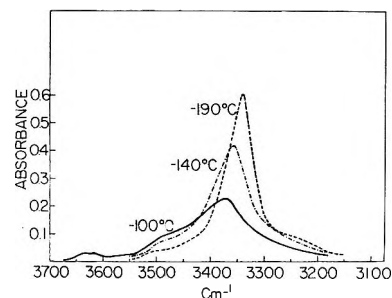


Figure 6. The OH stretching fundamental of 2,2,4-trimethyl-3-pentanol at different temperatures. Concentration at 20°: 0.07C *M* in FR; cell length: 0.183 mm.

and associated alcohols.^{9,12,17} The tetramer probably contributes to the observed intensity at the low-frequency side of the 6725- cm^{-1} band.

At -140°, the free-OH overtone is still quite strong, while at the same temperature, it is weak at the fundamental level. At -190°, the trimer band becomes the strongest band, while the tetramer band has not yet emerged from the background. Thus we again see that the bands of the less associated species are favored at the overtone level. (The first overtone of these oligomers is difficult to measure in FM because of solvent absorption.)

C. 2,2,4-Trimethyl-3-Pentanol. The spectra taken in FR (Figure 6) and FM are not very different for this molecule. The free and oligomer bands become very weak upon cooling, and at the lowest temperatures, we find a prominent polymer band at 3340 cm^{-1} . The band has a pronounced asymmetry, however, indicating the presence of a weak band at about 3390 cm^{-1} . There is also a weak band at 3500 cm^{-1} . These indicate the presence of a moderate amount of oligomer. At the level of the first overtone (Figure 7), we are again in the presence of a much better representation of the monomer and oligomer bands. At -97° (Figure 7), the monomer still gives the highest peak, and the oligomer peak at 6715 cm^{-1} appears to be stronger than the polymer band. At -190° we find a well defined oligomer band at 6645 cm^{-1} , and a very strong polymer band at 6405 cm^{-1} .

Discussion

Although at low temperatures the bands become significantly sharper, they remain quite broad, showing that each associated species is accompanied by a continuum due to a distribution of O---O distances and solvent configurations.¹⁸ Under these circumstances,

(15) A. S. N. Murthy, R. E. Davis and C. N. R. Rao, *Theoret. Chim. Acta (Berlin)*, **13**, 81 (1969).

(16) M. Asselin and C. Sandorfy, *Chem. Phys. Lett.*, **8**, 601 (1971).

(17) M. Asselin, G. Bélanger, and C. Sandorfy, *J. Mol. Spectrosc.*, **30**, 96 (1969).

(18) J. Schiffer and D. F. Hornig, *J. Chem. Phys.*, **49**, 4150 (1968).

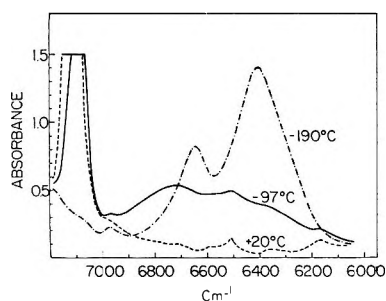


Figure 7. The first overtone of 2,2,4-trimethyl-3-pentanol at different temperatures. Concentration at 20°: 0.050 *M* in FR; cell length: 10 cm; 10× scale expansion used.

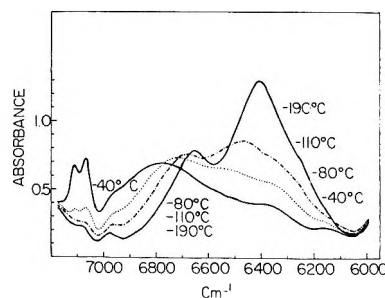


Figure 8. The first overtone of the OH stretching vibration of 2,2,4-trimethyl-3-pentanol (7:3 mixture with CCl_3F) at different temperatures; cell length: 1 cm.

we can only hope to distinguish between species which widely differ from each other in hydrogen bond energy.

For DMP, Dos Santos, Cruège, and Pineau¹⁹ have shown that at room temperature and for a 0.05 mole fraction, the proportion of cyclic species with respect to the total amount of polymers is much higher than for phenol itself. Our results are in qualitative agreement with this. In fact, we found that steric hindrance increases the proportion of cyclic oligomers, which can still be clearly identified at -190° in the case of DMP and DIPP.

As for mechanical anharmonicities, the values we have found are similar to those reported previously.¹² ($X_{12} \sim 130 \text{ cm}^{-1}$ at -190°). The mutual overlap between the broad oligomer bands and polymer bands prevents us from computing anharmonicity constants for the former. The cyclic trimer of DIPP gives $X_{12} = 110 \text{ cm}^{-1}$, a value intermediate between normal values for free OH bands (about 80 cm^{-1}) and polymer bands.

In all the spectra there is a weak band at about 3200 cm^{-1} . A similar band was found in the spectrum of methanol in CCl_4 by Van Ness, Van Winkle, Richtol, and Hollinger²⁰ who assigned it to "waterlike" structures in which the oxygen atom is acceptor for two protons.

All alcohols and phenols possess a few weak bands in the 6500-cm^{-1} region which are due to $\nu_{\text{CH}} + \nu_{\text{OH}}$ type combinations involving the free OH stretching vibration. When the temperature is lowered and hydrogen bond formation proceeds, these become gradually weaker and finally disappear. We find shoulders of the $\nu_{\text{CH}} + \nu_{\text{OH}}$ type in the $6200\text{-}6300$ region involving the associated OH group. These, however, cannot be mistaken for the associated OH stretching overtone, which is much stronger. This can be substantiated by measuring the spectrum of alcohols deuterated on the carbons. Asselin and Sandorfy¹⁰ examined the spectra

of 2-propanol and 2-propanol-*d*₇ (not deuterated in the OH) at -190° , and found the polymer overtone at the same frequency, and with the same general appearance. The same was found with methanol. (See following paper.) On this ground, we can rule out a proposal made by Luck and Ditter,²¹ according to which the weaker band (our oligomer band) would be the polymer band, and the strong and broad band (our polymer band), a combination of the $\nu_{\text{CH}} + \nu_{\text{OH}}$ type.

The weaker associated band in the first overtone region of TMP (6645 cm^{-1}) resembles a band in the spectrum of tertiary butanol which Asselin and Sandorfy¹⁰ ascribed to double excitation (simultaneous excitation by one quantum in two OH groups bound together by a hydrogen bond). They used deuteration and isolation techniques and have also shown that it cannot be due to Fermi resonance.

We measured the spectrum of the 2,2,4-trimethyl-3-pentanol by mixing it with CCl_3F in a proportion of 7:3 by volume (Figure 8). At -190° , the spectrum was practically the same as in FR or FM. (Showing that our using of mixed solvents does not produce additional bands in the spectra.) In addition, it can be seen that the oligomer band gradually shifts toward 6645 cm^{-1} upon cooling and becomes gradually sharper. This shows that this band can be assigned to oligomers. A coincidence is possible, however, and the matter is not definitely settled. Measurements at temperatures lower than -190° could provide additional evidence.

Acknowledgment. We acknowledge financial assistance from the National Research Council of Canada.

(19) J. Dos Santos, F. Cruège, and P. Pineau, *J. Chim. Phys.*, **67**, 826 (1970).

(20) H. C. Van Ness, J. Van Winkle, H. H. Richtol, and H. B. Hollinger, *J. Phys. Chem.*, **71**, 1483 (1967).

(21) W. A. P. Luck and W. Ditter, *Ber. Bunsenges. Phys. Chem.*, **72**, 365 (1968).

A Vibrational Overtone Study of Association in Liquid Methanol

by C. Bourdéron, J.-J. Péron, and C. Sandorfy*

Département de Chimie, Université de Montréal, Montréal, Québec, Canada (Received September 27, 1971)

Publication costs assisted by Université de Montréal

An attempt has been made to demonstrate the presence of oligomers and monomers in liquid methanol, by a study of the OH stretching fundamental, and its first and second overtones. The key to the solution of this problem is the previously made observation that a decrease in the intensity of the polymer overtones gives the bands of the less associated species a chance to appear.

Introduction

It was shown in the preceding paper¹ that hydrogen-bonded oligomers of sterically hindered alcohols subsist in solutions even at liquid nitrogen temperature. The identification of monomers and oligomers was seen to be facilitated in the region of the first overtone by a strong decrease in the intensity of the polymer bands.

We now present results pertaining to an alcohol not affected by steric hindrance, methanol. For this molecule, the OH stretching fundamental and its first and second overtones were studied in the liquid state.

Interpretation of the Spectra

(a) At room temperature in the fundamental region, we find only one nearly symmetrical broad band, centered at 3340 cm^{-1} , which is obviously due to the polymer. There is no evidence for the presence of either monomer or oligomers in this part of the spectrum of liquid methanol. (See the preceding paper for the sense given to the word "polymer".)

(b) The region of the first overtone (Figure 1), also measured at room temperature, is much more complex. We find a broad feature containing a well defined peak at about 6340 cm^{-1} (A), with three apparent subbands (B,C,D). The peak at 6340 cm^{-1} corresponds to the polymer; this is confirmed by the fact that at low temperatures it becomes preponderant (curve 3, Figure 1). C and B have the right frequency for being oligomer bands (see the preceding paper), and D the monomer band. One might argue that B is not really due to the OH stretching overtone of oligomers, but to combinations of the $\nu_{\text{CH}} + \nu_{\text{OH}}$ type, as was proposed by Fletcher and Heller.^{2,3} Curve 1 in Figure 1 shows the spectrum of 0.05 *M* methanol in CCl_3F at room temperature. (This spectrum was measured in a 10-cm cell using the 10 \times scale expansion of the Cary 17 instrument. The spectrum of the pure liquid was measured in a 0.2-cm cell so that the products of concentration by optical path were approximately the same in both cases). Under these conditions the monomer band, at about 7135 cm^{-1} (which has a peak absorbance of 4.7 on the scale of Figure 1) is preponderant, and a few weak

bands are found between 6500 and 6400 cm^{-1} . These bands are absent in the spectrum of both CH_3OD and CD_3OH , so they must be of the $\text{OH} + \text{CH}_3$ type. The OH bands entering these combinations are due to the free OH groups, however, and are much too weak to interfere with the observation of the B band (Figure 1). Clearly, then, oligomer bands are present in the first overtone region.

As for the D band, the contribution of free OH groups to its observed intensity is hard to estimate because of possible CH and CD absorption in the 7100-cm^{-1} region.⁴

We now have to examine the possibility that, as proposed by Luck and Ditter,⁵ the band at 6340 cm^{-1} is due to a combination of the $\text{OH} + \text{CH}_3$ type, involving the polymer OH stretching frequency. We therefore measured the spectrum of liquid CD_3OH . At room temperature, observation is made difficult because of interference from the $3\nu_{\text{CD}}$ bands. At -100° , as polymers become preponderant, we find a strong band at the same frequency as for CH_3OH . This is seen even more clearly in a solution of CD_3OH in a 1:1 mixture of CCl_3F and $\text{C}_2\text{F}_4\text{Br}_2$ at -190° . The same observation was made previously by Asselin and Sandorfy⁶ in the case of 2-propanol-*d*₇ and 2-propanol. Thus it is confirmed that the band at 6340 cm^{-1} is due to the polymer.

Whereas at the level of the fundamental only polymer bands are seen, monomer and oligomer bands appear at the first overtone level, the polymer still being the strongest.

(c) In order to interpret the second overtone region, we have to eliminate any possible absorption due to the methyl group. To do this we measured the spectrum of CH_3OH against CH_3OD . Since OD does not absorb

(1) C. Bourdéron, J.-J. Péron, and C. Sandorfy, *J. Phys. Chem.*, **76**, 864 (1972).

(2) A. N. Fletcher and C. A. Heller, *J. Phys. Chem.*, **71**, 3472 (1967).

(3) A. N. Fletcher and C. A. Heller, *ibid.*, **72**, 1839 (1968).

(4) R. F. Goddu and D. A. Delker, *Anal. Chem.*, **32**, 140 (1960).

(5) W. A. P. Luck and W. Ditter, *Ber. Bunsenges. Phys. Chem.*, **72**, 365 (1968).

(6) M. Asselin and C. Sandorfy, *J. Chem. Phys.*, **52**, 6130 (1970).

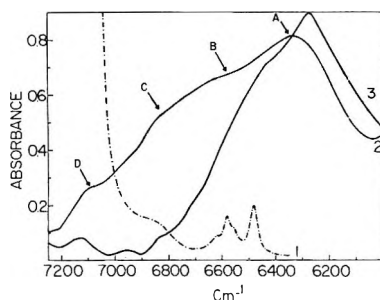


Figure 1. The first OH stretching overtone of liquid methanol. Curve 1: 0.05 *M* solution in CCl_3F at room temperature in a 10-cm cell using the 10 \times scale expansion. Curve 2: liquid at room temperature in a 0.2-cm cell. Curve 3: 0.24 *M* solution in a 1:1 mixture of CCl_3F and $\text{C}_2\text{F}_4\text{Br}_2$ at -190° . Cell length: 10 cm, using a 2 \times scale expansion.

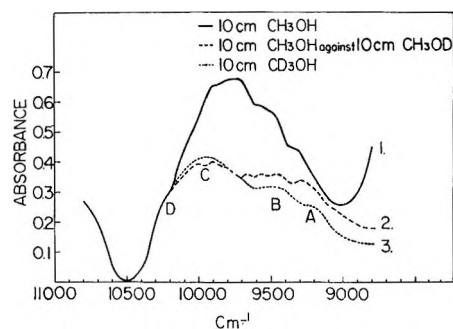


Figure 2. The second OH stretching overtone of liquid methanol. Curve 1: liquid in a 10-cm cell. Curve 2: CH_3OH compensated by CH_3OD in 10-cm cells. Curve 3: liquid CD_3OH in a 1-cm cell using the 10 \times scale expansion.

in this part of the spectrum, all the observed absorption must be due to the OH group. The result was curve 2 in Figure 2. It is very different from curve 1 which belongs to liquid methanol. Then, we went on measuring the spectrum of CD_3OH and obtained curve 3. The resemblance between curves 2 and 3 shows that they are both due to OH absorption. It is seen that in the second overtone region, the center of gravity is in the oligomer part (C). The free species is represented by a strong shoulder (D) at its high frequency side and there are two more bands at lower frequencies (A and B) which must correspond to more highly associated species (A surely being due to the polymer).

It may be difficult to believe that the broad C band corresponds to oligomers and the polymers give the weaker A and perhaps B bands. Thus we measured the spectrum at -100° , and found a spectacular decrease in the intensity of C, while the intensity of A increased (Figure 3). Since the lowering of temperature certainly favors the polymer, the C band cannot be the polymer band.

Discussion

We assign the 3340-cm^{-1} band to the polymer fundamental, 6340 cm^{-1} to its first overtone, and 9220 cm^{-1} to its second overtone. The last assignment takes into account the effect of CH_3 absorption (see above), and is different from the one proposed by Luck and Ditter⁵ who put it at 9760 cm^{-1} . From these frequencies we obtain the following (approximate) anharmonicity constants

$$X_{12} = \nu_{01} - \frac{\nu_{02}}{2} = 170\text{ cm}^{-1}$$

$$X_{23} = \frac{\nu_{02}}{2} - \frac{\nu_{03}}{3} = 100\text{ cm}^{-1}$$

$$Y_{123} = \frac{1}{2} \left(\nu_{02} - \nu_{01} - \frac{\nu_{03}}{3} \right) = -35\text{ cm}^{-1}$$

The latter value is of the same order as the one ob-

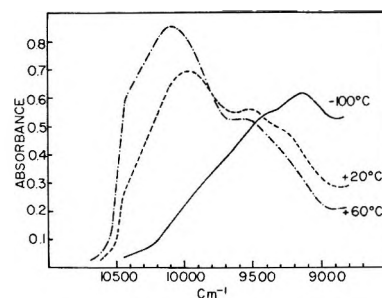


Figure 3. The second OH stretching overtone of liquid CD_3OH at different temperatures. Cell length: 3 cm, scale expansion 5 \times .

tained by Asselin and Sandorfy⁷ for other alcohols, using isotopic ratios rather than the second overtone.

In liquid methanol at room temperature, polymers, oligomers, and monomers are present. At the level of the OH stretching fundamental, the polymer bands are much stronger than the others, which are completely hidden under the polymer band envelope. At the level of the first overtone the polymer bands become weaker, and the oligomer band appears strongly.

At the level of the second overtone, the oligomer band becomes the strongest band in the spectrum. Even at low temperature, the intrinsically weak polymer band undergoes but a slight increase.

The oligomer band contains in all probability several different species. We cannot identify them.

The observed bands cannot be due to different OH groups of the same species. If they were, they could not exhibit the observed temperature changes.

Thus, thanks to our previous observations made on sterically hindered alcohols, the spectrum of methanol can be interpreted at all levels in a coherent way.

Acknowledgment. We express our thanks for financial support by the National Research Council of Canada.

(7) M. Asselin and C. Sandorfy, *J. Mol. Struct.*, **8**, 145 (1971).

Hydrogen Bonding and Complex Formation of Dimethylamine.

Infrared Investigations on the NH Stretching Vibration Bands

by H. Wolff* and G. Gamer

Physikalisch-Chemisches Institut, Universität Heidelberg, 69 Heidelberg, Germany (Received September 20, 1971)

Publication costs borne completely by The Journal of Physical Chemistry

The infrared spectra of dimethylamine in the fundamental and in the first overtone range of the NH stretching vibration have been investigated as a function of concentration and of temperature. In the fundamental range, in CCl_4 and *n*-hexane solutions bands of hydrogen-bonded and of free NH groups have been observed. A reduction of the frequency of the bonded groups in CCl_4 solution relative to the frequency in hexane solution is attributed to the increase in proton-donor ability of the amino group due to complexation with the solvent. A significant frequency decrease in hexane with increasing amine concentration is explained by an increase of proton-donor ability due to self-association. In the overtone range, except at the lowest temperatures, only the band of free groups has been detected. A decrease of its frequency in hexane with increase of amine concentration is attributed to the change from amino groups of monomers to the free groups of self-associates. The rather slight frequency shift in CCl_4 is explained by the transition from the free groups of CCl_4 complexes of monomers to the free groups of self-associates. From localization of the associate overtone at wave numbers 60 to 100 cm^{-1} lower than the free groups overtone, it follows that the decrease of mechanical anharmonicity caused by hydrogen bonding does not have the significance assumed previously. The enthalpy of association is determined to be about -1900 cal/mol in hexane and about -1100 cal/mol in CCl_4 . The fraction of the free NH groups in the pure compound is calculated to be about 60% at $+20^\circ$ and about 40% at -20° .

A. Introduction and Measurements

Hydrogen bonding of primary aliphatic amines was studied by infrared investigations of the NH stretching vibrations.^{1,2} It was of interest to extend these investigations to secondary aliphatic amines. Therefore, concentration and temperature dependence of infrared bands in the fundamental and the first overtone range of the NH stretching vibration of dimethylamine were analyzed. The measurements were performed at temperatures between $+20$ and -100° , mainly on solutions in *n*-hexane and CCl_4 , but as well on solutions in triethylamine and methanol, even covering some ternary mixtures.

The procedure used for obtaining the low-temperature spectra included the use of special cells into which the previously purified and degassed samples were condensed from a vacuum apparatus.^{1,2} By use of the Perkin-Elmer 125 spectrometer the spectral slit width could be selected sufficiently small to guarantee the measurement of the true band shape. Cell and solvent absorption were compensated.^{1,2} The extinction coefficients $\epsilon = 1/cl \log I_0/I$ (c expressed as mol/l.) were corrected for the changes of densities with temperature.^{1,2} To determine the location and the integrated absorption intensities of overlapping bands, a least-square-fit computer program³ was utilized.

Dimethylamine was prepared from its hydrochloride by addition of KOH. It was dried with LiAlH_4 before purifying and degassing by fractionation. Triethylamine ("purissimum" grade, Fluka AG) was dried with

sodium. CCl_4 and *n*-hexane (both "Uvasol" grade, E. Merck) were dried with P_2O_5 . Methanol ("Uvasol" grade, E. Merck) was dried with molecular sieve 3 Å previously heated at $300\text{--}350^\circ$ under vacuum.

B. Results and Discussion

Observed Bands. Figure 1 contains the spectra of hexane and of carbon tetrachloride solutions of dimethylamine which were obtained in the range of the NH stretching fundamental at -20° .⁴ The spectra are presented as extinction coefficients *vs.* wave number, concentration as parameter. Measured wave numbers are listed in Table I. Two bands are observed: the one at higher frequencies, increasing with dilution and increase of temperature, is assigned to the free NH groups (3361 cm^{-1} in hexane solution, 3356 cm^{-1} in CCl_4 solution). The other band, decreasing with dilution and increase of temperature, occurring at approximately $40\text{--}70$ cm^{-1} lower wave numbers, is assigned to

(1) H. Wolff and U. Schmidt, *Ber. Bunsenges. Phys. Chem.*, **68**, 579 (1964).

(2) (a) H. Wolff, *Z. Elektrochem.*, **66**, 529 (1962); (b) *J. Chem. Phys.*, **52**, 2800 (1970).

(3) H. Wolff and D. Horn, *Ber. Bunsenges. Phys. Chem.*, **72**, 419 (1968).

(4) The spectra in the fundamental range of *n*-hexane solutions of dimethylamine at $+20$, -60 , and -80° , and of the undiluted compound at 0 , -40 , and -80° will appear following these pages in the microfilm edition of this volume of the journal. Single copies may be obtained from the Business Operations Office, Books and Journals Division, American Chemical Society, 1155 Sixteenth St., N.W., Washington, D. C. 20036, by referring to author, title of article, volume, and page number. Remit check or money order for \$3.00 for photocopy or \$2.00 for microfiche.

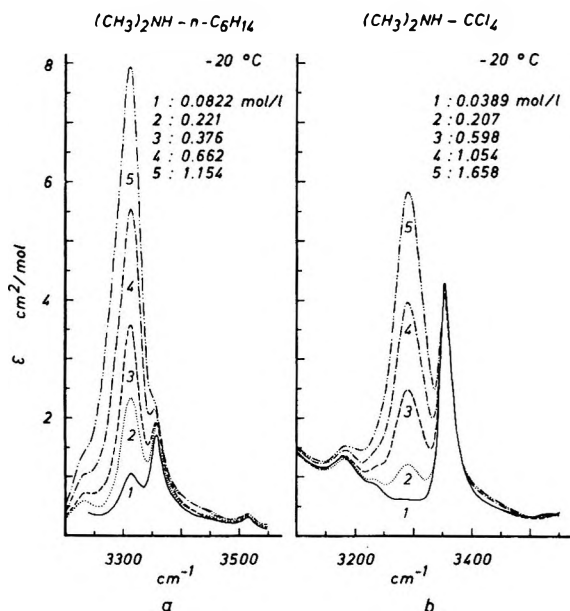


Figure 1. NH stretching fundamental of dimethylamine at -20° : a, hexane solutions; b, CCl_4 solutions.

the hydrogen-bonded NH groups (3322 cm^{-1} in hexane solution, 3302 cm^{-1} in CCl_4 solution, and 3294 cm^{-1} in the pure compound).

Table I: Wave Numbers of the NH Stretching Fundamental of Dimethylamine

Temp, $^\circ\text{C}$	Monomers in $n\text{-C}_6\text{H}_{14}$	Monomers in CCl_4	Associates in $n\text{-C}_6\text{H}_{14}$	Associates in CCl_4	Associates pure compound
+20	3360.5	3356	3322	3301.5	3293.5
-20	3359	3353	3315	3291	3279
-60	3357.5	...	3308.5	...	3262
-100	3247

Figure 2 shows the spectra of CCl_4 solutions in the range of the first overtone of the NH stretching vibration at -20° , concentration as parameter (spectra of hexane solutions are not reproduced because they behave similarly). Likewise, in Figure 2 the overtone spectra of the undiluted compound are shown, temperature as parameter. Measured wave numbers are listed in Table II. The wave numbers of the pure compound and of dilute CCl_4 solutions differ only by about 5 cm^{-1} . Moreover, the extinction coefficients increase with dilution. These observations lead to the conclusion that in the range of the first harmonics solely the band of free groups is visible. Earlier authors⁵ assumed that the band in the overtone range of undiluted secondary aliphatic amines belongs to the bonded groups. According to the low-temperature spectra of the pure compound only a weak absorption at $6420\text{--}6430\text{ cm}^{-1}$ can be assigned to the bonded NH.

Figure 3 shows the overtone spectra of a solution of

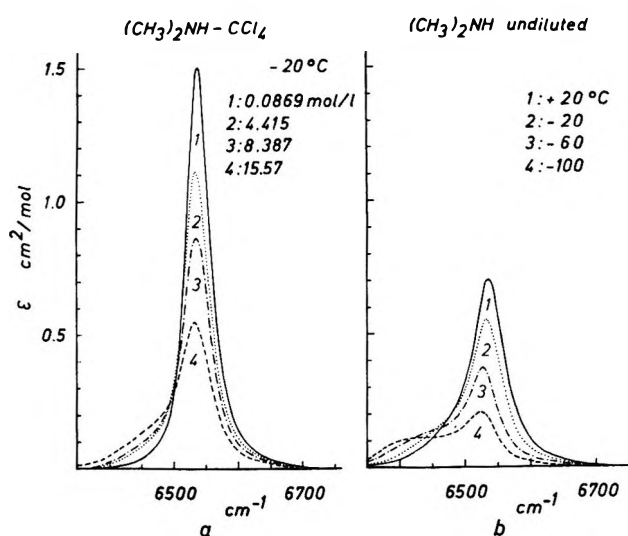


Figure 2. NH stretching overtone of dimethylamine: a, CCl_4 solutions at -20° ; b, pure dimethylamine at $+20$, -20 , -60 , and -100° .

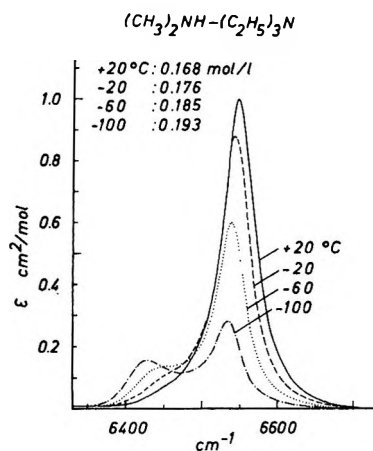


Figure 3. NH stretching overtone of dimethylamine in triethylamine solution (mole fraction 0.0231) at $+20$, -20 , -60 , and -100° .

dimethylamine in triethylamine (measured wave numbers in Table II). Besides the band of amine monomers the band of the bonded groups is observed more distinctly than in case of undiluted dimethylamine. This is most obvious in the -100° spectrum, thereby strengthening the assignment chosen for the pure compound.

Figure 4 shows the overtone spectra of hexane solutions of dimethylamine with added methanol. With increase of amine mole fraction the band at 6553 cm^{-1} of solutions in pure hexane is shifted to about 6510 cm^{-1} . This shift parallels a change from free monomeric NH groups to free NH groups of methanol adducts.

In the spectrum of a rather dilute solution of dimeth-

(5) C. Berthomieu and C. Sandorfy, *J. Mol. Spectrosc.*, **15**, 15 (1965).

Table II: Wave Numbers of the NH Stretching Overtone of Dimethylamine^a

Temp °C	Monomers in $n\text{-C}_6\text{H}_{14}$	Monomers in CCl_4	Free groups pure compound	Associates pure compound	Monomers in $\text{N}(\text{C}_2\text{H}_5)_3$	Adducts in $\text{N}(\text{C}_2\text{H}_5)_3$	Free groups in CH_3OH
+20	6553	6542.5	6538	(6479)	6548	(6467)	6511.5
-20	6549.2	6538	6534	(6469)	6543	(6464)	6506.5
-60	6545.6	...	6529	(6453)	6538	6450	6502
-100	6523	6426	6532	6433	...

^a The wave numbers of the pure compound and of the triethylamine solution were obtained from band separation procedure (section A). The data in parentheses were derived from weak band shoulders. They are less precise.

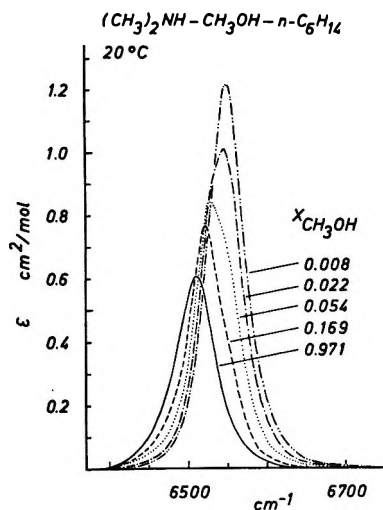


Figure 4. NH stretching overtone in dimethylamine + hexane + methanol as a function of mole fraction of methanol. $c_{(\text{CH}_3)_2\text{NH}}$ decreases from 0.117 mol/l. ($x_{\text{CH}_3\text{OH}} = 0.008$) to 0.110 mol/l. ($x_{\text{CH}_3\text{OH}} = 0.169$) and finally results in $c = 0.697$ mol/l. ($x_{\text{CH}_3\text{OH}} = 0.971$) at the binary mixture dimethylamine + methanol.

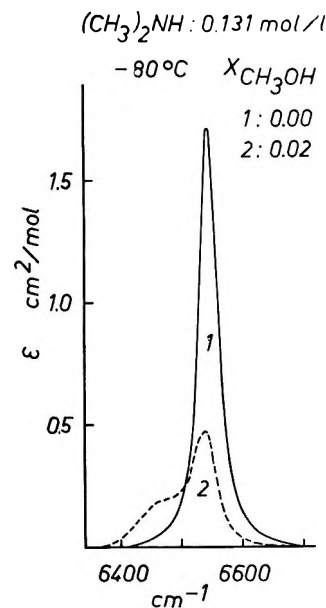
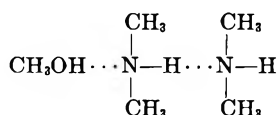


Figure 5. NH stretching overtone of dimethylamine in hexane solution (0.131 M) at -80° : —, pure solution; ----, with added methanol (mole fraction = 0.0215).

ylamine with added methanol at -80° (Figure 5) a second band is detected apart from the free group's band which is considerably reduced in intensity. The width and the shift of more than 100 cm^{-1} suggest an assignment of this band to the bonded NH groups of the dimethylamine-methanol adducts. If methanol is assumed as a proton-donor,^{6,7} the adducts may be described by the formula



The intensity of the adduct band is comparable with the intensity of the band of the bonded groups of pure dimethylamine at -100° (Figure 2b). Considering the lower amine concentration as well as the higher temperature of the solution, we conclude that the added methanol promotes the association to a larger degree than the increase in amine concentration.

Frequency Behavior

In Figure 6 the wave numbers of the associate fun-

damental are plotted vs. amine mole fraction, temperature as parameter. The values decrease with decrease of temperature, especially in more concentrated solutions and in the pure compound. The value of the pure compound at -110° amounts to 3244.5 cm^{-1} . This decrease must be at least partially attributed to the formation of stronger hydrogen bonds caused by the reduction of bond distances.

As can be seen, the wave numbers are lower in CCl_4 solutions than in hexane solutions, and they decrease with increasing amine mole fraction far more pronounced in hexane solutions than in CCl_4 solutions. Following the ideas developed by Hallam⁸ and by Bellamy, *et al.*,⁹ the lower values in CCl_4 have to be in-

(6) Th. Zeegers-Huyskens, *Spectrochim. Acta*, **21**, 221 (1965).

(7) Even diethyl ether, a stronger Brønstedt base than methanol, does not show any associate band in mixture with dimethylamine.

(8) H. E. Hallam in M. Davies, "Infrared Spectroscopy and Molecular Structure," Elsevier, Amsterdam, 1963.

(9) (a) L. J. Bellamy and R. J. Pace, *Spectrochim. Acta*, **22**, 525 (1966); (b) L. J. Bellamy, K. J. Morgan, and R. J. Pace, *ibid.*, **22**, 535 (1966).

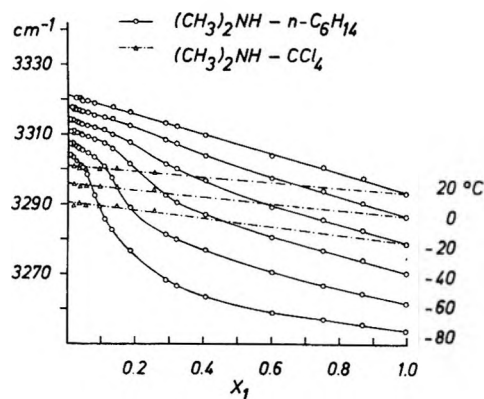


Figure 6. Wave numbers of the associate band of dimethylamine in hexane and CCl_4 solutions as a function of amine mole fraction and of temperature.

terpreted as a result of complexation with the solvent.^{10,11} This increases the polarization of the NH bond, and therewith the proton-donor ability of the amino group, thus leading to the formation of stronger $\text{N-H}\cdots\text{N}$ bonds.

In self-association an amine molecule takes over the role, which in CCl_4 solutions carbon tetrachloride plays with respect to the monomer. The dimer formed still has a weak hydrogen bond; it shows, therefore, a small shift of the associate band. Starting with the trimer, however, the polymers possess the stronger bonds resulting from the improved proton-donor ability. Therefore, the frequency decrease with increasing association can be explained by passing from the dimers to the trimers and higher polymers. The frequency decrease in the range of mole fractions from 0.1 to 0.3, especially at low temperatures, may be considered as a direct indication of that transition. The lack of a pronounced frequency decrease in CCl_4 solutions has to be interpreted in terms of that transition missing.

The explanation of the frequency shift by the improvement of the proton-donor ability due to complexation or self-association is based upon the assumption of chain-like association. The formation of chain-like associates may also be concluded from the observation of the band of the dimethylamine-triethylamine adducts at approximately the same position as the self-associate band, namely at 3302 cm^{-1} in hexane solutions and at 3281.5 cm^{-1} in CCl_4 solutions. With these adducts, there is no possibility of forming cyclic aggregates.

In Figure 7 the wave numbers of the overtone are plotted vs. amine mole fraction. Again a decrease of wave numbers with increasing amine mole fraction is observed. The decrease arises in hexane from the transition of the free groups of monomers to the free groups of self-associates, in carbon tetrachloride from the transition of the free groups of CCl_4 complexes of monomers to the free groups of self-associates. The rather small decrease in the latter case reveals that the

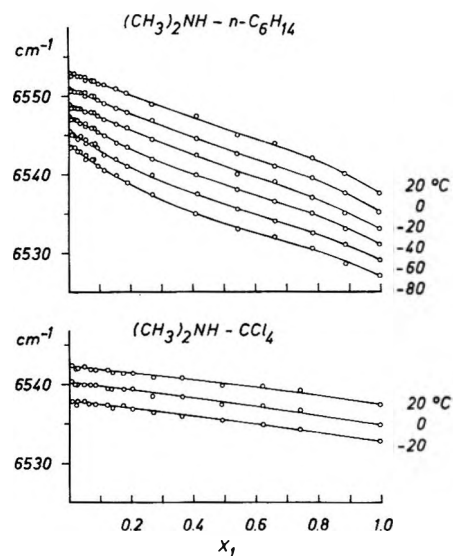


Figure 7. Wave numbers of the NH stretching overtone of dimethylamine in hexane and CCl_4 solutions as a function of amine mole fraction and of temperature.

complexation influences the free NH bond to nearly the same extent as the self-association.

In dilute solutions with added methanol a shift of the overtone of about 30 cm^{-1} occurs at methanol fractions below 0.1.¹² This shift corresponds with the transition from the free NH groups of monomers or CCl_4 complexes of monomers to the free groups of methanol complexes.

The associate overtone lies at wave numbers 60 to 100 cm^{-1} lower than the free groups overtone. From this it is concluded that the mechanical anharmonicity of the associated homologs, calculated from $|\nu_{02}/2 - \nu_{01}|$, is 30 to 50 cm^{-1} greater than determined in previous investigations.⁵ Therefore, the decrease of mechanical anharmonicity caused by hydrogen bonding does not have the significance assumed previously. (For dimethylamine solutions forming rigid glasses at low temperatures, this has been confirmed by Sandorfy, *et al.*,¹³ who found the monomer and associate anharmonicities to be nearly equal.)

Intensity Behavior

The most conspicuous feature of the intensity behavior of the NH stretching vibration bands is the low intensity of the free group's band in the fundamental range and the high intensity in the overtone range. Changing to the more active solvent, the extinction coefficient of the free NH fundamental increases. The

(10) A. N. Sharpe and S. Walker, *J. Chem. Soc. (London)*, 2974 (1961).

(11) H. Wolff and R. Würtz, *Ber. Bunsenges. Phys. Chem.*, 72, 101 (1968).

(12) The frequency-concentration plot of *n*-hexane and CCl_4 solutions of dimethylamine at increasing amounts of added methanol is reproduced in the microfilm edition. See ref 4.

(13) C. Sandorfy, private communication.

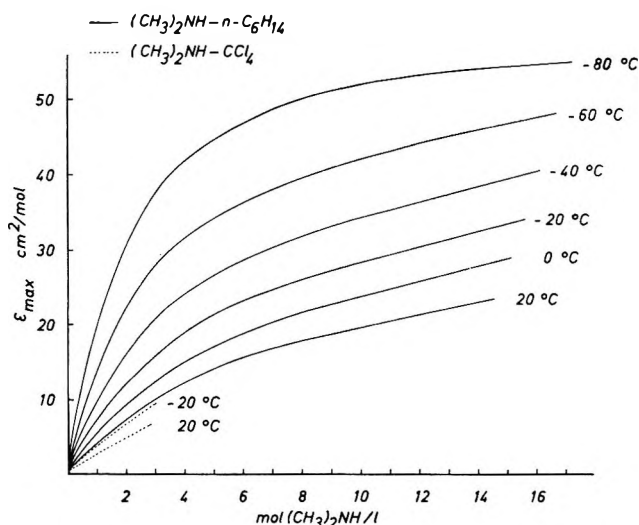


Figure 8. Maximum extinction coefficients of the associate band of dimethylamine in hexane and CCl_4 solutions as a function of amine concentration and of temperature.

integrated extinction coefficient in CCl_4 is about twice that in hexane solutions. In the overtone range the integrated extinction coefficients of both solutions are nearly the same, the ratio of overtone to fundamental intensity being 3:2 in hexane solutions and 2:3 in CCl_4 solutions.

In Figure 8 the maximum extinction coefficients of the band of bonded NH groups are plotted *vs.* concentration. At hexane solutions after a steep rise the extinction coefficients continue rather flattened. At CCl_4 solutions they are smaller and reveal a linear dependence upon concentration.

Thermodynamic Data

In undiluted dimethylamine and its solutions in hexane and CCl_4 the equilibria $\text{A}_1 + \text{A}_1 \rightleftharpoons \text{A}_2$, $\text{A}_2 + \text{A}_1 \rightleftharpoons \text{A}_3$, $\text{A}_3 + \text{A}_1 \rightleftharpoons \text{A}_4$, etc., are to be assumed. Denoting the equilibrium constants as $K_{1,2}$, $K_{2,3}$, $K_{3,4}$, etc., respectively, $K_{1,2}$ can be calculated from the maximum extinction coefficients of the overtone by the methods of Liddell and Becker¹⁴ and of Geiseler and Stöckel.¹⁵ The results of these calculations are listed in Table III. They are similar to the values obtained for $K_{1,2}$ from vapor pressure measurements^{16a} which are included in Table III. Besides, because of the larger frequency distance (Figure 7) the error resulting from superposition of the bands of free groups of monomers and of associates is smaller at hexane solutions than at CCl_4 solutions. The $K_{1,2}$ values for hexane solutions, therefore, can be assumed to be more precise than the values in CCl_4 .

The enthalpy of association was calculated from the equilibrium constants (Table III) as well as from the concentrations at which the maximum extinction coefficients of the associate band (Figure 8) are equal.^{1,2a} The average of these determinations in hexane, -1850

Table III: Association Constants $K_{1,2} = c_2/c_1^2$ of Dimethylamine in l./mol

Temp. °C	In hexane		From vapor pressure measurements ^a	In carbon tetrachloride	
	From ϵ_{max}			from ϵ_{max}	
	(Liddell/Becker)	(Geiseler-Stöckel)		(Liddell-Becker)	(Geiseler-Stöckel)
+20	0.108	0.102	0.118	0.0521	0.0576
-20	0.144	0.165	0.190	0.0735	0.0726
-60	0.232	0.318

^a Calculated by multiplying the mole fraction constants from ref 16a by the molar volume of the solvent.

cal/mol (-1110 and -1680 cal/mol from equilibrium constants, -2760 cal/mol from concentrations), is in satisfactory agreement with the value of -1820 cal/mol which was derived from vapor pressure data.^{16a} The average in CCl_4 , -1130 cal/mol (-1270 and -850 cal/mol from equilibrium constants, -1270 cal/mol from concentrations) is lower since the solvent complex must be dissociated at first.

The fraction of free NH groups in undiluted dimethylamine and in a $0.168 M$ solution in triethylamine could be determined from the ratio of overtone intensities of the pure compound or the triethylamine solution and of a dilute solution of dimethylamine in hexane. The results of these calculations are listed in Table IV.

Table IV: Fractions of Free NH Groups Calculated from the Integrated Absorption Intensities of the Overtone. In Parentheses: Fractions Calculated from the Maximum Extinction Coefficients

	Temp. °C			
	+20	-20	-60	-100
Pure dimethylamine	0.59 (0.49)	0.41 (0.33)	0.25 (0.20)	0.16
0.168 M solution in triethylamine	0.76 (0.69)	0.60 (0.53)	0.40 (0.33)	0.21

In accord with the results from investigations of the vapor pressure isotope effect^{16b} the fraction of free groups in the pure compound is found to be about 60% at $+20^\circ$ and about 40% at -20° . In the triethylamine solution the fraction was determined to be about 75% at $+20^\circ$ and about 55% at -20° . Fractions of 15–30% below -20° suggest the formation of considerable quantities of higher polymers in the pure compound at the lower temperatures.

(14) U. Liddell and E. D. Becker, *Spectrochim. Acta*, **10**, 70 (1958).

(15) G. Geiseler and E. Stöckel, *ibid.*, **17**, 1185 (1961).

(16) (a) H. Wolf and R. Würtz, *Z. Phys. Chem. (Frankfurt am Main)* **69**, 67 (1970); (b) *J. Phys. Chem.*, **74**, 1600 (1970).

Acknowledgment. We gratefully acknowledge support of this work by the Deutsche Forschungsgemein-

schaft, Bad Godesberg, and by the Fonds der Chemischen Industrie, Frankfurt.

The Role of the Diffuse Layer in Water-in-Oil Microemulsions

by S. Levine*

Department of Chemistry, University of Southern California, Los Angeles, California 90007

and K. Robinson

Department of Mathematics, The University, Manchester, M13 9PL, England (Received July 5, 1971)

Publication costs borne completely by The Journal of Physical Chemistry

The model proposed by Adamson for water-in-oil microemulsions is modified to allow for the diffuse layer in the aqueous droplet interior. For a 1-1 electrolyte, a relation governing the equilibrium of the droplet is derived which is based on a balance between the surface tension of the film at the boundary in its uncharged state, the osmotic pressure due to the ion concentrations, and the Maxwell electrostatic stress associated with the electric field in the internal diffuse layer. The corresponding Donnan equilibrium condition used by Adamson is obtained as the limiting case for very dilute electrolytes. Assuming that the potential distribution inside the droplet obeys the Poisson-Boltzmann equation, various approximate solutions to this equation are derived and the results compared with (exact) numerical calculations; one simple approximate solution gives particularly good agreement. Substitution of the approximate solutions into the droplet equilibrium condition gives estimates for the surface tension of the film at the droplet boundary in the form of a difference of two large but approximately equal quantities, each of which is strongly dependent on the surface potential. The determination of the surface tension is thus a sensitive measure of the accuracy of the various approximate solutions. For surface potentials ~ 50 mV the different values are in broad agreement; however at higher potentials (~ 100 mV) only one of our methods gives plausible results when compared with the computational values. Calculations of the ratios of salt concentration in the droplet to that in the bulk aqueous phase for various droplet radii seem consistent with the available experimental results.

1. Introduction

In a recent paper, Adamson¹ proposed a model for water-in-oil microemulsions (Schulman²⁻⁵) or micellar emulsions (Adamson¹) in terms of a balance between Donnan osmotic pressure due to the higher total ionic concentration in the emulsion unit and Laplace pressure associated with the interfacial tension. The surface of the emulsion droplets (with radii in the range 50-500 Å) are mixed films of surfactant and cosurfactant (*e.g.*, alcohol), which separate the aqueous interior of the droplet from the surrounding nonpolar (hydrocarbon) medium. The emulsion phase can exist in equilibrium with an essentially noncolloidal aqueous second phase provided there is some added electrolyte distributed between the droplets' aqueous interior and the external aqueous medium. Both aqueous media contain some alcohol and the total ionic concentration inside the droplet is found to exceed that in the external aqueous phase. The above model is depicted schematically in Figure 1.

Adamson¹ assumed that the ions in the aqueous

droplets were uniformly distributed at uniform electrostatic potential, which implies, by Poisson's equation, that the volume charge density inside the droplet is zero. This would only apply if the surfactant in the mixed film on the surface of the droplet were completely undissociated. A potential difference, $\Delta\chi$ say, between the droplet interior and the bulk of the aqueous phase would then be due to dipole orientation in the mixed film and at the boundary between the bulk hydrocarbon and aqueous phases. Suppose that the added electrolyte is univalent (say NaCl) and that its concen-

* Permanent address: Department of Mathematics, The University, Manchester, M13 9PL, England.

(1) A. W. Adamson, *J. Colloid Interface Sci.*, **29**, 261 (1969).

(2) J. E. Bowcott and J. H. Schulman, *Z. Elektrochem.*, **59**, 283 (1955).

(3) J. H. Schulman, W. Stoeckenius, and L. M. Prince, *J. Phys. Chem.*, **63**, 1677 (1959).

(4) J. H. Schulman and J. B. Montagne, *Ann. N. Y. Acad. Sci.*, **92**, 366 (1961).

(5) C. E. Cooke and J. H. Schulman, in "Surface Chemistry," P. Ekwall, K. Groth, and V. Runnstrom-Reio, Ed., Munksgaard, Copenhagen, 1965, p 231.

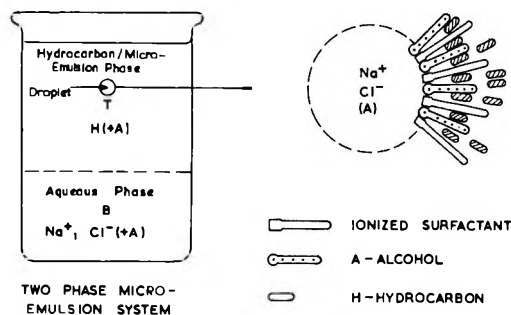


Figure 1. (a) Microemulsion phase in equilibrium with an aqueous phase. (b) Schematic representation of a droplet (from ref 17).

trations (number densities of molecules) in the droplet and external aqueous phases are n^* and n , respectively. Then the conditions of thermodynamic equilibrium with respect to Na^+ and Cl^- ions between the two aqueous phases may be expressed in the forms

$$\mu_1^0 + kT \ln n = \bar{\mu}_1^0 + kT \ln n^* + e_0 \Delta\chi \quad (1.1)$$

$$\mu_2^0 + kT \ln n = \bar{\mu}_2^0 + kT \ln n^* - e_0 \Delta\chi \quad (1.2)$$

where the four "standard" chemical potentials μ_1^0 , etc., depend on pressure, temperature T , and water-alcohol compositions. k is Boltzmann's constant and e_0 is the proton charge. It follows that

$$e_0 \Delta\chi = \frac{1}{2}(\mu_1^0 - \bar{\mu}_1^0 - \mu_2^0 + \bar{\mu}_2^0) \quad (1.3)$$

If the water-alcohol compositions are equal in the two phases then $\mu_1^0 = \bar{\mu}_1^0$, $\mu_2^0 = \bar{\mu}_2^0$, and $\Delta\chi = 0$. We conclude that if $\Delta\chi \neq 0$ and the film is uncharged, then thermodynamic equilibrium with respect to ions is possible only if the single ion free energies of solvation for each ion species differ in the two phases and this implies different compositions with respect to water and alcohol in these phases.

When the surfactant molecules become ionized, then a nonzero volume charge density is built up within the spherical volume of a droplet and it follows from Poisson's equation that a uniform potential is impossible. A diffuse layer potential gradient must prevail within the droplet when the mixed film is charged. The purpose of the present paper is to obtain the modifications to Adamson's work when the Gouy-Chapman theory (Poisson-Boltzmann equation) is applied to the diffuse layer. The Poisson-Boltzmann (P.B.) equation for the spherically symmetric potential distribution inside a droplet cannot be solved exactly by analytical methods except at low potentials, where the classical approach of Gronwall, La Mer, and Sandved⁶ is available. An equivalent but more convenient treatment has been developed by Bagchi, *et al.*,^{7,8} and we shall apply their method to the present problem. Two other approximate analytical methods which provide upper and lower bounds to the potential function under certain conditions will be described. Two purely

numerical techniques are also used to check the accuracy of the analytical results. Numerical methods based on variational principles⁹⁻¹² will not be considered.

2. Equilibrium Condition for the Charged Droplet

2a. The Net Charge on the Droplet. We assume that a surfactant molecule on the surface of the droplet becomes negatively charged by losing an Na^+ ion to the droplet interior. If the concentration of added electrolyte (NaCl) inside the droplet is n^* , and the additional concentration of Na^+ ions due to the dissociation of the surfactant film is n_s , then the total concentrations of Na^+ and Cl^- inside the droplet are $n_1^* = n^* + n_s$, $n_2^* = n$, respectively. If V_m is the droplet volume, then the total charge in the droplet interior, q_i , is just $e_0 V_m (n_1^* - n_2^*)$. The total charge on the film, q_f , is $4\pi a^2 \sigma$, where a is the droplet radius and σ is the film charge density. In general $q_f + q_i \neq 0$, and thus there is a net charge $Q = q_i + q_f$, on the droplet: we shall show that the magnitude of this net charge Q is much less than $|q_i|$ or $|q_f|$.

In the microemulsion water-in-oil system studied by Tosch, Jones, and Adamson,¹³ the oil phase contains 10-30% of water by volume, indicating a fairly concentrated dispersion of emulsion droplets. Similar concentrations are shown on the electron microscope photographs of Stoeckenius, Schulman, and Prince.¹⁴ If we consider a regular array of emulsion droplets, then a simple model of the diffuse layer in the oil medium surrounding a given droplet is a spherical shell carrying a charge $-Q$ to balance the charge Q on the droplet. The outer radius b of this shell is such that $4\pi b^3/3$ is the volume in the oil phase assigned to a droplet. If the charge distribution within this volume is assumed to be spherically symmetric, then the potential $\Psi = \Psi(r)$ will satisfy the boundary condition $[d\Psi/dr]_{r=b} = 0$. As we are only interested in the order of magnitude of Q , it is sufficient to consider the linear Debye-Hückel equation. The potential in the region $a \leq r \leq b$ is therefore¹⁵

(6) T. H. Gronwall, V. K. La Mer, and K. Sandved, *Phys. Z.*, **29**, 358 (1928).

(7) S. N. Bagchi, G. P. Das, and S. Chakravarti, *Bull. Nat. Inst. Sci. India*, **29**, 28 (1961).

(8) S. N. Bagchi and M. Plischke, *J. Indian Chem. Soc.*, **45**, 923 (1968).

(9) P. D. Robinson and A. M. Arthurs, *J. Math. Phys.*, **9**, 1364 (1968).

(10) N. Anderson and A. M. Arthurs, *ibid.*, **9**, 2037 (1968).

(11) A. M. Arthurs and P. D. Robinson, *Proc. Cambridge Phil. Soc.*, **65**, 535 (1969).

(12) A. M. Arthurs, "Complementary Variational Principles," Clarendon Press, Oxford, 1970.

(13) W. C. Tosch, S. C. Jones, and A. W. Adamson, *J. Colloid Interface Sci.*, **31**, 297 (1969).

(14) W. Stoeckenius, J. H. Schulman, and L. M. Prince, *Kolloid-Z.*, **169**, 170 (1960).

(15) J. R. Philip, *J. Chem. Phys.*, **52**, 1387 (1970).

$$\Psi(R) = \Psi_0 \frac{R_0 [\sinh(R_1 - R) - R_1 \cosh(R_1 - R)]}{R [\sinh(R_1 - R_0) - R_1 \cosh(R_1 - R_0)]} \quad (2.1)$$

where $\Psi_0 = \Psi(a)$, the potential just outside the droplet, $R = \kappa_h r$, $R_0 = \kappa_h a$ and $R_1 = \kappa_h b$, $1/\kappa_h$ being the Debye-Hückel thickness. From Gauss' theorem

$$Q = -a^2 \epsilon_h \left[\frac{d\Psi}{dr} \right]_{r=a} = \Psi_0 a^2 \epsilon_h \kappa_h \times \left[\frac{1}{R_0} - \left\{ \frac{R_1 \tanh(R_1 - R_0) - 1}{\tanh(R_1 - R_0) - R_1} \right\} \right] \quad (2.2)$$

For the extremely small ionic concentration in the oil medium ($10^{-9} M$, say) and an oil dielectric constant $\epsilon_h = 4$, we find that $R_0 \simeq 0.023$ for $a = 500 \text{ \AA}$, and R_1/R_0 lies in the range 1.4–2.1 for the concentration range mentioned above. We can therefore expand the hyperbolic tangent in powers of $R_1 - R_0$ to obtain

$$Q \approx \frac{\Psi_0 a \epsilon_h}{3R_0} (R_1^3 - R_0^3) \quad (2.3)$$

A typical value for the area per ionized surfactant molecule on the droplet surface is 100 \AA^2 . Thus $|q_f| \sim \pi \times 10^4 e_0$ for $a = 500 \text{ \AA}$, giving $|Q/q_f| \lesssim 3.5 \times 10^{-7}$ for $\Psi_0 = 50 \text{ mV}$. This fraction varies linearly with a and Ψ_0 . It should be noted that (2.3) gives $Q \rightarrow 0$ as $R_1 \rightarrow R_0$, as might be expected on physical grounds; the net charge on the droplet must vanish as the surrounding hydrocarbon volume falls to zero.

2b. The Effects of Dipole Orientation and Water-Alcohol Composition. If the diffuse layer in the hydrocarbon medium is ignored, so that each droplet carries zero charge, then the potential difference between the negatively charged inner side of the droplet film and the external bulk phase is $\Delta\chi$, the potential due to dipole orientation at the interfaces, to which we referred above. We shall now show how $\Delta\chi$ is related to the charge on the droplet. Let $n_1 = n_1(r)$ and $n_2 = n_2(r)$ be the number densities of Na^+ and Cl^- ions at some interior point of the droplet, at a radial distance r from the center, and $\psi = \psi(r)$ the mean potential at this point referred to the bulk aqueous medium as the zero. The conditions of thermodynamic equilibrium replacing (1.1) and (1.2) read

$$\mu_1^0 + \mathbf{kT} \ln n = \tilde{\mu}_1^0 + \mathbf{kT} \ln n_1 + e_0 \psi \quad (2.4)$$

$$\mu_2^0 + \mathbf{kT} \ln n = \tilde{\mu}_2^0 + \mathbf{kT} \ln n_2 - e_0 \psi \quad (2.5)$$

If we consider conditions at the surface of the droplet, where $n_1 = n_1(a)$, $n_2 = n_2(a)$, and write the potential just inside the drop as $\psi = \psi(a) = \psi_0 + \Delta\chi$, then by combining (2.4) and (2.5) we obtain

$$e_0 \Delta\chi = -e_0 \psi_0 + \mathbf{kT} \ln [n_2(a)/n_1(a)] + \frac{1}{2} [\mu_1^0 - \tilde{\mu}_1^0 - \mu_2^0 + \tilde{\mu}_2^0] \quad (2.6)$$

Even if the alcohol/water compositions are identical in the two media so that $\mu_1^0 = \tilde{\mu}_1^0$, $\mu_2^0 = \tilde{\mu}_2^0$, by com-

parison with eq 1.3 we see that $\Delta\chi$ is now nonzero because of the charge on the droplet. If the compositions were identical in the two aqueous media and the droplets were uncharged, then $\Delta\chi$ would be zero (neglecting a possible effect of droplet curvature). This is because the contribution to $\Delta\chi$ from the plane film at the hydrocarbon-bulk aqueous phase boundary would cancel with that from the spherical film at the droplet-hydrocarbon boundary. These two films are different when the droplet is charged and thus basically $\Delta\chi$ is nonzero due to the dependence on this charge of the proportions and concentrations of surfactant and alcohol molecules in the droplet film. The above argument also implies that the presence of the electrolyte is essential to microemulsion formation.

We may write the equilibrium conditions 2.4 and 2.5 in the form

$$\begin{aligned} n_1 &= n_1^0 \exp[-e_0 \psi / \mathbf{kT}]; \\ n_1^0 &= n \exp[(\mu_1^0 - \tilde{\mu}_1^0) / \mathbf{kT}] \end{aligned} \quad (2.7)$$

$$\begin{aligned} n_2 &= n_2^0 \exp[e_0 \psi / \mathbf{kT}]; \\ n_2^0 &= n \exp[(\mu_2^0 - \tilde{\mu}_2^0) / \mathbf{kT}] \end{aligned}$$

On introducing the quantities

$$m = (n_1^0 n_2^0)^{1/2}; \quad \alpha = \frac{\mathbf{kT}}{e_0} \ln (n_1^0 / n_2^0) \quad (2.8)$$

(2.7) becomes

$$\begin{aligned} n_1 &= m \exp[-e_0(\psi - \alpha) / \mathbf{kT}]; \\ n_2 &= m \exp[+e_0(\psi - \alpha) / \mathbf{kT}] \end{aligned} \quad (2.9)$$

Here m is proportional to the NaCl concentration n in the external aqueous phase; in the particular case of identical water-alcohol composition in the two phases, $m = n$ and $\alpha = 0$.

2c. The Equilibrium Condition. For equilibrium between the microemulsion phase and the external aqueous phase, the Helmholtz free energy of the whole system must be a minimum with respect to any small change, subject to constant total volume and constant temperature. Such a change could be the hypothetical transfer of a small number of water and alcohol molecules from the aqueous bulk phase to the droplet interior. We may suppose that this is carried out in two stages. In stage I, water and alcohol molecules are transferred from the bulk aqueous medium to the droplet interior, increasing the droplet volume by δV_m and causing a corresponding change in the volume of the bulk aqueous phase of $-\delta V_m$. However, the numbers of ions Na^+ and Cl^- and the numbers of surfactant molecules (ionized and un-ionized) in the droplet interior and in the film on the droplet surface are kept fixed. (For simplicity we may assume that the water-alcohol media are incompressible.) The changes pro-

duce an infinitesimal departure from equilibrium, which is restored in stage II when we transfer ions and surfactant molecules from the bulk aqueous medium to the droplet. Also, surfactant molecules may be adsorbed into the film from the droplet interior, and a change may occur in degree of dissociation. If we have equilibrium, no free energy change occurs in stage II. The change in the Helmholtz free energy in stage I may be obtained from the general treatment by Bell and Levine¹⁶⁻¹⁸ (referred to as B.L. Parts I, II, III) of the electric double layer free energies and forces in concentrated colloidal suspensions. We assume that the electric double layers inside the droplet and in the surrounding oil medium are governed by the Poisson-Boltzmann equation. The particular system considered by B.L. which is pertinent here is the one where diffuse layers are present in both the particle interiors (here aqueous) and the external dispersion medium (here oil). The "electrical" free energy associated with the double layer is obtained by a Debye-Hückel charging process and can be written in the form (Part I) $F_e = E_e - TS_e$ where E_e is the familiar electrostatic field energy and S_e is the change in entropy which is due to the re-arrangement of ions in the diffuse layers during the charging process. In addition we need to include the entropic term in the free energy in the completely discharged state which is part of the "chemical" free energy F_c . If this is denoted by $-TS_0$ then for each droplet we have

$$S_e + S_0 = -k \int_V [n_1(\ln n_1 - 1) + n_2(\ln n_2 - 1)] dv \quad (2.10)$$

where n_1 and n_2 are the number densities of Na^+ and Cl^- ions at an arbitrary point inside the droplet. B.L. show that if the surface of a typical particle at any sol concentration undergoes a general displacement $\delta\mathbf{r}$ which may vary with position on the surface, then the change in F_e is (Part II, eq 7.4, 7.5)

$$\delta F_e = - \int_S \mathbf{X} \cdot \delta\mathbf{r} dS \quad (2.11)$$

where

$$\mathbf{X} = \{ \mathbf{T} - \mathbf{T}' - (\Delta\Pi - \Delta\Pi')\mathbf{U} \} \cdot \mathbf{n}_s \quad (2.12)$$

\mathbf{T} and \mathbf{T}' are the Maxwell stress tensors just outside and inside the particle, $\Delta\Pi$ and $\Delta\Pi'$ are the corresponding ideal osmotic pressure terms, \mathbf{U} is the unit tensor, and \mathbf{n}_s is the unit outward vector normal to the particle surface. The corresponding change in the chemical free energy F_c is

$$\delta F_c = \int_S kT(n_1^* + n_2^*)\mathbf{U} \cdot \delta\mathbf{r} dS \quad (2.13)$$

In Part III, B.L. apply this general formula to the outer boundary of their system, here considered as a single

droplet, by imagining solvent molecules transferred into the system. In our case, we may ignore the contributions from the oil phase (\mathbf{T} and $\Delta\Pi$) and because of the spherical symmetry obtain simply (Part II, eq 4.15, 5.12, Part III, eq 2.1, 2.2)

$$\Delta\Pi' = kT[n_1(a) + n_2(a) - n_1^* - n_2^*];$$

$$\mathbf{T}' \cdot \mathbf{n}_s = \frac{\epsilon}{8\pi} \left[\frac{d\psi}{dr} \right]_{r=a}^2 \mathbf{n}_s \quad (2.14)$$

where $n_1(a)$, $n_2(a)$ are the number densities of Na^+ and Cl^- ions just inside the droplet. Noting that $\int_S \mathbf{U} \cdot \delta\mathbf{r} \cdot dS$ is just δV_m , the total change in the free energy in stage I is therefore

$$\left\{ kT[n_1(a) + n_2(a)] - \frac{\epsilon}{8\pi} \left[\frac{d\psi}{dr} \right]_{r=a}^2 \right\} \delta V_m \quad (2.15)$$

where ϵ is the dielectric constant of the droplet interior. To the same approximation the free energy change associated with the ideal ion entropy in the bulk aqueous phase is

$$-2nkT\delta V_m \quad (2.16)$$

If γ is the non-Coulombic part of the surface tension of the mixed film and $S_m = 4\pi a^2$ the area of the droplet film, then the free energy change attributed to this surface tension is

$$-\gamma\delta S_m = -(2\gamma/a)\delta V_m \quad (2.17)$$

There will also be a contribution to the free energy change due to any difference in the water-alcohol concentrations of the two phases. Because little is known about such a possible change in water-alcohol concentration and about the surface tension γ , in the rest of this paper we shall assume identical water-alcohol compositions in the two phases and therefore put $m = n$ and $\alpha = 0$. The equilibrium condition is therefore that the sum of (2.15)–(2.17) equals zero, *i.e.*

$$\frac{2\gamma}{a} = kT[n_1(a) + n_2(a) - 2n] - \frac{\epsilon}{8\pi} \left[\frac{d\psi}{dr} \right]_{r=a}^2 \quad (2.18)$$

Schulman and his coworkers^{2-5,19} have proposed that negative interfacial tension is responsible for the formation of microemulsions. Thus if $(\gamma_{w/o})_a$ is the interfacial tension between the water and the oil phase in the presence of added alcohol and Π is the spreading pressure in the film due to the surfactant, then the total interfacial tension $\gamma_i = (\gamma_{w/o})_a - \Pi < 0$ in the non-equilibrium state. It is postulated that an equilibrium state is attained through the formation of the microemulsion when γ_i tends to zero. However, the effect

(16) G. M. Bell and S. Levine, *Trans. Faraday Soc.*, **53**, 143 (1957).

(17) G. M. Bell and S. Levine, *ibid.*, **54**, 785 (1958).

(18) G. M. Bell and S. Levine, *ibid.*, **54**, 975 (1958).

(19) L. M. Prince, *J. Colloid Interface Sci.*, **23**, 165 (1967).

of the electric double layer is not taken into account. In the present theory, the total change in the free energy is represented by the sum of (2.15)–(2.17), which we may write as $\delta F = \gamma_i \delta S_m$; eq 2.18 then expresses the condition $\gamma_i = 0$. If Π_u is the spreading pressure of the uncharged surfactant and Π_e is the Coulombic contribution to Π , then we can identify our non-Coulombic surface tension γ with $(\gamma_{w/0})_a - \Pi_u$. Thus (2.18) may also be expressed as $\gamma = \Pi_e$. We observe that if the double layer is absent and $\Delta\chi = 0$, the right-hand side of (2.18) vanishes and we obtain $\gamma = 0$.

3. Linear Debye–Hückel Approximation

The potential $\psi(r)$ is assumed to satisfy the Poisson–Boltzmann equation

$$\frac{1}{r^2} \frac{d}{dr} \left(r^2 \frac{d\psi}{dr} \right) = -4\pi e_0 (n_1 - n_2) / \epsilon = \frac{8\pi n e_0}{\epsilon} \sinh \left(\frac{e_0 \psi}{kT} \right) \quad (3.1)$$

where we have put $m = n$ and $\alpha = 0$ in (2.9). At small potentials, this becomes

$$\frac{1}{r^2} \frac{d}{dr} \left(r^2 \frac{d\psi}{dr} \right) = \kappa^2 \psi \quad (3.2)$$

where κ is the Debye–Hückel parameter, characteristic of the electrolyte in the bulk aqueous medium, given by

$$\kappa^2 = 8\pi n e_0^2 / \epsilon kT \quad (3.3)$$

The solution of (3.2) which is finite at the centre $r = 0$ has the form

$$\psi(r) = B \frac{\sinh \kappa r}{r} \quad (3.4)$$

where the constant B is determined by applying Gauss's flux theorem at $r = a$. If we ignore the charge $-Q$ in the diffuse layer of the hydrocarbon medium, then

$$\frac{4\pi\sigma}{\epsilon} = \left(\frac{d\psi}{dr} \right)_{r=a} \quad (3.5)$$

from which, if $x_0 = \kappa a$

$$B = \frac{4\pi a^2 \sigma}{\epsilon (x_0 \cosh x_0 - \sinh x_0)} \quad (3.6)$$

In the linear approximation of the Debye–Hückel theory, we write

$$kT [n_1(a) + n_2(a) - 2n] = 2nkT [\cosh \Lambda_s - 1] \approx nkT \Lambda_s^2 \quad (3.7)$$

where

$$\Lambda_s = \frac{e_0 \psi(a)}{kT} \quad (3.8)$$

Using (3.4)–(3.8), the equilibrium condition (2.18) becomes

$$\frac{2\gamma}{a} = \frac{2\pi\sigma^2}{\epsilon} \left[\frac{x_0 \sinh 2x_0 - \sinh^2 x_0 - x_0^2}{(x_0 \cosh x_0 - \sinh x_0)^2} \right] \quad (3.9)$$

At the two extremes in the range of x_0

$$\begin{aligned} \frac{2\gamma}{a} &\rightarrow \frac{4\pi\sigma^2}{\epsilon x_0} \quad (x_0 \rightarrow \infty); \\ \frac{2\gamma}{a} &\rightarrow \frac{18\pi\sigma^2}{\epsilon x_0^2} \quad (x_0 \rightarrow 0) \end{aligned} \quad (3.10)$$

According to the second limiting expression $a \rightarrow \infty$ as $\kappa \rightarrow 0$, *i.e.*, the electrolyte tends to zero, for given γ and σ_0 , confirming that microemulsion formation is impossible in absence of electrolyte. An estimate of γ predicted by (3.9) is easily obtained. For $a = 100$ Å and an electrolyte concentration of $0.1 M$, $\kappa \sim 10^7$ cm⁻¹ and $x_0 \sim 10$. If A is the area per univalent ionized surfactant molecule in the micelle film, and $\sigma_0 = -e_0/A$, on combining (3.4) and (3.6), the potential at the film is given by

$$\Lambda_s = \frac{4\pi a e_0^2}{kTA} \frac{1}{(x_0 \coth x_0 - 1)} \approx \frac{4\pi a e_0^2}{kTA(x_0 - 1)} \quad (3.11)$$

for $x_0 \gg 1$. A typical value of 1 for the left-hand member of (3.11) requires $A \sim 1000$ Å² and then (3.10) gives the very small surface tension $\gamma \sim 1/4$ dyn/cm indicating that the surface charge density σ is outside the range of the Debye–Hückel approximation.

The equilibrium condition which corresponds to (2.18) and is used by Adamson reads

$$kT(n_1^* + n_2^* - 2n) = \frac{2\gamma}{a} \quad (3.12)$$

where the mean concentrations n_1^* and n_2^* of Na⁺ and Cl⁻ ions in the droplet interior are

$$n_1^* = \frac{1}{V_m} \int_{V_m} n_1 dv, \quad n_2^* = \frac{1}{V_m} \int_{V_m} n_2 dv \quad (3.13)$$

Making use of (2.9) and introducing the Debye–Hückel approximation, (3.12) becomes

$$\begin{aligned} \frac{2\gamma}{a} &= \frac{2nkT}{V_m} \int_{V_m} \left[\cosh \left(\frac{e_0 \psi}{kT} \right) - 1 \right] dv \approx \\ &\frac{3nkT}{a^3} \int_0^a \left(\frac{e_0 \psi}{kT} \right)^2 r^2 dr = \frac{x_0 (\sinh 2x_0 - 2x_0)}{(x_0 \cosh x_0 - \sinh x_0)^2} \end{aligned} \quad (3.14)$$

Then

$$\begin{aligned} \frac{2\gamma}{a} &\rightarrow \frac{3\pi\sigma^2}{2\epsilon x_0} \quad (x_0 \rightarrow \infty); \\ \frac{2\gamma}{a} &\rightarrow \frac{18\pi\sigma^2}{\epsilon x_0^2} \quad (x_0 \rightarrow 0) \end{aligned} \quad (3.15)$$

Comparison of (3.15) with (3.10) shows that the formula (3.14) underestimates the value of γ by a factor of $3/4$ at large x_0 , but at small x_0 (3.9) gives the same limiting form as (3.14). The latter result is to be ex-

pected because the ion distribution in the micelles should become uniform as the electrolyte concentration tends to zero.

4. Estimates of the Potential Distribution

This section contains descriptions of various approximate solutions of the P.B. equation, since a better physical insight can be obtained from a good analytical approximation than from an anonymous table of numbers in a computer printout. Also, these solutions may be useful in related problems. Numerical methods will be described in the following section to test the accuracy of our approximations but these are very time-consuming and thus are not convenient in use. For the large values of κa relevant here, an approximate analytical method is described which is very useful because of its simplicity; it also leads to a simple expression for the surface tension (§5d). Furthermore, we apply the exact series solution of Bagchi, *et al.*,^{7,8} which is not widely known, to our problem, and calculate the first two terms. In describing these approximate solutions to the P.B. equation, it is convenient to assume that the potential and hence σ are positive. Making the substitutions

$$x = \kappa r, y = \frac{e_0 \psi}{kT} x = \Lambda x \quad (4.1)$$

the P.B. eq 3.1 becomes

$$\frac{d^2 y}{dx^2} = x \sinh (y/x) \quad (4.2)$$

Multiplying both sides of (4.2) by dy/dx and integrating, we have

$$\left(\frac{dy}{dx}\right)^2 - \left(\frac{dy}{dx}\right)_{x=0}^2 = 2 \int_0^y x \sinh (y/x) dy \quad (4.3)$$

where $(dy/dx)_{x=0} = e_0 \psi(0)/kT = \Lambda_0$. Since $0 \leq x \leq x_0$, we have the inequalities

$$x \sinh (y/x) > x_0 \sinh (y/x_0) > y \quad (4.4)$$

which allow us to derive convenient approximate expressions for the potential. If we replace the integrand in the right-hand member of (4.3) by y , then it is easily seen that (4.3) yields the linear Debye-Hückel solution (3.4), which we may write as

$$\psi(r) = \psi(0) \frac{\sinh \kappa r}{\kappa r} = \frac{x_0 \psi(a)}{\sinh x_0} \frac{\sinh x}{x} \quad (4.5)$$

If $\psi(0)$ is specified, then the inequalities (4.4) ensure that (4.5) yields an underestimate of the exact solution of the P.B. equation.

In the following subsections we derive three closer approximations to the exact solution of (4.2).

4a. "One-Part" Solution. If the integrand in (4.3) is replaced by $x_0 \sinh (y/x_0)$, we obtain

$$\left(\frac{dy}{dx}\right)^2 - \left(\frac{dy}{dx}\right)_{x=0}^2 = 2x_0^2 [\cosh (y/x_0) - 1] \quad (4.6)$$

Introducing $z = y/x_0$ and

$$b^2 = 1 - \frac{1}{2x_0^2} \left(\frac{dy}{dx}\right)_{x=0}^2 = 1 - \frac{\Lambda_0^2}{2x_0^2} \quad (4.7)$$

(4.6) simplifies to

$$\frac{dz}{dx} = \sqrt{2}(\cosh z - b^2)^{1/2} \quad (4.8)$$

The solution of (4.8) can be expressed in terms of the incomplete elliptic integral of the first kind (ref 20, p 185, eq 297.00), namely

$$x = F(\phi, k) = \int_0^\phi d\theta / (1 - k^2 \sin^2 \theta)^{1/2} \quad (4.9)$$

where

$$k^2 = 1/2(1 + b^2); \quad k'^2 = 1 - k^2 = (\Lambda_0/2x_0)^2 \quad (4.10)$$

and

$$\sin \phi = \frac{\sqrt{2}}{[1 + b^2 + (1 - b^2) \coth^2 (1/2z)]^{1/2}} = \frac{1}{[1 + k'^2/\sinh^2 (y/2x_0)]^{1/2}} \quad (4.11)$$

By the first inequality in (4.4) we see that (4.9) must be a lower bound to the exact solution of (4.2) if $\psi(0)$, the potential at the centre of the droplet, is given.

The surface charge density, σ , is given by

$$\sigma = \frac{\epsilon}{4\pi} \left[\frac{d\psi}{dr} \right]_{r=a} = \frac{\kappa \epsilon kT}{4\pi e_0 x_0} \left[\frac{dy}{dx} - \frac{y}{x} \right]_{x=x_0} = \frac{\kappa \epsilon kT}{4\pi e_0 x_0} [(4x_0^2 \sinh^2 \{1/2\Lambda_s\} + \Lambda_0^2)^{1/2} - \Lambda_s] \quad (4.12)$$

using (4.6) and (4.10); $\Lambda_s = e_0 \psi(a)/kT$, the reduced surface potential. Also the equilibrium condition (2.18) can be written as

$$\frac{2\gamma}{a} = 4\pi \kappa T \sinh^2 (1/2 \Lambda_s) - \frac{2\pi \sigma^2}{\epsilon} \quad (4.13)$$

with σ given by (4.12). For given electrolyte concentration, droplet radius, and Λ_0 , the relations (4.9)–(4.11) determine Λ_s . Thus σ and γ can be obtained from (4.12) and (4.13).

For droplet radii in the range 50–500 Å and electrolyte concentrations 0.01–0.1 M, κa lies between 2 and 50. When $\kappa a > 5$, say, the thickness of the diffuse layer inside the droplet is much less than the droplet radius. In these circumstances Λ_0 and hence k' are small, suggesting that we approximate $F(\phi, k)$ in (4.9) by writing²¹

$$x = F(\phi, k) = \ln (\sec \Phi + \tan \Phi) + O(k'^2) \simeq \sinh^{-1} (\tan \Phi) \quad (4.14)$$

(20) P. F. Byrd and M. D. Friedmann, "Handbook of Elliptic Integrals for Engineers and Physicists," Springer-Verlag, Berlin, 1954.

where

$$\sin^2 \Phi = k \sin^2 \phi \quad (4.15)$$

This approximation is only valid for $k' \tan \phi \ll 1$. Using (4.11), substituting for Φ into (4.14) from (4.15), and rearranging, we obtain

$$y = 2x_0 \sinh^{-1} \left\{ \frac{k'}{(k-1 + k/\sinh^2 x)^{1/2}} \right\} \quad (4.16)$$

For $k' \tan \phi \gtrsim 1$, we make the transformation (ref 22, p 593, eq 17.4.13)

$$\tan \psi = \frac{1}{k' \tan \phi} \quad (4.17)$$

when (4.9) becomes

$$x = F(\phi, k) = K(k) - F(\psi, k) \quad (4.18)$$

where $K(k)$ is the complete elliptic integral of the first kind. We now find that $k' \tan \psi < 1$, and therefore

$$F(\psi, k) \simeq \sinh^{-1}(\tan \psi); \quad \sin^2 \Psi = k \sin^2 \psi \quad (4.19)$$

By using eq 4.10, 4.11, and 4.19, 4.18 becomes after rearrangement

$$y = 2x_0 \times \sinh^{-1} \left\{ \left[\frac{k}{\sinh^2 \{K(k) - x\}} - (1-k) \right]^{1/2} \right\} \quad (4.20)$$

$K(k)$ may be conveniently estimated from (ref 22, eq 17.3.11, p 591)

$$K(k) \simeq \ln(4/k') \quad (4.21)$$

valid for small k' .

4b. "Two-Part" Solution. An alternative approach is to use the linear Debye-Hückel approximation, eq 4.5, over that part of the range where the potential is small enough so that the approximation is valid. Let the limit of validity be x_1 . For $x > x_1$, we replace the integrand in (4.3) by $x_1 \sinh(y/x_1)$ and obtain

$$\left(\frac{dy}{dx} \right)^2 - \left(\frac{dy}{dx} \right)^2_{x=x_1} = 2x_1^2 [\cosh(y/x_1) - \cosh(y_1/x_1)] \quad (4.22)$$

where

$$y_1 = \Lambda_0 \sinh x_1, \quad \left(\frac{dy}{dx} \right)^2_{x=x_1} = (\Lambda_0 \cosh x_1)^2 = \Lambda_0^2 + y_1^2 \quad (4.23)$$

By substituting $v = y/x_1$, $\Lambda_1 = y_1/x_1$ into (4.22), the resulting equation can be integrated (ref 20, p 188, eq 297.75). With

$$k^2 = 2/(1 + \cosh \Lambda_1 - {}^{1/2}\Lambda_1^2 \coth^2 x_1) = 1 - k'^2 \quad (4.24)$$

$$\sin^2 \epsilon = 1 - \frac{k'^2}{k^2 \sinh^2({}^{1/2}v)}; \quad \tan \psi = \frac{1}{k' \tan \epsilon}$$

the solution is

$$\frac{1}{k} (x - x_1) = F(\epsilon, k) - F(\epsilon_1, k) \quad (4.25)$$

$$= F(\psi_1, k) - F(\psi, k) \quad (4.26)$$

using (4.18). Investigation of the higher order terms in the series expansion of $F(\phi, k)$ in powers of k' shows that it is preferable to expand the elliptic integrals in (4.26) rather than those in (4.25). Proceeding in a manner similar to that in §4a, we obtain

$$y = 2x_1 \sinh^{-1} \left\{ \left[\frac{1}{k} \left(1 - k + \frac{1}{\sinh^2 [F(\psi_1, k) - (x - x_1)/k]} \right) \right]^{1/2} \right\} \quad (4.27)$$

where

$$F(\psi_1, k) \simeq \sinh^{-1} \{ [k - 1 + k \sinh^2({}^{1/2}\Lambda_1)]^{-1/2} \} \quad (4.28)$$

We should note that equation (4.26) gives $\psi = 0$, $y = \infty$ for $x = x_m$, where

$$x_m = x_1 + kF(\psi_1, k) \quad (4.29)$$

Thus x has a maximum value, x_m , beyond which the solutions (4.26) and (4.28) do not exist. Depending on the chosen values of x_0 and x_1 , it is possible to find $x_m < x_0$. This occurs for small x_0 , when $x_1 \sinh(y/x_1)$ is not a good approximation to $x \sinh(y/x)$. This solution is an overestimate for $x > x_1$ and an underestimate for $x < x_1$ relative to the exact solution specified by $y(0) = 0$, $y(x_1) = \Lambda_1 x_1$.

4c. Power Series for $y(x)$. We now apply the method of Bagchi, *et al.*,^{7,8} to the present problem by expanding $y(x)$ as a power series in the reduced potential at the centre of the droplet, Λ_0 . With $\Lambda = y/x$, eq 4.2 may be written

$$(x\Lambda)'' - (x\Lambda) = x(\sinh \Lambda - \Lambda) \quad (4.30)$$

If we write Λ in the form

$$\Lambda = \frac{1}{x} \sum_{s=0}^{\infty} \alpha^{2s+1} b_{2s+1}(x) \quad (4.31)$$

then (4.30) becomes

$$\sum_{s=0}^{\infty} \alpha^{2s+1} [b''_{2s+1} - b_{2s+1}] = \sum_{s=0}^{\infty} \alpha^{2s+1} G_{2s+1}(x) \quad (4.32)$$

where $G_1 = 0$ and

$$G_{2s+1} = \frac{x}{(2s+1)!} \left\{ \frac{\partial^{2s+1}}{\partial \alpha^{2s+1}} \times \left[\sinh \left(\sum_{i=0}^{\infty} \frac{\alpha^{2i+1}}{x} b_{2i+1} \right) - \sum_{i=0}^{\infty} \frac{\alpha^{2i+1}}{x} b_{2i+1} \right] \right\}_{\alpha=0} \quad (4.33)$$

(21) S. Levine and A. Suddaby, *Proc. Phys. Soc., London, Sect. A*, **64**, 287 (1951).

(22) M. Abramowitz and I. A. Stegun, "Handbook of Mathematical Functions," Dover Publications, New York, N. Y., 1965.

Equating powers of α in (4.32) and integrating the resulting second-order equation for $b_{2s+1}(x)$, we find that

$$b_{2s+1}(x) = \int_0^x G_{2s+1}(\xi) \sinh(x - \xi) d\xi \quad (4.34)$$

Our boundary conditions $y(0) = 0, y'(0) = \Lambda_0$ give $\alpha = \Lambda_0$. We find that

$$b_1(x) = \sinh x \quad (4.35)$$

$$b_3(x) = \frac{\sinh x}{24} [Ei(2x) + 3E_1(2x) - 2E_1(4x)] - \frac{e^{-x}}{24} [Ei(4x) - 2Ei(2x) - 2E_1(2x) + E_1(4x)] \quad (4.36)$$

where $Ei(x)$ and $E_1(x)$ are the exponential integrals as defined in ref 22 (p 288, eq 5.1.1, 5.1.2). At large x (>10 , say), only the first term in each of the square brackets need be considered and we find that $b_3(x)$ behaves essentially as e^{3x}/x . The determination of the higher terms in the series (4.31) becomes increasingly laborious and will not be attempted here.

5. Numerical Results and Discussion

Before describing the results, we shall first outline two purely numerical methods for the solution of eq 4.2.

5a. Linearization Method. Let $\eta(x) = Y(x) - y^{(0)}(x)$ where $Y(x)$ is the true solution of (4.2) and $y^{(0)}(x)$ is an approximate solution. Then, assuming $\eta(x)$ small, linearization of (4.2) with respect to $\eta(x)$ and replacement of derivatives by finite differences with step $h = x_0/n$, yields

$$\eta_{i+1} - \eta_i [2 + h^2 \cosh(y_i^{(0)}/x_i)] + \eta_{i+1} = h^2 x_i \sinh(y_i^{(0)}/x_i) - (y_{i+1}^{(0)} - 2y_i^{(0)} + y_{i-1}^{(0)}) \quad (5.1)$$

where $y_i^{(0)} = y^{(0)}(x_i), \eta_i = \eta(x_i), x_i = ih, i = 1(1)n-1$. Since the formulation is that of a boundary value problem, the conditions $y_0^{(0)} = y(0), y_n^{(0)} = y(x_0)$ are required. This set of equations can be written in matrix form $A\eta = B$, where η, B are vectors and A is a square tri-diagonal matrix ($A_{ij} = 0, |i - j| > 1$). Special algorithms are available for the solution of (5.1) in this case. The new solution $y_i^{(1)} = y_i^{(0)} + \eta_i$ is substituted for $y_i^{(0)}$ into (5.1) and the process repeated until $y_i^{(n)} - y_i^{(n-1)}$ is smaller than some accuracy criterion. The errors involved in the final solution are $O(h^2)$.

5b. An Integral Equation Formulation. From (4.31), (4.32), and (4.34) we obtain

$$y = \alpha b_1 + \int_0^x \left\{ \sum_{s=1}^{\infty} \alpha^{2s+1} G_{2s+1}(\xi) \right\} \times \sinh(x - \xi) d\xi \quad (5.2)$$

$$= \Lambda_0 \sinh x + \int_0^x \xi \sinh(x - \xi) [\sinh(y/\xi) - (y/\xi)] d\xi \quad (5.3)$$

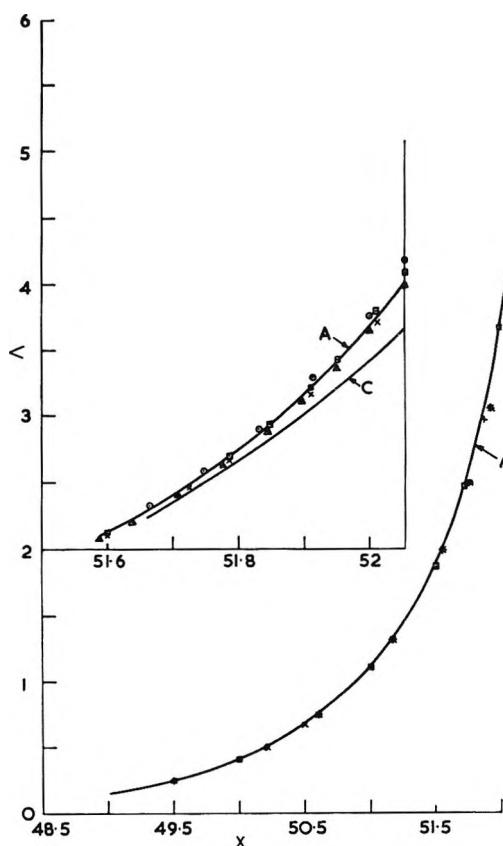


Figure 2. Potential distributions within the micelle for radius $a = 50 \text{ \AA}$. Plots of $\Lambda(x) = e_0\psi(x)/kT$ vs. x with 1-1 electrolyte concentration of 0.1 M, $\epsilon = 78.3$ and $T = 25^\circ$. Except for the curve B and the points marked Δ , boundary conditions $y(0) = 0, y'(0) = \Lambda_0 = 0.174$ have been chosen, with Λ_0 such that the reduced surface potential Λ_s as calculated by the method of §4a is exactly 4. Curve A: Numerical solution (the two methods of §5a, 5b agree to within 0.1% for step-length chosen). \times : "One part" solution described in §4a. Curve E and points \circ : "Two part" solution of §4b with reduced potential $\Lambda_1 = 0.2$ at the join. Curve D and points \square : "Two part" solution with $\Lambda_1 = 0.4$ at join. Curve C and points $*$: series solution of §5c. Curve B and points Δ : Numerical solution of §5a with reduced surface potential $\Lambda_s = 4$. Inset: Same as in main figure, but with x scale in range $(x_0 - 1/2, x_0)$ enlarged fivefold. Letters and point symbols have same meanings in Figures 3-5.

using (4.30) and the relation $G_1(\xi) = 0$. The solution is obtained by iteration, using equations (4.16) and (4.20) to give initial values. This method is much less efficient than that described in §5a, because of the need to integrate (5.3) numerically for every y value in each cycle.

5c. Numerical Results. Figures 2-5 show plots of the normalized potential Λ against x for droplet radii $a = 50-500 \text{ \AA}$ and 1-1 electrolyte concentration 0.1 M. Only those portions of the curves which lie outside the region where the linear Debye-Hückel theory is applicable are given. We readily see that the method of §4a gives the best approximate solution near the surface. The two-part method (§4b) gives no solution near x_0 for small a . For fixed thickness $(1/\kappa)$ of the

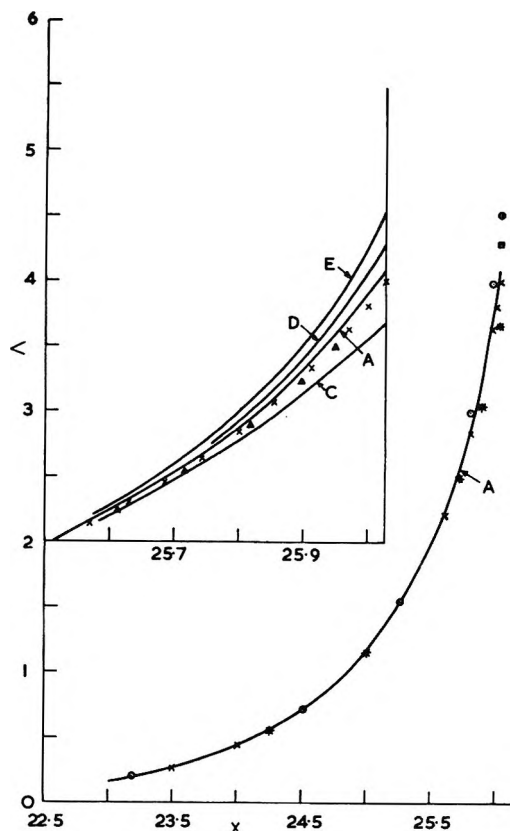


Figure 3. Plots similar to those in Figure 2, with $a = 100 \text{ \AA}$, $\Lambda_0 = 1.91 \times 10^{-3}$.

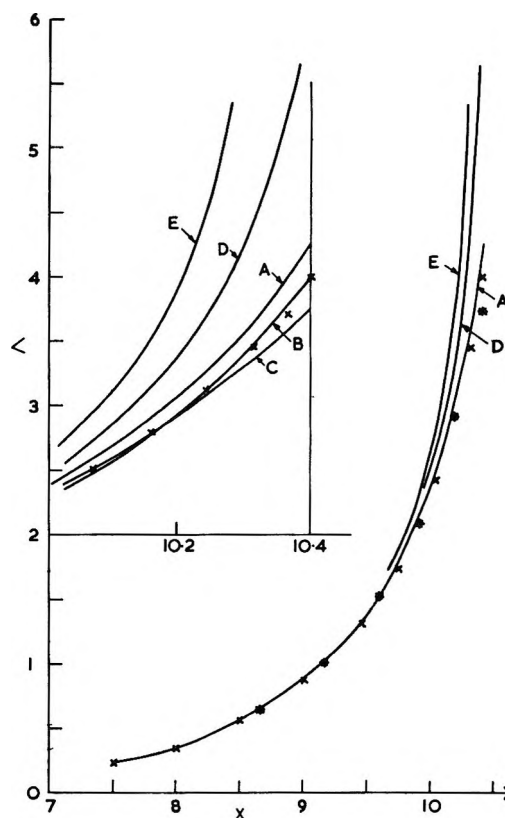


Figure 4. Plots similar to those in Figure 2, with $a = 250 \text{ \AA}$, $\Lambda_0 = 7.89 \times 10^{-10}$.

diffuse layer, the approximation of replacing $x \sinh (y/x)$ in (4.3) by $x_0 \sinh (y/x_0)$ or $x_1 \sinh (y/x_1)$ improves as x_0 increases. Consequently, the differences between the various methods decrease as x_0 increases.

Examination of the form of the solutions derived above shows that the curves obtained are functions only of x and the reduced central potential Λ_0 . Each curve represents a continuous range of the pair of quantities: reduced surface potential and the equivalent value of x_0 , as defined by the common central conditions. (For example, in Figure 2, curve A is the solution of (4.2) for $y(0) = 0$, $y'(0) = 0.174$; the surface parameters may be $x_0 = 5.21$, $\Lambda_s = 4.88$ or $x_0 = 4.53$, $\Lambda_s = 2$ and so on). Solutions at different concentrations may also be found by a similar argument. Since $\kappa \propto (\text{concentration})^{1/2}$ curve A gives the exact solution for the boundary conditions shown for different concentrations if we multiply the x scale by the factor $(0.1/\text{new concentration})^{1/2}$. Similarly, these solutions can be used when the dielectric constant ϵ of the droplet interior changes with the water-alcohol composition, since $\kappa \propto \epsilon^{-1/2}$.

5d. *The Surface Tension.* The surface tension γ is determined from (4.13), which can be written as

$$\frac{2\gamma}{a} = 4n\kappa T \sinh^2 (1/2\Lambda_s) - \frac{\epsilon}{8\pi} \left[\frac{d\psi}{dr} \right]_{r=a}^2 \quad (5.4)$$

For $\Lambda_s \sim 4$, γ is given by the difference of two fairly

large quantities, and its calculation constitutes a good test of the accuracy of our approximate methods. For large x_0 , the method of §4a permits a simple approximate form of (5.4). Since $\Lambda_0 \ll \Lambda_s$, Λ_0^2 can be ignored in (4.12), which can therefore be written as

$$\left[\frac{d\psi}{dr} \right]_{r=a}^2 \simeq \frac{\kappa^2 k^2 T^2}{e_0^2 x_0^2} \left\{ 4x_0^2 \sinh^2 (1/2\Lambda_s) - 4x_0\Lambda_s \sinh (1/2\Lambda_s) \right\} \quad (5.5)$$

Substituting into (5.4), and assuming x_0 large, we have

$$\gamma \simeq \frac{2}{\kappa} n\kappa T \Lambda_s \sinh (1/2\Lambda_s) \quad (5.6)$$

Equation 5.6 shows that γ is approximately proportional to $\sqrt{n\epsilon}$ for fixed Λ_s . If the Maxwell stress terms in (2.12) were ignored, then we should obtain the "Donnan equilibrium" expression

$$\gamma = \frac{2}{\kappa} n\kappa T x_0 \sinh^2 (1/2\Lambda_s) \quad (5.7)$$

which grossly overestimates γ for typical values of x_0 and Λ_s . Table I compares the calculations of γ from the various methods. The negative values obtained for $\Lambda_s = 4$ by our two-part solution require comment. These arise because $x_1 \sinh (y/x_1)$ is a good approximation to $x \sinh (y/x)$ only near $x = x_1$ and for $x \simeq x_0$ overestimates the value of $y'(x_0)$ and hence $(d\psi/dr)_{r=a}$.

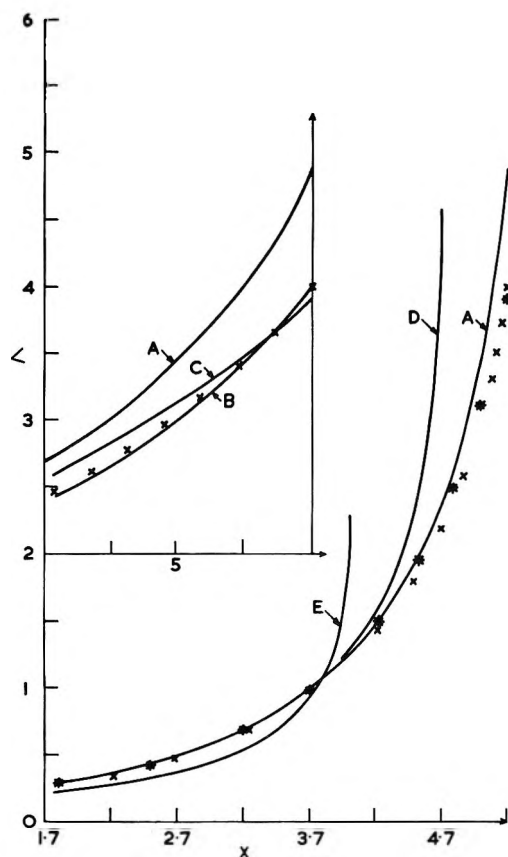


Figure 5. Plots similar to those in Figure 2, with $a = 500 \text{ \AA}$, $\Lambda_0 = 7.84 \times 10^{-21}$.

Reasonable agreement is found from comparison of the results from the numerical methods and those of §4a; for $\Lambda_s = 4$ the errors are $\sim 25\%$. A more favorable situation obtains at $\Lambda_s = 2$, where most of the methods (the exception being the two-part solution) agree within $\sim 25\%$. It should be noted that the methods of §4a and §4c always overestimate γ at any given potential, because the potential and hence the slope are underestimated.

5e. The Concentration Ratios. The ratio of the concentration of electrolyte in the emulsion phase to that in the bulk (aqueous) phase is given by

$$R = \frac{1}{V_m} \int_0^a \exp(-e_0\psi/kT) 4\pi r^2 dr = \frac{3}{x_0^3} I \quad (5.8)$$

It is convenient to divide the range of integration into two parts, taking as the division point $x = x_1$, the limit of the Debye-Hückel approximation. Thus we can write $I = I_1 + I_2$, where for large x_1

$$I_1 = \int_0^{x_1} e^{-\Lambda x^2} dx \approx \frac{1}{3}x_1^3 - x_1^2\Lambda_1 + \frac{1}{4}x_1^2\Lambda_1^2 \quad (5.9)$$

on expanding the exponential term in the integrand up to $0(\Lambda^2)$. Also

$$I_2 = \int_{x_1}^{x_0} e^{-\Lambda x^2} dx < I_2' = e^{-\Lambda_1} \int_{x_1}^{x_0} x^2 dx = \frac{1}{3}e^{-\Lambda_1}(x_0^3 - x_1^3) \quad (5.10)$$

Table I: Values of the Surface Tension γ for Various Droplet Radii and Surface Potentials^a

Method ^b	Radius $a, \text{ \AA}$	Λ_s	$\gamma, \text{ dyn/cm}$	Radius $a, \text{ \AA}$	Λ_s	$\gamma, \text{ dyn/cm}$
A		4	4.95	44.5		1.05
B		4	6.91	...		1.12
C	50	4	6.54	44.2	2	1.33
D		3.92	17.3	32.6		1.42
E		no	...	42.3		-1.62
solution						
A		4	5.13	94.9		1.03
B		4	6.91	...		1.12
C	100	4	6.73	94.8	2	1.33
D		3.74	23.2	94.7		1.52
E		6.48	-2150	94.4		0.18
A		4	5.56	245.1		1.04
B		4	6.91	...		1.12
C	250	4	6.87	245.0	2	1.32
D		3.67	46.2	245.1		2.33
E		4.30	-44.6	245.0		0.40
A		4	5.74	495.1		1.04
B		4	6.91	...		1.12
C	500	4	6.81	495.0	2	1.32
D		3.65	85.8	495.2		3.36
E		4.10	-27.7	495.1		0.91

^a Concentration = 0.1 M, 1-1 electrolyte in pure water droplet interior, $\epsilon = 78.3$, $T = 25^\circ$. ^b The letters A-E refer to the different methods as follows: A, linearization (§5a); B, eq (5.6) (independent of a); C, "one-part" (§4a); D, series (§4c); E, "two-part" (§4b), with $\Lambda_1 = 0.4$.

Hence $I_1 < I < I_1 + I_2'$, and we can place limits on the value of R .

Table II contains the calculated limits of I for the four cases previously considered, with $\Lambda_1 = 0.5, 1$. Numerical integrations of (5.7) based on the method of §4a are also shown. We find that R is in the range 0.3-0.9, which is to be compared with the range 0.3-0.5 as found by Tosch, *et al.*,¹³ for the 2-1 electrolyte Na_2SO_4 . The differences may be attributed partly to the different electrolyte type and partly to the possible

Table II: Electrolyte Concentration Ratios between Aqueous Emulsion and Bulk Phases^a

a	Λ_1	I_1	I_2'	R_{\min}	R_{\max}	I_n	R_n
50	0.5	3.70	24.2	0.08	0.59	14.7	0.31
50	1	7.23	10.7	0.15	0.38		
100	0.5	166	109	0.44	0.73	218	0.58
100	1	193	44	0.51	0.63		
250	0.5	4430	720	0.75	0.88	4780	0.81
250	1	4650	281	0.79	0.84		
500	0.5	41100	2930	0.87	0.94	42500	0.90
500	1	42000	1130	0.89	0.92		

^a a = radius of micelle, \AA , Λ_1 = maximum reduced potential in Debye-Hückel range, $R_{\min} = \frac{3}{x_0^3} I_1$, $R_{\max} = \frac{3}{x_0^3} (I_1 + I_2')$, I_n, R_n are values I, R from numerical integration.

presence of potential drops due to dipole orientation in the droplet film and at the oil-water interface.

Acknowledgments. K. R. is indebted to the Science Research Council of the United Kingdom for a post-

doctoral research associateship. The authors are greatly indebted to Professor A. W. Adamson of the University of Southern California for having brought this problem to their attention and for invaluable discussions.

Relations between Crystal Structure, Molecular Electronic Polarizability, and Refractive Properties of Ice I

by Allen P. Minton

National Institute of Arthritis and Metabolic Diseases, National Institutes of Health, Public Health Service, U. S. Department of Health, Education and Welfare, Bethesda, Maryland 20014 (Received June 30, 1971)

Publication costs assisted by the National Institute of Arthritis and Metabolic Diseases

A relation is derived which expresses the refractive index of a crystalline array of isotropically polarizable molecules as a function of the density, the scalar molecular electronic polarizability, and a structure factor calculated from the geometry of the array. The structure factor for the hexagonal ice I lattice is evaluated utilizing a theoretical lattice model and from the existing experimental data by means of the relation previously derived. The two values so obtained are found to be in fair agreement, and possible reasons for the discrepancy between them are discussed.

I. Introduction

It is now well known that the permanent dipole moment μ of a water molecule in condensed phases is larger than in the vapor phase, due to the polarizing effect of its neighbors.¹ The magnitude of μ in ice I can be fairly reliably estimated at 2.4 debyes compared with the vapor phase value of 1.8 debyes.² In contrast, the effect of local structure upon the molecular electronic polarizability and refractive properties of water does not appear to have received systematic study, although the results of Eisenberg,³ studying liquid water, and Batsanov,⁴ studying crystalline hydrates, have indicated that changes in the local environment of a water molecule are coupled to significant variations in refractive properties.

The birefringence of ice is of intrinsic interest because, unlike that of ordinary molecular crystals, it cannot be accounted for on the basis of an anisotropic molecular electronic polarizability. Dielectric measurements indicate that at temperatures slightly below freezing, the relaxation time for random reorientation of H₂O molecules in ice is of the order of 10⁻⁴ to 10⁻⁵ sec.⁵ During the course of a birefringence measurement each molecule in the bulk of the crystal therefore assumes all six possible alternate hydrogen-bonded positions in the ice lattice. Since the birefringence of

ice is independent of field strength (in the linear region) there can be no correlation between the average molecular orientation and the direction of the applied optical frequency field. Thus even though a single water molecule appears to be slightly anisotropically polarizable with respect to molecular coordinates,⁶ the time-average polarizability α must be isotropic with respect to crystal or laboratory coordinates, and is given by

$$\alpha = \frac{\alpha_{ll} + \alpha_{mm} + \alpha_{nn}}{3} \quad (1)$$

where the α_{ii} are the diagonal elements of the molecular polarizability tensor defined with respect to molecular cartesian coordinates l, m, n .

Since the polarizability is effectively isotropic, the birefringence must therefore be due to anisotropy of the local field at the site of a water molecule in ice. We present here a simple extension of the Lorentz-

(1) D. Eisenberg and W. Kauzmann, "The Structure and Properties of Water," Oxford Press, New York, N. Y., 1969, p 105 ff.

(2) A. P. Minton, *Chem. Phys. Lett.*, **7**, 606 (1970).

(3) H. Eisenberg, *J. Chem. Phys.*, **43**, 3887 (1965).

(4) S. S. Batsanov, *Russ. J. Phys. Chem.*, **34**, 32 (1960).

(5) D. Eisenberg and W. Kauzmann, ref 1, p 112 ff.

(6) W. H. Orttung and J. A. Meyers, *J. Phys. Chem.*, **67**, 1905 (1963).

Lorentz theory⁷ which relates the structure of a crystal to anisotropy of the local field. The results obtained are equivalent to those obtained earlier by Bragg⁸ in a rather less straightforward manner. We next apply these relations to the hexagonal lattice of ice I and show that the simple model is consistent with the existing experimental data.

We shall assume for the sake of ease in calculation that the water molecules in ice are electronically discrete. Possible consequences of this assumption will be discussed subsequently. Having made the assumption, it is a simple matter to show that the dipoles induced in these discrete molecules by an external field are of sufficiently small extension so that the electrostatic interactions between them are well described by the classical formulae for point dipoles. Finally, we neglect the permanent dipoles present in ice as not contributing to the induced polarization at optical frequencies.

II. The Refractive Index Equation for a Crystalline Array of Isotropically Polarizable Molecules

Lorentz⁹ showed that the effective field at the center of a spherical cavity of radius r_c in an isotropic dielectric continuum of refractive index n was given by

$$\vec{E}_{\text{Lorentz}} = \frac{n^2 + 2}{3} \vec{E}_c \quad (2)$$

where E_0 is the externally applied polarizing field. The effective field at the site of a reference molecule in a crystal is equal to the sum of the Lorentz field and that due to the molecules in the immediate vicinity of the designated site (lying inside the boundary of the Lorentz cavity), which we shall designate as E_{loc} , the local field

$$\vec{E}_{\text{eff}} = \vec{E}_{\text{Lorentz}} + \vec{E}_{\text{loc}} \quad (3)$$

The local field E_{loc} at the site of a reference molecule (placed at the origin) is equal to the sum of the fields of the dipoles induced in neighbor molecules by the externally applied field. (The externally applied field itself is included in the Lorentz field.) The electric field of induced dipole i of moment $\vec{\mu}_i$ oriented in the field direction (designated here as z) and located at x_i, y_i, z_i has a z component at the origin given by

$$E_i^z = \frac{-\mu_i}{r_i^3} \left[\frac{3z_i^2 - r_i^2}{r_i^5} \right] \quad (4)$$

where $r_i^2 = x_i^2 + y_i^2 + z_i^2$. If the field direction z is either parallel or perpendicular to the crystallographic axes, the internal field components perpendicular to the applied field will average to zero. In this case, because all molecules are taken as identical, $\vec{\mu}_i = \vec{\mu}$ (oriented in the z direction) and we therefore obtain

$$\vec{E}_{\text{loc}} = \sum_{i=1}^{N_c} E_i^z = \vec{\mu} \sum_{i=1}^{N_c} \left[\frac{3z_i^2 - r_i^2}{r_i^5} \right] \quad (5)$$

where N_c is the number of particles inside the Lorentz cavity of radius r_c . We denote the sum on the right-hand side of (5) by f_z (for structure factor in the z direction) and remark that it must converge; it is not a function of N_c (or r_c) provided that they are sufficiently large. The converse would lead to the absurd result that the refractive properties are a function of the radius of an imaginary spherical boundary constructed for the purpose of calculation.

Classical electrostatics yield the following relations

$$\vec{\mu} = \alpha \vec{E}_{\text{eff}} \quad (6)$$

and

$$\frac{n_z^2 - 1}{4\pi} = N\alpha \frac{E_{\text{eff}}^2}{E_0^2} \quad (7)$$

where all quantities are defined for electric field directed along the z coordinate. We can thus replace each term in eq 3 with an expression which is a function of n_z and is linear in \vec{E}_0 . Canceling out \vec{E}_0 , and replacing N by a function of density ρ , molecular weight M , and Avogadro's number N_a , we may rearrange (3) to obtain

$$\frac{n_z^2 - 1}{n_z^2 + 2} = \frac{4\pi N_a \rho}{3M} \frac{\alpha}{1 - \alpha f_z} \quad (8)$$

The refractive index is thus expressed as a function of a molecular property (α) and a property of the crystal lattice (f_z). It should be noted that α , even though a molecular property, would not be expected to be entirely independent of the molecular environment. The optical spectrum of an isolated molecule is altered upon its incorporation into a molecular crystal and this would presumably be reflected in its electronic polarizability as well. However, if the crystal structure is known, f_z can be calculated in principle and, in conjunction with refractive index and density data, may be used to determine α in the crystal.

III. The Structure Factor

Lorentz showed long ago⁹ that in a cubic crystal f_z is identically zero due to the symmetry of the lattice. A similar argument can be used to show that this is also the case for face-centered cubic crystals. For $f_z = 0$, equation 8 reduces to the familiar Clausius-Mossotti relation. However, if the crystal is not isotropic, then f_z will not in general be equal to zero (although it may be infinitesimal) and there may be as many as three nonidentical structure factors. For a uniaxial crystal such as ice I there will be two such, corresponding to external electric fields applied parallel and perpendicular to the optic axis, which coincides with the crystallographic axis. A further simplifica-

(7) C. J. Böttcher, "Theory of Electric Polarization," Elsevier, Amsterdam, 1952, Chapter 8.

(8) W. L. Bragg, *Proc. Roy. Soc., Ser. A*, **106**, 346 (1924).

(9) H. A. Lorentz, "Theory of Electrons," Teubner Verlagsgesellschaft, Leipzig, 1909.

tion follows from the uniaxial symmetry requirement that $\sum_i x_i^2/r_i^5 = \sum_i y_i^2/r_i^5$ where the sum is taken over all lattice sites enclosed in a sphere about the reference molecule as origin. Upon writing out the expressions for f_x , f_y , and f_z as indicated in eq 5, replacing r_i^2 by $x_i^2 + y_i^2 + z_i^2$ and eliminating either x or y , it becomes apparent that $f_x = f_y = -f_z/2$. Henceforth f_z shall be denoted by $f_{||}$ and $f_x (=f_y)$ by f_{\perp} to indicate applied field direction with respect to the crystallographic axis. Depending upon the magnitude of $f_{||}$ (and hence the difference between $f_{||}$ and f_{\perp}), the crystal will exhibit greater or lesser birefringence. The ordinary ray will correspond to light propagated such that its electric field vector is perpendicular to the optic (crystallographic, z) axis, and the extraordinary ray will correspond to light propagated such that its electric field vector is parallel to this axis. Thus calculation of $f_{||}$ (and thereby f_{\perp}) in conjunction with a scalar molecular electronic polarizability will account for both ordinary and extraordinary refractive indices.

The structure factor $f_{||}$ was evaluated for the ice I lattice by performing the indicated sum in the following way. A computer program was written to generate the coordinates of the oxygen atoms on a hexagonal ice I lattice with $r_{0-0} = 2.77 \text{ \AA}$. ($f_{||}$ is proportional to the crystal density so that direct calculation at one intermolecular spacing—or crystal density—permits evaluation at any.) The sites were then ranked in order of their distance from a reference molecule set at the origin, and $f_{||}$ summed over all molecules out to a given radius.

In Figure 1 the sum accumulated out to radius r is plotted as a function of r . The calculation was carried out to a radius of 32.32 \AA from the reference site, which includes the 4340 nearest neighbors of the reference molecule. It can be clearly seen that even at the largest radius to which the calculation was carried, the sum fluctuates with successive contributions of small numbers of molecular induced dipoles equidistant from the reference molecule. These fluctuations cannot be attributed to round-off error in the double-precision

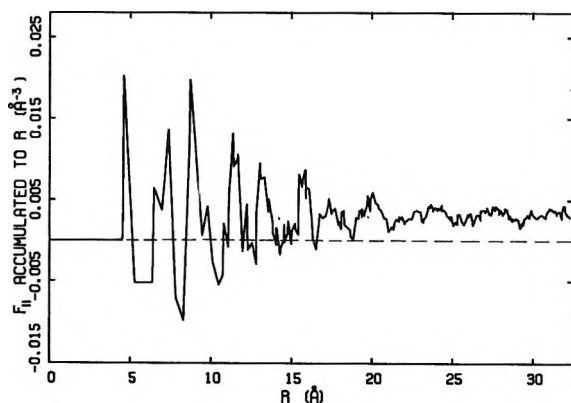


Figure 1. $f_{||}$ accumulated to r as a function of r .

calculation and therefore indicate (surprisingly) that even at a radius of $>30 \text{ \AA}$, the hexagonal ice lattice does not appear as a dielectric continuum to the reference molecule. Nevertheless, we may obtain from Figure 1 a fairly reliable estimate of $f_{||}$. A statistical analysis of points beyond 22 \AA indicates that they are distributed randomly about a mean value of $3.2 \times 10^{-3} \text{ \AA}^{-3}$ with a standard deviation of $0.7 \times 10^{-3} \text{ \AA}^{-3}$.

IV. Discussion

Analogs of equation 8 may be written for both extraordinary (ϵ) and ordinary (ω) rays in terms of the parallel and perpendicular structure factors, respectively

$$\frac{n_{\epsilon} - 1}{n_{\epsilon}^2 + 2} = \frac{4\pi N_a \rho}{3M} \frac{\alpha}{1 - \alpha f_{||}} \quad (9)$$

$$\frac{n_{\omega}^2 - 1}{n_{\omega}^2 + 1} = \frac{4\pi N_a \rho}{3M} \frac{\alpha}{1 - \alpha f_{\perp}} \quad (10)$$

The refractive indices and birefringence of crystalline ice were measured by Ehringhaus¹⁰ who reported that at the sodium D-line (5894 \AA) and $\sim -3^{\circ}$, $n_{\epsilon} = 1.3105$ and $n_{\omega} = 1.3090$. Inserting these values into equations 9 and 10, recalling that $f_{||} = -1/2 f_{\perp}$, and setting $\rho = 0.9164 \text{ g/cm}^3$ ¹¹ and $M = 18.016$, one obtains $\alpha = 1.5001 \text{ \AA}^3$ and $f_{||} = 2 \times 10^{-3} \text{ \AA}^{-3}$. Data at other wave lengths and temperatures yield different values of α but the same value of the structure factor. In Table I, experimental values of the refractive index at several wavelengths and two temperatures are compared with those calculated from eq 9 and 10 using a structure factor $f_{||} = 2 \times 10^{-3}$. Note that excellent agreement is obtained across the visible spectrum and at two widely varying temperatures. The polarizability varies with wavelength as expected and slightly with temperature. This latter effect is probably due to slight changes in the electronic structure of the H-bonded water molecules arising from temperature variation in the equilibrium O—O distance in ice, a variation which is too small to significantly affect the structure factor.

Table I: Experimental and Calculated Values of the Ordinary (n_{ω}) and Extraordinary (n_{ϵ}) Refractive Indices of Ice I

Temp, °C	λ , Å	ρ , g/cm ³	Calcd		Experimental		α , Å ³
			n_{ω}	n_{ϵ}	n_{ω}	n_{ϵ}	
~ -3	4047	0.9164	1.3184	1.3200	1.3184	1.3200	1.5419
	5894		1.3090	1.3105	1.3090	1.3105	1.5001
	6907		1.3065	1.3080	1.3066	1.3079	1.4891
-65	4047	0.9237	1.3206	1.3222	1.3206	1.3222	1.5392
	6239		1.3116	1.3101	1.3117	1.3101	1.4932

(10) A. Ehringhaus, *Neues Jahrb. Mineral., Geol., Beilage Band, B*, **41**, 342 (1917).

(11) N. E. Dorsey, "Properties of Ordinary Water-Substance," Reinhold, New York, N. Y., 1940, p 484.

The value of f_{11} obtained from the experimental data is somewhat (20–50%) lower than that predicted by the ice lattice calculation described in the preceding section. One possible source of this discrepancy may be an oversimplification in the model due to the assumption of electronically discrete molecules. The O–H···O hydrogen bond in ice is known to be partially covalent,¹² but by assuming that the molecules are discrete we are neglecting the covalent character of this bond. To the extent that electrons are shared between neighboring H₂O molecules in ice, it is incorrect to utilize the classical point dipole model to calculate the contribution of a molecule to the local field at the lattice site of its neighbor.

Another possible source of the discrepancy is the experimental sample itself, a prism cut from ice formed on the surface of a vessel of conductivity water exposed to subfreezing temperatures.¹³ Although Ehringhaus describes his sample as homogeneous with an optical axis perpendicular to the water–air interface at which the ice was formed, there is a distinct possibility that this sample was not a single crystal, but rather a conglomerate of preferentially oriented crystallites which are too small to be discerned using crossed polarizers under low magnification. Such a conglomerate would

indeed exhibit birefringence due to the preferential orientation of the crystallites but this birefringence would be less than that of a single crystal. In support of this hypothesis let it be noted that reliable methods of forming large single crystals of ice¹⁴ were only reported much later than the study of Ehringhaus. These procedures appear to require considerably more apparatus, time, and effort than that described in the earlier study.

In conclusion, the extension of the Lorentz–Lorenz theory described here appears to account quite well for the birefringence of ice by considering the anisotropy of the local field in the crystal. The apparent experimental structural factor is somewhat less than that calculated from a perfect lattice model, but it is not known whether the discrepancy arises from oversimplification in the theory or from microheterogeneity in the experimental sample.

The author wishes to acknowledge that stimulating discussions with Professor Henryk Eisenberg led to the initiation of this study.

(12) See A. P. Minton, *Trans. Faraday Soc.*, **67**, 1226 (1971) and references therein.

(13) A. Ehringhaus, ref 10, p 363.

(14) F. Jona and P. Scherrer, *Helv. Phys. Acta*, **25**, 35 (1952).

Intermolecular Forces in Gases of Associating Substances

by L. S. Moore and J. P. O'Connell*

University of Florida, Gainesville, Florida 32601 (Received August 31, 1971)

Publication costs borne completely by The Journal of Physical Chemistry

The forces between two isolated water molecules are essentially completely described by an intermolecular potential energy function which is consistent with recent molecular orbital calculations and correlates all macroscopic data dependent on the pair interactions. The sum of the overlap and dispersion forces (derived from water-nonpolar gas data using the spherically symmetric Kihara core model) and classical electrostatic forces (dipole, quadrupole, induction) generally agrees with the total forces given by molecular orbital calculations of several investigators. In some orientations (hydrogen atoms opposed) the spherical repulsion term is in error but these differences apparently are inconsequential for calculating macroscopic properties. In the "open-chain" dimer configuration, the energies are insufficiently attractive indicating that nonclassical "chemical" forces are present. The transport coefficients of pure water are well predicted from the "physical" forces. However, second virial coefficient data indicate that the "chemical" forces are important for this property. Analytic functions for the spatial distribution of these "chemical" forces have been developed which fit the data over a wide temperature range. These functions are consistent in distribution with the MO calculations but are about 2 kcal less negative energy. The same methods have also been applied to ammonia with equal success.

Because of the practical importance of understanding and predicting the macroscopic properties of substances such as water and ammonia whose intermolecular forces are complex, a large number of models have been developed for describing pair interactions as the beginning of multibody descriptions. (See, for example, references cited in Hirschfelder, *et al.*,¹ Pimentel and McClellan,² and Hadzi.³) Although there has been some controversy about whether the forces between molecules of such substances as water and ammonia are only electrostatic, it has become apparent that treatments based on ideal multipole moments are not adequate and additional weak "chemical" interaction must be included.

It is the purpose of this work to present an approach to modeling weak chemical bonding in associating substances by relating these forces to the second virial coefficient. In water and ammonia we have chosen to call the chemical effect hydrogen bonding, and we have studied these substances principally because extensive data are available.

Intermolecular Potential

Although it is an approximation to do so, the intermolecular forces in complex systems can be separated into contributions from overlap (repulsion), dispersion, induction, dipolar, and higher electrostatic moments, and from nonclassical delocalization of electrons from their monomolecular orbitals.⁴⁻⁸ For the purpose of predicting macroscopic properties, London dispersion and repulsion can be approximated by the Kihara potential with a spherical core.^{9,10} Although it is not a completely satisfactory description of the pair potential,¹¹ we have elected to use this model potential because the effects of these two contributions are small in

water and ammonia and any errors are not likely to severely affect our conclusions.

In addition to the Kihara core potential, terms are included to account for dipole-dipole, dipole-quadrupole, quadrupole-quadrupole, and induction forces (assuming spherical polarizability).^{12,13} The permanent dipole moment is assumed to be an ideal point vector at the center of mass, and an axially symmetric quadrupole moment is used. Energies given by the sum of these terms and the Kihara model are said to be the physical contributions to the intermolecular energy. Expressions for the complete physical potential model are given in Appendix A.

O'Connell and Prausnitz^{14,15} have used this potential

- (1) J. O. Hirschfelder, C. F. Curtis, and R. B. Bird, "Molecular Theory of Gases and Liquids," Wiley, New York, N. Y., 1954.
- (2) G. C. Pimentel and A. L. McClellan, "The Hydrogen Bond," W. C. Freeman, San Francisco, Calif., 1962.
- (3) D. Hadzi, Ed., "Hydrogen Bonding," Pergamon Press, Oxford, England, 1959.
- (4) C. A. Coulson, *Research*, **10**, 149 (1957).
- (5) J. N. Murrell, M. Randic, and D. R. Williams, *Proc. Roy. Soc., Ser. A*, **284**, 566 (1965).
- (6) F. B. Van Duijneveldt and J. N. Murrell, *J. Chem. Phys.*, **46**, 1759 (1967).
- (7) F. B. Duijneveldt, *ibid.*, **49**, 1424 (1968).
- (8) J. L. Lippert, M. W. Hanna, and P. J. Trotter, *J. Amer. Chem. Soc.*, **91**, 4035 (1969).
- (9) J. P. O'Connell and J. M. Prausnitz, "Thermodynamic and Transport Properties at Extreme Pressure and Temperatures," S. Gratch, Ed., ASME, New York, N. Y., 1965, p 19.
- (10) L. S. Tee, S. Gotoh, W. E. Stewart, *Ind. Eng. Chem., Fundam.*, **5**, 363 (1966).
- (11) J. P. O'Connell, Ph.D. Thesis, University of California, 1967.
- (12) A. D. Buckingham, *Quart. Rev.*, **13**, 183 (1959).
- (13) A. D. Buckingham and J. A. Pople, *Trans. Faraday Soc.*, **51**, 1173 (1955).

function to predict the transport properties of steam using the Kihara potential parameters of Rigby, *et al.*,¹⁶ determined from mixtures of water with nonpolar gases. Lee, *et al.*,¹⁷ have determined the Kihara parameters for ammonia by the same method. The complete sets of physical parameters for water and ammonia are given in Table I.

Table I: Potential Function Parameters for Water and Ammonia^a

	Water	Ammonia
$\epsilon/k, ^\circ\text{K}$	170	215
$\sigma, \text{\AA}$	2.65	2.70
$2a, \text{\AA}$	0.265	0.540
$a^* = 2a/\sigma$	0.1	0.2
$\mu, \text{esu-cm}$	1.84×10^{-18}	1.47×10^{-18}
$Q, \text{esu-cm}^2$	1.0×10^{-26}	0.3×10^{-26}
$\alpha, \text{\AA}^3$	1.59	2.24

^a See ref 15 and 17.

Second Virial Coefficients

Although the polar Kihara potential function completely describes the classical interactions, it ignores weak chemical association. It is likely that nonspherical repulsive forces and association forces tend to cancel in predicting transport properties, but the second virial coefficient is sensitive to errors in attractive forces. Thus, failure of the potential function to predict pure water vapor second virial coefficients indicates that weak chemical bonding must be important.

Lambert, *et al.*,¹⁸ show that the second virial coefficient can be written as

$$B = B_{\text{phys}} + B_{\text{chem}} = B_{\text{phys}} + RTK_p \quad (1)$$

where B_{phys} may be obtained in any of several ways,^{11,17-19} and K_p is an equilibrium constant which can be correlated macroscopically.

$$R \ln K_p = -\frac{\Delta H}{T} + \Delta S \quad (2)$$

This equation is often an excellent description of $B_{\text{exptl}} - B_{\text{phys}}$, if ΔH and ΔS are empirical constants.

In Appendix B it is shown that if the pair potential can be partitioned as

$$\Gamma_{\text{tot}} = \Gamma_{\text{phys}} + \Gamma_{\text{chem}} \quad (3)$$

where Γ_{phys} is as described above and Γ_{chem} is due to hydrogen bonding, then

$$B_{\text{phys}} = -\frac{N_0}{4} \int_{\Omega} \int_0^{\infty} [e^{-\Gamma_{\text{phys}}/kT} - 1] r^2 dr d\Omega \quad (4a)$$

$$B_{\text{chem}} = -\frac{N_0}{4} \int_{\Omega} \int_0^{\infty} e^{-\Gamma_{\text{phys}}/kT} [e^{-\Gamma_{\text{chem}}/kT} - 1] r^2 dr d\Omega \quad (4b)$$

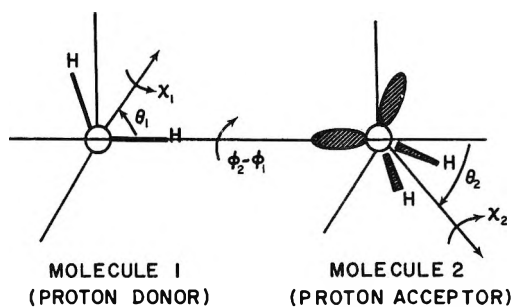


Figure 1. Orientation of open-chain water dimer.

where Ω is all orientations. Models for Γ_{chem} can be developed and tested by comparing values of B_{chem} obtained from $B_{\text{exptl}} - B_{\text{phys}}$ with values determined through use of eq 4b.

Hydrogen Bonding Potential Function

One source of an expression for Γ_{chem} is from subtracting Γ_{phys} from *ab initio* molecular orbital calculations of Γ_{tot} . The authors have recently²⁰ discussed these differences from available calculations and shown that only the open-chain dimer Figure 1 contributes any significant attractive energies which cannot be described by the potential of Appendix A. The differences from several sources²¹⁻²⁴ were essentially the same with varying orientations about the O-O line but calculations based on Gaussian basis sets^{23,24} yielded a distance dependence much different from those based on Slater sets.^{21,22} (See Figure 2.) We have chosen the latter dependence, which is monotonic as $(r - 2a)^{-6}$, since it is a simpler function, seems more consistent with the concept of an "additional" nonclassical attractive force, yields more accurate monomolecular polar moments and also has a significant negative value at the separation in ice which would be required to yield the experimental energy of sublimation²⁵ without unreasonably large nonadditive effects in the classical interactions.

(14) J. P. O'Connell and J. M. Prausnitz, *Ind. Eng. Chem., Fundam.*, **8**, 453 (1969).

(15) J. P. O'Connell and J. M. Prausnitz, *ibid.*, **9**, 579 (1970).

(16) M. Rigby, J. P. O'Connell, and J. M. Prausnitz, *ibid.*, **8**, 460 (1969).

(17) C. S. Lee, J. P. O'Connell, C. D. Myrat, and J. M. Prausnitz, *Can. J. Chem.*, **48**, 2993 (1970).

(18) J. D. Lambert, G. A. H. Roberts, J. S. Rowlinson, and V. J. Wilkinson, *Discuss. Faraday Soc.*, **15**, 113 (1948).

(19) J. S. Rowlinson, *Trans. Faraday Soc.*, **45**, 974 (1949).

(20) L. S. Moore and J. P. O'Connell, *J. Chem. Phys.*, **55**, 2605 (1971).

(21) J. Del Bene and J. A. Pople, *ibid.*, **52**, 4858 (1970).

(22) K. Morokuma and J. R. Winick, *ibid.*, **52**, 1301 (1970).

(23) D. Hankins, J. W. Moskowitz, and F. H. Stillinger, Jr., *ibid.*, **53**, 4544 (1970).

(24) P. A. Kollman and L. C. Allen, *ibid.*, **51**, 3286 (1969).

(25) D. Eisenberg and W. Kauzmann, "Structure and Properties of Water," Oxford University Press, 1969.

$$\Gamma_{\text{chem}} = 4\epsilon P_1 \left[\frac{\sigma}{r - 2a} \right]^6 G \quad (5)$$

where G is the orientation dependent factor, and P_1 is a parameter.

Although the MO calculations show slight functional interaction among the angular coordinates, we have assumed for simplicity that the orientation dependence of chemical energy is separable.

$$G(\theta_1, \theta_2, \phi_2 - \phi_1) = g_1(\theta_1)g_2(\theta_2)g_3(\phi_2 - \phi_1) \quad (6)$$

The basic premise in modeling the orientation dependence is that association occurs with a hydrogen of one molecule interacting with either or both of the lone-pair orbitals of the oxygen on the other molecule, and consequently the minimum chemical energy is when this hydrogen is located on the O-O line.

It is assumed that the chemical energy decreases as the cosine of rotation normal to the O-O line; *i.e.*, for the proton donor molecule (molecule 1 in Figure 1), as $\cos [P_2(\theta_1 - \theta_1^\circ)]$. The period is given by an unknown parameter P_2 while θ_1° is the experimentally measured HOH angle for water, 52.3° . Thus

$$g_1(\theta_1) = \cos [P_2(\theta_1 - 52.3^\circ)] \quad (7)$$

and the cosine is taken to be zero for arguments less than -90° or greater than $+90^\circ$.

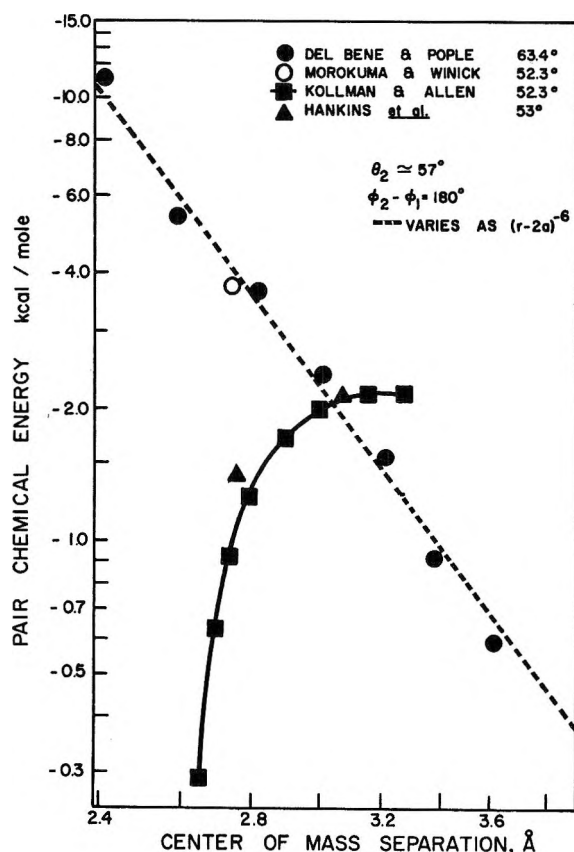


Figure 2. Distance dependence of difference between MO and empirical potential energies in open-chain water dimer.

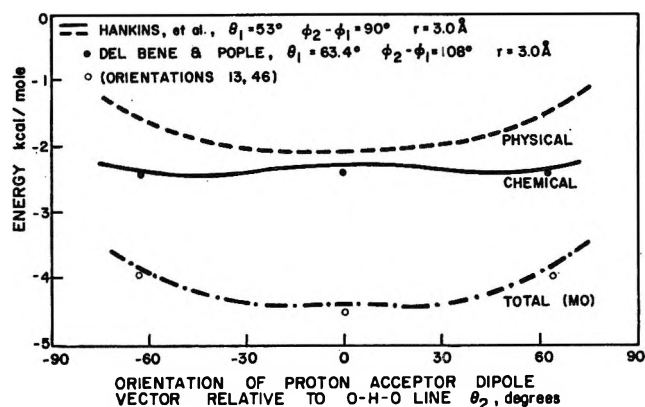


Figure 3. Orientation dependence of water-water intermolecular energies at 3.0 \AA separation of open-chain dimer.

The θ_2 dependence is of the same form, except that the water acceptor molecule has two lone-pair orbitals to associate. The chemical energy can be considered to vary as $\cos [P_3(\theta_2 - \theta_2^\circ)] + \cos [P_3(\theta_2 + \theta_2^\circ)]$ if the bonding with each orbital is additive. Hanks, *et al.*,²² have made extensive calculations of the angular dependence of the molecular orbital energies for two open-chain water dimer configurations. Figure 3 shows the effect of variation of θ_2 on the total (MO), physical, and chemical energies for these two cases when the center of mass distance is 3 \AA . Chemical energies from Del Bene and Pople for orientations which were nearly the same are also included in the figures and are in good agreement at that distance. In Figure 3 is seen the expected θ_2 dependence, with distinct, smooth minima at approximately the tetrahedral angles. The shape of this curve changes to a slight degree as a function of separation (in the calculations of Del Bene and Pople the separate minima disappear at center of mass distances greater than 3.2 \AA and are more pronounced at shorter distances) and rotation (when $\phi_2 - \phi_1$ is changed by 90° , the difference between the $+63.4^\circ$ and -63.4° orientations is 0.3 kcal). However, ignoring these effects an excellent approximation to the chemical energy in Figure 3 is given by

$$g_2(\theta_2) = \cos [1.15(\theta_2 - 52.3^\circ)] + \cos [1.15(\theta_2 + 52.3^\circ)] \quad (8)$$

where, again, the cosine is taken to be zero for arguments less than -90° or greater than $+90^\circ$. For $|\theta_2| > 131$, $g_2(\theta_2) = 0$.

However, the θ_2 dependence can also be expressed in another, simpler form; g_2 is nearly constant over the range of θ_2 because of the additive effect of bonding with either lone-pair orbital. Thus, we also have used

$$g_2(\theta_2) = 1 \quad \begin{cases} |\theta_2| < P_3 \\ = 0 & |\theta_2| > P_3 \end{cases} \quad (9)$$

It should be noted that this function does not give the

Table II: The Chemical Second Virial Coefficient of Water Calculated with Several Sets of Parameters with Varying Width of Step Function in θ_2

$T, ^\circ\text{C}$	B_{exptl}^a	Max error ^d	B_{phys}^b	$B_{\text{exptl}} - B_{\text{phys}}$	Calculated B_{chem}				
					100°	120°	150°	180°	1.15^d
25	-1165	150	-622.7	-542.3	-582.0	-563.6	-548.5	-554.3	-580.2
50	-800	40	-455.0	-345.0	-361.2	-354.6	-349.6	-352.8	-360.5
75	-590	13	-347.0	-243.0	-242.5	-240.5	-239.2	-241.1	-242.2
100	-454	7	-274.2	-179.8	-173.1	-173.0	-173.0	-174.2	-173.1
125	-357	10	-222.8	-134.2	-129.3	-130.3	-130.9	-131.6	-129.3
150	-290	7	-184.9	-105.1	-101.2	-102.0	-103.6	-103.1	-101.3
175	-237	7	-155.9	-81.1	-81.5	-82.3	-82.0	-83.2	-81.6
200	-200	7	-133.4	-66.6	-67.4	-68.1	-68.5	-68.8	-67.5
225	-172	5	-115.4	-56.6	-56.9	-57.5	-67.9	-58.1	-57.0
250	-149	5	-100.7	-48.3	-49.0	-49.5	-49.7	-49.9	-49.1
300	-116.5	5	-78.4	-38.1	-37.9	-38.2	-38.3	-38.4	-37.9
350	-93.5	4	-62.2	-31.1	-30.7	-30.6	-30.8	-30.8	-30.7
400	-76.5	4	-50.2	-26.3	-25.7	-25.6	-25.5	-25.6	-25.7
450	-63.0	4	-41.0	-22.0	-22.0	-21.9	-21.8	-21.8	-22.0
500	-53.0	4	-33.6	-19.4	-19.3	-19.1	-19.9	-19.0	-19.3
600	-35.0	4	-22.8	-12.2	-15.5	-15.2	-15.0	-15.0	-15.4
700	-25.0	3	-15.3	-9.7	-13.0	-12.6	-12.4	-12.4	-12.4
800	-18.0	3	-9.9	-8.1	-11.2	-10.8	-10.6	-10.6	-11.1
900	-13.0	3	-5.8	-7.2	-9.8	-9.4	-9.2	-9.3	-9.8
1000	-9.0	3	-2.6	-6.4	-8.8	-8.4	-8.2	-8.3	-8.7
			P_1		-0.575	-0.608	-0.786	-0.850	-0.62
			P_2		0.448	1.106	2.093	2.380	0.64
			Minimum total pair energy, ^e kcal/mol		-3.6	-3.7	-4.0	-4.1	-3.7
			at $R_{\text{CM}}, \text{\AA}$		2.83	2.82	2.80	2.79	2.82
			$\partial^2\Gamma_{\text{chem}}/\partial\theta_1^2$, kcal/rad ²		0.2	1.2	6.1	8.7	1.3 ^g
			Rms deviation, ^f cc/mol		2.7	2.6	2.6	2.3	2.7

^a Compiled from several sources by O'Connell.¹¹ Limits suggested by experimenters and comparison of data from different workers. Units of cm^3/mol . ^b Recalculated values from O'Connell and Prausnitz.¹⁶ ^c $g_2(\theta_2)$ defined by eq 9. Fitted at $T = 348, 448, 573,$ and 723°K points only. ^d $g_2(\theta_2)$ defined by eq 8. Fitted at $T = 348, 448, 573,$ and 723°K points only. ^e $\theta_1 = 52.3^\circ, \theta_2 = 52.3^\circ, \phi_2 = 180^\circ$. ^f For data from 348 to 1273°K . ^g $\partial^2\Gamma_{\text{chem}}/\partial\theta_2^2$, kcal/rad² = 1.38.

curvature of $\partial^2\Gamma_{\text{chem}}/\partial\theta_2^2$ of Del Bene and Pople of 5.55 kcal/rad².

Finally since there is essentially no dependence of the chemical energy on $\phi_2 - \phi_1$ we have set

$$g_3 = 1 \quad (10)$$

Comparisons with Experiment

Experience in fitting the parameters in Γ_{chem} to $B_{\text{tot}} - B_{\text{phys}}$ indicates that there is not a unique set of three parameters required to fit the data. One parameter may always be fixed *a priori* within a fairly wide range of values.

Table II shows the results of the fitting where we have specified P_3 (the width of the energy in θ_2 as 100, 120, 150, and 180°) using eq 9. It is not clear that there is any best set of parameters which result, since all values of P_3 fitted the data. The rms deviation in O'Connell and Prausnitz¹⁶ for the same data was about 3.0 cm^3/mol . However, for $P_3 < 150^\circ$, $\partial^2\Gamma_{\text{chem}}/\partial\theta_1^2$ becomes very small and thus considerably different from the value of Del Bene and Pople of 22.24 kcal/rad². (Examining the difference between the minimum energy of the lowest energy dimer and the energy of orientation

Table III: A Comparison of the Minimum Energy Water Dimer Structure from MO and Empirical Calculations

	$R, \text{\AA}$	θ_1, deg	θ_2, deg	Γ_{tot} , kcal	$\delta\Gamma_{\text{tot}}/\delta\theta_1^2$, kcal/rad ²
Del Bene and Pople ^c	2.73	51	58	-6.09	25.7 ^b
Morokuma and Winick ^d	2.78	52.3	54	-6.55	...
Hankins, <i>et al.</i> ^e	3.00	52.3	40	-4.72	...
Kollman and Allen ^f	3.00	52.3	25	-5.3	...
Equation 9	2.79	52.3	52.3	-4.1	12.2
Equation 8	2.82	52.3	52.3	-3.7	5.8

^a Oxygen-oxygen and center of mass distances are very nearly equal. ^b See parenthetical sentence in Comparisons with Experiment section. ^c See ref 21. ^d See ref 22. ^e See ref 23. ^f See ref 24.

50 at 2.6 and 2.8 \AA separation indicates that this value should be closer to 11 kcal/rad².) It is not clear whether Γ_{chem} actually exists at θ_2 up to the limit of 180° since an error using the empirical expression for repulsion appears for $150^\circ < \theta_2 < 180^\circ$ and this would tend to include the chemical energy in this range. However, it is apparent that only with the large values of P_3 do

Table IV: The Chemical Second Virial Coefficient for Ammonia for Different Γ_{chem} Parameter Sets

$T, ^\circ\text{C}$	$B_{\text{exptl.}}^a$ cm ³ /mol	B_{phys}^b	$B_{\text{exptl.}} - B_{\text{phys}}$	Calculated B_{chem}^c		
				0.5	1.00	1.50
50	-201.5	-125.5	-76.0	-81.4	-81.1	-81.0
75	-164.5	-104.4	-60.1	-61.7	-61.8	-61.7
100	-137.0	-87.8	-49.2	-48.8	-49.0	-49.0
125	-116.5	-74.6	-41.9	-39.9	-40.1	-40.0
150	-99.0	-63.8	-35.2	-33.4	-33.6	-33.6
175	-86.0	-54.9	-31.1	-28.6	-28.8	-28.7
200	-74.0	-47.4	-26.6	-24.9	-25.0	-24.9
225	-63.5	-41.0	-22.5	-22.0	-22.1	-22.0
250	-56.0	-35.5	-20.5	-19.6	-19.7	-19.6
275	-48.5	-30.7	-17.8	-17.7	-17.7	-17.7
300	-42.0	-26.5	-15.5	-16.1	-16.1	-16.1
325	-38.5	-22.8	-15.2	-14.8	-14.8	-14.7
			P_1	-1.559	-1.588	-1.445
			P_2	9.168	3.78	1.48
		Minimum total pair energy, kcal/mol ^d		-3.6	-3.7	-3.4
		Center of mass separation, Å		3.10	3.10	3.12
		Rms deviation, cc/mol		2.1	2.0	2.0

^a Smoothed values of Cheh²⁶ and O'Connell.¹¹ ^b Recalculated values from Lee, *et al.*¹⁷ ^c Fitted at 348, 423, 498, and 573°K only. ^d $\theta_1 = 68.2^\circ$, $\theta_2 = 0^\circ$, $\phi_2 - \phi_1 = 0^\circ$.

the total energy at the minimum and the curvative approach the expected values. The eq 8 form of $g_2(\theta_2)$ was also used to fit B_{chem} data to determine some measure of the differences in the minimum total energy between a step function and a smoothed function. Table II indicates that this difference is less than 0.5 kcal/mol, but that the smoothed function is not sufficiently broad in θ_2 and is too broad in θ_1 to give the MO curvatures. The total pair energies were calculated at the orientation where $G = 1$ which is close to the orientations where the first derivatives of Γ_{tot} are all zero. Table III is a comparison of the final results from this work and the molecular orbital calculations for water. The energy is not extremely sensitive to changes in distance, θ_1 , or θ_2 , so the present work gives results which are about 2 kcal/mol less negative than those of Del Bene and Pople, and Mørökuma and Winick. Although this difference is large, any larger value of $P(1)$ in eq 8 and 9 always gave values of B_{chem} which were too negative over the entire temperature range.²⁵

Potential Function for Ammonia

There are insufficient MO calculations to establish the spatial distribution of the chemical energy in ammonia. We have arbitrarily used the same type of Γ_{chem} function as found for water, except using one lone-pair orbital for nitrogen. From the geometry of the molecules, we have chosen

$$g_1 = \cos [P_2(\theta_1 - 68.2^\circ)] \quad (11)$$

$$g_2 = \cos [P_3\theta_2] \quad (12)$$

Then Γ_{chem} for ammonia is assumed to be defined by eq 5, 6, 10, 11, and 12. Table IV shows the calculated

B_{chem} fitted to $B_{\text{exp}} - B_{\text{phys}}$ for three sets of parameters. Just as was found with water, one parameter may always be specified over a limited range of values. The fit obtained in Cheh, *et al.*,²⁶ for the same data had an rms deviation of 2.0 cm³/mol. In each case the data point at 50° accounted for over half the contribution to the sum squared deviation.

Conclusions

It appears that for the purposes of the second virial coefficient, the present model is essentially a two parameter intermolecular potential function to include the nonclassical attractive forces between two molecules. While the calculations for eq 4b are nontrivial, the dependence of B_{chem} on temperature appears to be more flexible than that of eq 1 plus 2 and the requirements of the analysis are considerably simpler than in ref 17. Further, the obvious agreement in relative distance and orientation dependence between the present model and MO calculations places this method on a firmer basis. Finally, it is possible that this model may also be useful for describing dense-phase interactions.

Acknowledgment. The authors are grateful to the University of Florida Computing Center for use of its facilities.

Appendix A

Contributions to "Physical" Pair Intermolecular Potential.

(26) H. Y. Cheh, J. P. O'Connell, and J. M. Prausnitz, *Can. J. Chem.*, **44**, 429 (1966).

$$\Gamma_{\text{physical}} = \Gamma_{\text{repulsion}} + \Gamma_{\text{dispersion}} + \Gamma_{\text{dipole-dipole}} + \Gamma_{\text{dipole-quadrupole}} + \Gamma_{\text{quadrupole-quadrupole}} + \Gamma_{\text{induction}} \quad (\text{A1})$$

$$\Gamma_{\text{repulsion}} + \Gamma_{\text{dispersion}} = 4\epsilon \left\{ \left[\frac{\sigma}{r-2a} \right]^{12} - \left[\frac{\sigma}{r-2a} \right]^6 \right\} \quad (\text{Kihara}) \quad (\text{A2})$$

$$\Gamma_{\text{dipole-dipole}} = \frac{-\mu^2}{r^3} [2 \cos \theta_1 \cos \theta_2 - \sin \theta_1 \sin \theta_2 \cos (\phi_2 - \phi_1)] \quad (\text{A3})$$

$$\Gamma_{\text{dipole-quad}} = \frac{3\mu Q}{2r^4} [\cos \theta_1 (3 \cos^2 \theta_2 - 1) - \cos \theta_2 (3 \cos^2 \theta_1 - 1) + 2 \sin \theta_1 \sin \theta_2 \times (\cos \theta_1 - \cos \theta_2) \cos (\phi_2 - \phi_1)] \quad (\text{A4})$$

$$\Gamma_{\text{quad-quad}} = \frac{3Q^2}{4r^5} [1 - 5 \cos^2 \theta_1 - 5 \cos^2 \theta_2 - 15(\cos \theta_1 \cos \theta_2)^2 + 2(\sin \theta_1 \sin \theta_2 \cos (\phi_2 - \phi_1) - 4 \cos \theta_1 \cos \theta_2)^2] \quad (\text{A5})$$

$$\Gamma_{\text{induction}} = \frac{-\mu^2 \alpha}{2r^6} [3 \cos^2 \theta_1 + 3 \cos^2 \theta_2 + 2] \quad (\text{A6})$$

See Figure 1 for definitions of angles θ_1 , θ_2 , $\phi_2 - \phi_1$. r is the distance between centers of mass.

Appendix B

For a pair potential of the form

$$\Gamma_{\text{tot}} = \Gamma_{\text{phys}} + \Gamma_{\text{chem}} \quad (\text{B1})$$

the second virial coefficient can be split into additive terms

$$B_{\text{tot}} = B_{\text{phys}} + B_{\text{chem}} \quad (\text{B2})$$

by simply performing the separation

$$\begin{aligned} B_{\text{tot}} &\equiv -\frac{N_0}{4} \int_{\Omega} \int_0^{\infty} [e^{-\Gamma_{\text{tot}}(r,\Omega)/kT} - 1] r^2 dr d\Omega \\ &= -\frac{N_0}{4} \int_{\Omega} \int_0^{\infty} [e^{-\Gamma_{\text{phys}}/kT} - 1] + \\ &\quad [e^{-(\Gamma_{\text{phys}}/kT + \Gamma_{\text{chem}}/kT)} - e^{-\Gamma_{\text{phys}}/kT}] r^2 dr d\Omega \quad (\text{B3}) \\ &= -\frac{N_0}{4} \int_{\Omega} \int_0^{\infty} [e^{-\Gamma_{\text{phys}}/kT} - 1] r^2 dr d\Omega - \\ &\quad \frac{N_0}{4} \int_{\Omega} \int_0^{\infty} e^{-\Gamma_{\text{phys}}/kT} [e^{-\Gamma_{\text{chem}}/kT} - 1] r^2 dr d\Omega \end{aligned}$$

Then B_{phys} and B_{chem} are defined as in eq 4. The same result can also be derived from the formal perturbation methods of Zwanzig²⁷ and Vives²⁸ which also provide expressions for the higher order virial coefficients.

(27) R. W. Zwanzig, *J. Chem. Phys.*, **22**, 1420 (1954).

(28) D. L. Vives, Chemical Engineering Department, Auburn University, Auburn, Ala., private communication.

The Volume Changes of Ionic Association Reactions

by Paul Hemmes

Department of Chemistry, Rutgers University, Newark, New Jersey 07102 (Received September 1, 1971)

Publication costs borne completely by The Journal of Physical Chemistry

Using the Fuoss and Bjerrum association constants, estimates of the volume changes which occur upon ionic associates can be calculated. It is concluded that volume changes are of little use in distinguishing between inner-sphere and outer-sphere complexes but may be of value in distinguishing the type of binding of small counterions to macromolecules. The relevance of the calculated volume changes to the interpretation of ultrasonic absorption studies of electrolyte solutions is discussed.

One of the most difficult problems arising in the investigation of the solution chemistry of associated electrolytes is the experimental distinction between outer-sphere (solvent separated) and inner-sphere (contact) ion pairs. A similar difficulty arises in the study of ionic binding by polyelectrolytes where distinction

must be made between site binding and general electrostatic binding. The volume changes which accompany ionic association reactions have been used previously^{1,2}

(1) T. G. Spiro, A. Revesz, and J. Lee, *J. Amer. Chem. Soc.*, **90**, 4000 (1968).

(2) U. P. Strauss and Y. P. Leung, *ibid.*, **87**, 1476 (1965).

in an attempt to make such distinctions. In the case of inner-sphere-outer-sphere complexes¹ it was found that no distinction could be made since both types of ion pairs gave similar values for the molar volume change of formation.

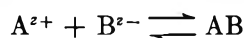
One of the most successful methods for distinguishing between these complexes is the technique of ultrasonic absorption. This method has been applied to the investigation of both substitutionally labile³ and inert⁴ systems. In the latter case, a relaxation process was observed which was interpreted as being due to the formation of an outer-sphere complex, while in the former case multiple relaxations are found which are due to the formation of both types of complexes.

Molar volume changes for complex formation can be calculated from the magnitude of the excess sound absorption.⁵ The calculated values depend on the assumed mechanism, however, and hence have been subject to numerous revisions.⁶

An investigation of theoretical estimates of the volume changes for complex formation was undertaken in order to determine the potential utility of experimental volume changes for the purpose of distinguishing the type of ion pairs in solution and hopefully to shed light on the interpretation of sound absorption spectra.

Theoretical Aspects

To estimate the volume changes which occur in an association reaction, first consider the formation of an outer-sphere complex according to the reaction



The association constant for this reaction can be estimated using either the Fuoss⁷ (1) or the Bjerrum equation⁸ (2)

$$K_F = \frac{4\pi a^3 N e^b}{3000} \quad (1)$$

with N = Avogadro's number, $b = |Z_A Z_B| e_0^2 / a D k T$, a = distance of closest approach of ions, D = dielectric constant, and e_0 = charge on the electron. Other symbols have their usual meanings.

$$K_{Bj} = \frac{4\pi N a^3 b^3}{1000} \cdot Q(b) \quad (2)$$

with⁹

$$Q(b) = \int_2^b \frac{e^Y}{Y^4} dY$$

Both of these equations have been tested repeatedly and are known to give reasonable estimates of the experimental association constant.

The volume change which occurs on forming the outer-sphere complex can now be estimated using the equation

$$\left(\frac{d \ln K_m}{dp} \right)_T = \frac{-\Delta V}{RT} \quad (3)$$

where K_m is the association constant on the molality scale. The Fuoss and Bjerrum equations refer to the molarity scale. Hence

$$\ln K_{F(Bj)} + \ln \rho = \ln K_m \quad (4)$$

where $K_{F(Bj)}$ is the Fuoss (Bjerrum) association constant and ρ is the density of the solution.

If we now take the pressure derivative of the natural logarithm of eq 1 holding T constant, we obtain

$$\left(\frac{d \ln K_F}{dp} \right)_T = \frac{db}{dp} = \frac{-|Z_A Z_B| e_0^2}{a D k T} \frac{d \ln D}{dp} \quad (5)$$

which yields a value of

$$\Delta V_F = \frac{|Z_A Z_B| e_0^2 N}{a D} \left(\frac{d \ln D}{dp} \right)_T - RT \beta \quad (6)$$

or

$$\Delta V_F = RT \left[b \left(\frac{d \ln D}{dp} \right)_T - \beta \right] \quad (7)$$

where β = solution compressibility.

According to Owens and Brinkley¹⁰ and Fuoss,¹¹ the density and dielectric constant of a liquid have similar pressure dependences, namely

$$1 - \frac{D(1)}{D(p)} = A D(1) \log \frac{B + P}{B + 1} \quad (8)$$

where $D(1)$ = dielectric constant at 1 atm, $D(p)$ = dielectric constant at pressure P , and A and B are constants.

$$1 - \frac{\rho(1)}{\rho(p)} = C \rho(1) \log \frac{B + P}{B + 1} \quad (9)$$

where $\rho(1)$ = density at 1 atm, $\rho(p)$ = density at pressure P , and C is a constant. These two equations can be combined to give

$$1 - \frac{D(1)}{D(p)} = \frac{A}{C} \frac{D(1)}{\rho(1)} \left[1 - \frac{\rho(1)}{\rho(p)} \right] \quad (10)$$

Differentiation of eq 10 yields

$$\frac{1}{D} \left(\frac{d \ln D}{dp} \right)_T = \frac{A}{C \rho} \left(\frac{d \ln \rho}{dp} \right)_T \quad (11)$$

or since

(3) P. Hemmes, F. Fittipaldi, and S. Petrucci, *Acustica*, **21**, 228 (1969).

(4) A. Elder and S. Petrucci, *Inorg. Chem.*, **9**, 19 (1970).

(5) M. Eigen and K. Tamm, *Z. Elektrochem.*, **66**, 93 (1962).

(6) A. Bechtler, K. G. Breitschwerdt, and K. Tamm, *J. Chem. Phys.*, **52**, 2975 (1970).

(7) R. M. Fuoss, *J. Amer. Chem. Soc.*, **80**, 5059 (1958).

(8) N. Bjerrum, *Kon. Danske Vidensk. Selskab*, **7** (1926).

(9) R. M. Fuoss and F. Accascina, "Electrolytic Conductance," Interscience, New York, N. Y., 1959, p 155.

(10) B. B. Owen and S. R. Brinkley, *Phys. Rev.*, **64**, 32 (1943).

(11) J. F. Skinner, E. L. Cussler and R. M. Fuoss, *J. Phys. Chem.*, **72**, 1057 (1968).

$$\left(\frac{d \ln \rho}{dp}\right)_T = \beta \quad (12)$$

$$\left(\frac{d \ln D}{dp}\right)_T = \frac{A}{C} \cdot \frac{D}{\rho} \cdot \beta \quad (13)$$

Using values of A , C , D , and ρ from ref 10 and 11 and from Harned and Owen,¹² it seems that for all liquids, for which data are available, the quantity $AD/C\rho$ is greater than unity. The calculated volume change for association is therefore positive. This is the expected behavior since when ions associate to form a neutral pair there is a release of the solvent molecules which had been oriented by the free ions. Equation 7 predicts that for very small b or for $b = 0$ the volume change is negative. Physically this is very unlikely since in the absence of strong long-range forces the pressure dependence of K_m would tend toward zero. That is, the change in the equilibrium constant on the molarity scale should be a consequence of the decreased volume of liquid only. The increase in density with pressure would then compensate yielding a pressure-independent K_m . The failure of eq 7 to give the expected result for small values of b indicates that the Fuoss equation may not have the correct functional form in this region.¹³

To differentiate the Bjerrum formula, it is convenient to express $Q(b)$ as⁹

$$Q(b) = \frac{1}{6} \left[e^2 + Ei(-2) - Ei(-b) - \frac{e^b}{b} \left(1 + \frac{1}{b} + \frac{2}{b^2} \right) \right] \quad (14)$$

where e is the base of natural logarithm, Ei represents the exponential integral defined as

$$-Ei(-x) = \int_{-\infty}^x \frac{e^t}{t} dt \quad (15)$$

Taking the logarithmic derivative of eq 2 yields

$$\left(\frac{d \ln K_{Bj}}{dp}\right)_T = \left(\frac{3}{b} + \frac{e^b}{Q(b)b^4} \right) \frac{db}{dp} \quad (16)$$

The calculated volume change is then

$$\Delta V_{Bj} = RT \left[\left(3 + \frac{e^b}{Q(b)b^4} \right) \frac{d \ln D}{dp} - \beta \right] \quad (17)$$

For large values of b , the compressibility term is negligible compared to the first term in both eq 7 and 17. The ratio of the calculated terms is

$$\frac{\Delta V_{Bj}}{\Delta V_F} \cong \frac{3}{b} + \frac{e^b}{Q(b)b^4} \quad (18)$$

For large values of b , $Q(b) \rightarrow e^b/b^4$, hence $\Delta V_{Bj}/\Delta V_F \rightarrow 1$. As b decreases to 2, however, $Q(b) \rightarrow 0$ and $\Delta V_{Bj}/\Delta V_F \rightarrow \infty$. The singular behavior of the Bjerrum function is due to the following: two ions are associated in the Bjerrum sense when the ratio of elec-

trical potential energy to the quantity kT is greater than 2. Consider some electrolyte which is associated by this criterion, that is

$$\frac{|Z_A Z_B| e_0^2}{a D k T} > 2$$

When the solution is compressed, the dielectric constant increases and if the above ratio is only slightly greater than 2 at 1 atm, the increased dielectric constant may cause the ratio to be less than 2. According to Bjerrum, the electrolyte is no longer associated. Hence a small change in D causes a change in the classification of the electrolyte from associated to unassociated.

Inner-Sphere-Outer-Sphere Equilibria

For an electrolyte which associates to form both inner-sphere and outer-sphere complexes, the total equilibrium constant is

$$K_{\Sigma} = K_o(1 + K_1) \quad (19)$$

where K_o is the outer-sphere association constant and K_1 is the ratio of inner-sphere to outer-sphere complexes. Taking the pressure derivative of the logarithmic form of eq 19 yields

$$\Delta V_T = \Delta V_o + \frac{K_1}{1 + K_1} \Delta V_1 \quad (20)$$

where ΔV_T is the total volume change, ΔV_o is the volume change for the formation of the outer-sphere complex, and ΔV_1 is the volume change which occurs when the outer-sphere complex is converted into an inner-sphere one. It is evident from eq 20 that if the extent of inner-sphere substitution is small ($K_1 \ll 1$), the total volume change is approximately ΔV_o . If, however, inner-sphere species are favored ($K_1 \gg 1$), the total volume change is approximately $\Delta V_o + \Delta V_1$. Hence, if volume changes are to be useful in distinguishing between the two classes of complexes, $|\Delta V_1|$ must be sufficiently large that differences between ΔV_T and ΔV_o can be meaningful. Reliable values for ΔV_1 are not readily available. We can therefore use only theoretical estimates and the values for similar reactions.

Consider a highly idealized picture of the substitution process, in which the metal ion has one hard-sphere solvent molecule coordinated to it and has a hard-sphere ligand in the second coordination sphere. Further assume that the radius of the ligand equals that of the solvent molecule. The volume change will be given by

$$V_1 = \bar{V}_{is} + \bar{V}_{sol} - \bar{V}_{os} \quad (21)$$

where \bar{V}_{is} is the partial molar volume of the inner-sphere complex, \bar{V}_{sol} is the partial molar volume of the solvent, and \bar{V}_{os} is the partial molar volume of the outer-sphere

(12) H. S. Harned and B. B. Owen, "The Physical Chemistry of Electrolyte Solutions," 3rd ed, Reinhold, New York, N. Y., 1958.

(13) S. Petrucci, P. Hemmes, and M. Battistini, *J. Amer. Chem. Soc.*, **89**, 5552 (1967).

complex. For this idealized case, substitution of the ligand for the solvent molecule causes zero volume change. This treatment is too crude to be very useful. A better estimate of the volume change can be obtained by treating the two complexes as dipoles of large moment and estimating the electrostatic contribution to the free-energy change of this dipolar equilibrium. According to Kirkwood,¹⁴ the free energy of a dipole of radius r and moment μ (standard state of $D = 1$) is

$$\Delta G_i = \frac{-\mu_i^2}{r_i^3} \cdot \frac{D-1}{2D+1} \quad (22)$$

For the formation of an inner-sphere complex, the total free-energy change is

$$\Delta G^\circ = -\left[\frac{\mu_{is}^2}{r_{is}^3} + \frac{\mu_{sol}^2}{r_{sol}^3} - \frac{\mu_{os}^2}{r_{os}^3} \right] \frac{D-1}{2D+1} \quad (23)$$

This value of the free energy leads to a value for the equilibrium constant for the reaction. It is possible to choose values for the radii of the various species such that experimental values of K_1 can be reproduced, but the calculated values are far too sensitive to the assumed radii to be valuable, *a priori*. The volume change calculated from this equation, however, is useful in setting limits on the values of ΔV_1 . The calculated dipolar volume change is

$$\Delta V_1 = -RT(\ln K_1) \frac{3D}{(2D+1)(D-1)} \left(\frac{d \ln D}{dp} \right)_T \quad (24)$$

In water ($D = 78$), assuming that K_1 is between 10 and 0.1, which are typical values, the electrostatic contribution to the volume change due to this equilibrium is only about ± 0.5 cc. Even in low dielectric media ($D = 5$), the volume change is small ($\Delta V \cong 5$ cc). It should be understood that the nonelectrostatic contribution to volume change may not be zero. For example, the reaction $I_3^- = I_2 + I^-$ has a volume change of $+5.4$ cc/mol.¹⁵ Since most of the interest in inner-sphere-outer-sphere equilibria involves the first row transition metal ions, it is best to obtain an estimate for the volume changes for these ions. A rough indication of ΔV_1 was obtained by the following process. The molar volume of solid $NiSO_4 \cdot 7H_2O$ and $CoSO_4 \cdot 7H_2O$ were calculated from the salt densities. Similarly the molar volume of $NiSO_4 \cdot 6H_2O$ and $CoSO_4 \cdot 6H_2O$ were calculated. Using the value 18.0 cc/mol for the molar volume of water, the calculated value of ΔV for the process



is about $+4$ cc/mol. Since the crystal structure of the heptahydrates¹⁶ is quite similar to the model proposed by Eigen¹⁷ for the first stage of an ionic association reaction, this estimate of the volume changes for anion desolvation processes can be useful in the interpretation of the ultrasonic spectra of metal sulfates.

Experimental Tests

Tests of either eq 7 or 17 are difficult for two reasons. First, only electrolytes which form outer-sphere complexes exclusively can be used for these tests and, second, both equations depend on the ion size parameter a . With regard to the second point, it is always possible to solve either eq 1 or 2 for the a parameter if the experimental association constant is available. The values of a so obtained, however, are generally incorrect since the experimental association constant includes the effects of ion-solvent and nonelectrostatic factors which are not considered in the derivation of eq 1 and 2.⁹

Hamann, *et al.*,¹⁸ measured the volume change for the formation of $LaFe(CN)_6$ ion pairs in water. These two ions must form only an outer-sphere complex. The value they obtained was $+8.0$ cc/mol. Using the Fuoss equation (eq 1) with a calculated from K equal to 7.36 \AA yields a calculated $\Delta V = +8.98$ cc/mol from eq 7. Similarly, ΔV calculated from the Bjerrum equation ($a = 4.19 \text{ \AA}$) and eq 17 gives $\Delta V = +6.89$ cc/mol.

Despite quantitative differences in the value of the association constants, it is generally agreed that $MgSO_4$ and $MnSO_4$ ion pairs in water are mainly of the outer-sphere type, and hence K_1 is generally small. Under these conditions, the total ΔV is approximately equal to the volume change for the formation of the outer-sphere complex. The value of ΔV measured¹⁸ for $MgSO_4$ is $+7.3$ cc/mol while ΔV_F is $+7.42$ cc/mol and $\Delta V_{Bj} = +4.86$ cc/mol. For $MnSO_4$ the experimental results are $\Delta V = 7.4$ cc/mol while the calculated values of $\Delta V_F = 8.3$ cc/mol and $\Delta V_{Bj} = 5.0$ cc/mol. In all cases the value of a used is not too different from the sum of hydrated ionic radii.

Applications

Since the calculated volume changes depend on the reciprocal of the center to center ion separation parameter a , the volume changes may be used as probes for the nature of bonding of ion to polyelectrolytes. If there is a general electrostatic interaction, all distances between charges will be large, and hence ΔV should be small. If instead of this general "ionic atmosphere bonding"² there should be a strong interaction between the ion and a specific site, then the distances involved would be relatively small and the ΔV considerably larger. These expectations have been confirmed by experiment.² It should be noted that Strauss and Leung attributed the large ΔV for site binding to the release of coordinated solvent molecules. This is not

(14) J. G. Kirkwood, *J. Chem. Phys.*, **2**, 351 (1934).

(15) S. D. Hamann, "High Pressure Physics and Chemistry," Vol. 2, R. S. Bradley, Ed., Academic Press, New York, N. Y., 1963.

(16) A. F. Wells, "Structural Inorganic Chemistry," Oxford University Press, London, 1962.

(17) C. Langford and H. Gray, "Ligand Substitution Dynamics," W. A. Benjamin, New York, N. Y., 1965.

(18) J. W. Larson, *J. Phys. Chem.*, **74**, 3392 (1970).

the case, since that process should have only a small ΔV . It is the electrostatic ordering of solvent molecules which when destroyed by ionic association causes a large volume change. In this regard the ΔV is more diagnostic than Raman spectra since the formation of outer-sphere complexes gives a large ΔV but no Raman bond.

Comparison with Ultrasonic Results

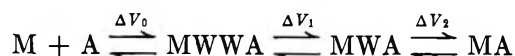
Before numerical results of volume changes obtained from ultrasonic absorption studies can be compared with the calculated values from eq 7 and 17, corrections must be made to account for the fact that these equations yield the isothermal volume change while ultrasonics measures the adiabatic volume change. The two quantities are related by

$$\Delta V_s = \Delta V_T - \frac{\alpha}{\rho C_p} \Delta H \quad (25)$$

where α is the coefficient of thermal expansion, ρ is the density, and C_p is the heat capacity. For water, at 25° and using the experimental values of ΔH ¹⁸ for association of divalent sulfates, eq 25 gives a correction term of about 0.3 cc. This term is therefore insignificant under these conditions but may be substantial in other solvents.

We can summarize much of what has been said about the ion-pair conversions very simply. In general, the volume changes from outer-sphere complex to inner sphere are small in magnitude and positive in sign.

Two grossly different interpretations of the ultrasonic spectrum of $MnSO_4$ in water have appeared. Tamm¹⁹ has proposed a three-step mechanism of the type



where W represents water molecules intervening in the ion pairs. Tamm fit his data to this model in terms of the six rate constants and calculated the volume changes for the processes. His results are shown in Table I.

Table I^a

	Tamm	Yeager
V_1	+18.3	+9
V_2	-13.3	+2
V_3	+3.5	...

^a All values are in cc/mol for association processes.

Jackopin and Yeager²⁰ used a two-step model for the same process. This fit therefore involves four parameters rather than six. Little can be said about the merits of the data fitting procedure, since Tamm used a theoretical estimate of one rate constant and an inde-

pendently determined value of another. Hence he had only four free parameters also. The calculated volume changes, however, provide an alternate means of comparing the data fitting process. Tamm's proposed mechanism leads to two unusual features. First, the volume change for the formation of the outer-sphere complex is very large compared to the estimates of either eq 7 or 17. Also, if the relative population of inner-sphere species is low, then the overall ΔV measured by conductance techniques should be approximately equal to ΔV_1 . This is clearly not the case. The second step of Tamm's mechanism is supposedly an anion desolvation process. While ultrasonics cannot determine the sign of ΔV , Tamm had to take ΔV_2 negative in order to make the calculated overall volume change agree with the total ΔV . From the previous discussions it seems that the volume change for such a process should be small in magnitude. If the dipolar model (eq 24) is used, the calculated volume change will be positive since $\ln K$ is negative. On the basis of the crystal volume model, the volume change for this process was +4 cc/mol. Hence a large negative value of ΔV_2 cannot be justified physically. It has only a mathematical significance, which will be discussed below. The model used by Yeager, however, is quite compatible with the ideas presented here. That is, the volume change for the formation of the outer sphere complex is +9 cc/mol, as opposed to a calculated estimate of +8 cc/mol from the Fuoss equation. The volume change for the inner-sphere formation is +2 cc/mol in satisfactory agreement with expectations.

It is not the purpose of this discussion to find fault with the work of Tamm. It is important to analyze the approach used in that work to find reasons for the anomalous volume changes. The ultrasonic data of divalent metal sulfates show that at very high frequencies there is an excess of absorption relative to water, which covers too large a frequency range to be a single relaxation process. Three explanations have been offered for this effect. (a) There may be a distribution of relaxations; (b) there may be two processes; and (c) there may be an ion-solvent interaction which would lead to an apparent excess absorption by the solution. Tamm chose alternative b while Yeager chose c. If alternative c is correct, then Tamm's interpretation incorporates a large physical contribution besides the chemical one. Hence his estimate of ΔV for the first (highest frequency) process, based upon the magnitude of the excess sound absorption, is too large. Since the total ΔV is known and is considerably below the calculated value for ΔV , for the outer-sphere complex, Tamm was forced to take a negative sign for the second process in order to compensate for the excessive

(19) K. Tamm, "Report of the 6th International Congress on Acoustics," Paper 6P-3-3, Tokyo, 1968.

(20) L. G. Jackopin and E. Yeager, *J. Phys. Chem.*, **74**, 3766 (1970).

ΔV_1 . The calculations presented in the present work indicate that the negative sign and the magnitude are improbable. Hence the choice of alternative c leads to a much more physically reasonable result than alternative b.

The study of outer-sphere association of substitutionally inert systems was performed by Petrucci and Elder. The calculated volume change from this work was about 16 to 20 cc/mol, decreasing with concentration. Extrapolating the data to infinite dilution gives $\Delta V = 15.6 \pm 0.5$ cc/mol for both $[\text{Co}(\text{NH}_3)_6](\text{SO}_4)_3$ and $[\text{Co}(\text{en})_2](\text{SO}_4)_3$. Spiro¹ found $\Delta V = 15.2$ cc/mol

at ionic strength 1 *M*. Both of these figures are above the estimates of ΔV from eq 7 which is 10 cc/mol. While the error in the use of ΔV_F is about 60%, this result does not conflict with the divalent sulfate case where Tamm's calculated ΔV_1 was about 220% greater than the Fuoss estimate. The deviations are not due only to the higher charge, since a symmetrical 3:3 electrolyte gave adequate agreement. The fact that the ion pairs are charged may be significant. Experimental studies of this possibility are in progress. This deviation may represent a significant quantitative failure of the continuum model.

Radioisotope Determination of the Surface Concentrations of Calcium and Phosphorus on Hydroxyapatite in Aqueous Solution

by M. Kukura, L. C. Bell,* A. M. Posner, and J. P. Quirk

Department of Soil Science and Plant Nutrition, Institute of Agriculture, University of Western Australia
Nedlands, Western Australia 6009 (Received August 5, 1971)

Publication costs borne completely by The Journal of Physical Chemistry

The areas per PO_4^{3-} ion and Ca^{2+} ion on the surface of calcium hydroxyapatite $[\text{Ca}_{10}(\text{OH})_2(\text{PO}_4)_6]$ at the point of zero charge were found to be 33.1 ± 2.7 and 23 ± 2.1 , respectively; these values are in reasonable agreement with those expected from crystal parameters. The presence of PO_4^{3-} (or its hydrolysis products) Ca^{2+} , Na^+ , K^+ , CHCl_3 , or barbiturate ion in suspension of hydroxyapatite did not alter the area per PO_4^{3-} or Ca^{2+} . These areas did however change with pH. At pH values sufficiently less than 7.5 the area per PO_4^{3-} ion decreased.

Hydroxyapatite $[\text{Ca}_{10}(\text{OH})_2(\text{PO}_4)_6]$ is the structural prototype of the main inorganic constituent of bone and teeth, and the structure of this compound differs only slightly from that of the common ore of phosphorus, fluorapatite $[\text{Ca}_{10}\text{F}_2(\text{PO}_4)_6]$. Hydroxyapatite is the end product resulting from the application of superphosphate containing $\text{Ca}(\text{H}_2\text{PO}_4)_2$ to calcareous soils. The surface chemistry of hydroxyapatite is thus of interest to mineral processors in addition to those engaged in agricultural, dental, and medical research. The surface concentrations of calcium and phosphorus on hydroxyapatite are useful parameters in studying phenomena such as chemisorption, physical adsorption, and ionic substitution at the hydroxyapatite-solution interface.

The concentration of atoms per unit area on the surface of sparingly soluble solids can be calculated provided the specific surface area of the solid is known with the use of radioisotopes. Conversely, the specific surface can be evaluated from the measured surface con-

centrations of atoms and a knowledge of the area per atom at the crystal surface.¹⁻⁷

The theoretical basis of this method is that when a radioisotope X^* is introduced into the aqueous phase in chemical equilibrium with a sparingly soluble salt XY , the isotope X^* will exchange only with some of the X atoms in the solid surface until at isotope equilibrium the specific activity of X^* will be the same on the solid surface as in solution, *i.e.*

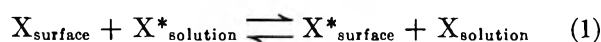
* Address correspondence to this author at the Department of Agriculture, University of Queensland, Brisbane, Australia.

- (1) I. M. Kolthoff, *J. Phys. Chem.*, **40**, 1027 (1936).
- (2) I. M. Kolthoff and W. M. MacNevin, *J. Amer. Chem. Soc.*, **58**, 499 (1936).
- (3) I. M. Kolthoff and A. S. O'Brien, *ibid.*, **61**, 3409 (1939).
- (4) I. M. Kolthoff and C. Rosenblum, *ibid.*, **55**, 2656 (1933).
- (5) C. D. McAuliffe, N. S. Hall, L. A. Dean, and S. B. Hendricks, *Proc. Soil Sci. Soc. Amer.*, **12**, 119 (1947).
- (6) F. Paneth and W. Vorwerk, *Pulver. Sci. Phys. Chem.*, **101**, 445 (1922).
- (7) M. Falkenheim, W. F. Neuman, and H. C. Hodge, *J. Biol. Chem.*, **169**, 713 (1947).

Table I: Measured Areas per Phosphorus and Calcium on the Surface of Hydroxyapatite in Aqueous Solution^a

Sample no.	Specific surface area, m ² /g	% Ca	% P	% CO ₃ ²⁻	pH of suspension	Area per P, Å ²	Area per Ca, Å ²
B34	9.2	39.5	18.2	0.05	7.4	38	26
B56	13.6	39.4	18.2	0.10	7.4	35	24
B1617	26.1	39.1	18.1	...	7.7	33	24
B1617	26.1	39.1	18.1	...	7.5	30	21
B1617	26.1	39.1	18.1	...	7.8	32	22
B18	26.6	38.8	18.1	0.03	7.4	31	20
B9	29.6	38.8	18.1	0.15	7.7	33	24

^a P and Ca concentrations in solution range from 0.63 to 0.82 and 1.68 to 3.04 ppm, respectively. Ca/P mole ratio in the solid ranges from 1.66 to 1.67.



Now

$$K = \frac{a_{X^*_{\text{surface}}} \cdot a_{X_{\text{solution}}}}{a_{X_{\text{surface}}} \cdot a_{X^*_{\text{solution}}}} \quad (2)$$

where a = chemical activity.

Since X and X^* are chemically equivalent it follows that

$$X_{\text{surface}} = \frac{X^*_{\text{surface}} [X_{\text{solution}}]}{[X^*_{\text{solution}}]} \quad (3)$$

$[X^*_{\text{solution}}]$ and $[X_{\text{solution}}]$ can be measured directly and X^*_{surface} determined either directly by analysis of the solid or, more commonly, by measurement of the difference between the amount of isotope in solution at time zero and that at equilibrium. X_{surface} is then readily calculated from eq 3. If the area each group or atom occupies in the surface is known from crystallographic data, the specific surface of the solid can then be calculated from the measured value of X_{surface} . Alternatively, if the specific surface area is known, the concentration of surface ions on the solid $[X_{\text{surface}}]$ can be determined. This paper describes the use of the latter technique to measure the surface concentrations of calcium and phosphorus on hydroxyapatite in aqueous solutions using the radioisotopes P³² and Ca⁴⁵.

Experimental Section

Synthetic hydroxyapatite was prepared by the reaction of Ca(OH)₂ and Ca(H₂PO₄)₂ solutions at 100° and CO₂-free conditions as detailed by Bell, *et al.*⁸ Each sample was well characterized by chemical (Table I), X-ray diffraction, and infrared methods.

Each of these analyses confirmed the purity of the samples. Electron micrographs showed the preparations to consist of well-defined prismatic-shaped crystals from 0.5 to 10 μ long, 0.02 to 0.2 μ wide, and 0.01 to 0.2 μ high. Specific surface areas of the samples were calculated from BET measurements using nitrogen and/or krypton, and these values were in reasonable agreement with the areas calculated from crystal size.

The following procedure was used to measure the dis-

tribution of P³² and Ca⁴⁵ between the solid surface and its equilibrium solution. Suspensions containing 200 mg of solid per 200 ml were prepared using double-distilled CO₂-free water. Prior to addition of any isotope, suspensions were continuously shaken at 24 ± 0.5° for 2–4 weeks to allow attainment of dissolution equilibrium as indicated by solution phosphorus and calcium analyses. Blank solutions were prepared, and these contained the same calcium and phosphorus concentrations as the solutions in equilibrium with the hydroxyapatite samples. The blank solutions provided a correction for radioactive decay and adsorption of isotope onto the container walls.

The P³² (as H₃PO₄ in dilute HCl) and Ca⁴⁵ (as CaCl₂) were diluted with hydroxyapatite equilibrium solution so that the calcium and phosphorus concentrations in the equilibrated suspensions would be virtually unchanged by the isotope addition. Sampling of the tagged suspensions was continued until measurable uptake of isotope had ceased. The proportion of isotope taken up by the solid varied from 10 to 60% but most commonly was around the optimum value of 50%. All sampling operations were carried out under an atmosphere of N₂ to prevent entry of CO₂ into the suspensions. This was to preclude the replacement of surface phosphate groups by carbonate. The replacement of phosphate by carbonate in naturally occurring apatites is well documented.⁹

When isotope exchange was judged to be complete, a sample of the suspension (or blank solution) was passed through an 0.22-μ millipore filter and 1-ml aliquots added to 10 ml of Bray's scintillation solution.¹⁰ Simultaneous counting of P³² and Ca⁴⁵ was provided by a Packard Tricarb 3320 liquid scintillation counter. The total calcium concentration in the filtered solutions was measured by atomic absorption spectroscopy and the total phosphorus concentration by the method of Murphy and Riley.¹¹

(8) L. C. Bell, A. M. Posner, and J. P. Quirk, submitted to *J. Colloid Interface Sci.*

(9) R. Z. LeGeros, O. R. Trautz, J. P. LeGeros, and E. Klein, *Bull. Soc. Chim. Fr.*, 1712 (1968).

(10) G. A. Bray, *Anal. Biochem.*, 1, 279 (1960).

In most instances the suspensions were adjusted with KOH to pH 8.5, the pH corresponding to the point of zero charge for the synthetic hydroxyapatite samples.⁸ This adjustment was designed to eliminate the effect of surface charge on the possible accumulation of phosphorus or calcium at the solid surface. Despite precautions, slight downward drifts in pH did occur over the 3–5-week duration of each experiment. The change occurring during isotope exchange was small and did not affect the solubility equilibrium to any measurable degree.

Results and Discussion

Theoretical Surface Concentrations of Calcium and Phosphorus on Hydroxyapatite. From a knowledge of the crystal morphology, the structure of the unit cell and the orientation of the unit cell in the crystal, the theoretical area per phosphorus and calcium atoms can be calculated. The unit cell of hydroxyapatite $[\text{Ca}_{10}(\text{OH})_2(\text{PO}_4)_6]$ exhibits hexagonal symmetry with an a axis = 9.432 Å and c axis = 6.881 Å.¹² Electron micrographs of synthetic stoichiometric hydroxyapatite crystals in this and other studies^{9,13} have shown the crystals to be prismatic in shape. Electron diffraction analysis of the solids used in this study confirmed the observation of other workers^{13,14} that the c axis runs parallel to the longest axis of the crystals. The planes most commonly developed on the crystal exterior are the ones described by the Miller indices $[10\bar{1}0]$, $[10\bar{1}1]$, $[0001]$, and sometimes $[1121]$.¹⁵ The latter three planes intersect the c axis and will, in well-crystallized solids, show significant development only at the ends of the crystal. Thus the $[10\bar{1}0]$ plane, which corresponds to the a - c face of the unit cell, will contribute most to the crystal surface. (The a - c face is defined here as the plane bounded by the a and the c axes.) Inspection of an atomic model of the hydroxyapatite unit cell shows that there are three fairly distinct planes of atoms parallel to the a - c face. These planes contain all six phosphorus atoms and all ten calcium atoms in the unit cell. There is no "a priori" reason for assuming that the plane represented by the a - c face of the unit cell should be preferred to the other two planes parallel to it. It is reasonable to assume, therefore, that all three planes will contribute to the surface exposed at a $[10\bar{1}0]$ crystal face. The number of phosphorus and calcium atoms per unit cell at the surface should then be an average of the numbers of these ions per unit cell in each of these three planes (Figure 1), *i.e.*, 2 phosphorus and 3.33 calcium atoms. If one uses the unit cell dimensions $a = 9.43$ Å and $c = 6.88$ Å, the calculated area per phosphorus atom is 32.4 Å² and for calcium 19.5 Å². The calculated areas per phosphorus and calcium for faces occurring at the ends of the crystals are different from those calculated for the $[10\bar{1}0]$ face. For the $[0001]$ face the calculated area per phosphorus atom is 25.6 Å² and the area per calcium

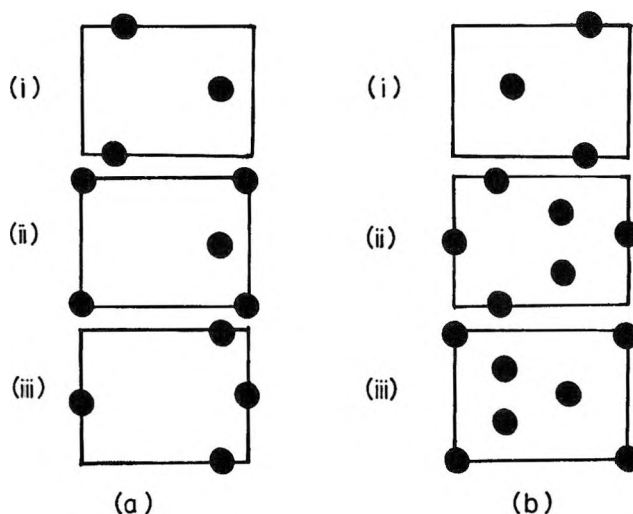


Figure 1. Diagrammatic representation of the number of (a) phosphorus or (b) calcium atoms in various planes of the unit cell parallel to the $[10\bar{1}0]$ or a - c face of hydroxyapatite.

atom is 29.6 Å². Electron micrographs of crystals used in this study, however, showed that the contribution of faces other than the $[10\bar{1}0]$ to the total crystal surface was less than 1%. The area for each phosphorus and calcium atom should then be close to values predicted for the $[10\bar{1}0]$ face.

Measured Areas for Surface Phosphorus and Calcium Atoms. The areas for phosphorus and calcium calculated from measurements of specific surface area and isotope exchange on hydroxyapatite samples of varying specific surface area are shown in Table I. The values obtained for phosphorus are close to the theoretically predicted value of 32.4 Å² calculated on the assumption that the contribution from planes at the ends of the crystals is small. The mean value for all samples is 33.1 Å² with a standard deviation of 2.7. The measured areas per calcium atom, although not as close to the theoretically predicted value of 19.5 Å², are nonetheless reasonable (mean 23.0 ± 2.1). In relation to this result it is of interest to note that in Figures 1a and b there are two phosphate atoms in each of the three possible atomic planes parallel to the a - c face, whereas the number of calcium atoms varies, being two, four, and four. This result may mean that there is a tendency for plane i shown in Figure 1b to contribute a greater proportion to the surface area than the other two planes.

The close agreement between theoretical and experimental areas for phosphorus and calcium suggests that surface dissolution and recrystallization processes

(11) J. Murphy and J. P. Riley, *Anal. Chim. Acta*, **27**, 31 (1962).

(12) M. I. Kay, R. A. Young, and A. S. Posner, *Nature*, **204**, 1050 (1964).

(13) R. C. Likins, H. G. McCann, A. S. Posner, and D. B. Scott, *J. Biol. Chem.*, **235**, 2152 (1960).

(14) A. S. Posner, *Phys. Rev.*, **49**, 760 (1969).

(15) C. Palache, H. Berman, and C. Frondel, "Dana's System of Mineralogy," Vol. II, Wiley, New York, N. Y., 1951.

("thermal aging") were reduced to a minimum by ensuring that chemical equilibrium had been reached prior to addition of isotope. Previous studies of this type 1-4 have indicated that erroneous results were obtained if thermal aging processes were appreciable.

Hydroxyapatite is known to be amphoteric and for the samples used in this investigation the solid had a net zero charge at about pH 8.5.⁸ All suspensions were initially adjusted to this pH as it was considered that a test of the technique of using isotope exchange to measure the area per phosphorus and calcium atoms would best be made on a solid with net zero charge. In suspensions having high solid to solution ratios of charged particles, errors in calculating the surface concentration of atoms could arise with highly charged solids due to negative adsorption. (In this work low solid to solution ratios were employed.) It is also conceivable that a solid with a high surface charge density might preferentially adsorb ions of opposite charge, and this might be reflected in a change in its measured surface concentration. At the pH values of the suspensions in this investigation (7.4-7.9) the hydroxyapatite surface would have had a net positive charge. Apparently this charge development was sufficiently small not to affect the relative adsorption of phosphorus and calcium.

A limited investigation involving the variation of pH of the suspensions over wide limits, however, indicated a change in the measured area per phosphorus on the hydroxyapatite surface. At low pH values the area per phosphorus atom was significantly lower than the theoretical value of 32.4 \AA^2 indicating an accumulation of phosphorus on the positively charged surface. At high pH values the reverse was observed. The trend in calcium areas was not as definite.

The good agreement between the area per phosphate ion determined experimentally near the point of zero charge with the area expected from crystallographic data indicates that the isotopic exchange involves only atoms in the first layer of the crystal. The results for the area occupied by calcium ions in the surface show a deficiency of calcium ions compared with what would be expected; however, as indicated above, the planes parallel to the a - c face of the crystal will have different numbers of calcium ions. When this factor is taken into account, it seems reasonable to conclude that near the point of zero charge only calcium ions from the first layer of the crystal are involved. The results for the area occupied for phosphate and calcium ions at pH values appreciably removed from the point of zero charge can be interpreted as being due to a surface excess of calcium or phosphate ions; that is, ad-atoms are present on the surface. Further work is being undertaken to investigate the possible change in surface concentration of phosphorus and calcium with pH.

It is of interest to compare the results presented in this paper with those obtained in a similar study on hy-

droxyapatite by Olsen.¹⁶ The latter author obtained a value of 21.6 \AA^2 for the average area per surface phosphorus atom, and this agreed well with his predicted value of 21.5 \AA^2 . Olsen based his calculation, however, on the assumption that one of the possible faces of the hydroxyapatite crystal, the a - c face, contained three phosphorus atoms and had an area of 9.37×6.88 or 64.5 \AA^2 . This gave an area per atom of 21.5 \AA^2 . Examination of an atomic model of hydroxyapatite, however, indicates that two of these three phosphorus atoms are shared with neighboring unit cells (Figure 1a(i)) and thus the true area per phosphorus atom for this plane should be $64.5/2 = 32.2 \text{ \AA}^2$. The relatively low experimental value obtained by Olsen for the phosphorus area could possibly be explained by the fact that the solid used in that study was phosphate-rich having a Ca/P mole ratio of 1.52 compared with the value of 1.67 for a solid of ideal composition.

After the surface concentrations of phosphorus and calcium on hydroxyapatite in the absence of foreign ions had been established, these parameters were then used to measure the extent of reaction with the solid of a number of additives commonly employed in hydroxyapatite solution studies at pH values (7.4-7.9) near the point of zero charge.

The presence in hydroxyapatite suspensions of barbiturate ($0.01 M K^+$ or Na^+ salt), a commonly used buffer, or chloroform ($1\% v/v$), an antibacterial agent, had no significant effect on the area per phosphorus and calcium. If significant adsorption of these species had occurred, then a change in the surface concentrations of phosphorus and calcium would have been expected.

The surface concentrations of phosphorus and calcium were unaltered by the presence of KCl ($0.1 M$). If K^+ can exchange with surface calcium atoms on hydroxyapatite as has been suggested by Pak and Bartter,¹⁷ then the measured area per calcium atom should have increased, *i.e.*, the surface concentration decreased. The result obtained in this study supports the finding by Bell, *et al.*,⁸ that K^+ acts as an indifferent ion towards hydroxyapatite in aqueous solutions.

Excess phosphorus or calcium is often added to aqueous suspensions of hydroxyapatite to prevent adsorption of added isotope onto the walls of the supporting vessel or to hasten the approach to solubility equilibrium prior to the addition of the isotope. The measured areas per phosphorus and calcium were unaffected by varying the Ca concentration from 0.15 to 12.8 ppm with P concentrations of 18.7 and 0.32 ppm, respectively, indicating that the formation of a calcium- or phosphorus-rich phase on the hydroxyapatite surface did not occur.

It seems that P^{32} and Ca^{45} can be used to advantage

(16) S. R. Olsen, *J. Phys. Chem.*, **56**, 630 (1952).

(17) C. Y. C. Pak and F. C. Bartter, *Biochim. Biophys. Acta*, **141**, 410 (1967).

to measure the specific surface area of hydroxyapatite in aqueous solutions provided that (1) the hydroxyapatite has the theoretical composition, (2) the equilibration conditions are such that the surface of the solid has the same composition as the bulk, *e.g.*, pH close to the point of zero charge, and (3) sufficient equilibration time is allowed prior to addition of isotope to reduce "aging" effects during isotope exchange. Alternatively, knowing the specific surface area, isotope exchange of P^{32} and Ca^{45} can be used to investigate sur-

face reactions such as chemisorption, physical adsorption, and ionic substitution.

Acknowledgments. The authors are grateful to I. D. Sills for the surface area measurements and to T. Armitage for his valuable assistance with the electron microscope. One of us (L. C. Bell) wishes to acknowledge his support as a Queen Elizabeth Fellow during this research project. The work reported forms part of a research program supported by the Australian Research Grants Committee.

Effects of High-Pressure HCl on Transport Properties of the Molten

46 Mol % KCl-54 Mol % $ZnCl_2$ Eutectic System¹

by Billy R. Hubble and James L. Copeland*

Department of Chemistry, Kansas State University, Manhattan, Kansas 66502 (Received June 21, 1971)

Publication costs assisted by The National Science Foundation

Effects of chemically interacting high-pressure HCl gas on the electrical conductance and viscosity of molten 46 mol % KCl-54 mol % $ZnCl_2$ eutectic were investigated in comparison with those of inert argon. Specific conductance, κ , was measured at 275° and 300° with HCl pressures from 1 to 205 atm at 275°, to 163 atm at 300°, and with argon pressures from 1 to 272 atm at 275° to 350°. Viscosity was measured by means of a capillary flow technique at HCl pressures from 1 to 136 atm at 300° and to 96 atm at 320°. The effect of argon pressure on κ was as expected a depressive one presumably caused by the pressure and dilution with dissolved gas. HCl, on the other hand, greatly enhanced κ at each temperature with increasing saturation pressure. Viscous flow time was found to decrease considerably less sharply with HCl pressure than κ increased with HCl pressure. These experimental results are interpreted in terms of a breakup of polymeric ions by the HCl and a Grotthus-type conduction process, *i.e.*, proton exchange. Such a mechanism would bring about a rapid enhancement of conductivity with increasing HCl concentration, together with a decrease in viscosity as a result of the formation of smaller units of flow from the polymeric ion breakdown.

Introduction

Only in recent years have investigations of the effects of pressure on transport properties of molten systems been undertaken. Technological difficulties associated with the simultaneous maintenance of high pressures and temperatures appear to be the main obstacles to such studies. Experimentally, high pressures have been generated in two ways: (a) hydrostatic techniques, and (b) use of inert gases as pressurizing media. For examples, Angell, Pollard, and Strauss^{2,3} have measured electrical conductances of $Ca(NO_3)_2 + KNO_3$ glass forming melts under hydrostatic pressure transmitted by a Teflon plug, and Barton, Cleaver, and Hills⁴ have determined conductances of molten alkali nitrates under pressure communicated by mercury columns. Copeland and Christie⁵ recently have studied viscous properties of molten $NaNO_3$ and KNO_3 under hydro-

static pressure transmitted by a stainless steel Sylphon bellows. Diffusion coefficients have been measured under pressure for Na^+ in $NaNO_3$, and for Cs^+ in $CsNO_3$ and $NaNO_3$,⁶ however, pressure was applied by

(1) This paper was presented in part at the sixth Midwest Regional Meeting of the American Chemical Society, Lincoln, Neb., Oct. 1970.

(2) C. A. Angell, L. J. Pollard, and W. Strauss, *J. Chem. Phys.*, **43**, 2899 (1965).

(3) C. A. Angell, L. J. Pollard, and W. Strauss, *ibid.*, **50**, 2694 (1969).

(4) A. F. M. Barton, B. Cleaver, and G. J. Hills, *Trans. Faraday Soc.*, **64**, 208 (1968).

(5) J. L. Copeland and J. R. Christie, *J. Chem. Phys.*, **55**, 4925 (1971).

(6) (a) S. B. Tricklebank, L. Nanis, and J. O'M. Bockris, *Rev. Sci. Instrum.*, **35**, 807 (1964); (b) M. K. Nagarajan, L. Nanis, and J. O'M. Bockris, *J. Phys. Chem.*, **68**, 2726 (1964); (c) M. K. Nagarajan and J. O'M. Bockris, *ibid.*, **70**, 1854 (1966).

direct contact of N₂ with the melts, and the effect of gas solubility is in doubt.⁴ In the past our laboratory has reported its findings concerning the effects of pressurization with He, Ar, and N₂ on the conductivities of molten NaNO₃ and AgNO₃,⁷⁻⁹ and more recently the effects of such gas pressurizations on the viscous properties of NaNO₃ and KNO₃.^{10,11} Although our crude determinations of the high pressure solubilities of the foregoing gases in these melts have been shown to be inaccurate,¹² the transport measurements serve to show that a dissolved inert gas acts as a diluent by virtue of its molecules creating their own holes in a melt rather than by occupancy of any inherent liquid free volume.

In the present work, we report the results of a first study of the effects of a chemically reactive high-pressure gas on the transport properties of a molten electrolyte system. This study includes: (a) specific conductance measurements on the molten 46 mol % KCl-54 mol % ZnCl₂ eutectic system (mp 228°)¹³ from 275° to 350° while pressurized with Ar from 1 to 272 atm, (b) specific conductance measurements at 275° with this melt pressurized with HCl from 1 to 205 atm, (c) specific conductance measurements at 300° with the melt pressurized with HCl from 1 to 163 atm, (d) viscosity measurements at 300° while pressurized with HCl from 1 to 136 atm, and (e) viscosity measurements at 320° while pressurized with HCl from 1 to 96 atm.

Experimental Section

Materials. Reagent grade KCl and ZnCl₂ were obtained from the Mallinckrodt Co. The KCl was dried in an oven at 130° for over a week before being weighed. The ZnCl₂ was dried in an oven at 150° for over 24 hr, while under vacuum, by constant pumping on the system with a mechanical vacuum pump.¹⁴ All weighings and handling of the salts were done in a Model 50004/50005 Lab Con Co. drybox with an Ar atmosphere. Argon and electronic grade HCl were used directly from cylinders obtained from the National Cylinder Gas Co. and the Matheson Gas Products Co., respectively. The purity of each gas was claimed to be better than 99.99% by the respective manufacturers.

Apparatus. A 500-ml capacity Inconel X-750 autoclave (Type A364HC of the Parr Instrument Co., and provided with Conax lava-packed glands) was used. Conductivity measurements were made with a Leeds and Northrup Co. No. 4660 Jones-type bridge. A Heathkit Model IG-82 sine wave generator provided a 1000-Hz signal. Stray capacitance was balanced by an Industrial Instruments Co. Model DK2A decade capacitance box. Null detection was provided by a Heathkit Model 10-12 oscilloscope. Shielded cable was employed in all connections, and the bodies of the electric furnace and autoclave were grounded. Temperatures were transduced by means of chromel-alumel thermocouples, using an ice-water reference junction

and a Leeds and Northrup Co. No. 8691 millivolt potentiometer.

A Pyrex capillary conductance cell, similar to one previously employed in our laboratory,⁷ was used. The cell constant was found in the conventional manner using known conductance data for molten NaNO₃ over the temperature range of the present study. The cell constant was 260.0 cm⁻¹, and was temperature independent in this temperature region.

The general apparatus and method employed in the viscosity determinations are identical with those employed in the alkali nitrate work.^{10,11} The capillary flow viscometer used in the present study was the same as employed earlier,¹¹ where it was found that the effective viscometer constant, *K*, was expressible as

$$K = (6.220 \pm 0.021) \times 10^{-2} - (3.644 \pm 0.054) \times 10^{-5} T' \text{ cP cm}^3 \text{ g}^{-1} \text{ sec}^{-1} \quad (1)$$

where *T'* is temperature in °C and the errors are least squares probable errors.

Procedure. In the conductance experiment, 1.6070 mol of KCl and 1.8865 mol of ZnCl₂ were weighed in the drybox environment and mixed together to prepare the 46 mol % KCl-54 mol % ZnCl₂ eutectic mixture. The mixture was melted in a casserole and was decanted several times to remove any insoluble matter before being allowed to solidify in a desiccator that was kept evacuated for over 24 hr by means of a mechanical vacuum pump. In the drybox environment, a 300.93-g sample of the prepared eutectic was transferred to the conductance cell. The latter was installed in the autoclave. The assembled autoclave was then removed from the drybox environment and was placed in an electric furnace. Evacuation by means of the vacuum pump was maintained while the temperature of the furnace was slowly increased to the melting point of the eutectic. Once the eutectic was in the liquid phase, equilibration of the system at a particular temperature was followed by conductance measurements.

Conductance was first determined at atmospheric pressure over *ca.* 25° temperature intervals, in each instance allowing the system to reach thermal equilibrium over a period of at least a day before taking resistance measurements at a particular temperature. These results are reported in detail elsewhere.¹⁵

(7) J. L. Copeland and W. C. Zybko, *J. Phys. Chem.*, **70**, 181 (1966).

(8) J. L. Copeland and S. Radak, *ibid.*, **70**, 3356 (1966).

(9) J. L. Copeland and S. Radak, *ibid.*, **71**, 4360 (1967).

(10) J. L. Copeland and J. R. Christie, *ibid.*, **73**, 1205 (1969).

(11) J. L. Copeland and J. R. Christie, *ibid.*, **75**, 103 (1971).

(12) B. Cleaver and D. E. Mather, *Trans. Faraday Soc.*, **66**, 2469 (1970).

(13) P. V. Clark, "Fused Salt Mixtures: Eutectic Compositions and Melting Points," SC-R-68-1680, U. S. Dept. of Commerce/National Bureau of Standards, 1968, p 83.

(14) J. D. Mackenzie and W. K. Murphy, *J. Chem. Phys.*, **33**, 366 (1960).

For the Ar pressure studies, performed before those with HCl to provide a basis for comparison of the HCl results, the desired temperature was first attained. Equilibrium pressure, temperature, and resistance readings were obtained, in order, at pressures of 1000, 2000, 3000, and 4000 psig. The procedure was then reversed at 3500, 2500, 1500, and 500 psig. The resistance reading at atmospheric pressure, at the particular temperature, was then repeated. Such runs were performed at *ca.* 25° increasing temperature intervals.

In the HCl gas pressure studies, the autoclave was first evacuated to remove any Ar left from the Ar studies, then HCl gas pressure was applied. For the 275° run, the HCl pressure was increased in intervals to a maximum of 3000 psig and was then decreased in intervals back to atmospheric pressure. The conductance measurement at atmospheric pressure was repeated before increasing the temperature. For the 300° run, HCl pressure was increased in intervals to a maximum of 2400 psig and was then decreased in intervals back to atmospheric pressure. Experimental problems were encountered with the gradual corrosion of the stainless steel needle valve which permitted access to the autoclave. Thus, eventually this valve became incapable of retaining the higher pressures of HCl (*e.g.*, a maximum of 2400 psig in the 300° run) and forced the termination of measurements at the end of the 300° run. The HCl also corroded the thermocouples.

In the viscosity experiment, the eutectic was prepared in the same manner as that described for the conductance experiment. In the drybox environment a 100.000-g sample of the prepared eutectic (calculated from the molten salt density data¹⁶ to fill the viscometer adequately with the liquid surface slightly below the rim of the subreservoir) was placed in the viscometer assembly. The latter was installed in the autoclave, which was in turn assembled and removed from the drybox environment and placed in the furnace. The evacuation treatment described for the conductance study was followed while the eutectic was being heated and fused.

Viscosity measurements were first performed at atmospheric pressure in the temperature range between 286° and 505°. These results are described in detail elsewhere.¹⁵ The viscosity measurement technique has been described earlier.^{10,11} In the HCl gas pressure study, for the 300° viscosity run the HCl pressure was increased in intervals to a maximum of 2000 psig and was then decreased in intervals back to atmospheric pressure. The viscosity measurement at atmospheric pressure was repeated before increasing the temperature. For the 320° run, the HCl pressure was increased in intervals to a maximum of 1420 psig and was then decreased in intervals back to atmospheric pressure. The viscosity measurement at atmospheric pressure was then repeated. The needle valve again became incapable of retaining the higher pressures of

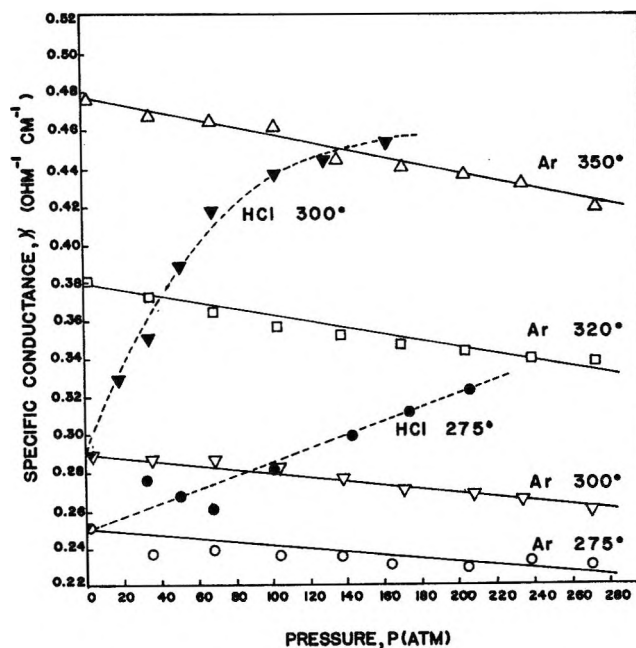


Figure 1. Isotherms of specific conductance, κ , of the molten 46 mol % KCl-54 mol % ZnCl₂ eutectic vs. saturating gas pressure of Ar and HCl.

HCl in the 320° run (*i.e.*, at a maximum of 1420 psig) and measurements were forced to be terminated at the end of this sequence.

Results

Specific conductance was calculated as $\kappa = C/R$, the cell constant, C , equaling 260.0 cm⁻¹. The results obtained with Ar and HCl pressurizing media are summarized in Table I.¹⁷ Isotherms of κ vs. pressure, P (atm) are shown in Figure 1, where solid curves represent pressurization with Ar and dashed curves pressurization with HCl. So-called apparent activation volumes for the specific conductance, defined as

$$\Delta V_{\kappa}^* = -RT(d \ln \kappa / dP)_T \quad (2)$$

may be computed from least-squares slopes of $\ln \kappa$ vs. P plots and are included in Table II.

The viscosity results obtained with HCl pressurization are summarized in Table III. Figure 2 shows isotherms of flow time, t (sec) vs. P (atm). Apparent coefficients of viscosity, η (cP) = $K\rho t$, were computed with an effective viscometer constant, K , as given by eq 1. For these relative apparent viscosities atmospheric pressure density data, ρ , were used, with the tentative as-

(15) B. R. Hubble, Ph.D. Thesis, Kansas State University, Manhattan, Kans., 1971.

(16) F. R. Duke and R. A. Fleming, *J. Electrochem. Soc.*, **104**, 251 (1957).

(17) Table I will appear following these pages in the microfilm edition of this volume of the journal. Single copies may be obtained from the Business Operations Office, Books and Journals Division, American Chemical Society, 1155 Sixteenth St., N.W., Washington, D. C. 20036, by referring to author, title of article, volume, and page number. Remit check or money order for \$3.00 for photocopy or \$2.00 for microfiche.

Table II: Summary of Computed Apparent Specific Conductance Activation Volumes for the Molten 46 mol % KCl-54 mol % ZnCl System while Pressurized with Ar. Errors are Least-Squares Probable Errors

Temp, ^a °C	Slope of ln κ vs. pressure, × 10 ⁴	Intercept of ln κ vs. pressure	Activation volume, ΔV _κ [*] , cm ³ mol ⁻¹
275	2.38 ± 0.42	1.4139 ± 0.0067	10.7 ± 1.9
300	4.15 ± 0.19	1.2326 ± 0.0030	19.5 ± 0.9
320	4.40 ± 0.23	0.9772 ± 0.0038	21.4 ± 1.1
350	4.69 ± 0.20	0.7388 ± 0.0032	24.0 ± 1.0

^a Maximum expt. error in temp. is ±1°.

Table III: Summary of Viscosity Calculations for the Molten 46 mol % KCl-54 mol % ZnCl System while Pressurized with HCl

Temp, ^a °C	HCl Press, ^b atm	Flow time, ^c sec	Visc. const., ^d cP cm ² g ⁻¹ sec ⁻¹	Melt density, ^e g cm ⁻³	Apparent rel. visc., ^f cP
300	1	203.8	0.05130	2.248	23
300	5	193.0	0.05130	2.248	22
300	37	143.0	0.05130	2.248	16
300	75	132.0	0.05130	2.248	15
300	102	120.5	0.05130	2.248	14
300	136	116.0	0.05130	2.248	13
320	1	128.5	0.05048	2.234	15
320	17	122.1	0.05048	2.234	14
320	29	120.7	0.05048	2.234	14
320	33	117.8	0.05048	2.234	13
320	54	112.0	0.05048	2.234	13
320	78	89.6	0.05048	2.234	10
320	97	81.0	0.05048	2.234	9

^a Maximum expt. error in temp. is ±1°. ^b Maximum expt. error in press. is ±3 atm, except at 1 ± 0 atm. ^c Probable error for a single measurement is at most ±0.6 sec. ^d Calculated from eq 1. ^e Ignoring effect of press. and gas density. ^f Very approx.

sumption that these data were reasonably valid with pressurization as well. The gas density was also assumed to be negligible at the pressures employed in this work, compared with the liquid salt density.

Discussion

Figure 1 shows that the effect of Ar pressure on κ is normal, *i.e.*, a depressive one presumably due to pressure and dilution by gas solubility.⁷ Hydrogen chloride, on the other hand, greatly enhances κ at each temperature with increasing saturation pressure. The effect on κ at 300° may flatten out at pressures in excess of 163 atm, or may even go through a maximum above that pressure. It is a possibility that this curving over above 80 atm may be the result of the onset of corrosion, so that the measurements at this temperature may only be reliable to about 70 atm. Unfortunately the corrosion problem mentioned forced termination of the 300° run with the highest pressure used being that at 163 atm.

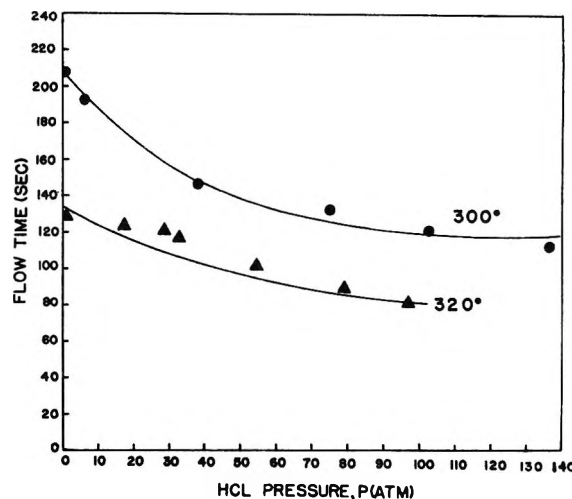
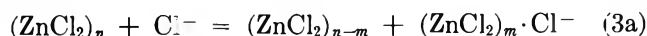


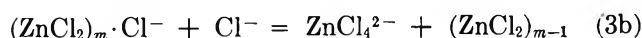
Figure 2. Isotherms of viscous flow time, *t*, of the molten 46 mol % KCl-54 mol % ZnCl₂ eutectic vs. saturating gas pressure of HCl.

Figure 2 illustrates that the isothermal effect of HCl pressure on viscous flow time is a reducing one. If one takes the tentative position of ignoring the inert gas solubility effect, other than assuming that the dilution hypothesis⁷ extends to the KCl-ZnCl₂ system, one can advance an interpretation of the Ar pressurization results. Two conflicting trends exist, due to temperature and pressure effects on the conductance process. The results, as seen in Table II where ΔV_κ^{*} values increase with increasing temperature, show that the depressive pressure effect becomes more pronounced with temperature; *i.e.*, slopes of ln κ vs. *P* plots, also tabulated in Table II, become more negative with increasing temperature. Increasing temperature, *per se*, serves to augment conductance at a given pressure.

Pure ZnCl₂ melts at 318°, and the liquid is thought to be made up of polymeric networks of ZnCl₄²⁻ tetrahedra.¹⁴ As the temperature is raised, or as additional Cl⁻ ions, for example as KCl, are added, these networks may break up to some extent into smaller units such as ZnCl₄²⁻, ZnCl₃⁻, ZnCl⁺, and Zn²⁺ (and, of course, Cl⁻ ions from dissociation, if any). Moyer, *et al.*,¹⁸ feel that Raman studies of the KCl-ZnCl₂ melts indicate that added Cl⁻ ions serve to dissociate the networks into essentially individual ZnCl₄²⁻ tetrahedra alone, according to a "depolymerization" reaction



at Cl⁻ added up to a KCl:ZnCl₂ mole ratio of *ca.* 0.2, followed by



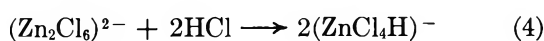
etc., above a mole ratio of 0.2. Ellis,¹⁹ in additional Raman work, feels that some ZnCl₃⁻ units are formed,

(18) J. R. Moyer, J. C. Evans, and G. Y-S. Lo, *J. Electrochem. Soc.*, **113**, 158 (1966).

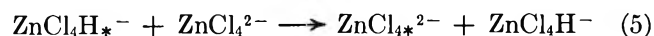
(19) R. B. Ellis, *ibid.*, **113**, 485 (1966).

as well as a ZnCl_2 monomer and a small amount of ZnCl^+ . Whatever the specific natures of the dissociated species may be, electrical conductance of the KCl-ZnCl_2 system certainly increases noticeably with KCl concentration and with temperature,¹⁶ as would be expected, leading to non-Arrhenius behavior with an inconstant "activation energy." Our measurements of η for the eutectic melt of this study, at atmospheric pressure, also indicate non-Arrhenius behavior for this transport property, with an "activation energy" becoming smaller with increasing temperature.¹⁵

As a tentative interpretation of our results we advance the following hypothesis. Hydrogen chloride gas dissolving in the melt acts to break up $(\text{Zn}_n\text{Cl}_{3n})^{n-}$ polymer ions into smaller units, analogous to the action of Cl^- ; e.g., for $n = 2$



This may be followed by a "Grotthus process" of conduction



for example, as in water: $\text{H}_3\text{O}_*^+ + \text{H}_2\text{O} \rightarrow \text{H}_2\text{O}_* + \text{H}_3\text{O}^+$. Such a protonic chain transfer mechanism would enhance κ significantly, in addition to another (smaller) increase in κ due to the breakdown of the larger polymeric ions into smaller entities. These effects would be expected to increase with increasing HCl saturating pressure (Figure 1). At higher temperatures (e.g., 300° in our study) the solubility of HCl may be expected to be somewhat greater at a given pressure (assuming endothermic dissolution^{20,21}), and this increase in HCl concentration should result in an even greater enhancement of κ via the mechanism of eq 4 and 5. This is in addition to the normal increase in κ observed to occur at higher temperatures as a result of thermal breakdown of the polymeric ions, as is believed to occur.¹⁴ Some weight is given to the case for a Grotthus process by the work of Siew and Sundheim²² on the viscosity, density, electrical conductivity, chemical shift, and proton relaxation times for solutions of HNO_3 in the $\text{LiNO}_3\text{-KNO}_3\text{-NaNO}_3$ eutectic. These workers felt that, although not strictly analogous, the Grotthus type model provided a reasonable interpretation of the unusually high mobility for the hydrogen ion observed in their work.

The interpretation of the conductivity results is not inconsistent with our findings of the viscous flow properties. If viscous flow is dominated by the larger species in a liquid,²³ it would be reasonable to assume that the viscosity of the KCl-ZnCl_2 eutectic melt, saturated

with HCl , should reflect essentially the extent to which the large $(\text{ZnCl}_2)_n$ lattice networks have been dissociated into smaller entities as a result of the HCl presence. This appears to be the trend in Figure 2. It would not be meaningful to attempt to illustrate any quantitative relationship between viscosity and conductivity via calculated Walden's rule products, $\eta\Lambda$, for a number of reasons: (a) Walden's rule is known generally not to be applicable to molten salts, due primarily to the inapplicability of the Nernst-Einstein equation to such systems; (b) Walden's rule is not applicable to systems of mixed composition; (c) the equivalent fraction of HCl existing in the melt at a particular pressure is unknown, and therefore the contribution of this equivalent fraction to the equivalent conductance, Λ , is unknown; and (d) the only common temperature at which both conductance and viscosity measurements were obtained under HCl pressure was 300° , and the curving over of the 300° conductance isotherm, in Figure 1, might add to the complexity of such an analysis. (Viscous flow times were not possible to be obtained at 275° because the melt was too viscous to flow through the capillary viscometer; the corrosion problem precluded further common temperature measurements of η and κ .)

Summary

In conclusion, we feel that our results indicate the likely breakup of polymeric ions in the KCl-ZnCl_2 melt by dissolved HCl molecules, followed by a Grotthus-type conduction process accounting for an apparent high proton mobility. The consequent increase of κ with increasing HCl concentration becomes more pronounced at higher temperatures as the result of greater HCl solubility and greater thermal breakdown of polymeric ions. The viscosity of the system is apparently reduced as a result of the breakdown of the larger polymeric ions into smaller entities by dissolved HCl molecules.

Acknowledgments. The authors gratefully acknowledge the support of this research by the National Science Foundation, Grant No. GP-12002. This work is based in part on the thesis of Billy R. Hubble, which has been accepted by the Graduate School of Kansas State University as partial fulfillment of the requirements for the Ph.D. degree.

(20) E. A. Ukshe and B. N. Devyatkin, *Russ. J. Phys. Chem.*, **39**, 1222 (1965).

(21) E. A. Ukshe and B. N. Devyatkin, *ibid.*, **39**, 1641 (1965).

(22) L. C. Siew and B. R. Sundheim, *J. Phys. Chem.*, **73**, 4139 (1969).

(23) J. Frenkel, "Kinetic Theory of Liquids." Dover Publications, New York, N. Y., 1955, pp 439-445.

The Physicochemical Properties of Aqueous Solutions of Fluorinated Surfactants

by Kōzō Shinoda,* Masakatsu Hatō, and Takao Hayashi

Department of Chemistry, Faculty of Engineering, Yokohama National University, Ooka-2, Minami-ku, Yokohama, Japan
(Received August 2, 1971)

Publication costs borne completely by The Journal of Physical Chemistry

The surface tension and the solubility of aqueous solutions of fluorinated surfactants ($C_nF_{2n+1}SO_3M$, $C_7F_{15}COOM$, etc.) have been measured. The cmc's and the Krafft points of the fluorinated surfactants were determined from these data. The cmc of fluorinated surfactant is close to that of ordinary surfactant whose hydrocarbon chain length is about 1.5 times longer than a fluorocarbon chain. This relation is explained assuming the free energy change of transferring the $-CF_2-$ group from the singly dispersed state (aqueous environment) to the micellar state is $1.6kT$. The surface tension of several fluorinated surfactants whose chain length is longer than ~ 8 or 9 was not depressed as low as expected. This is because the Krafft points of these surfactants are higher than the experimental temperature at which the hydrated solid form precipitates and the concentration of singly dispersed material does not increase. If the Krafft point were low, the surface tension would have attained as low as 20 dyn/cm above the cmc, as in the case of ethanolanmonium perfluorooctanesulfonate. The correlation between the Krafft points and the structure of fluorinated surfactants is explained by the theory that a Krafft point is a melting point of hydrated solid agent.

Introduction

Fluorinated surfactants are much more surface active than ordinary surfactants and stable against acidic, alkaline, oxidative, and reductive reagents as well as elevated temperature. Several papers¹⁻³ dealing with the surface and colloidal properties of fluorinated surfactants in aqueous solution have been published, but they deal with only limited types of surfactants due to the difficulty of the synthesis of fluorinated compounds. In the present paper, (1) the effect of fluorocarbon chain length on the solubility and surface tension, (2) the effect of the kinds of gegenions on the Krafft point,⁹ and (3) the effect of the structure of fluorocarbon chain on the Krafft point have been studied in order to increase the solubility and to attain lower surface tension. If the Krafft point is depressed by use of the appropriate gegenion, the surface tension attains low values and the solubility increase enormously.

Experimental Section

Materials. Metal salts of perfluorooctanoic acid, $n-C_7F_{15}COOM$, were the same materials described in earlier papers.^{8,10} Potassium perfluorooctanesulfonate, $C_8F_{17}SO_3K$, obtained from the Minnesota Mining and Manufacturing Co. was repeatedly washed by water to remove water soluble impurities after the recrystallization with absolute ethanol and dried at 110° . Perfluorooctanesulfonic acid, $C_8F_{17}SO_3H$, was obtained by distillation of the potassium salt in the presence of 95% sulfuric acid (bp 150° ; 14 mm).¹¹ Metal salts were obtained neutralizing the acid by respective metal hydroxides. $C_7F_{15}SO_3Na$, $C_9F_{19}SO_3^{1/2}Mg \cdot 2H_2O$, $C_{11}F_{23}SO_3^{1/2}Mg \cdot 2H_2O$, $(CF_3)_2CF(CF_2)_4COOH$ (mp = $13 \sim 14^\circ$), and $(CF_3)_2CF(CF_2)_4CH=CHCH_2COOH$ (mp = $63 \sim 68^\circ$) were synthesized by T. H. The procedure of the synthesis will be published elsewhere.

$C_7F_{15}SO_3Na$ and $C_9F_{19}SO_3^{1/2}Mg \cdot 2H_2O$ were recrystallized from water and dried at 110° . $C_9F_{19}SO_3K$ was prepared by adding excess aqueous KCl solution to an aqueous solution of $C_9F_{19}SO_3^{1/2}Mg \cdot 2H_2O$ at 80° , well above the Krafft point of $C_9F_{19}SO_3^{1/2}Mg \cdot 2H_2O$, then filtered and washed at $70 \sim 80^\circ$. Potassium salt of $(CF_3)_2CF(CF_2)_4CH=CHCH_2COOH$ was obtained neutralizing by an aqueous KOH solution at $70 \sim 80^\circ$. Excess amount of KOH (2%) was added in order to suppress hydrolysis. $(CF_3)_2CF(CF_2)_4COOM$ were prepared by neutralizing an aqueous $(CF_3)_2CF(CF_2)_4COOH$ solution with respective metal hydroxides. The electrical conductivity of water used was $1.2 \sim 1.4 \mu\text{mho/cm}$ at 25° .

Procedures. Solubility Measurement. The solubility of surfactants was determined either by electrical conductivity (at low solubility) or by weighting the dried solution (at high solubility) after vigorous stirring of solutions over 1-2 hr which were kept in a

(1) J. H. Simons, Ed., "Fluorine Chemistry," Vol. 5, Academic Press, New York, N. Y., 1964, p 370.

(2) N. O. Brace, *J. Org. Chem.*, **27**, 4491 (1962).

(3) M. K. Bennett and W. A. Zisman, *J. Phys. Chem.*, **63**, 1911 (1959).

(4) C. H. Arrington and G. D. Patterson, *ibid.*, **57**, 247 (1953).

(5) H. M. Scholberg, R. A. Guenther, and R. I. Coon, *ibid.*, **57**, 923 (1953).

(6) H. B. Klevens and M. Raison, *J. Chim. Phys.*, **51**, 1 (1954).

(7) L. A. Schits, Ξ/III , 143, 5th International Congress on Surface Active Substances, Barcelona, Spain, 1968.

(8) K. Shinoda and H. Nakayama, *J. Colloid Sci.*, **18**, 705 (1963).

(9) The Krafft point is a temperature above which the hydrated solid surfactant melts and dissolves as micelles in water. So the solubility of surfactant increases enormously. Cf. K. Shinoda, *et al.*, "Colloidal Surfactants," Academic Press, New York, N. Y., 1963, pp 7-9.

(10) H. Nakayama and K. Shinoda, *Bull. Chem. Soc. Jap.*, **40**, 1797 (1967).

(11) T. Gramstad and R. N. Haszeldine, *J. Chem. Soc.*, 2640 (1957).

thermostat controlled within $\pm 0.02^\circ$. Further stirring caused no change in the solubility. Prior to the determination of the concentration the solution was allowed to stand about 30 min. The relations between the concentrations *vs.* the conductivity at various temperature were determined using solutions of known concentration. These relations were used as calibration curves to determine the concentrations. It is confirmed that both measurements agree with each other. The solubility data are the means of more than two determinations. The respective values did not deviate more than 0.5% from the mean.

Surface Tension Measurement. Surface tension was measured by a drop-weight method in an air thermostat controlled within $\pm 0.2^\circ$. The correction by Harkins and Brown¹² was applied. The time duration for 1 drop was 3–45 min depending on the time required to attain the equilibrium. The surface tensions are average values of 2–4 measurements whose accuracy was ± 0.1 dyn/cm around the cmc and ± 0.3 dyn/cm at lower concentration.

Results and Discussion

Surface Properties of Fluorinated Surfactants. The surface tension *vs.* the concentration curves of metal salts of perfluoroalkanesulfonic acids are shown in Figure 1. Dotted lines illustrate the surface tension of solutions in which the hydrated solid agent precipitates. The surface tension of sodium dodecanesulfate is also shown for comparison. The surface tension *vs.* the concentration curves of normal and branched perfluoroalkancarboxylates are plotted in Figure 2. The minima of surface tension and the cross sectional areas per molecule at 25° are listed in Table I. The cross

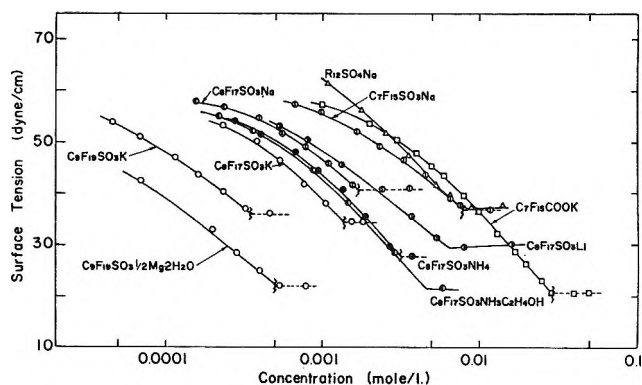


Figure 1. The surface tension of $C_nF_{2n+1}SO_3M$ in water at 25° . Purity of $C_9F_{19}SO_3K$ is lower than the other surfactants (see text).

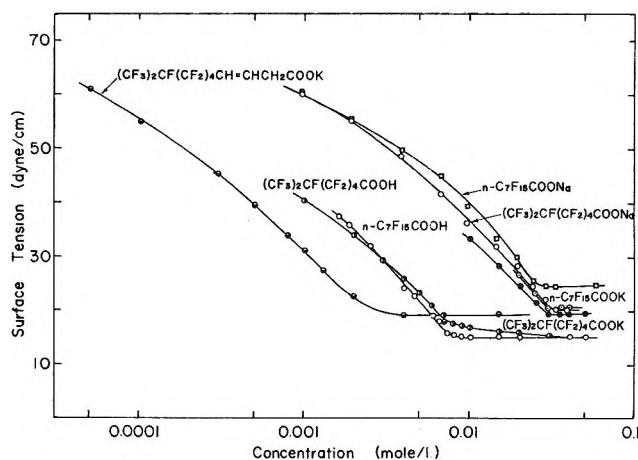


Figure 2. The surface tension of $n-C_7F_{15}COOM$ and $(CF_3)_2CF(CF_2)_4COOM$ in water at 25° . The surface tension of $(CF_3)_2CF(CF_2)_4CH=CHCH_2COOK$ was measured in 0.02 *N* KOH aqueous solution in order to suppress hydrolysis.

Table I: The Surface Tension Minima and Cross Sectional Areas of Fluorinated Surfactants at 25°

Compound	Minima of surface tension, dynes/cm	Cross sectional area, $\text{Å}^2/\text{molecule}$
$n-C_7F_{15}SO_3Na$	37.3	52.5
$n-C_8F_{17}SO_3Li$	29.8	55.2
$n-C_8F_{17}SO_3Na$	40.5	52.5
$n-C_8F_{17}SO_3K$	34.5	45.1
$n-C_8F_{17}SO_3NH_4$	27.8	41.0
$n-C_8F_{17}SO_3NH_3C_2H_4OH$	21.5	42.5
$n-C_9F_{19}SO_3^{1/2}Mg \cdot 2H_2O$	22.0	45.2
$n-C_7F_{15}COONa$	24.6	42.0
$(CF_3)_2CF(CF_2)_4COONa$	20.2	43.5
$n-C_7F_{15}COOK$	20.6	43.0
$(CF_3)_2CF(CF_2)_4COOK$	19.5	47.5
$n-C_7F_{15}COOH$	15.2	41.5
	15.3 ^b	...
$(CF_3)_2CF(CF_2)_4COOH$	~ 15.5	48.0
$(CF_3)_2CF(CF_2)_4CH=CHCH_2COOK^a$	19.4	...

^a In 0.02 *N* aqueous KOH solution.

sectional area of surface active ion, $\alpha_2 = 1/\Gamma_2N$, is calculated from the equation^{8,13}

$$-\left(\frac{\partial \gamma}{\partial \ln C_2}\right)_T = RT \left(1 + \frac{K_g}{Z}\right) \Gamma_2 \quad (1)$$

where C_2 is the concentration of surface active ion, Γ_2 is the surface excess of surface active ion, z is the number of charges of gegenion, and K_g is 0.52 for $n-C_7F_{15}COOK$ ¹³ and assumed 0.5 for the other surfactants. This equation takes into account the effect of gegenions on the surface tension *vs.* the concentration curve.⁸ The slope, $(\partial \gamma / \partial \ln C_2)_T$, was determined by curve fitting a linear relationship in surface tension *vs.* the concentration just below the cmc. It is clear from Figures 1 and 2 that the surface activity of fluorinated surfactants is much larger than corresponding ordinary surfactants with the same chain length. The minima of the surface tension of fluorinated surfactants whose

(12) W. D. Harkins and F. E. Brown, *J. Amer. Chem. Soc.*, **41**, 519 (1919).

(13) K. Shinoda and K. Katsura, *J. Phys. Chem.*, **68**, 1568 (1964).

Table II: The Effects of the Kinds of Gegenions and the Structure of Fluorocarbon on the Krafft Points

Compound	Krafft point, °C	Compound	Krafft point, °C
$n\text{-C}_7\text{F}_{15}\text{SO}_3\text{Na}$	56.5	$n\text{-C}_7\text{F}_{15}\text{COOLi}^{10}$	below 0
$n\text{-C}_8\text{F}_{17}\text{SO}_3\text{Li}$	below 0	$n\text{-C}_7\text{F}_{15}\text{COONa}^{10}$	8.0
$n\text{-C}_8\text{F}_{17}\text{SO}_3\text{Na}$	75	$n\text{-C}_7\text{F}_{15}\text{COOK}^{10}$	25.6
$n\text{-C}_8\text{F}_{17}\text{SO}_3\text{K}$	80	$n\text{-C}_7\text{F}_{15}\text{COORb}^{10}$	20.2
$n\text{-C}_8\text{F}_{17}\text{SO}_3\text{NH}_4$	41	$n\text{-C}_7\text{F}_{15}\text{COOCs}^{10}$	below 0
$n\text{-C}_8\text{F}_{17}\text{SO}_3\text{H}$	below 0	$n\text{-C}_7\text{F}_{15}\text{COOH}^{10}$	20
$n\text{-C}_8\text{F}_{17}\text{SO}_3\text{NH}_3\text{C}_2\text{H}_4\text{OH}$	below 0	$n\text{-C}_7\text{F}_{15}\text{COONH}_4^{10}$	2.5
$n\text{-C}_9\text{F}_{19}\text{SO}_3^{1/2}\text{Mg}\cdot 2\text{H}_2\text{O}$	41	$(\text{CF}_3)_2\text{CF}(\text{CF}_2)_4\text{COOK}$	below 0
$n\text{-C}_{11}\text{F}_{23}\text{SO}_3^{1/2}\text{Mg}\cdot 2\text{H}_2\text{O}$	90 ± 5	$(\text{CF}_3)_2\text{CF}(\text{CF}_2)_4\text{COONa}$	below 0
		$(\text{CF}_3)_2\text{CF}(\text{CF}_2)_4\text{COOH}$	below 0
		$(\text{CF}_3)_2\text{CF}(\text{CF}_2)_4\text{CH}=\text{CHCH}_2\text{COOK}$	below 0

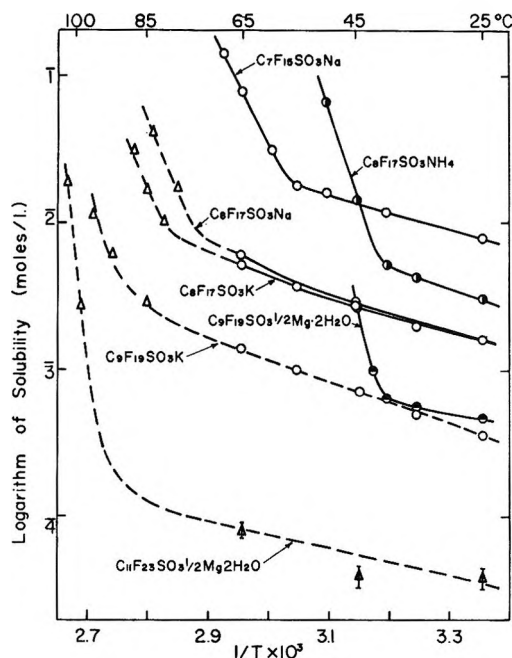


Figure 3. The solubility of $\text{C}_n\text{F}_{2n+1}\text{SO}_3\text{M}$ in water as a function of temperature. Purity of $\text{C}_9\text{F}_{19}\text{SO}_3\text{K}$ is lower than the other surfactants (see text).

Krafft points are higher than 25° is generally high, whereas surfactants whose Krafft points are lower than 25° attain lower surface tension. The Krafft point of ethanolammonium salt is below 0° and the surface tension of aqueous solution is 21.5 dynes/cm.

The Krafft Points and the Solubility of Fluorinated Surfactants in Water. The solubility of fluorinated surfactants in water was determined as a function of temperature and shown in Figures 3 and 4. The dotted curves indicate that the data were less accurate than the other owing to the measurement at high or low temperature or to the small solubility. The temperature at which the solubility increases abruptly corresponds to the Krafft point, as summarized in Table II. It is clear from Figures 3 and 4 that one should select surfactants whose Krafft points are lower than the experimental temperature in order to increase the solubility.

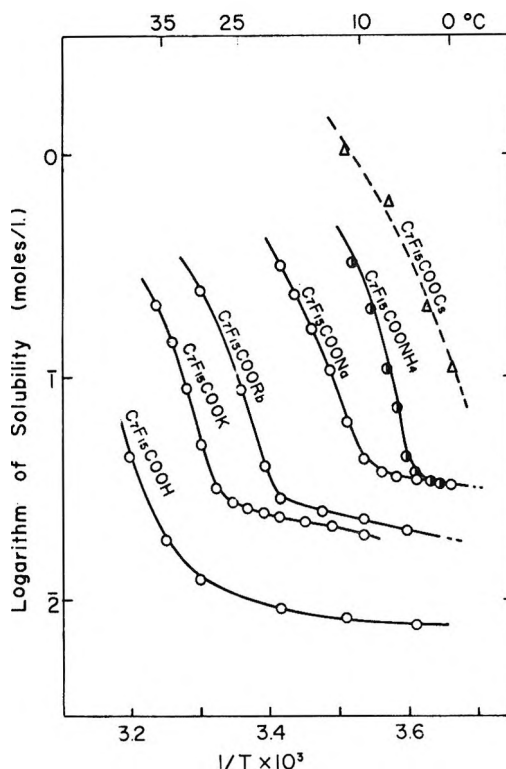


Figure 4. The solubility of $n\text{-C}_7\text{F}_{15}\text{COOM}$ in water as a function of temperature.

The saturation concentration of singly dispersed species, cmc, is not directly related to the solubility.

It is evident from Table II that the Krafft points are raised with an increase of chain length as in the case of ordinary surfactants and the increment of the Krafft points with an increase of chain length of fluorinated surfactants is much larger¹⁴ than that of corresponding ordinary sodium alkanesulfonate.¹⁵ Thus, the chain length of surfactants which form micelles around room temperature is restricted. It is also important to select a suitable gegenion of fluorinated surfactant whose

(14) M. Hatō, and K. Shinoda, *J. Chem. Soc. Jap.*, 91, 27 (1970).

(15) N. V. Tartar and K. A. Wright, *J. Amer. Chem. Soc.*, 61, 539 (1939).

Krafft point is low in order to dissolve the surfactant at lower temperature.

The Effect of the Kinds of Gegenions on the Krafft Point. It is evident from Table II that the Krafft points are markedly dependent on the kinds of gegenions. Krafft points may be affected by several factors such as bond nature between surface active ion and gegenion, structure of hydrated solid agents, or degree of hydration. Among these factors, the degree of hydration of solid agent seems most important. In many cases, the more hydrated the gegenions, the lower the Krafft point. Rb and Cs salts are exceptions. The low Krafft point of ethanolammonium salt can be explained in that the ethanolammonium is an organic group of low melting point and is likely to hydrate well.

The Relation between Krafft Point and the Structure of Fluorocarbon Chain. It is well known that melting points of organic compounds change drastically with the structure such as branching of and double bond in a hydrocarbon chain. This is also the case for Krafft point as can be seen in Table II. A moderately branched compound shows a much lower Krafft point as well as melting point than a corresponding straight chain compound as shown in Table III, but the melting point of

Table III: The Melting Points and the Krafft Points of Straight and Branched Perfluorooctanoic Acids

Compound	mp, °C	Krafft point, °C
$n\text{-C}_7\text{F}_{15}\text{COOH}$	56.4–57.9	20
$(\text{CF}_3)_2\text{CF}(\text{CF}_2)_4\text{COOH}$	13–14	below 0

symmetrically branched compounds such as $(\text{CF}_3)_2\text{-CFCF}(\text{CF}_3)_2$ (mp = -16.7° ¹⁶) is higher than $n\text{-C}_6\text{F}_{14}$ (mp = $-87.1\text{--}86.05^\circ$ ¹⁷) just as in $(\text{CH}_3)_3\text{CC}(\text{CH}_3)_3$ (mp = $100.63\text{--}100.69^\circ$ ¹⁸) and $n\text{-C}_8\text{H}_{18}$ (mp = $-56.8\text{--}56.9^\circ$ ¹⁸).

The Krafft Point of Binary Surfactant Mixtures. It is expected that the Krafft point is depressed by mixing with another surfactant or by replacing with suitable gegenions.^{19,20} It seems interesting to examine whether the Krafft point of surfactant mixtures can be explained quantitatively by our model.^{19,20} The Krafft points of binary surfactant mixtures are estimated from the solubility of 5% solution of respective mixtures and shown in Figures 5 and 6 as a function of mole fraction. It is clear from Figures 5 and 6 that the Krafft points are depressed by adding another surfactant. The lower the Krafft point of surfactant added, the larger the depression of the Krafft point. The addition of a suitable salt into an aqueous solution of surfactant is also an efficient way to obtain the lower Krafft point, *i.e.*, to increase the solubility. Actually the solubility of $\text{C}_8\text{F}_{17}\text{SO}_3\text{K}$ in water increases by adding sulfuric acid²¹ because the Krafft point of $\text{C}_8\text{F}_{17}\text{SO}_3\text{H}$ is below 0° .

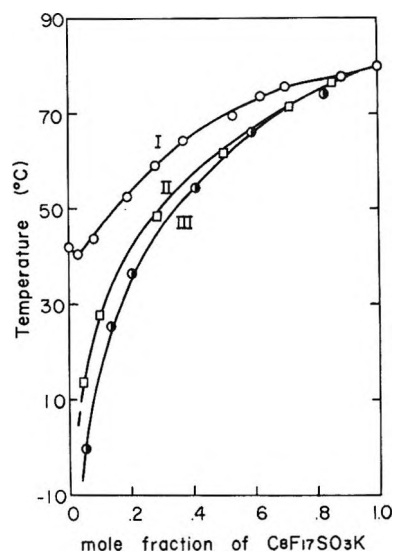


Figure 5. The Krafft point of binary surfactant mixtures. Key: I, $\text{C}_8\text{F}_{17}\text{SO}_3\text{NH}_4 + \text{C}_8\text{F}_{17}\text{SO}_3\text{K}$; II, $\text{C}_8\text{F}_{17}\text{SO}_3\text{H} + \text{C}_8\text{F}_{17}\text{SO}_3\text{K}$; III, $\text{C}_8\text{F}_{17}\text{SO}_3\text{NH}_2\text{C}_2\text{H}_4\text{OH} + \text{C}_8\text{F}_{17}\text{SO}_3\text{K}$.

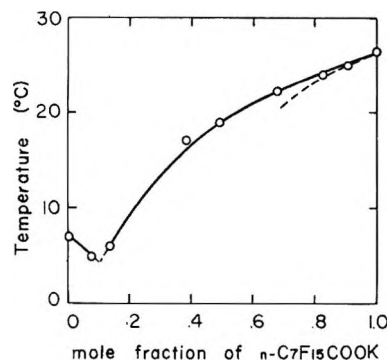


Figure 6. The Krafft point of binary surfactant mixture: $n\text{-C}_7\text{F}_{15}\text{COONa} + n\text{-C}_7\text{F}_{15}\text{COOK}$.

By the analogy of a phase diagram of melting points of binary mixture, the curves in Figures 5 and 6 can be explained, since the curves illustrate a temperature at which a solid phase appears from the liquid mixture (mixed micelle). If the mole fraction of the second component in the micelle is small, the activity of the first component is estimated by the Raoult's law. Then, the change in Krafft point of surfactant mixtures may be expressed just as the well-known equation on freezing point depression²²

(16) G. A. Crowder, M.S. Thesis, University of Florida, (1961); p 177 in ref 3.

(17) V. E. Stiles and G. H. Cady, *J. Amer. Chem. Soc.*, **74**, 3771 (1952).

(18) J. Timmermans, "Physico-Chemical Constants of Pure Organic Compounds," Elsevier, Amsterdam, 1950, pp 85, 96.

(19) K. Shinoda, T. Nakagawa, B. Tamamushi, and T. Isemura, "Colloidal Surfactants," Academic Press, New York, N. Y., 1963, p 7.

(20) K. Shinoda and E. Hutchinson, *J. Phys. Chem.*, **66**, 577 (1962).

(21) Reference 1, pp 374–377.

(22) W. J. Moore, "Physical Chemistry," Prentice-Hall, Englewood Cliffs, N. J., 1962, p 134.

Table IV: Cmc of Fluorinated Surfactants

Compound	Cmc mol/l.	Temp, °C	Method
<i>n</i> -C ₇ F ₁₅ SO ₃ Na	0.0175	56	Solubility
<i>n</i> -C ₈ F ₁₇ SO ₃ Li	0.0063	25	Surface tension
<i>n</i> -C ₈ H ₁₇ SO ₃ Na	0.0085	75	Solubility
<i>n</i> -C ₈ F ₁₇ SO ₃ K	0.0080	80	Solubility
<i>n</i> -C ₈ F ₁₇ SO ₃ NH ₄	0.0055	41	Solubility
<i>n</i> -C ₈ F ₁₇ SO ₃ NH ₃ C ₂ H ₄ OH	0.0046	25	Surface tension
<i>n</i> -C ₉ F ₁₉ SO ₃ ^{1/2} Mg·2H ₂ O	0.00064	41	Solubility
<i>n</i> -C ₁₁ F ₂₃ SO ₃ ^{1/2} Mg·2H ₂ O	~0.00014	90-100	Solubility
<i>n</i> -C ₇ F ₁₅ COONa	0.036	8.0	Solubility ¹⁰
<i>n</i> -C ₇ F ₁₅ COOK	0.027	25.6	Solubility ¹⁰
	0.027		Dye method ⁶
<i>n</i> -C ₇ F ₁₅ COORb	0.028	20.2	Solubility ¹⁰
<i>n</i> -C ₇ F ₁₅ COOH	0.0090	20	Solubility ¹⁰
	0.0080, 0.0091	25	Surface tension ^{10,3}
<i>n</i> -C ₇ F ₁₅ COONH ₄	0.033	2.5	Solubility ¹⁰
(CF ₃) ₂ CF(CF ₂) ₄ COONa	0.032	25	Surface tension
(CF ₃) ₂ CF(CF ₂) ₄ COOK	0.030	25	Surface tension
(CF ₃) ₂ CF(CF ₂) ₄ COOH	0.0085	25	Surface tension
(CF ₃) ₂ CF(CF ₂) ₄ CH=CHCH ₂ COOK	~0.0015 ^a	25	Surface tension

^a In 0.02 *N* KOH aqueous solution.

$$\ln X_1^m = -(\Delta H_1^f/R)(1/T - 1/T_f^0) \quad (2)$$

where X_1^m is the mole fraction of first component in the micellar phase, ΔH_1^f is the heat of fusion of hydrated solid surfactant (component 1), T is the absolute temperature and T_f^0 is the Krafft point of surfactant (component 1). Introducing the heat of fusion, $\Delta H_1^f = 9.6$ kcal/mol,²³ and the Krafft point 25.6° of C₇F₁₅COOK into eq 2, we can evaluate the change of Krafft point of mixtures as a function of mole fraction of first component in the micelle. The calculated values are shown in Figure 6 by a dotted curve. The initial slope well agrees with the experimental curve. Change of the Krafft point over the mole fraction range will be discussed in the succeeding paper which deals with the Krafft point of mixtures of calcium salts.

Cmc of Fluorinated Surfactants. Cmc's were determined either from the solubility *vs.* temperature curves or from surface tension *vs.* concentration curves and are summarized in Table IV.

It can be concluded from Table IV that the cmc values of fluorinated surfactants are mainly determined by the fluorocarbon chain length and the valency of gegenions. Difference in species of gegenion of the same valency has less effect on the cmc. The smaller cmc values of C₇F₁₅COOH than those of corresponding salts may be the result of the incomplete dissociation of the acid. Cmc values of univalent salts of perfluoronanesulfonic acid (C₉F₁₉SO₃M) are estimated to be 0.003-0.001 mol/l. from the change in cmc with chain length. This value is about 4-5 times larger than that of the bivalent salt C₉F₁₉SO₃^{1/2}Mg·2H₂O in Table IV, just as the relation of the cmc values of univalent and bivalent salts of ordinary alkanesulfonate.²⁴ This dif-

ference is explained by the smaller electrical potential of the micellar surface, ψ_0 , of bivalent salt²⁴

$$\psi_0 = \frac{kT}{Z_i e} \left(\ln \frac{2000\pi\sigma^2}{DNkT} - \ln C_i \right) \quad (3)$$

where Z_i is the number of charges of the gegenions, C_i is the concentration of gegenions, and σ is the charge density of micellar surface. Thus, it is clear that the electrical contribution for the micelle formation of fluorinated surfactants is also explained as a function of the number of charges of the gegenions, the concentration of gegenions, and the charge density of the micelle surface.²⁴

The cmc values of fluorinated surfactants and ordinary surfactants^{25,26} are compared in Table V. The cmc is expressed as a function of chain length, in the case where no salt added.^{27,28}

Table V: The Comparison between the cmcs of Fluorinated Surfactants and those of Ordinary Surfactants

Compound	cmc, mol/l.	Temp, °C	Compound	cmc, mol/l.	Temp, °C
C ₈ F ₁₇ SO ₃ Na	0.0085	75	C ₁₂ H ₂₅ SO ₃ Na	0.0081 ²⁴	25
C ₈ F ₁₇ SO ₃ K	0.0080	80	C ₁₂ H ₂₅ SO ₄ Na	0.0081	25
C ₇ F ₁₅ COONa	0.036	8	C ₁₁ H ₂₃ COONa	0.026 ²⁵	25
C ₇ F ₁₅ COOK	0.027	25.6	C ₁₁ H ₂₃ COOK	0.0255 ²⁵	25

(23) K. Shinoda, S. Hiruta, and K. Amaya, *J. Colloid Interface Sci.*, **21**, 102 (1966).

(24) See p 56, eq 1.52 in ref 19.

(25) R. J. Williams, J. N. Phillips, and K. J. Mysels, *Trans. Faraday Soc.*, **51**, 728 (1955).

(26) H. B. Klevens, *J. Amer. Oil Chem. Soc.*, **30**, 74 (1953).

$$\ln \text{cmc} = - \frac{1}{1 + K_g} \left(\frac{m\omega}{kT} \right) + K \quad (4)$$

where m is the number of carbon atoms in the chain, ω is the free energy difference per methylene group between micellar state and singly dispersed state, K and K_g are the experimental constants, T is the absolute temperature, and k is the Boltzmann constant. K_g and K are determined experimentally from the change of cmc with the concentration of the gegenions and the change of cmc with the number of carbon atoms in a paraffin chain. The free energy difference of transferring a $-\text{CH}_2-$ group from aqueous environment to micellar aggregate is estimated to be $1.08kT$ for ordinary surfactants²⁷ and that for $-\text{CF}_2-$ is estimated to be $1.6kT$ from

the change of the cmc values with the fluorocarbon-chain length. As the K value in eq 4 does not change much with the kinds of surfactants, the cmc of a fluorinated surfactant is close to that of an ordinary surfactant whose hydrocarbon chain length is about 1.5 times longer than the fluorocarbon chain.²⁹

(27) P 37-42, eq (1.44) and (1.45) in ref 19.

(28) K. Shinoda, *Bull. Chem. Soc. Jap.*, **26**, 101 (1953).

(29) Tables of surface tension and solubility data will appear following these pages in the microfilm edition of this volume of the journal. Single copies may be obtained from the Business Operations Office, Books and Journals Division, American Chemical Society, 1155 Sixteenth St., N.W., Washington, D. C. 20036, by referring to author, title of article, volume, and page number. Remit check or money order for \$3.00 for photocopy or \$2.00 for microfiche.

Studies of the Vaporization Kinetics of Hydrogen-Bonded Liquids

by F. R. McFeely and G. A. Somorjai*

Inorganic Materials Research Division, Lawrence Berkeley Laboratory, and Department of Chemistry, University of California, Berkeley, California 94720 (Received July 23, 1971)

Publication costs assisted by the U. S. Atomic Energy Commission

The vacuum evaporation rates of glycerol, ethylene glycol, and triethylene glycol have been measured in the temperature range 5–50° using a microbalance. The activation enthalpies of vaporization of the three liquids were found to be different from their enthalpies of vaporization. The vacuum evaporation rates for glycerol and triethylene glycol were about one-third of the maximum rate that can be calculated from the vapor pressures, and one-twentieth of the maximum rate for diethylene glycol. It appears that breaking one or more hydrogen bonds at the surface is the rate-limiting step in the mechanism of vaporization of these largely hydrogen-bonded liquids.

Introduction

To date there have been many studies of the vaporization kinetics of single crystal surfaces. These investigations have revealed a variety of vaporization mechanisms.¹ For some of the solids the desorption of loosely bound surface species was rate limiting (most metals). For other compounds, bond-breaking at well-defined surface sites, surface chemical reactions, association or dissociation were rate limiting. In cases where desorption of molecules at the vaporizing surface was not the rate limiting step, the observed vaporization rate was frequently found to be less than the maximum possible rate, J_{max} , that can be calculated from the kinetic theory of gases. The vaporization coefficient $\alpha_v = J_{\text{obsd}}/J_{\text{max}}$ has been used to indicate the magnitude of the deviation of the observed rate, J_{obsd} , from the maximum rate.

In contrast, the vaporization kinetics of liquids have not been investigated. Wyllie² has measured the vac-

uum vaporization rates of several liquids at one temperature and has thus obtained values for the vaporization coefficient α_v . However the lack of information about the activation enthalpy of vaporization, ΔH_v^* , which can only be obtained from studies of the vaporization rates as a function of temperature, precludes any deduction of the vaporization mechanism.

We have studied the vacuum vaporization rates of glycerol ($\text{CH}_2\text{OHCHOHCH}_2\text{OH}$), diethylene glycol ($\text{CH}_2\text{OHCH}_2\text{OCH}_2\text{CH}_2\text{OH}$), and triethylene glycol ($\text{CH}_2\text{OHCH}_2\text{OCH}_2\text{CH}_2\text{OCH}_2\text{CH}_2\text{OH}$) in the temperature ranges 18–50°, 5–30°, and 10–40°, respectively. From the data the vaporization rates and ΔH_v^* for each liquid were obtained. The experimental results indicate that the breaking of a specific number of hydrogen bonds may be the rate limiting step in each case.

(1) G. A. Somorjai and J. E. Lester, *Progr. Solid State Chem.*, **4**, 1 (1967).

(2) G. Wyllie, *Proc. Roy. Soc., Ser. A*, **197**, 383 (1949).

Experimental Section

The vacuum vaporization experiments were carried out using a Cahn microbalance mounted in a vacuum chamber. The weight change of the balance was displayed on a recorder as a function of time so that the weight of the vaporizing sample could be monitored continuously. The balance could measure weight changes of less than 10 μg .

The liquid that was to be vaporized (spectrograde for glycerol, and reagent grade for the two glycols) was placed in a cylindrical aluminum sample holder and was maintained at a pressure of $5\text{--}50 \times 10^{-3}$ Torr for a period of up to 5 hr to remove dissolved gases and other more volatile impurities (water, etc.). Since degassing of the liquid samples was carried out in the vaporization chamber the samples could be transferred onto the microbalance in 30 sec thus eliminating any possibility of recontamination. The sample was then placed on the balance and the chamber evacuated by means of an oil diffusion pump to an ambient pressure of $\sim 5 \times 10^{-6}$ Torr. At this pressure, the flux of vaporized or ambient molecules striking the vaporizing liquid surface is negligible.

During the experiments the temperature of the liquid was monitored by a 0.005-in. copper-constantan thermocouple placed in the liquid. We were able to place the thermocouple directly on the vaporizing surface where it was held by the surface tension. In order to assure that there would be no surface cooling the total vaporization rates were kept lower than rates reported in single crystal vaporization studies where no temperature gradients across the vaporizing sample could be found.³ [During the vaporization of NaCl crystal surfaces rates as high as 4.8×10^{-5} mol/cm² min were measured as compared to 0.7×10^{-5} mol/cm² min, the rate measured for glycerol at 34°, and only the two highest temperature rate measurements for diethylene glycol exceeded the NaCl vaporization rate. Although the activation enthalpy of sublimation of NaCl was much higher than for any of the liquids in this study the temperature of the solid surface was within 0.25° of the bulk temperature.] While diethylene glycol cooled from 22° to 5° and triethylene glycol to 10° due to heat loss by vaporization, the temperature measured by the thermocouple was found to be independent of its position in the crucible. It therefore appears that under the given experimental conditions there was no detectable temperature gradient between the surface and the bulk and that we therefore had an accurate measure of the temperature of the vaporizing surface.

The liquid was heated by radiation from a coil of nichrome resistance wire placed near the sample. The liquid was maintained at a constant temperature within $\pm 0.2^\circ$ by means of a variable gain feedback control unit. Reproducible steady state vaporization rates at as many as five different temperatures could be measured before the sample surface receded significantly

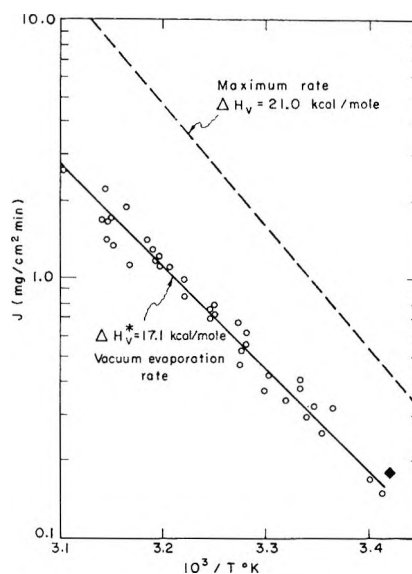


Figure 1. Key: —, vacuum vaporization rate of glycerol; ---, maximum rate;⁵ ◆, determination by Heideger and Boudart.

into the holder. The evaporation rates were measured by both starting at low temperature and increasing the temperature and also by starting at high temperature and decreasing the temperature. The vacuum evaporation rates were reproducible regardless of the thermal history of the sample. Fifty vaporization rates were measured with the various glycerol samples, forty were made using diethylene glycol, and thirty-five using triethylene glycol in the indicated temperature ranges.

Results

Figure 1 shows a plot of the logarithm of the evaporation rate (mg/cm² min) as a function of the reciprocal of the absolute temperature for glycerol. The solid line indicates the experimental vacuum vaporization rate, while the dotted line represents the maximum rate predicted by the kinetic theory of gases using the well-known Langmuir equation⁴ $J(\text{mg}/\text{cm}^2 \text{ min}) = P_{\text{eq}}/(2\pi MRT)^{1/2}$ using the equilibrium vapor pressure data of Stedman.⁵ Here P_{eq} is the equilibrium vapor pressure, M is the molecular weight of the vapor (assumed to be monomer), and R and T have their usual meaning. The isolated point on the graph represents the vacuum vaporization rate of glycerol as calculated from the data obtained at a single temperature by Heideger and Boudart.⁶

Figures 2 and 3 give the vacuum vaporization rates of diethylene and triethylene glycol, along with the maximum rates calculated from the equilibrium vapor pressure data of Gallagher and Hibbert.⁷ The equi-

(3) J. E. Lester, Ph.D. thesis, University of California, Berkeley, 1967.

(4) I. Langmuir, *J. Amer. Chem. Soc.*, **35**, 931 (1913).

(5) D. F. Stedman, *Trans. Faraday Soc.*, **24**, 289 (1928).

(6) W. J. Heideger and M. Boudart, *Chem. Eng. Sci.*, **17**, 1 (1962).

(7) A. F. Gallagher and J. Hibbert, *J. Amer. Chem. Soc.*, **59**, 2523 (1937).

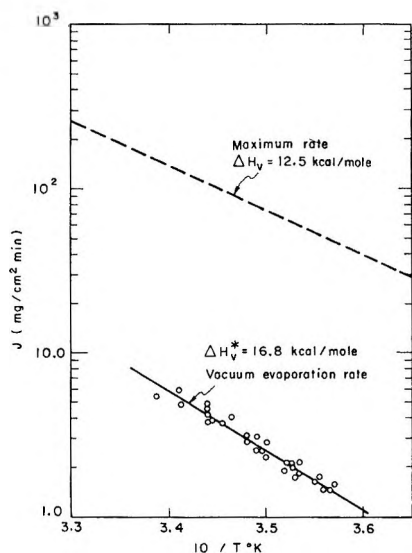


Figure 2. Key: —, vacuum vaporization rate of diethylene glycol; ---, maximum rate.⁷

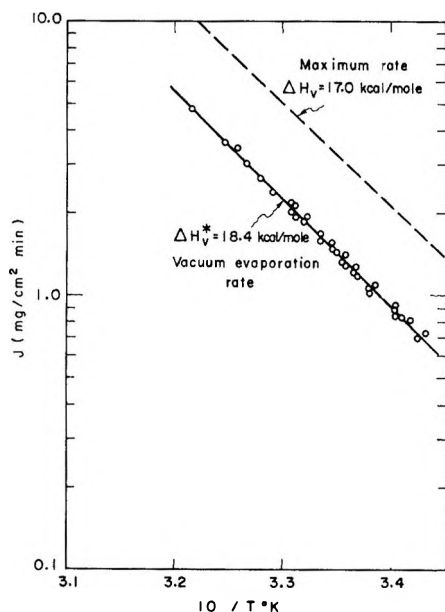


Figure 3. Key: —, vacuum vaporization rate of triethylene glycol; ---, maximum rate.⁷

librium heats of vaporization, ΔH_v , and the experimentally determined activation enthalpies, ΔH_v^* for all three liquids are summarized in Table I, along with $\alpha_v(300^\circ\text{K})$, the ratio of the observed vacuum evaporation rate to maximum rate for each of the liquids at 300°K . It should be noted that α_v is not constant throughout the studied temperature range due to the difference in ΔH_v and ΔH_v^* .

Discussion

In the three organic liquids studied, the energy binding a molecule to its neighbors at the liquid surface is primarily due to hydrogen bonding and attractive interactions through dispersion forces. Bondi and Simkin⁸

Table I: The Heat of Vaporization, ΔH_v , the Activation Enthalpy of Vaporization, ΔH_v^* , and the Evaporation Coefficient, $\alpha_v(300^\circ\text{K})$, for Glycerol, Diethylene Glycol, and Triethylene Glycol

	ΔH_v , kcal/mol	ΔH_v^* , kcal/mol	$\alpha_v(300^\circ\text{K})$
Glycerol	21.0	17.1	0.34
Diethylene glycol	12.5	16.8	0.05
Triethylene glycol	17.0	18.4	0.46

have devised a method of separating these two major contributions. The interaction energy due to dispersion forces is estimated by the heat of vaporization of a compound in which methyl groups are substituted for the hydroxyl groups. For example the dispersion force contribution for glycerol is taken to be the ΔH_v of 3-methylpentane. The hydrogen bonding contribution is then accounted for using a semiempirical parameter, $\delta(\text{OH})$, the hydrogen bond energy increment per OH group. For the purposes of our analysis we chose $\delta(\text{OH}) = 4.3$ kcal/mol since that is the average reported value of the hydrogen bond energies for alcohols given by Pimentel⁹ and since that value fits the data well. The predicted enthalpies of vaporization with varying hydrogen bonding contributions (assuming the additivity of hydrogen bond energies) are shown in Table II along with the experimental enthalpies and activation enthalpies of vaporization. The homologous compounds used to estimate the dispersion force contribution to ΔH_v were, for glycerol, 3-methylpentane, for diethylene glycol, dipropyl ether, and for triethylene glycol, dipropoxyethane. The heats of vaporization of 3-methylpentane and dipropyl ether are given by Jordan.¹⁰ Unfortunately we could find no reliable data for dipropoxyethane, but judging by the variations in heats of vaporization of similar compounds we can be reasonably confident that its heat of vaporization is

Table II: Comparison of the Enthalpies and Activation Enthalpies of Vaporization with the Enthalpies of Vaporization Calculated by Adding Different Hydrogen Bond Contributions to the Enthalpy of Vaporization of the Homologous Molecules ΔH_H

	ΔH_H	$\Delta H_H + \delta(\text{OH})$	$\Delta H_H + 2\delta(\text{OH})$	$\Delta H_H + 3\delta(\text{OH})$	ΔH_v	ΔH_v^*
Glycerol	8.0	12.3	16.6	20.9	21.0	17.1
Diethylene glycol	8.7	13.0	17.3	...	12.5	16.8
Triethylene glycol	>8.7	>13.0	>17.3	...	17.0	18.4

(8) A. Bondi and P. J. Simkin, *AIChE J.*, **3**, 473 (1957).

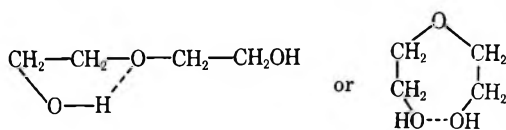
(9) G. C. Pimentel and A. L. McClellan, "The Hydrogen Bond," W. H. Freeman, San Francisco, Calif., 1960.

(10) T. E. Jordan, "Vapor Pressures of Organic Compounds," Interscience, New York, N. Y., 1954.

greater than that of dipropyl ether by no more than 1–2 kcal/mol.

Inspection of Table II reveals that the three liquids studied have vaporization energy requirements that are distinctly different. For glycerol, which exhibits the strongest total hydrogen bonding, $\Delta H_v^* < \Delta H_v$. Thus the activation enthalpy of vaporization is less than the total enthalpy of vaporization. It is apparent from Table II that the enthalpy of vaporization reflects the breaking of three hydrogen bonds. It is also apparent that the activation enthalpy corresponds to the breaking of only two hydrogen bonds. It is assumed that the molecules vaporize as monomers.

For the vaporization of diethylene glycol $\Delta H_v^* > \Delta H_v$. There is strong experimental evidence that this molecule exists in a ringlike form caused by internal hydrogen bonding.



Its enthalpy of vaporization $\Delta H_v = 12.5$ kcal/mol is appreciably smaller than that for ethylene glycol (17.0 kcal/mol).⁷ Similarly the entropy of vaporization at the boiling point indicates weaker association in liquid diethylene glycol ($\Delta S_v \approx 24.14$ e.u.)⁷ than in liquid ethylene glycol ($\Delta S_v \approx 29.0$ e.u.)⁷ or triethylene glycol ($\Delta S_v \approx 30.9$ e.u.)⁷ Thus vaporization near equilibrium is likely to require the breaking of only one hydrogen bond per molecule, in addition to overcoming the attractive dispersion forces between the molecules in the liquid.

The activation enthalpy of vaporization, however, indicates a much greater energy requirement (16.8 kcal/mol) for breaking the molecule away at the vaporizing surface. This larger energy requirement would indicate that two hydrogen bonds must be broken before the molecule could vaporize into vacuum.

For triethylene glycol ($\text{CH}_2\text{OHCH}_2\text{OCH}_2\text{CH}_2\text{OCH}_2\text{CH}_2\text{OH}$) the activation enthalpy of vaporization is only slightly larger (18.4 kcal/mol) than the heat of vaporization (>17.0 kcal/mol).⁷ Also this liquid has a large evaporation coefficient. The breaking of two hydrogen bonds is clearly necessary for vaporization to occur, both in equilibrium and in vacuum. The less than unity evaporation coefficient indicates that although the energetics of vaporization far from equilibrium are not much different from the equilibrium case, the surface concentration of molecules that may vaporize is less than their surface concentration at equilibrium. Since the presence of minute impurities at the vaporizing surface that could block the vaporization cannot be ruled out, a more detailed analysis of this effect would not be useful.

Studies of the vaporization of ice single crystals¹¹ have revealed that the breaking of one hydrogen bond

can be a rate limiting step in the sequence of reaction steps leading to the vaporization of water molecules. At low temperatures ($\leq -80^\circ$), $\Delta H_v^* \approx \Delta H_v = 12.2$ kcal/mol and $\alpha_v = 1$. This value reflects the energy necessary to break two hydrogen bonds. However, above -45° ΔH_v^* approaches the values of $1/2\Delta H_v$ and $\alpha_v \ll 1$, reflecting the breaking of only one hydrogen bond. A typical log rate *vs.* $1/T$ curve for the vacuum vaporization of ice is shown in Figure 4. It appears

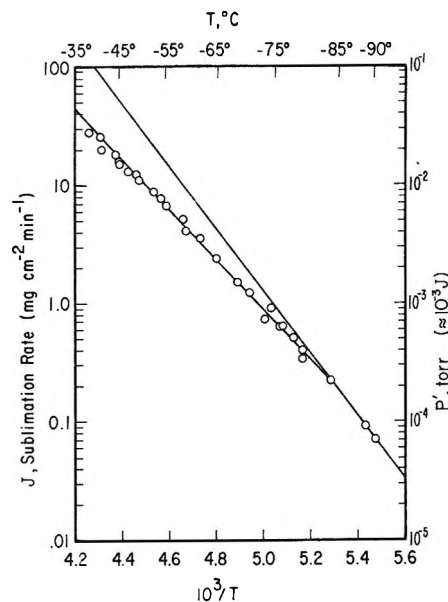


Figure 4. Vacuum vaporization rate and maximum vaporization rate of ice.

that ice at equilibrium with the vapor has a surface population of a highly mobile species, thought to be water molecules hydrogen bonded to only one nearest neighbor. These molecules are the source of vapor flux leaving the surface. At sufficiently low temperatures the vacuum vaporization rate is low enough so as not to significantly alter the equilibrium surface population. However, sublimation at high temperatures depletes this population and the rate limiting step in the vaporization changes from the desorption of the mobile water molecules at low temperatures, to their *formation* at high temperatures.

From these studies it appears that the breaking of one or more hydrogen bonds can be a rate determining step in the vaporization of hydrogen bonded liquids. This effect is likely to be more pronounced for smaller molecules where the proportion of hydrogen-bonding groups is large (ice, glycerol, diethylene glycol). For longer carbon chain organic molecules (*e.g.*, triethylene glycol) the activation enthalpy of vaporization may not be markedly different from the enthalpy of vaporization, as these experimental data suggest. Their evaporation rates may be reasonably approximated by the

(11) J. G. Davy and G. A. Somorjai, *J. Chem. Phys.*, **55**, 3624 (1971).

Langmuir equation assuming an evaporation coefficient near unity.

Acknowledgment. This work was performed under the auspices of the U. S. Atomic Energy Commission.

A Comparison of Stabilization Energy and Resonance Energy as a Measure of the Delocalization Energy in Free Radicals^{1a}

by A. S. Rodgers,* M. C. R. Wu,^{1b} and L. Kuitu

Thermodynamics Research Center, Department of Chemistry, Texas A & M University, College Station, Texas 77840 (Received August 30, 1971)

Publication costs assisted by the Robert A. Welch Foundation

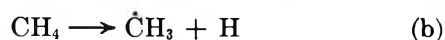
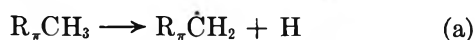
There are, in the literature, two measures of the π -delocalization energy for free radicals: the resonance energy, RE° , introduced by Szwarc² and defined as $RE^\circ = \Delta H_b^\circ - \Delta H_a^\circ$, and the stabilization energy, SE° , introduced by Benson⁵ and defined as $SE^\circ = \Delta H_c^\circ - \Delta H_a^\circ$.



In reactions a and c, \dot{R}_π represents a π -delocalized radical and \dot{R}_s represents the analogous, hydrogen-saturated radical. It is evident that these two definitions will yield different values for the delocalization energy of the same radical as they use different models for the localized radical. It is reasonable to expect that the delocalization energy should be a property of the radical and not depend on the particular bond that is broken. As a result, both definitions have been generalized to include dissociation reactions of the R-X bond where X is any atom or group and have been tested for consistency. It was found that only the stabilization energy of Benson was properly invariant to changes in the bond being broken. On this basis it was concluded that the stabilization energy is the preferred measure of the delocalization energy in free radicals.

In 1948, Szwarc² studied the pyrolysis of toluene and deduced a value of 77.5 kcal mol⁻¹ for the bond dissociation energy of the primary C-H bond. He noted that this was 24.5 kcal mol⁻¹ less than the then accepted value for the C-H bond dissociation energy (BDE) in methane and attributed this difference to the resonance energy of the benzyl radical. While these numbers have changed with time, the definition of resonance energy for delocalized radicals introduced by him has persisted.³ If one considers the example of a delocalized radical obtained from the scission of a primary C-H bond,⁴ as in benzyl and allyl radicals, then the resonance energy, RE° , is given as (298.15 K is implied unless otherwise stated)

$$RE^\circ(R_\pi\dot{C}H_2) = \Delta H_b^\circ - \Delta H_a^\circ \quad (1)$$



In 1965, Benson⁵ suggested an alternative definition. Rather than comparing the C-H BDE of the unsat-

urated compound with that of methane, he suggested that it be compared with the analogous C-H BDE in the corresponding fully hydrogenated compound (R_sCH_3). He recognized that such a definition would yield numerical results different from those of Szwarc² so that he suggested the term "stabilization energy" be applied.⁵ Thus, the stabilization energy, SE° , is given by⁶

$$SE^\circ(R_\pi\dot{C}H_2) = \Delta H_c^\circ - \Delta H_a^\circ \quad (2)$$

(1) (a) This work was supported by the Robert A. Welch Foundation. (b) Robert A. Welch Foundation Predoctoral Fellow 1969-1971.

(2) M. Szwarc, *J. Chem. Phys.*, **16**, 128 (1948).

(3) See, for example, R. T. Morrison and R. N. Boyd, "Organic Chemistry," 2nd ed, Allyn and Bacon Inc., Boston, Mass., 1966, p 390.

(4) While we shall consider this particular example, the results are readily generalized to radicals derived from the scission of secondary and tertiary bonds.

(5) S. W. Benson, *J. Chem. Educ.*, **42**, 510 (1965).

(6) Corrections to eq 2 for changes in strain and resonance energies may be necessary in particular cases.

Table I: Dissociation Enthalpies for the C-X Bond at 298 K in kcal mol⁻¹

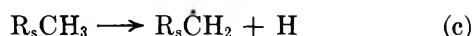
X	C ₆ H ₅ CH ₂ X	CH ₂ =CHCH ₂ X	<i>trans</i> -CH ₃ CH=CHCH ₂ X	CH ₃ X	C ₂ H ₅ X
H ^a	85.0 ^{b,c}	88.6 ^c	85.2 ^c	104.0 ^{b,c}	98.0 ^{b,c}
OH ^a	78.2 ^{e,f}	82.3 ^e	...	91.4 ^{e,f}	91.1 ^e
CH ₃	71.8 ^d	75.4 ^d	72.0 ^d	88.2 ^d	84.5 ^d
C ₂ H ₅	68.7 ^d	72.1 ^d	68.7 ^d	84.7 ^d	81.5 ^d
(CH ₃) ₂ CH ^g	68.1 ^f	71.2 ^{d,f}	...	84.3 ^d	80.7 ^{d,f}
Br ^a	54.7 ^f	57.2 ^f	...	69.8 ^{e,f}	67.6 ^{e,f}
I ^a	40.0 ^e	43.9 ^h	...	56.2 ^e	53.2 ^{e,f}

^a ΔH_f° (X, g, 298 K), ref 12. ^b Reference 7; these data and ΔH_f° (RH, g, 298 K) from ref 13 determine ΔH_f° (R, g, 298 K). ^c Reference 8; these data and ΔH_f° (RH, g, 298 K) from ref 13 determine ΔH_f° (R, g, 298 K). ^d ΔH_f° (RX, g, 298 K), ref 13. ^e ΔH_f° (RX, g, 298 K), ref 14. ^f ΔH_f° (RX, g, 298 K), ref 15. ^g ΔH_f° (R, g, 298 K), ref 8. ^h ΔH_f° (RX, g, 298 K), ref 16.

Table II: Resonance and Stabilization Energies at 298 K for the Benzyl, Allyl, and Methallyl Radicals (Eq 3 and 4a) for Various Groups

X	Benzyl ^a		Allyl ^a		Methallyl ^a	
	RE ^o , kcal mol ⁻¹	SE ^o , kcal mol ⁻¹	RE ^o , kcal mol ⁻¹	SE ^o , kcal mol ⁻¹	RE ^o , kcal mol ⁻¹	SE ^o , kcal mol ⁻¹
H	19.0	13.0	15.4	9.4	18.8	12.8
OH	13.2	12.9	9.1	8.8
CH ₃	16.4	12.7	12.8	9.1	16.2	12.5
C ₂ H ₅	16.0	12.8	12.6	9.4	16.0	12.8
(CH ₃) ₂ CH	16.2	12.6	13.1	9.5
Br	14.1	12.9	12.6	10.4
I	16.2	13.2	12.4	9.3

^a Based on data of Table I.

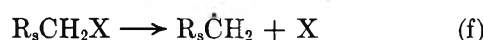
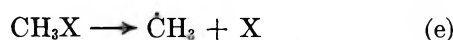
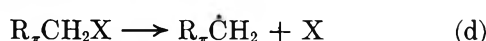


The evaluation of eq 2 is greatly simplified by the fact that ΔH_c° is not significantly affected by changes in the alkyl moiety R_s. The data^{7,8} show that $\Delta H_c^\circ = 98 \pm 1$ kcal mol⁻¹ for R_s equal to methyl, ethyl, *n*-propyl, isopropyl, and *tert*-butyl. As $\Delta H_b^\circ = 104 \pm 1$ kcal mol⁻¹,^{7,8} these two measures of the delocalization energy of a radical differ by 6 kcal mol⁻¹. One naturally asks the question "Is one to be preferred over the other?" The answer to this is "yes," and it is based on considerations of transferability and utility.

One can reasonably expect the delocalization energy of a radical to be a property of that radical and, therefore, its value should not depend upon the particular bond that is broken. Both the definitions of Szwarc and of Benson can be generalized to include dissociation reactions involving the C-X bond where X is any atom or group. Thus, eq 1 and 2 become eq 3 and 4.

$$RE^\circ(R_\pi\dot{\text{C}}\text{H}_2) = \Delta H_e^\circ - \Delta H_d^\circ \quad (3)$$

$$SE^\circ(R_\pi\dot{\text{C}}\text{H}_2) = \Delta H_f^\circ - \Delta H_d^\circ \quad (4)$$



Again, the evaluation of eq 4 is facilitated by the fact that ΔH_f° is nominally independent of R_s to the extent

that group additivity applies to compounds^{9,10} and radicals.¹¹ Thus, reaction f may be replaced by g and eq 4 becomes eq 4a.



$$SE^\circ(R_\pi\dot{\text{C}}\text{H}_2) = \Delta H_g^\circ - \Delta H_d^\circ \quad (4a)$$

The resonance and stabilization energies of the benzyl, allyl, and methallyl radicals are calculated according to eq 3 and 4a using the dissociation enthalpies of Table I.¹²⁻¹⁶ The results are summarized in Table

(7) J. A. Kerr, *Chem. Rev.*, **66**, 494 (1966).

(8) D. M. Golden and S. W. Benson, *ibid.*, **69**, 125 (1969).

(9) S. W. Benson and J. H. Buss, *J. Chem. Phys.*, **29**, 546 (1958).

(10) S. W. Benson, F. R. Cruickshank, D. M. Golden, G. R. Haugen, H. E. O'Neal, A. S. Rodgers, R. Shaw, and R. Walsh, *Chem. Rev.*, **69**, 279 (1969).

(11) H. E. O'Neal and S. W. Benson, *Int. J. Chem. Kinet.*, **1**, 221 (1969).

(12) D. R. Stull, Ed., "JANAF Thermochemical Tables," The Thermal Research Laboratories, Dow Chemical Co., Midland, Mich., 1965.

(13) Selected Values of Properties of Hydrocarbons and Related Compounds," API Research Project 44, Thermodynamics Research Center, Texas A & M University, College Station, Texas, 1967.

(14) D. R. Stull, E. F. Westrum, Jr., and G. C. Sinke, "The Chemical Thermodynamics of Organic Compounds," Wiley, New York, N. Y., 1969.

(15) J. D. Cox and G. Pilcher, "Thermochemistry of Organic and Organometallic Compounds," Academic Press, New York, N. Y., 1970.

(16) A. S. Rodgers, D. M. Golden, and S. W. Benson, *J. Amer. Chem. Soc.*, **88**, 3194 (1966).

II, from which it is seen that only the stabilization energy of Benson is properly invariant to changes in the character of the bond being broken. The transferability of the stabilization energy is further supported by calculations for the benzyl radical with the following additional groups and their corresponding stabilization energies in kilocalories per mole: $-\text{COCH}_3$, 14.7;¹⁵ $-\text{SH}$, 13.7;¹⁰ $-\text{SCH}_3$, 13.4;¹⁰ $-\text{SC}_2\text{H}_5$, 13.2;¹⁰ $-\text{CH}_2\text{C}_6\text{H}_5$, 11.3;¹⁵ and $-\text{C}_6\text{H}_5$, 10.5.¹⁵

The utility of the stabilization energy results from its transferability. Equation 4a may be expanded to

$$SE^\circ(\text{R}_\pi\dot{\text{C}}\text{H}_2) = \Delta H_f^\circ(\text{C}_2\text{H}_5\cdot, \text{g}, 298 \text{ K}) - \Delta H_f^\circ(\text{R}_\pi\dot{\text{C}}\text{H}_2, \text{g}, 298 \text{ K}) + \Delta H_f^\circ(\text{R}_\pi\text{CH}_2\text{X}, \text{g}, 298 \text{ K}) - \Delta H_f^\circ(\text{C}_2\text{H}_5\text{X}, \text{g}, 298 \text{ K}) \quad (5)$$

Once the stabilization energy has been established by bond dissociation energy measurements for one X (usually H), then eq 5 may be used to estimate values of $H_f^\circ(\text{R}_\pi\text{CH}_2\text{X}, \text{g}, 298 \text{ K})$ for other groups X. For the benzyl radical, BDE measurements on toluene and ethane have established these quantities so that

$$\Delta H_f^\circ(\text{C}_6\text{H}_5\text{CH}_2\text{X}, \text{g}, 298 \text{ K}) = \Delta H_f^\circ(\text{C}_2\text{H}_5\text{X}, \text{g}, 298 \text{ K}) + 32.2 \quad (6)$$

This equation should yield values of $\Delta H_f^\circ(\text{C}_6\text{H}_5\text{CH}_2\text{X}, \text{g}, 298 \text{ K})$ good to within 1–2 kcal mol⁻¹. This was, indeed, the case for nine of the above ten benzylic compounds. However, eq 5, and therefore eq 6, are subject to correction if (a) there exist steric interactions in $\text{R}_\pi\text{CH}_2\text{X}$ that do not exist in $\text{C}_2\text{H}_5\text{X}$ or (b) there exist electronic interactions between the groups R_π and X for which there are no counterparts in $\text{C}_2\text{H}_5\text{X}$. Indeed,

there is evidence from group additivity¹⁰ and uv spectra^{17,18} that suggest case b above may be the cause for the low values of $SE^\circ(\text{C}_6\text{H}_5\dot{\text{C}}\text{H}_2)$ from 1,2-diphenylethane and diphenylmethane (*i.e.*, X = $-\text{CH}_2\text{C}_6\text{H}_5$ and $-\text{C}_6\text{H}_5$).

With due consideration given to a and b above, the transferability of stabilization energies permits the estimation of the enthalpy of formation for a large class of compounds from just a few, critical measurements. Equation 6 is valid for $\text{C}_6\text{H}_5\text{CH}_2\text{X}$ compounds, eq 7 for $\text{CH}_2=\text{CHCH}_2\text{X}$ compounds, and eq 8 for *trans*- $\text{CH}_3\text{CH}=\text{CHCH}_2\text{X}$ compounds

$$\Delta H_f^\circ(\text{CH}_2=\text{CHCH}_2\text{X}, \text{g}, 298 \text{ K}) = \Delta H_f^\circ(\text{C}_2\text{H}_5\text{X}, \text{g}, 298 \text{ K}) + 25.1 \quad (7)$$

$$\Delta H_f^\circ(\textit{trans}\text{-CH}_3\text{CH}=\text{CHCH}_2\text{X}, \text{g}, 298 \text{ K}) = \Delta H_f^\circ(\text{C}_2\text{H}_5\text{X}, \text{g}, 298 \text{ K}) + 17.2 \quad (8)$$

Similar equations may be derived for delocalized radicals arising from the scission of a secondary C–X bond in which the hydrogenated reference compound is $\text{CH}_3\text{CHXCH}_3$.

In conclusion, two measures of the delocalization energy for radicals have been compared against the standards of transferability and utility, and it has been found that the stabilization energy, as opposed to the resonance energy originally introduced by Szwarc, is the preferable measure of the delocalization energy in radicals.

(17) D. S. McClure, *Can. J. Chem.*, **36**, 59 (1958).

(18) E. M. Layton, Jr., *J. Mol. Spectrosc.*, **5**, 181 (1960).

Thermodynamic Stability of Perylene-Iodine Charge-Transfer Complexes from Measurements of Iodine Vapor Absorption¹

by S. Aronson,* B. Strumeyer, and R. Goodman

Brooklyn College, City University of New York, Brooklyn, New York (Received August 9, 1971)

Publication costs assisted by the Petroleum Research Fund

The absorption of iodine vapor by solid perylene at temperatures of 60–120° was investigated over a range of iodine vapor pressures. The formation of two compounds, $P(I_2)_{1.50}$ and $P(I_2)_{2.90}$, was observed. Free energies, enthalpies, and entropies of formation were estimated from the data. The two compounds were found to be very similar in their thermodynamic stability.

Perylene, $C_{20}H_{12}$, a five-ring aromatic hydrocarbon, reacts with gaseous iodine or iodine in solution to form charge-transfer complexes. In a recent study of this reaction, Cobb and Wallis² measured the absorption and desorption of iodine vapor by solid perylene at 20–70° by following weight changes on a quartz spring balance. Their data show evidence for the existence of the solid compounds $P_3(I_2)_4$, $P_7(I_2)_{10}$, $P_2(I_2)_3$, $P(I_2)_2$, and $P_7(I_2)_{20}$ where the symbol, P, refers to perylene. Cobb and Wallis related their data to the results of previous investigations on the perylene-iodine system.

There has been much discussion about the nature of charge-transfer complexes.^{3–5} Most experimental work on these systems has been done in solution where a body of thermodynamic data has been accumulated.^{3–5} Little thermodynamic data are available on vapor-phase charge-transfer complexes^{3–5} and on solid-state charge-transfer complexes.⁶

In the present study, the absorption of iodine by solid perylene at 60–120° was investigated over a range of iodine vapor pressures. The higher temperature region used in this study as compared to that of Cobb and Wallis² permitted the system to come closer to thermodynamically reversible conditions. The results indicate that only two phases are present in the perylene-iodine system. The free energies, enthalpies, and entropies of formation of these solid phases are estimated from the data.

Experimental Section

Perylene, $C_{20}H_{12}$ (purity 99%), was obtained from the Aldrich Chemical Co. of Milwaukee, Wis. Reagent Grade iodine was obtained from the Fisher Scientific Co. of Fairlawn, N. J.

The apparatus used to study the absorption of iodine by perylene was similar to that of Cobb and Wallis and is shown in Figure 1. The iodine was distilled, *in vacuo*, into the tube at the bottom of the diagram from a reservoir not shown. A weighed amount of perylene, about 10 mg, was placed in the Pyrex bucket which was

suspended by a hook from a fine Pyrex glass wire. The wire was attached to a quartz spring. The extension of the spring was 0.70 mm/mg. A cross-hair attached to the spring below the spiral coil was used for measuring height. A mirror and vertical centimeter rule were placed behind the spring. Parallax errors were avoided by aligning the cross-hair and its image in the mirror adjacent to the centimeter rule. The position of the cross-hair could be read to ± 0.1 mm.

The perylene sample was heated by a tube-furnace which surrounded the sample. The temperature was measured by a chromel-alumel thermocouple connected to a Thermo Electric 400 temperature controller obtained from the Thermo Electric Co. of Saddle Brook, N. J. The iodine tube was surrounded by a water bath which was heated and controlled by a Bronwill constant temperature unit obtained from Bronwill Scientific Co. of Rochester, N. Y. Heating tapes were wound around the rest of the system and were heated to temperatures of 140–150° to avoid condensation of iodine. The temperatures produced by these tapes were monitored with chromel-alumel thermocouples embedded between the tape and the glass tube.

The procedure for initiating absorption measurements was as follows: The perylene sample was placed in the basket and was attached to the spring. The iodine had been previously distilled into its reservoir. The system was evacuated with all parts at room temperature and was then isolated from the vacuum pump. Under these conditions, the perylene absorbed a sig-

(1) Acknowledgment is made to the donors of The Petroleum Research Fund, administered by the American Chemical Society, for support of this research.

(2) C. M. Cobb and E. B. Wallis, *J. Phys. Chem.*, **72**, 2986 (1968).

(3) R. S. Mulliken and W. B. Person, "Molecular Complexes," Wiley, New York, N. Y., 1969.

(4) R. Foster, "Organic Charge-Transfer Complexes," Academic Press, London, 1969.

(5) L. J. Andrews and R. M. Keefer, "Molecular Complexes in Organic Chemistry," Holden-Day, San Francisco, Calif., 1964.

(6) W. E. Byrd, *Inorg. Chem.*, **1**, 762 (1962).

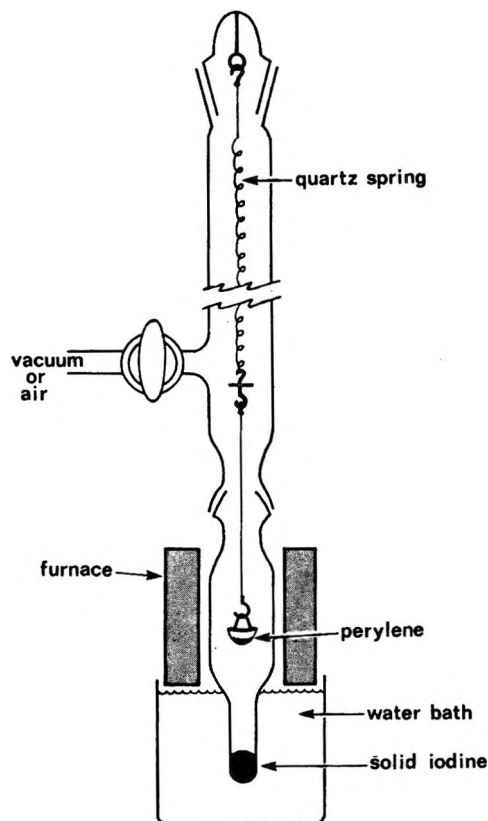


Figure 1. Apparatus for studying the absorption and desorption of iodine by perylene.

nificant amount of iodine in a few minutes. The sections of the system not containing the perylene or the iodine were heated to 140–150°. The perylene sample was then heated to the reaction temperature, between 60 and 120°. This resulted in the complete removal of iodine from the perylene. The pressure of the iodine vapor was then adjusted by regulating the temperature of the water bath.⁷ Many absorption and desorption runs could be made on the same perylene sample.

Results and Discussion

A number of experiments were first performed to determine which phases occur in the perylene–iodine system. Cobb and Wallis reported the existence of $P(I_2)_{1.33}$, $P(I_2)_{1.43}$, $P(I_2)_{1.50}$, and $P(I_2)_2$ and $P(I_2)_{2.86}$. Absorption and desorption data were obtained by us at a number of sample temperatures between 60 and 120°. Two of the plots are shown in Figures 2 and 3 for temperatures of 60 and 100°. It is observed that two plateaus occur, corresponding approximately to the compositions $P(I_2)_{1.50}$ and $P(I_2)_{2.90}$. The experimental error in determining the composition from the quartz spring height changes is estimated to be within $\pm 2\%$. The upper plateau occurred at a composition of $P(I_2)_{2.90}$ for all the sample temperatures studied. The composition at the first plateau was variable. For a sample temperature of 100°, the composition at the plateau

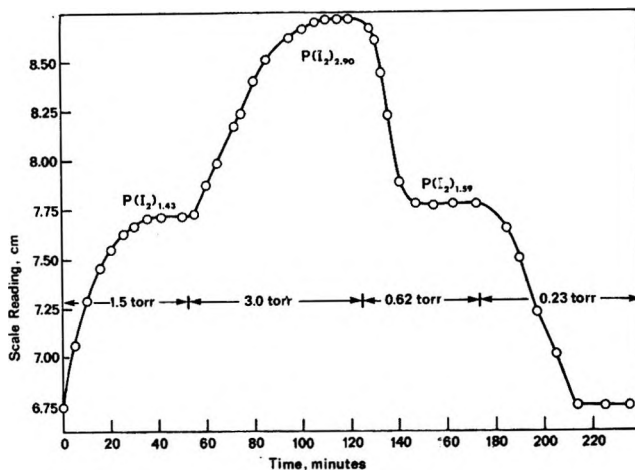


Figure 2. Formation and decomposition of perylene–iodine complexes at 60.0° at various iodine vapor pressures.

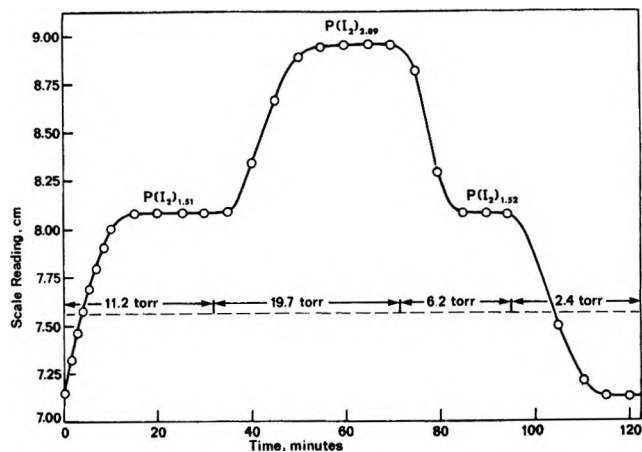


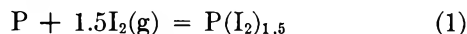
Figure 3. Formation and decomposition of perylene–iodine complexes at 100.0° at various iodine vapor pressures.

was close to $P(I_2)_{1.50}$ on absorption and desorption. At 60°, the composition of the plateau on absorption was $P(I_2)_{1.43}$ and that on desorption, $P(I_2)_{1.59}$. At 80° (not shown) intermediate values of $P(I_2)_{1.46}$ and $P(I_2)_{1.55}$ were obtained. It is our opinion that this variation in composition does *not* indicate that a number of compounds exist in this system in the range of $P(I_2)_{1.4}$ to $P(I_2)_{1.6}$. We are dealing with a nonequilibrium phenomenon involving hysteresis. This phenomenon may be related either to some nonequilibrium process involving gaseous iodine on the surface of the perylene particles or to the irregular crystal structure of our perylene powder as evidenced by the poor X-ray diffraction patterns which we obtained. In any event, it seems reasonable to assume that only one phase at the approximate composition $P(I_2)_{1.50}$ exists. The phases $P(I_2)_{1.43}$ and $P(I_2)_{1.50}$ reported by Cobb and Wallis very likely correspond to the single phase in the vicinity of

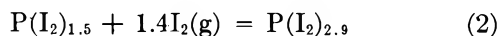
(7) Data relating the iodine vapor pressure to the temperature of solid iodine were obtained from "The Handbook of Chemistry and Physics," 51st ed, The Cleveland Rubber Co., Cleveland, Ohio, 1971, p D-168.

$P(I_2)_{1.50}$ observed by us. The phase $P(I_2)_{2.86}$ of Cobb and Wallis and our phase $P(I_2)_{2.90}$ are probably the same. The data presented by Cobb and Wallis which account for the existence of $P(I_2)_{1.33}$ and $P(I_2)_{2.00}$ are meager and may be attributed either to hysteretic effects or to experimental errors such as cold spots in their system leading to erroneous measurements of iodine vapor pressure.

The formation of the two complexes may be represented by the equations



and



where P refers to perylene. Assuming equilibrium conditions to apply, the relationships between free energy of reaction, per mole of I_2 , and iodine vapor pressure are

$$\Delta G_1^\circ = RT \ln p_1 \quad (3)$$

and

$$\Delta G_2^\circ = RT \ln p_2 \quad (4)$$

where eq 3 and 4 refer to reactions 1 and 2, respectively, and p_1 and p_2 are the vapor pressures of iodine in equilibrium with the solid phases in eq 1 and 2 (assuming ideal gas behavior).

Attempts were made to determine equilibrium vapor pressures experimentally. Threshold pressures for absorption and for desorption were measured in the following manner. First the general ranges of pressures at which absorption and desorption occurred at various sample temperatures were determined. More careful measurements were then made. At a particular sample temperature, the temperature of the iodine reservoir was raised in increments of 2–3° until absorption began. Some typical data for absorption threshold pressures for the formation of $P(I_2)_{1.50}$ are shown in Figures 4 and 5. It is observed that the transition from no absorption to rapid absorption occurs over a fairly narrow range of iodine pressures. Data on threshold pressures for absorption similar to those shown in Figures 4 and 5 were obtained at all sample temperatures and for the formation of both the phases $P(I_2)_{1.50}$ and $P(I_2)_{2.90}$. Desorption threshold pressures were also obtained by lowering the temperature of the iodine reservoir in increments of 2–3°. The threshold pressures for desorption were not as reproducible as those for absorption.

Threshold pressures for formation and decomposition of the complexes are shown in Table I for sample temperatures of 80 and 100°. Since the vapor pressures for desorption were somewhat variable, we list the minimum threshold pressure observed at each temperature. We note that the vapor pressure for absorption is not identical with the vapor pressure for desorption. The formation pressures were generally 2–3

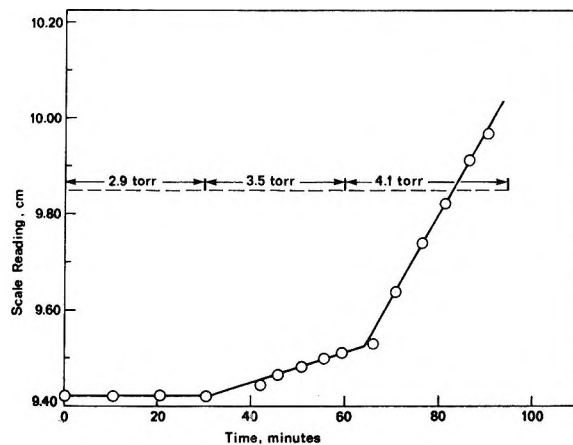


Figure 4. Determination of the threshold pressure for the formation of $P(I_2)_{1.5}$ with perylene at 100.0°.

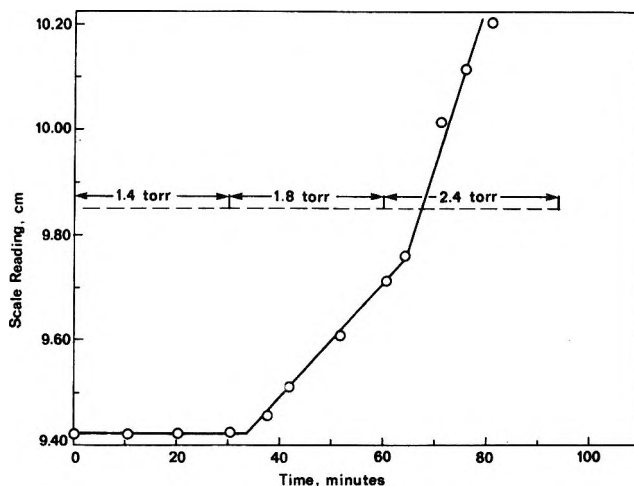


Figure 5. Determination of the threshold pressure for the formation of $P(I_2)_{1.5}$ with perylene at 80.0°.

times higher than the decomposition pressures. Since we do not have a single value of the vapor pressure of iodine for formation and decomposition of a particular compound we cannot calculate absolute values of thermodynamic parameters. We can, however, obtain ranges of values for the free energies of reactions corresponding to eq 1 and 2 which are quite narrow. At 80°, the standard free energy of formation of $P(I_2)_{1.50}$ (using iodine vapor at 1 atm pressure as the standard state) is between -4.3 and -5.1 kcal/mol of I_2 . The standard free energy of formation of $P(I_2)_{2.90}$ from $P(I_2)_{1.50}$ and iodine vapor is between -3.7 and -4.4 kcal/mol of I_2 . The free energies of formation and, hence, the stabilities of the compounds $P(I_2)_{1.50}$ and $P(I_2)_{2.90}$ are, thus, very similar. If the standard free energy of formation of $P(I_2)_{1.50}$ were 1 kcal less negative, it would not exist.

Estimates of the heats and entropies of formation of the compounds can be obtained from the variation of the free energy with temperature. It was most expedient to utilize the data obtained from the threshold

Table I: Threshold Pressures for Formation and Decomposition of Perylene-Iodine Compounds

Sample temp, °C	Compound	Formation pressure, Torr	Minimum decomposition pressure, Torr	Free energy of formation, ΔG° , kcal/mol I_2
80.0	$P(I_2)_{1.50}$	1.8	0.6	4.3-5.1
80.0	$P(I_2)_{2.90}$	3.8	1.4	3.7-4.4
100.0	$P(I_2)_{1.50}$	3.5	1.6	4.0-4.6
100.0	$P(I_2)_{2.90}$	11.4	4.2	3.3-3.9

pressures for absorption of iodine. These pressures were quite reproducible at all temperatures. A plot of the logarithm of the formation threshold pressure *vs.* reciprocal absolute temperature is shown in Figure 6 for $P(I_2)_{1.50}$ and $P(I_2)_{2.90}$ formation. From the data in Figure 6 we have calculated values for the heats and entropies of formation of the two compounds. These are shown in Table II. These values will be strictly accurate only if the threshold pressures for formation represent the true iodine vapor pressures in equilibrium with the compounds. Even if this is not the case, however, the error in these values is not large. Calculations based on free energy values averaged for absorption and desorption obtained from data including those in Table I gave similar results to those shown in Table II. We estimate on the basis of experimental factors and nonequilibrium considerations that the errors in the calculated free energies of formation of $P(I_2)_{1.5}$ and $P(I_2)_{2.9}$ at any temperature in the range investigated are within $+0.5$ kcal/mol of I_2 and -1.0 kcal/mol of I_2 . For convenience, we will assume an error of ± 1.0 kcal/mol of I_2 . The estimated errors in the enthalpies of formation of the two compounds, based on a least-square analysis of the data for the temperature dependence of the formation threshold pressures, are within ± 1.0 kcal/mol of I_2 . The errors in entropies of formation of the compounds are then estimated to be within ± 3 cal/°K-mol of I_2 . It should be noted that the errors for the two compounds are coordinated. For example, if the true value for the entropy of formation of $P(I_2)_{1.5}$ is somewhat higher than that listed in Table II,

Table II: Free Energies, Enthalpies, and Entropies of Formation of Perylene-Iodine Compounds Calculated from Threshold Pressures for Formation of the Compounds

Compound	$-\Delta G^\circ_{300^\circ K}$, kcal/mol of I_2^a	$-\Delta H^\circ$, kcal/mol of I_2	$-\Delta S^\circ$, cal/(°K mol of I_2)
$P(I_2)_{1.50}$	4.2	10.2	17.1
$P(I_2)_{2.90}^b$	3.6	10.4	19.1
$P(I_2)_{2.90}^c$...	10.3	18.1

^a Iodine vapor at 1 atm pressure considered as the standard state. ^b These values are for the reaction $0.71P(I_2)_{1.50} + I_2 = 0.71P(I_2)_{2.90}$. ^c These values are calculated from the above data for the reaction $0.35P + I_2 = 0.35P(I_2)_{2.90}$.

it is quite likely that the error in the entropy of formation of $P(I_2)_{2.9}$ is in the same direction and of the same magnitude.

We observe in Table II that the heats and entropies of formation of $P(I_2)_{1.50}$ and $P(I_2)_{2.90}$ are similar. It is reasonable that the entropy value for $P(I_2)_{2.90}$ is more negative than that for $P(I_2)_{1.50}$ since the iodine molecules are packed more closely in the former compound.

We conclude from the low (negative) values of the heats of formation that the bonding energies of the complexes are relatively small. There are no relevant data on solid complexes with which to compare the data in Table II. The results are qualitatively consistent with

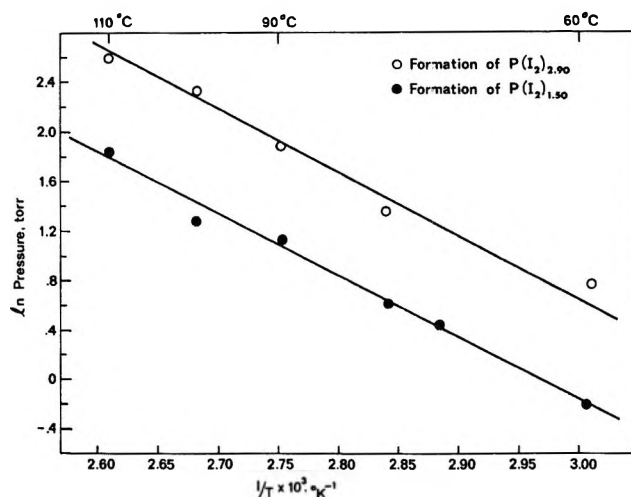


Figure 6. Plot of iodine threshold pressure as a function of the reciprocal of the absolute temperature.

the thermodynamic data obtained on a wide variety of charge transfer complexes in solution and in the gas phase.³⁻⁵ In those cases, heats of formation ranging from -2 to -14 kcal/mol of I_2 and entropies of formation ranging from -3 to -20 cal/(°K mol of I_2) have been observed, with the more negative enthalpy values generally associated with the more negative entropy values.

The large entropy values in Table II may be primarily attributed to the condensation of gaseous iodine in forming the solid complexes. It is interesting to compare the heats and entropies of formation of the complexes with the heats and entropies of condensation of gaseous iodine into liquid and solid iodine. These are, respectively, -10 kcal/mol and -23 cal/(°K mol) for liquid iodine (at 400°K) and -15 kcal/mol and -34 cal/(°K mol) for solid iodine (at 300°K).⁸ Thus, the values for the formation of the complexes are similar to those for the condensation of iodine into the liquid state. This agreement may be fortuitous. However, a similar situation occurs in the case of the alkali metal-

(8) D. R. Stull and G. C. Sinke, *Advan. Chem. Ser.*, No. 18, 107 (1956).

graphite layer compounds. These compounds have features in common with the aromatic charge transfer complexes. In the case of the graphite compounds, the entropies of formation are almost identical with the

entropies of condensation of the gaseous alkali metals into the liquid state.⁹

(9) S. Aronson and F. J. Salzano, *J. Chem. Phys.*, **49**, 434 (1968).

Phase Diagrams of Liquid Crystal Solvents Used in Nuclear

Magnetic Resonance Studies¹

by R. A. Bernheim* and T. A. Shuhler

Whitmore Laboratory, Department of Chemistry, The Pennsylvania State University, University Park, Pennsylvania 16802
(Received September 27, 1971)

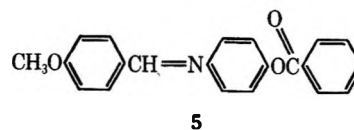
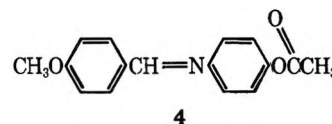
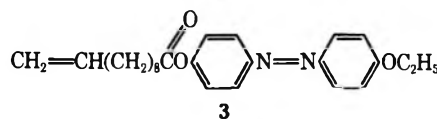
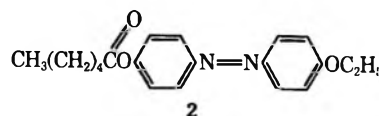
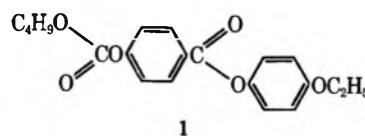
Publication costs assisted by the National Science Foundation

Phase diagrams are determined for a number of liquid crystal solvent mixtures useful as solvents in nuclear magnetic resonance spectroscopy.

In recent years the use of nematic liquid crystal solvents in nuclear magnetic resonance spectroscopy² has made possible a number of experiments that previously were very difficult or impossible to carry out. Molecular geometries,³ absolute signs of indirect spin-spin coupling constants,⁴ nuclear electric quadrupole interactions,⁵ magnetic shielding anisotropies,⁶ anisotropies in the indirect spin-spin interaction,⁵ as well as information concerning the degree and direction of the orientation of the solute molecules can be obtained.

One of the problems associated with nmr studies in liquid crystal solvents arises from the high temperature of the solid-nematic phase transition of most nematic substances. Temperature inhomogeneity and instability during the time required to perform the experiment give rise to spectral line broadening, and gaseous substances must be studied under very high pressures. These problems were greatly alleviated by the discovery of a number of low melting mixtures of nematic substances.⁷ It is of interest to nmr spectroscopists to know the phase transition behavior of these mixtures as a function of relative concentration which is the subject of this note.

The following compounds were used: butyl *p*-(*p*-ethoxyphenoxy-carbonyl)phenyl carbonate (1); (*p*-ethoxyphenylazo)phenyl heptanoate (2); *p*-(*p*-ethoxyphenylazo)phenyl undecylenate (3); *p*-[(*p*-methoxybenzylidene)amino]phenyl acetate (4); and *p*-[(*p*-methoxybenzylidene)amino]phenyl benzoate (5).



(1) This research was supported in part by the National Science Foundation.

(2) A. Saupe and G. Englert, *Phys. Rev. Lett.*, **11**, 462 (1963).

(3) L. C. Snyder and S. Meiboom, *J. Chem. Phys.*, **47**, 1480 (1967).

(4) R. A. Bernheim and B. J. Lavery, *J. Amer. Chem. Soc.*, **89**, 1279 (1967).

(5) J. C. Rowell, W. D. Phillips, L. R. Melby, and M. Panar, *J. Chem. Phys.*, **43**, 3442 (1965).

The compounds were obtained from Eastman Organic Chemicals and were used without further purification. Binary mixtures were prepared by weighing amounts of both components and then melting into the isotropic phase. After the mixture solidified a small part was placed between two clean glass slides and placed in the heating chamber of a microscope equipped with crossed

Occasionally phase separation was observed when compound 1 was present in less than 20 mol %.

The results are given in Table I and Figure 1. It is evident that the solid-nematic transition is lowered in temperature over a rather broad range of composition. In an nmr experiment this transition will generally be lowered further due to the addition of a third component. Coupled with the supercooling nature of the mixtures we conclude that there is considerable latitude in preparing solutions for study.

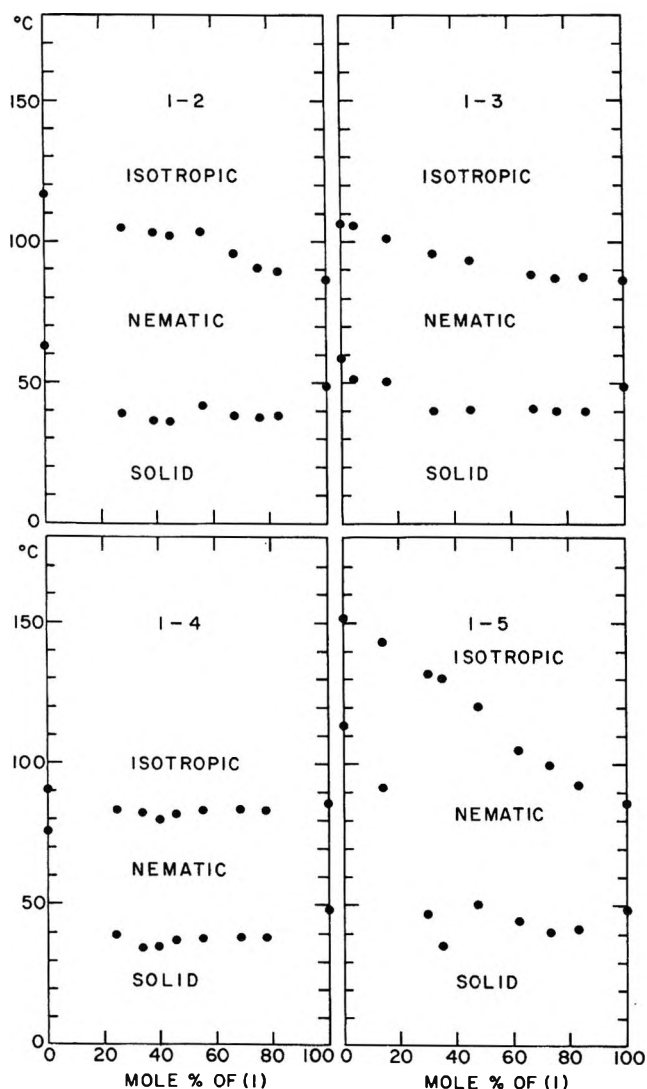


Figure 1. Phase diagrams of the liquid crystal mixtures commonly used as nmr solvents.

polarizing elements.⁸ A calibrated thermometer mounted in the heating block could be used to determine the sample temperature to $\pm 0.2^\circ$. The transition point between the solid and the nematic mesophase was recorded upon warming up through the transition as the mixtures are invariably supercooled upon lowering the temperature through the transition region.

Table I: Transition Temperatures as a Function of Composition for the Liquid Crystal Mixtures

Mol % of I	Transition, $^\circ\text{C}$		Mol % of I	Transition, $^\circ\text{C}$	
	Solid-nematic	Nematic-isotropic		Solid-nematic	Nematic-isotropic
1-2					
0	63.1	116.9	0	58.4	106.0
27.2	39.0	105.0	4.5	51.2	105.7
38.2	36.7	103.2	16.0	50.2	101.0
44.3	36.1	102.0	32.5	39.4	95.5
55.6	41.8	103.5	45.7	40.2	93.0
67.1	38.4	95.5	67.2	40.7	88.2
75.8	37.6	90.3	76.1	39.8	86.7
82.4	38.1	89.5	86.0	39.8	87.5
100	48.7	86.3			
1-4					
0	75.8	90.4	0	113.5	151.4
24.3	38.9	83.6	14.1	91.5	143.5
33.7	34.5	82.6	29.9	46.8	131.8
39.6	35.1	80.3	35.0	35.5	130.1
45.5	37.4	82.1	47.5	50.3	120.3
55.3	38.0	83.7	62.2	44.6	105.1
68.6	38.5	83.9	73.1	40.5	99.4
77.5	38.4	83.5	83.2	41.4	92.3

The properties of liquid crystal mixtures have been examined by numerous workers.⁹ The deviation from linearity of the isotropic-nematic transition temperature vs. composition is usually more marked when the two components differ greatly in molecular size and shape.¹⁰

(6) G. P. Ceasar, C. S. Yannoni, and B. P. Dailey, *J. Chem. Phys.*, **50**, 373 (1969); G. P. Ceasar and B. P. Dailey, *ibid.*, **50**, 4200 (1969); D. N. Silverman and B. P. Dailey, *ibid.*, **51**, 655 (1969); C. S. Yannoni, B. P. Dailey, and G. P. Ceasar, *ibid.*, **54**, 4020 (1971).

(7) H. Spieseke and J. Bellion-Jourdan, *Angew. Chem., Int. Ed. Engl.*, **6**, 450 (1967).

(8) Obtained from the Nagle Co., Rochester, N. Y.

(9) G. W. Gray, "Molecular Structure and the Properties of Liquid Crystals," Academic Press, New York, N. Y., 1962, Chapter 7.

(10) J. S. Dave and M. J. S. Dewar, *J. Chem. Soc.*, 4617 (1954); 4305 (1955).

An X-Ray Diffraction Investigation of the Vanadium-Deuterium System¹

by **Kenneth I. Hardcastle***

Department of Chemistry, San Fernando Valley State College, Northridge, California 91324

and **T. R. P. Gibb, Jr.**

Department of Chemistry, Tufts University, Medford, Massachusetts 02155 (Received May 3, 1971)

Publication costs assisted by San Fernando Valley State College

A partial phase diagram for the vanadium-deuterium system was determined from an X-ray diffraction investigation of vanadium deuterides of overall composition $VD_{0.1}$ to $VD_{1.7}$. The system consists of three primary phases: α , β , and γ . The α , solid solution phase consists of mobile, interstitial deuterium in a body-centered cubic vanadium atom lattice. The β phase is characterized by a body-centered tetragonal metal atom lattice, and the γ phase has a face-centered cubic arrangement of vanadium atoms and presumably has the CaF_2 -type structure. At room temperature the initial solid solution region (α) extends to $VD_{0.1}$. From $VD_{0.1}$ to $VD_{0.43}$ a two-phase region exists, $\alpha + \beta$. Pure β phase exists in the composition range $VD_{0.43}$ to $VD_{0.53}$. Beyond $VD_{0.53}$ to $VD_{0.7}$ the second two-phase region occurs and contains the β phase and α phase—now with a much larger lattice parameter. Pure α phase exists at compositions from $VD_{0.7}$ to $VD_{1.0}$, whereupon the third two-phase region is encountered and consists of the α phase and the γ phase. Vanadium deuterides with compositions between $VD_{0.1}$ and $VD_{1.0}$ were also studied with X-rays at higher and at lower temperatures. Above 130° only the α phase exists, while at lower temperatures two phase modifications were observed. The α' phase, which has an orthorhombic lattice of vanadium atoms, results when samples of overall composition $VD_{0.5}$ to $VD_{0.8}$ are cooled to approximately -70° or below. This distortion of the cubic metal atom lattice results from the "freezing-out" of the previously mobile deuterium atoms. The other phase observed, β' , occurs when samples of overall composition $VD_{0.1}$ to $VD_{0.8}$ are cooled to -25° or below. This phase also has a bcc lattice of vanadium atoms but a_0 decreases approximately 1% and c_0 increases approximately 3%. This is most likely due to additional ordering of the deuterium.

Introduction

During the course of a neutron diffraction investigation of several vanadium deuterides, it was found that the expected analogy to the vanadium-hydrogen system phase diagram² was not entirely valid; therefore, an X-ray powder diffraction study of the vanadium-deuterium system was undertaken. This paper presents the results of that study. The partial phase diagram obtained for the composition range studied, $VD_{0.1}$ to $VD_{1.7}$, is presented in Figure 1.

The vanadium-hydrogen system at room temperature (RT) is characterized by three phases:² α , which consists of hydrogen dissolved in a body-centered cubic vanadium metal lattice; β , a body-centered tetragonal phase (with respect to the vanadium atoms only, and this is true for all results presented in this paper); and γ , a face-centered cubic phase. The major differences exhibited by the vanadium-deuterium system are (1) the existence of a second bcc phase (RT) at compositions between those of the bcc and fcc phases and (2) a considerable shift in the temperature scale. The only prior publication on the structure of a vanadium-deuterium compound is by Roberts,³ who examined $VD_{0.66}$ and found that at room temperature the X-ray pattern could be interpreted as a bcc arrangement of vanadium atoms with $a = 3.148 \text{ \AA}$.

Experimental Section

The experimental procedures followed in this study are similar to those described by Maeland² with the following additions or changes.

Materials. Pure deuterium was obtained from the thermal decomposition of uranium deuteride. The deuterium used to prepare the uranium deuteride was purchased from the Stuart Oxygen Co., San Francisco, Calif., and was determined to be $99 + \% D_2$.

Preparation of the Deuterides. Samples of composition $VD_{0.1}$ to $VD_{0.8}$ were prepared in an all-glass high-vacuum line. Samples with $D/V > 1$ were made in the high-pressure system, which is described in detail elsewhere.⁴ Briefly, the high-pressure preparation method consisted of placing granules of cleaned vanadium metal (5–10 g) or of vanadium metal which previously had been heated in deuterium into the "magnadash" reactor. The reactor had been modified to accept an interchangeable boron carbide mortar and pestle unit.

(1) Presented in part before the Division of Physical Chemistry at the 158th National Meeting of the American Chemical Society, New York, N. Y., Sept 1969.

(2) A. J. Maeland, *J. Phys. Chem.*, **68**, 2197 (1964).

(3) B. W. Roberts, *Phys. Rev.*, **100**, 1257 (1955).

(4) A. J. Maeland, T. R. P. Gibb, Jr., and D. P. Schumacher, *J. Amer. Chem. Soc.*, **83**, 3728 (1961).

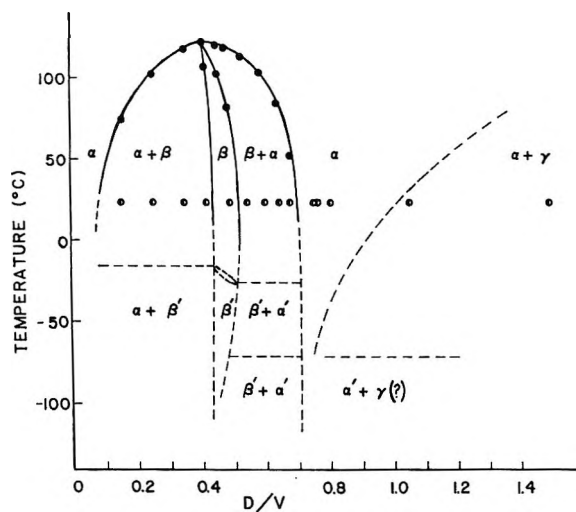


Figure 1. Partial phase diagram for the vanadium-deuterium system. Compositions of samples studied are indicated by half-filled circles.

The high-pressure apparatus with starting material was then cooled to approximately 0° , evacuated, and then pressured at 30–70 atm with deuterium. The vanadium sample was then crushed periodically for several hours and the progress of the reaction followed by observing the decrease in deuterium pressure. The composition of each vanadium deuteride was calculated from the pressure drop in the system and substantiated by analysis of the product. Analysis consisted of thermal decomposition of the deuteride and removal of the deuterium to a gas buret using a Toepler pump. The composition values obtained by analysis and by calculation from absorption agreed quite well. The maximum overall sample composition error as D/V is ± 0.03 .

X-Ray Diffraction Procedures. Diffraction photographs were obtained using a Straumanis-type General Electric powder camera and nickel-filtered copper radiation. The vanadium deuteride was sealed into a 0.3-mm diameter Pyrex capillary which had been filled with argon at 1 atm. For the high-temperature runs, the deuteride was heated by blowing hot air over the capillary. Several of the samples were also examined using a Seeman Heat Camera. For the low-temperature experiments, dried nitrogen gas was passed through a coil of copper tubing, cooled to -196° by immersion in liquid nitrogen, and then over the Pyrex capillary containing the deuteride. The temperature of the sample was adjusted primarily by changing the rate of flow of the nitrogen gas through the cold copper tubing. The open sides of the powder camera were closed off with thin plastic sheet to eliminate ice formation on the capillary and its holder. The temperature of the deuteride could thus be maintained quite easily in the range from -135 to 300° . The actual temperature of the sample was measured with thermocouples to an accuracy of $\pm 3^\circ$. In no run was any irreversible transformation observed. The unit cell dimensions for each

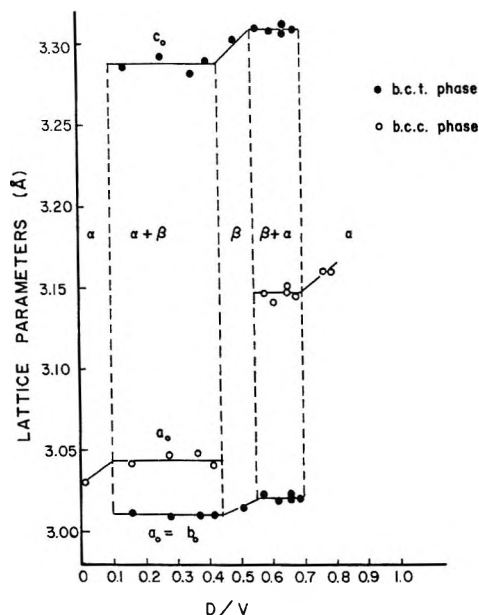


Figure 2. Variation of the lattice parameters with deuterium content at room temperature. Phase boundaries are indicated by dashed lines.

phase were subsequently determined from the diffraction lines by a least-squares extrapolation method using the Nelson–Riley,⁵ Taylor–Sinclair⁶ correction function. The diffraction lines were in general somewhat broad and diffuse, although α_1 – α_2 resolution at larger angles was observed in many films. The estimated accuracy of the parameters from a consideration of both the mathematical uncertainty in the least-squares procedure and the quality of the patterns is $\pm 0.003 \text{ \AA}$.

Results

Room Temperature Experiments. The diffraction results are summarized in Figure 2. The phase boundaries are indicated by dashed lines. The bcc α phase extends to approximately $VD_{0.1}$ and the lattice parameter increases from 3.030 to 3.045 \AA . This is the solid solution region wherein the deuterium atoms occupy interstitial positions in the vanadium atom lattice. Beyond $VD_{0.1}$ to $VD_{0.43}$ a two-phase region exists. This consists of the α phase and a β phase which has a body-centered tetragonal lattice of vanadium atoms. The parameter of the α phase in this region is 3.045 \AA , while the parameters of the β phase are $a_0 = 3.009 \text{ \AA}$ and $c_0 = 3.287 \text{ \AA}$. The β phase is the only phase in the composition range $VD_{0.43}$ to $VD_{0.53}$. The lattice parameters increase slightly with increasing deuterium content in this region, $a_0 = 3.009$ – 3.020 \AA and $c_0 = 3.287$ – 3.307 \AA . From $VD_{0.53}$ to $VD_{0.70}$ a second two-phase region exists. This consists of the β phase and the α phase—which has as before a body-centered cubic

(5) J. B. Nelson and D. P. Riley, *Proc. Phys. Soc. London*, **57**, 160 (1945).

(6) A. Taylor and H. Sinclair, *ibid.*, **57**, 126 (1945).

lattice of vanadium atoms. The lattice parameters of the β phase in this region are $a_0 = 3.020 \text{ \AA}$ and $c_0 = 3.307 \text{ \AA}$ while the parameter of the α phase has now increased to 3.143 \AA . Beyond $\text{VD}_{0.70}$ to approximately $\text{VD}_{1.0}$ only the α phase exists. The lattice parameter increases as before with increasing deuterium content in this region; a_0 changes from 3.143 \AA at $\text{VD}_{0.70}$ to 3.160 \AA at $\text{VD}_{0.80}$. The third two-phase region begins at approximately $\text{VD}_{1.0}$ and contains the α phase along with a γ phase—which has a face-centered cubic lattice of vanadium atoms. The parameter of the α phase in this region is approximately 3.16 \AA and the parameter of the γ phase is 4.27 \AA . Pure γ phase presumably exists at compositions near $\text{D/V} = 2$. The stability of the γ phase is much less than that of the α or β phases; therefore only minimal study was given this region and no attempt was made to prepare stoichiometric VD_2 .

Low-Temperature Experiments. Several of the samples were studied at low temperatures to correlate further with the neutron diffraction results. It was observed that the almost vertical phase boundaries for the $\alpha + \beta/\beta$ and $\beta + \alpha/\alpha$ regions remained essentially vertical down to 140°K (Figure 1). However, two significant modifications of the room temperature phases were observed. At approximately 250°K (-25°C) the lattice parameters of the β phase changed abruptly with $a_0 = 2.98 \text{ \AA}$ and $c_0 = 3.40 \text{ \AA}$. This phase is designated β' , and is characterized by a 1.3% shrinkage in a_0 and a 3.2% increase in c_0 . Also, the bcc α phase at higher compositions was observed to transform at low temperatures to an orthorhombic lattice—the α' phase. For example, a sample of $\text{VD}_{0.75}$ at 143°K (-130°C) has unit cell dimensions of $a_0 = 4.45 \text{ \AA}$, $b_0 = 4.48 \text{ \AA}$, and $c_0 = 3.15 \text{ \AA}$. Only approximate values for the cell edge lengths could be determined since the diffraction lines were quite broad in this low-temperature, unannealed sample. This orthorhombic modification of $\text{VD}_{0.75}$ is then analogous to $\text{NbH}_{0.9}$ ⁷ and $\text{TaH}^{8,9}$ at room temperature.¹⁰

High-Temperature Experiments. Each vanadium deuteride with $\text{D/V} < 1$ was also studied at elevated temperatures. The sample, contained in a sealed Pyrex capillary, was slowly heated to approximately 250° and held at this temperature for 45–60 min to ensure complete transformation to the α , solid solution phase. The sample was then cooled and the temperature arrested at the desired value, and after 1 hr at this temperature the X-ray exposure initiated. This procedure was followed in order to ensure that equilibrium phase distributions were being observed. This procedure was necessary since this system was particularly sluggish to phase transformations when approached from lower temperatures rather than high. These phenomena are now understood in the light of recent inelastic neutron scattering experiments on vanadium hydrides by Rush and Flotow.¹¹

Discussion

The results of this study indicate considerably more similarity between the vanadium–hydrogen and vanadium–deuterium systems than was originally indicated, the major difference being (1) a shift in the relative temperature scales of approximately 70° and (2) a broader field for the second two-phase region, the $\beta + \alpha$. Recent resistivity measurements of vanadium–hydrogen alloys by Westlake¹² indicate additional phase changes below 225°K (-48°C), and a $\beta/\beta + \alpha$ phase boundary (RT) at approximately $\text{VH}_{0.8}$. Maeland's phase diagram is quite reliable, we feel, from room temperature to higher temperatures for compositions from VH_0 to $\text{VH}_{0.8}$. Several independent investigators using quite different experimental methods have verified his results.^{11,12} Maeland made no attempt, however, to extend his study to low temperatures. Also, the relative instability of vanadium hydrides with $\text{H/V} > 0.8$ discouraged attempts to examine the higher compositions. We would expect to observe additional phases in the vanadium–hydrogen system analogous to those occurring in the vanadium–deuterium system, although the transition temperatures should be different. For example, α -vanadium hydride would have an orthorhombic lattice of vanadium atoms at low temperature.

The character of the various phases in the vanadium–deuterium or vanadium–hydrogen systems is rationalized as follows. The α phase consists of a bcc lattice of metal atoms containing interstitial deuterium "atoms" which are *quite mobile*.^{13,14} The α' phase is similar to the α phase except that the deuteriums are now "frozen" into specific lattice sites¹³—are not free to diffuse throughout the lattice—and this results in a slight distortion of the cubic metal atom lattice to the orthorhombic lattice observed. The β phase results when there is sufficient concentration of deuterium "atoms" such that the free-electron density of the vanadium atom lattice is decreased and the deuterium–deuterium repulsion is significant. As a result of these effects, the deuterium "atoms" occupy different lattice sites in the β phase and in such are not mobile but "frozen." The β' phase is similar to the β phase but probably represents additional ordering of the deuterium atoms. The

(7) G. Brauer and R. Hermann, *Z. Anorg. Allg. Chem.*, **274**, 11 (1953).

(8) T. R. Waite, W. E. Wallace, and R. S. Craig, *J. Chem. Phys.*, **24**, 634 (1956).

(9) B. Stalinski, *Bull. Acad. Polon. Sci., Cl. III*, **2**, 245 (1954).

(10) One reviewer has suggested that only α' phase might exist at temperatures below -75° in the composition range $\text{D/V} = 0.7\text{--}0.75$. While this might certainly be true and in fact would perhaps be the preferred description, any attempts to define the phase relationships in this low-temperature–high-composition region were hampered by the rather poor quality of the X-ray photographs which could be obtained (indicated by the dashed lines).

(11) J. R. Rush and H. E. Flotow, *J. Chem. Phys.*, **48**, 3795 (1968).

(12) D. G. Westlake, private communication.

(13) J. Rush, private communication.

(14) K. I. Hardcastle, unpublished results.

γ phase is most likely a CaF_2 type lattice with considerable deuterium-deuterium "atom" repulsion giving rise to high dissociation pressures and a high degree of nonstoichiometry. The results of a neutron diffraction investigation of $\text{VD}_{0.5}$ and $\text{VD}_{0.75}$ by Hardcastle¹⁴ will soon be published. Preliminary calculations support the requirements of the structural models for the vari-

ous phases and are in overall agreement with the neutron-scattering results of Rush and Flotow.¹¹

Acknowledgments. Financial support for this study by the U. S. Atomic Energy Commission is gratefully acknowledged. The authors also wish to thank Mr. Thomas Nunes and Mr. Ralph Bowman for their help with the calculations.

Radiation-Induced Polymerization of Pure Styrene at Low Temperature

by Suelo Machi,* Joseph Silverman,

*Laboratory for Radiation and Polymer Science, Department of Chemical Engineering,
University of Maryland, College Park, Maryland 20742*

and Donald J. Metz

Brookhaven National Laboratory, Upton, New York 11973

Publication costs assisted by Brookhaven National Laboratory

The radiation-induced polymerization of styrene was carried out over a range of temperature from 0 to -78° using superdry styrene and wet styrene. Molecular weight distributions were determined by gel permeation chromatography. In the course of the rate studies, the time of contact between styrene and silica gel was found to be an important factor. Partially dried liquid styrene shows a bimodal molecular weight distribution which reflects the simultaneous operation of ionic and radical processes. Upon solidification, superdry styrene exhibits a sharply decreased rate of polymerization, while wet styrene shows a marked increase. The polymer from superdry styrene shows a unimodal molecular weight distribution when formed in the liquid phase and a multimodal distribution when polymerized as a solid. At -78° , the rate of polymerization and the molecular weight of the product are rather low. In a sample irradiated at -78° and then stored at the freezing point of styrene (-30.5°) for a few hours, the polymer yield shows a large increase accompanied by the appearance of a very high molecular weight fraction in the distribution curve. Traces of water have no effect on the rate of polymerization and molecular weight distribution of frozen samples. A high yield of dimer and trimer, $G \approx 2.5$, is observed in wet liquid styrene. This can be attributed either to intraspur radical reactions or to water terminated ionic reaction in the bulk phase. The results in the solid state polymerization fit the assumption that a carbonium ion propagation predominates regardless of the water content.

Introduction

Metz and his coworkers¹ discovered that styrene polymerizes extremely rapidly by γ irradiation if it is exhaustively purified and dried. It has been well established by Metz, *et al.*,²⁻⁴ and Okamura, *et al.*,⁵⁻¹⁰ that the radiation-induced polymerization of superdry styrene proceeds *via* an ionic mechanism in the liquid state.

Chen,¹¹ Chapiro,^{12,13} and Phalangas, *et al.*,¹⁴ reported that the low temperature radiation-induced polymerization of styrene that was purified but not subjected to rigid drying procedures (wet styrene) showed a maximum rate slightly below the freezing point. In addition, Ueno, *et al.*,⁵ reported that the polymerization rate of superdry styrene at -78° is almost the same as that of wet styrene at that temperature.

The present communication involves studies on the polymerization of styrene at low temperatures in the

* Takasaki Radiation Chemistry Research Establishment, Japan Atomic Energy Research Institute, Takasaki, Gunma, Japan.

(1) D. J. Metz and C. L. Johnson, *Polym. Preprints*, **4**, 440 (1963).

(2) R. C. Potter, C. L. Johnson, R. H. Bretton, and D. J. Metz, *J. Polym. Sci., Part A-1*, **4**, 419 (1966).

(3) R. C. Potter, R. H. Bretton, and D. J. Metz, *ibid.*, **4**, 2295 (1966).

(4) R. C. Potter and D. J. Metz, *ibid.*, **9**, 441 (1971).

(5) K. Ueno, K. Hayashi, and S. Okamura, *ibid.*, *Part B*, **3**, 363 (1965).

(6) K. Ueno, K. Hayashi, and S. Okamura, *Polymer*, **7**, 431 (1966).

(7) K. Hayashi, H. Yamazawa, K. Ueno, K. Hayashi, K. Kamiyama, F. Williams, and S. Okamura, Abstracts of Symposium on Macromolecular Chemistry, Tokyo-Kyoto, Sept 1966.

(8) K. Ueno, F. Williams, K. Hayashi, and S. Okamura, *Trans. Faraday Soc.*, **63**, 1478 (1967).

liquid and solid states. The effect of phase change on polymerization rate and molecular weight distribution is described. Postirradiation polymerization was found to take place in the solid state with the formation of extremely high molecular weight products.

Experimental Procedures

The preparation of superdry styrene has been described earlier.³ In essence the procedure consists of vacuum distillation of monomer, vacuum bake-out of glassware, degassing of monomer, and drying with activated silica gel. In previous papers reproducible data had been reported. However irreproducibility has been a chronic problem for the last few years. In the present investigation the contact time between styrene and baked silica gel has been extended to 200 hr instead of the 17-hr period previously employed.³ In systematic studies we have observed that the polymerization rate increases with prolonged contact time and reaches constant reproducible values reported in previous work.³

Wet styrene was prepared by distillation through a 2-m Heli-Grid packed column under a reduced pressure of helium. It was then degassed by freeze-thaw cycles and transferred to ampoules by vacuum distillation in a sealed system. The glassware was not baked and contact with silica gel was omitted.

Irradiation of the samples was done in a ⁶⁰Co irradiation facility at BNL. Low temperature control was achieved by the use of liquid nitrogen slushes of organic compounds. Benzyl alcohol, styrene, furfural, benzyl acetate, and chloroform slushes were used to provide temperatures of -14, -30.5, -36, -49, and -64°, respectively. Ice-water and mixtures of Dry Ice and methanol were used to achieve temperatures of 0 and -78°. Styrene can be maintained as a supercooled liquid for several hours when it is cooled to its freezing point, -30.5°. If styrene is frozen at -78° for about 10 min and then raised to -30.5°, it remains in the solid crystalline state for at least several hours. By use of these techniques, both solid and liquid phase polymerizations were carried out at the melting point temperature.

Polystyrene was precipitated from irradiated liquid styrene by an excess of methanol. The polymer was filtered and dried in a vacuum oven. Per cent conversion was calculated from the weight of the dried polymer. In the case of the solid state polymerizations, each sample was quenched to liquid nitrogen temperature promptly after irradiation, after which the ampoule was opened and the frozen monomer-polymer mixture was contacted with a large amount of benzene. This rapid dissolution reduced postirradiation effects to negligible levels.¹⁴ In some cases polymer was separated from its benzene solution by methanol precipitation. In other cases, the freeze-dry method was used to minimize the loss of low molecular weight products

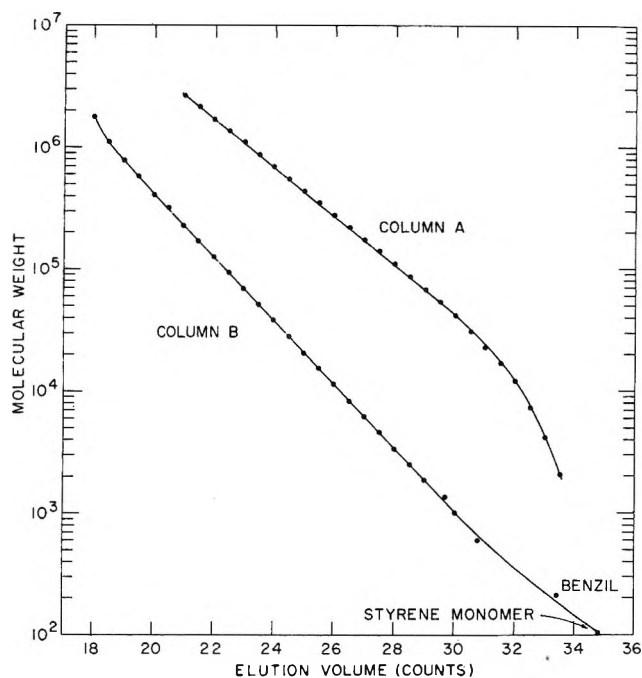


Figure 1. Calibration curves for chromatographic columns A and B.

such as dimers and trimers; the dilute benzene solution was frozen at -78° and evacuated for several hours.

The molecular weight distribution of the polymer collected was measured by gel permeation chromatography, using a Waters GPC Model 200 instrument. Two different sets of columns were used. Column set A was filled with polystyrene gel of pore sizes 5×10^6 , 1×10^6 , 1×10^5 , and 3×10^4 Å; set B with pore sizes of 1.5×10^5 , $1.5-5 \times 10^4$, 1×10^3 , and 350-700 Å. Each column was calibrated with 13 standard monodisperse ($1.06 \leq M_w/M_n \leq 1.20$) polystyrene samples which were obtained from several sources (Pressure Chemicals Co., Arro Laboratories, Inc., and Instruments for Industry and Research). Tetrahydrofuran (THF) was used as the eluting solvent. A polystyrene solution of 0.3% by weight was prepared in THF and filtered under pressure in a helium atmosphere. The polymer solution of 2 ml was injected for 120 sec. A THF flow rate of 1 ml/min and an oven temperature of 25° were used. The number average molecular weight, \bar{M}_n , was calculated from the chromatogram and the calibration curves (Figure 1).

In the subsequent paragraphs, illustrations, and Ta-

(9) K. Hayashi, H. Yamazawa, T. Takagaki, F. Williams, K. Hayashi, and S. Okamura, *Trans. Faraday Soc.*, **63**, 1489 (1969).

(10) F. Williams, K. Hayashi, K. Ueno, K. Hayashi, and S. Okamura, *ibid.*, **63**, 1501 (1967).

(11) C. S. H. Chen, *J. Polym. Sci.*, **58**, 389 (1962).

(12) Y. Amagi and A. Chapiro, *J. Chim. Phys.*, **59**, 537 (1962).

(13) A. Chapiro, *J. Polym. Sci., Part C*, **4**, 1551 (1964).

(14) C. J. Phalaragas, S. Srinivasan, and J. Silverman, *Trans. Amer. Nucl. Soc.*, **8** (2), 320 (1965).

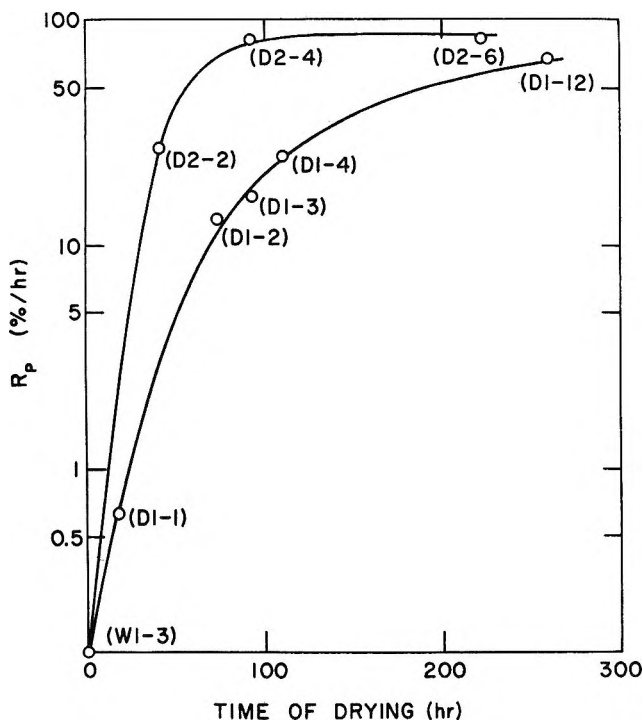


Figure 2. Rate of polymerization, at 0° and 50 krad/hr, after indicated times of contact between styrene and silica gel. Each experimental point is identified by a sample number.

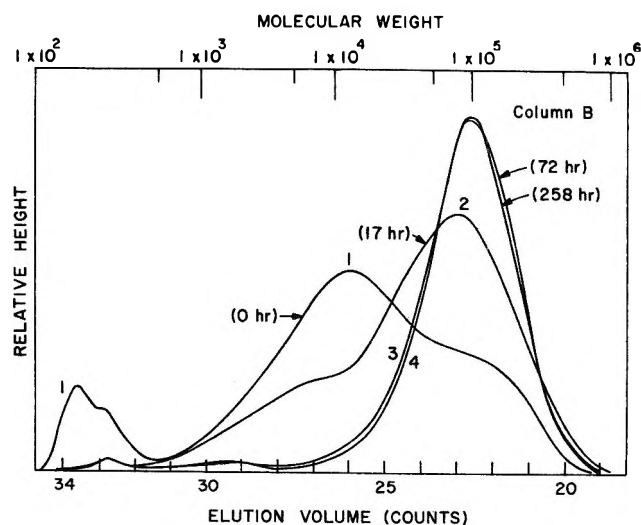


Figure 3. Effect of drying of monomer on the molecular weight distribution of the polystyrene produced by irradiation at 0° : curve 1 (W1-3); curve 2 (D1-1); curve 3 (D1-2); curve 4 (D1-12). The time of contact with silica gel is indicated for each chromatogram (column B).

ble I the prefix D denotes a superdry sample, and W denotes a wet sample.

Results and Discussion

Influence of Contact Time. Figure 2 shows the polymerization rate at 0° and 50 krad/hr vs. the contact time of styrene with two different batches of silica gel.

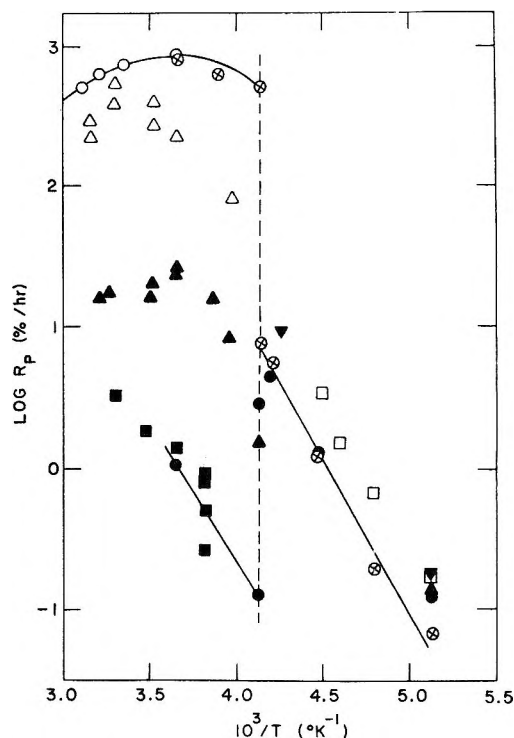


Figure 4. Rate of polymerization vs. reciprocal temperature. Where possible, rates of polymerization have been normalized to 2.8 Mrads/hr using the dose rate dependence reported by the author (column 4).

Symbol	System	Dose rate, Mrads/hr	Reported dose rate dependence	Ref
⊗	Superdry	2.8	..	This work
●	Wet	2.8	..	This work
○	Superdry	0.067	0.88	4
△	Superdry	0.014	0.62	8
▲	Dry	0.23	..	5
□	Wet	3.5	..	12
▼	Wet	0.76	1	14
■	Dry	0.82	0.53-0.71 (depending on water content)	15

In both cases the rate approaches a constant value after prolonged contact. To reach the asymptotic polymerization rate, the styrene was dried over silica gel more than 200 hr. The rate so obtained is reproducible and agrees with the rate reported by Potter, *et al.*³ In their work, a 17-hr contact time was sufficient to yield reproducible polymerization rates. The difference is in the activity of the baked silica gel. It appears that silica gels produced by different companies and even by the same company at different times can differ in drying behavior.

Figure 3 shows the molecular weight distributions for different contact times. The ordinate value is proportional to the weight fraction of polymer with the molecular weight characterized by the elution volume given as the abscissa. The data were obtained with liquid styrene at 0° . Curves 1 and 2 differ in shape,

but both show broad multimodal distributions. Wet styrene (curve 1) has a main peak at a molecular weight of approximately 1×10^4 and a secondary peak at approximately 8×10^4 . Curve 2 is the molecular weight distribution of the polymer from partially dried styrene which polymerized four times faster than the wet sample. The two main peaks of curve 2 are in the same positions as in curve 1, but the relative heights of the two peaks are different. With more complete drying, the first peak (1×10^4) disappears, and the second peak (8×10^4) increases. Eventually with continued drying (curves 3 and 4), a unimodal distribution curve is observed, whose single peak is in the same position as that of the second peak of the wet and the partially dried samples.

The change of polymerization rate with drying time (Figure 2) and the kinetic results of Potter, *et al.*,²⁻⁴ suggest that the second peak (8×10^4) of curves 1 and 2 arises from the water-sensitive ionic polymerization, and the lower peak (1×10^4) is caused by the water-insensitive free-radical polymerization. In the superdry styrene, the ionic polymer fraction is so large that the contribution from the free-radical polymerization is completely overshadowed.

For liquid styrene at 0° and at a dose rate of 50 krad/hr the molecular weight of the ionic polymer fraction is not influenced by a small amount of water, and the molecular weight is greater for the ionically formed polymer than for that formed by free-radical polymerization. Huang and Westlake¹⁵ also reported bimodal molecular weight distributions in the case of partially dried styrene and compared the relative heights of the two elution peaks obtained from various polymerization conditions. They did not obtain a unimodal distribution owing to insufficient removal of water from their styrene samples.

Effect of Phase Change and Temperature. An Arrhenius plot of the rate of radiation-induced polymerization of styrene is shown in Figure 4. Results from several other laboratories are included with our own data; where possible the data from previously published works are normalized to our dose rate of 2.8 Mrads/hr using the dose rate dependence reported by each author.

Above 0° a small negative temperature coefficient has been observed by Potter, *et al.*,³ for superdry styrene. Our 0° datum is in excellent agreement with that of Potter, *et al.*,³ and our two additional points for the liquid further extend the trend of their data. The temperature coefficient is observed to vanish at 0° and becomes slightly positive at lower temperatures. A similar trend was reported by Ueno, *et al.*,⁵ and led these workers to conclude that the radiation-induced ionic polymerization of styrene had a zero temperature coefficient between $+37$ and -21° .

In the present work we observed a sharp decrease in the rate of polymerization as superdry styrene changed from the liquid to the solid state. This discontinuity

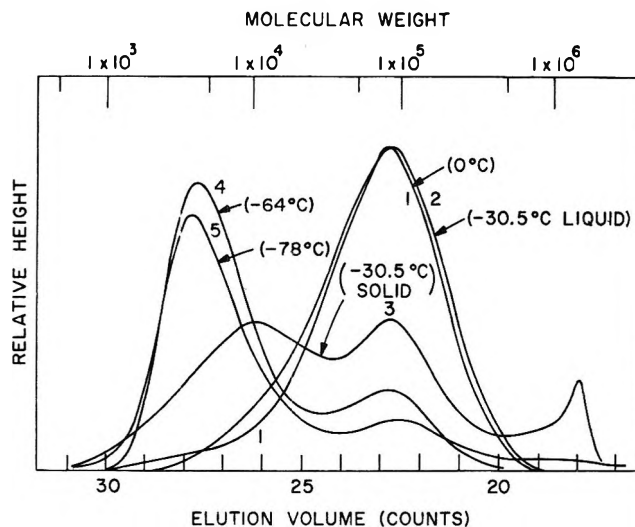


Figure 5. Molecular weight distributions formed at various temperatures using superdry styrene. (Dose rate, 2.8 Mrads/hr; column B.)

in rate is undoubtedly caused by the parallel similar discontinuous decrease in monomer diffusion rate when the styrene enters the solid state. The temperature coefficient for polymerization in the solid state observed here is much higher than that of the liquid. It agrees remarkably well with the value of 11.6 kcal/mol reported by Amagi and Chapiro,¹² and undoubtedly reflects the higher activation energy for diffusion in the solid state.

Chapiro¹³ classified monomers undergoing solid state polymerization into four groups depending on the polymerization rate change with monomer phase change. He placed styrene in the same group as bis(chloromethyl)-3,3-oxetane and acrylonitrile, whose polymerization rates increase greatly when they are solidified. This behavior is exhibited by wet styrene, as shown in Figure 4, but not for superdry styrene.

When the styrene is in the solid state, the polymerization rate is independent of water content. The rate for wet styrene, which would be expected to drop because of decreased mobility in the solid, instead rises to match the value for the superdry styrene. It appears, therefore, that in the solid state water is not able to deactivate the initiating or propagating species because of phase separation from the styrene. If this is the case, the polymerization in the solid state proceeds mainly by an ionic mechanism for both wet and superdry styrene.

The molecular weight distribution of polystyrene is markedly affected by phase change (Figure 5). The distribution of polymer formed from superdry liquid styrene is unimodal and does not change as the temperature is lowered from 0 to -30.5° (curves 1 and 2). If polymerization is carried out in the solid monomer, the

(15) R. Y. M. Huang and J. F. Westlake, *J. Polym. Sci., Part A-1*, **8**, 49 (1970).

molecular weight distribution of the polymer shows two or three peaks (curves 3, 4, and 5). One of these peaks, with a molecular weight of 8×10^4 , coincides with the peak of the unimodal distribution curve of the liquid phase polymerization. The height of this peak decreases to a great extent when the monomer is solidified and continues to decrease as the polymerization temperature is lowered. Another peak in the molecular weight region $(4-10) \times 10^3$ appears only in the solid state polymerization; its relative height increases as the temperature is lowered. The higher molecular weight species (8×10^4) is probably caused by polymerization under circumstances where the medium around the growing chains resembles the liquid; the lower molecular weight fraction may represent chains whose growth is limited by decreased mobility in more ordered or defect-free regions. At lower temperatures, the probability of the latter mode of polymerization becomes larger than that of the former.

In the solid state polymerization at -30.5° (the freezing point of styrene) another small peak corresponding to a very high molecular weight ($\sim 1 \times 10^6$) fraction is observed. Since the same peak is also observed in postirradiation polymerization (see below), this fraction may be caused by the slow growth of a long-lived species.

Postirradiation Polymerization in the Solid State. Samples irradiated at -78° and stored at that temperature for many hours undergo little postirradiation polymerization. When the postirradiation temperature is -30.5° , substantial postirradiation polymerization occurs. These kinetic effects are shown in Figure 6. A result worthy of note is the large effect obtained on heating a sample to -30.5° for 3 hr after a 15-hr storage at -78° .

In addition, it should be noted that the postirradiation kinetic behavior of wet and superdry styrene are

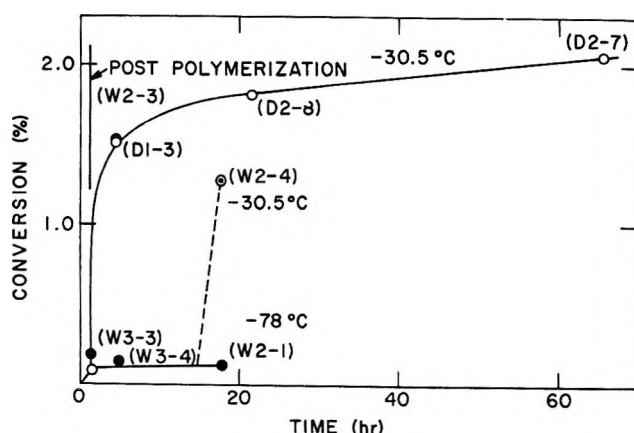


Figure 6. Postirradiation polymerization of styrene in the solid state as a function of time: \circ , superdry; \bullet , wet; \odot , wet; stored for 15 hr at -78° , then stored an additional 3 hr at -30.5° . All samples irradiated for 1.5 hr at -78° and at 2.8 Mrads/hr.

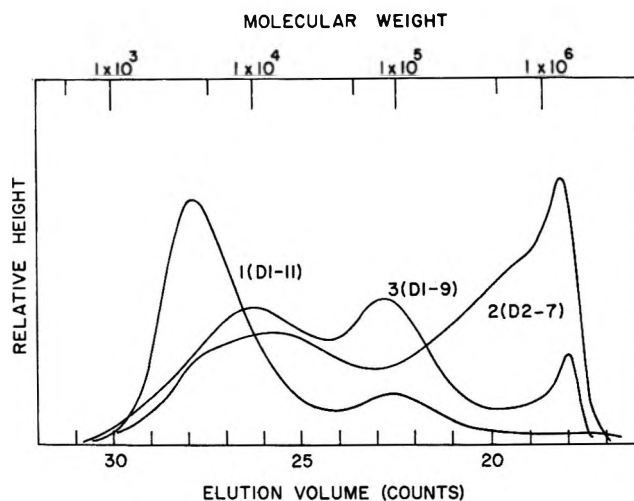


Figure 7. Molecular weight distributions formed in superdry styrene irradiated in the solid state at 2.8 Mrads/hr: curve 1 (D1-11), irradiated at -78° ; curve 2 (D2-7), irradiated at -78° for 1.5 hr, stored at -30.5° for 66 hr; curve 3 (D1-9), irradiated at -30.5° for 0.20 hr (column B).

similar, as are their in-source kinetics in the solid state.

Several molecular weight distribution curves of the polymer formed by in-source and postirradiation polymerization of superdry styrene are shown in Figure 7. The curve for the in-source product formed at -78° (curve 1) has two distinct peaks. One is a tall, narrow peak at 4×10^3 ; the other is a relatively small, broad peak at 6×10^4 . After postirradiation polymerization at -30.5° for 66 hr, the molecular weight distribution assumes a new shape (curve 2). The outstanding feature of curve 2 is a high molecular weight fraction at approximately 6×10^5 . The peak initially at 4×10^3 is shifted to 7×10^3 . Curve 3 in this figure is the distribution for the in-source product formed at -30.5° . It has peaks at 7×10^3 , 7×10^4 , and 1×10^6 .

The sample produced in the postirradiation polymerization at -30.5° was analyzed with a chromatographic column containing gel with a larger pore diameter (column A). Figure 8, which is the equivalent of curve 2 in Figure 7, shows no additional high molecular weight peaks.

Figure 9 shows the molecular weight distribution curves measured with column A for postirradiation polymerization experiments with wet styrene. Comparison with Figure 7 shows that the distribution curves in both wet and superdry styrene are similar, slight differences being attributable to errors in intercalibration of the two columns. Since the polymerization rates are also similar under comparable conditions, we conclude that both in-source and postirradiation polymerization in the solid state are independent of water content.

For several of the samples in Figures 7 and 9, as well as a number of other samples, the approximate yield of polymer molecules per gram under each peak was calculated by the following equation

$$N_p = 6 \times 10^{23} \left[\frac{CS_p}{(\bar{M}_n)_p S_t} \right]$$

where N_p = number of polymer molecules of molecular weight $(\bar{M}_n)_p$ per gram, $(\bar{M}_n)_p$ = number average molecular weight of the peak, C = fraction of styrene converted into polymer, S_p = area under the peak, and S_t = total area under the curve. From these values of N_p and the total irradiation dose delivered to the sample, the number of molecules of average molecular weight $(\bar{M}_n)_p$ isolated per 100 eV absorbed (G_p) was calculated. These calculated values appear in Table I, along with other pertinent information.

Table I is sufficiently detailed to allow the detection of certain trends from which useful generalizations can be drawn. Comparison of samples W2-3 and D3-1 offers quantitative confirmation of the statement made earlier concerning the independence of the rate of polym-

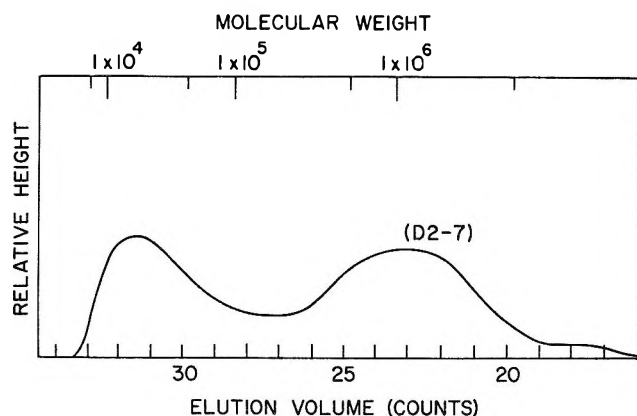


Figure 8. Molecular weight distribution of sample D2-7 measured with column A.

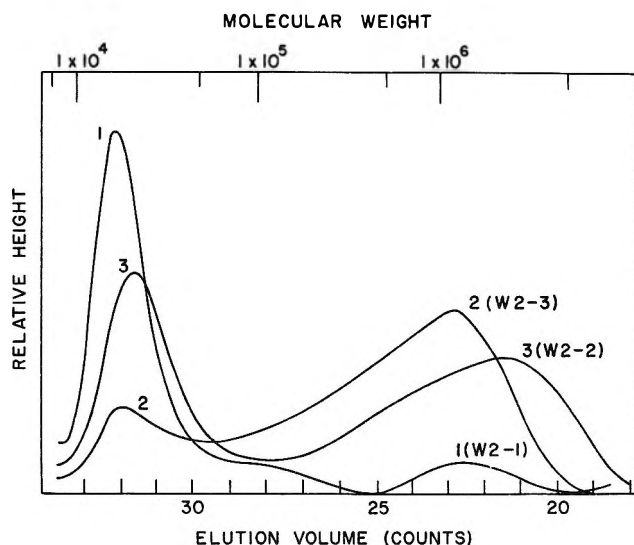


Figure 9. Molecular weight distributions formed in wet styrene irradiated in the solid state at 2.8 Mrads/hr: curve 1 (W2-1), irradiated at -78° for 1.5 hr, stored at -78° for 18 hr; curve 2 (W2-3), irradiated at -78° for 1.5 hr, stored at -30.5° for 3 hr; curve 3 (W2-2), irradiated at -30.5° for 0.20 hr, stored at -30.5° for 3 hr (column A).

erization and molecular weight distribution on water content in the postirradiation behavior of solid styrene. The data of samples W1-6 and D1-9, although not as close as the previous set, lead to a similar conclusion.

If we accept the general similarity between wet and dry styrene, comparison of samples W2-1, W2-4, and D1-11 indicates that the very high molecular weight species ($\sim 10^6$) arises from a postpolymerization process that occurs quite slowly at -78° , and more rapidly at higher temperatures (-30.5°). In fact, a relatively high molecular weight fraction appears in samples either irradiated or postpolymerized at temperatures near the melting point (samples W2-4, W2-3, D3-1, D2-7, W3-1, W3-2, W1-6, W2-2, and D1-9). The rate of appearance of this fraction and its relative contribution to the total weight of polymer formed appear to increase with postirradiation time and/or temperature.

This behavior is consistent with the viewpoint that some fraction of the polymerizing chains are nonterminated active centers, whose further growth, being limited by diffusion and "lattice" motion, is favored by increasing postirradiation time at any given temperature, or temperature for any given postirradiation time. A conservative working hypothesis is that the minimum number of trapped active centers per gram immediately following irradiation will be equal to the number of molecules per gram of the highest molecular weight fraction isolated ($\bar{M}_n > 5 \times 10^6$). From Table I it is seen that these values are all approximately equal to or greater than 10^{14} per gram. If these were trapped free radicals, they should have been readily observed by their electron spin resonance spectrum. We were not able to detect any esr signal above background at a dose of 5 Mrads at liquid nitrogen or Dry Ice temperature.

The appearance of a large amount of dimer and trimer in both the liquid (W1-3) and the solid (W1-6) phase irradiations is particularly significant. G values of approximately 0.7 have been reported for liquid styrene on the basis of kinetic studies^{16,17} and on the basis of DPPH scavenging studies.^{18,19} In both of these estimates only those radicals which escaped from or were formed outside of spurs are counted. In the present work the observed yield of polymer molecules, $G_p \approx 2.5$, may correspond to $G \approx 5$ for primary radical production. Under these circumstances the apparent discrepancy with the lower estimates would be due to our ability to count dimers and trimers formed in intraspur reactions. On a molar basis, dimers and trimers account for approximately 75% of the radiolytic yield of polymer molecules.

(16) A. Chapiro, "Radiation Chemistry of Polymeric Systems," Interscience, New York, N. Y., 1962.

(17) R. Y. M. Huang, F. J. Westlake, and S. C. Sharma, *J. Polym. Sci., Part A-1*, **7**, 1729 (1969).

(18) A. Chapiro, *C. R. Acad. Sci.*, **233**, 792 (1951).

(19) V. A. Krongauz and Kh. S. Bagdasarian, *Zh. Fiz. Khim.*, **32**, 1863 (1958).

Table I: Calculated Values of Number Average Molecular Weight ($(\bar{M}_n)_p$), Number of Polymer Molecules per Gram (N_p), and Number of Polymer Molecules per 100 eV (G_p) at Various Combinations of Irradiation and Postirradiation Conditions (Dose Rate = 2.8 Mrads per hr)

Sample	Irradiation temp, °C	Postpolymerization Temp, °C	Postpolymerization Time, hr	Yield, %	$(\bar{M}_n)_p$	S_p/S_t^a	N_p , molecules/g	Dose, Mrads	G_p , molecules/100 eV
D1-11	-78	0.09	3.7×10^3	0.78	1.1×10^{17}	4.2	4.2×10^{-2}
					6.1×10^4	0.22	2.0×10^{16}		7.7×10^{-4}
W2-1	-78	-78	18	0.12	5.0×10^3	0.74	1.1×10^{17}	4.2	4.2×10^{-2}
					8.1×10^4	0.12	1.1×10^{16}		4.2×10^{-4}
					1.2×10^6	0.14	8.4×10^{13}		3.2×10^{-5}
W2-4	-78	-78	15	1.27	5.4×10^4	0.12	1.7×10^{17}	4.2	6.5×10^{-2}
		-30.5	3		2.2×10^6	0.48	1.7×10^{16}		6.5×10^{-2}
					1.1×10^6	0.40	2.8×10^{16}		1.1×10^{-3}
W2-3	-78	-30.5	3	1.50	6.5×10^3	0.21	2.9×10^{17}	4.2	1.1×10^{-1}
					3.8×10^5	0.79	1.9×10^{16}		7.3×10^{-3}
D3-1	-78	-30.5	3	1.50	7.8×10^3	0.20	2.3×10^{17}	4.2	8.9×10^{-2}
					3.5×10^5	0.80	2.1×10^{16}		8.1×10^{-3}
D2-7	-78	-30.5	66	2.05	7.4×10^3	0.42	7.0×10^{17}	4.2	2.7×10^{-1}
					6.0×10^5	0.58	1.2×10^{16}		4.6×10^{-3}
W3-1	-35	3.30	5.3×10^3	0.74	2.8×10^{18}	2.1	2.2
					1.2×10^5	0.26	4.3×10^{16}		3.3×10^{-2}
W3-2	-35	-35	3	4.30	5.6×10^3	0.55	2.5×10^{18}	2.1	1.9
					2.3×10^5	0.45	5.1×10^{16}		3.9×10^{-2}
W1-6	-30.5	0.94	2.0×10^2	0.08	2.3×10^{18}	0.93	4.0
					3.0×10^2	0.04	7.5×10^{17}		1.3
					5.9×10^3	0.54	5.2×10^{17}		9.0×10^{-1}
					7.5×10^4	0.28	2.1×10^{16}		3.7×10^{-2}
					8.1×10^5	0.06	4.2×10^{14}		7.3×10^{-4}
W2-2	-30.5	-30.5	3	1.53	6.2×10^3	0.38	5.7×10^{17}	0.56	1.6
					5.6×10^5	0.62	9.8×10^{16}		2.8×10^{-2}
D1-9	-30.5	1.50	6.8×10^3	0.47	6.3×10^{17}	0.56	1.7
					6.7×10^4	0.41	5.5×10^{16}		1.5×10^{-1}
					1.0×10^6	0.12	1.1×10^{15}		3.0×10^{-3}
D1-8	-30.5	45.8	3.1×10^4	1.00	9.0×10^{18}	0.23	62
	(liquid)								
W1-3	0	1.10	2.0×10^2	0.07	2.3×10^{18}	2.8	1.3
	(liquid)				3.0×10^2	0.04	8.8×10^{17}		5.1×10^{-1}
					4.9×10^3	0.68	9.2×10^{17}		5.3×10^{-1}
					9.8×10^4	0.22	1.5×10^{16}		8.7×10^{-3}

^a S_p/S_t is the fractional area of each chromatogram corresponding to the indicated number average molecular weight species, $(\bar{M}_n)_p$.

Another possible explanation can be advanced on the basis of homogeneous reactions involving ionic species. The concentration of water in wet styrene is of the order of 10^{-2} mol/l. at 0° .²⁰ Assuming the values of the specific rate constants of the styryl carbonium ion for reaction with impurity, k_{tx} , and propagation, k_p , are 1×10^{10} and 5×10^6 l./mol sec,^{8,10} respectively, one finds that the probability of propagation relative to termination is

$$\frac{k_p[M]}{k_{tx}[H_2O]} \approx 0.5$$

Hence growth of a carbonium ion to the dimer or trimer stage prior to termination by proton transfer to water may be a reason for their great abundance.

Brown²¹ has shown that the radiolytic yield of dimer in neat liquid styrene containing 0.1% *tert*-butylcatechol is 0.64, of which 0.49 is attributed to excited species and the remainder to an anionic process. It is also

known that several substituted aromatic compounds undergo photoinduced dimerization in the solid^{22,23} and the liquid²⁴ state.

The general picture which emerges from the postirradiation polymerization data can be summarized as follows. Postirradiation polymerization occurs in solid styrene, and both the rate of the reaction and the molecular weight distribution of the product are essentially independent of water content. This indicates that the nature of the trapped, propagating species is the same in wet and dry styrene. Since we have not observed an esr signal in low temperature irradiated styrene, and the

(20) R. H. Boundy and R. F. Boyer, "Styrene, Its Polymers, Copolymers, and Derivatives," Reinhold, New York, N. Y., 1952.

(21) W. G. Brown, *J. Amer. Chem. Soc.*, **90**, 1916 (1968).

(22) G. M. J. Schmidt, "Reactivity of the Photoexcited Molecule," Interscience, New York, N. Y., 1967.

(23) M. Cohen, *Mol. Cryst.*, **9**, 287 (1969).

(24) E. J. Bowen and D. W. Tanner, *Trans. Faraday Soc.*, **51**, 475 (1955).

concentrations of the highest molecular weight fractions isolated are well above the threshold level of detection of free radicals, normal carbonium ions may be responsible for propagation.

Regardless of the nature of the propagating species, their growth is determined principally by factors associated with solid state effects, *i.e.*, defect population, diffusion, relief of strain by annealing, etc., in such a manner that bi- and multimodal molecular weight distributions are formed. The complex fashion in which

these effects interact is reflected in the complicated behavior of the molecular weight distribution with changes in temperature of irradiation, postirradiation time, and postirradiation temperature.

Acknowledgment. The authors express their gratitude to the Division of Research of the U. S. Atomic Energy Commission for supporting this work, and also to Althea Glines and Carl Johnson for their valuable technical assistance.

Detection of the Triphenylmethyl Radical by Electron Spin Resonance in the Thermal Decomposition of Sodium Triphenylacetate¹

by Edward G. Janzen* and Michael Buchheit

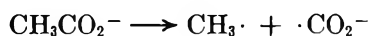
Department of Chemistry, University of Georgia, Athens, Georgia 30601 (Received May 21, 1971)

Publication costs borne completely by The Journal of Physical Chemistry

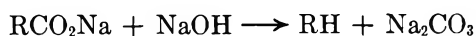
Triphenylmethyl radical is detected in the thermal decomposition of triphenylacetic acid and sodium triphenylacetate at temperatures above 195° and 55°, respectively. Triphenylmethyl radical is also detected when sodium triphenylacetate is warmed in quinoline, nitrobenzene, or bis(2-ethoxyethyl) ether at 65, 75, and 119°, respectively. A homolytic decarboxylation mechanism is proposed. Carbon dioxide radical anion is not detected. *n*-Butyllithium also produces triphenylmethyl radical from sodium triphenylacetate at room temperature. A nucleophilic addition to the carboxyl function followed by homolytic cleavage is proposed to account for this result.

Introduction

In a recent paper by Hisatsune and coworkers² on an infrared study of the thermal decomposition of sodium acetate in potassium halide matrices, it was concluded that the initial and rate-determining step of the decomposition was the formation of the methyl radical and carbon dioxide radical anion



This paper prompts us to report some electron spin resonance results we have obtained in the thermal decomposition of sodium triphenylacetate. Because of an interest in the classic reaction commonly taught in introductory organic courses wherein the sodium salt of a carboxylic acid is fused with sodium hydroxide to produce the hydrocarbon and sodium carbonate³



results on the thermal decomposition of triphenylacetate in the presence of sodium hydroxide are also included. Triphenylacetic acid has previously been used

in our laboratory as a convenient host for reactions of triphenylmethyl radical in the solid state. These include the reversible reaction of triphenylmethyl radical with oxygen in the temperature range 25–100°⁴ and the irreversible reaction of triphenylmethylperoxy radical with NO at room temperature.⁵

Results and Discussion

When triphenylacetic acid is heated in the absence of oxygen a weak esr signal is first detected at 195° which continues to increase in intensity with increase in tem-

(1) This work was supported by AFOS(SRC)-OAR U. S. Air Force Grant No. 1069-66.

(2) I. C. Hisatsune, E. C. Beahm, and R. J. Kempf, *J. Phys. Chem.*, **74**, 3444 (1970).

(3) M. P. E. Berthelot, *Ann. Chim. Phys.*, **9**, 444 (1866); see however T. S. Oakwood and M. R. Miller, *J. Amer. Chem. Soc.*, **72**, 1849 (1950).

(4) C. L. Ayers, E. G. Janzen, and F. J. Johnston, *J. Amer. Chem. Soc.*, **88**, 2610, (1966); E. G. Janzen, F. J. Johnston, and C. L. Ayers, *ibid.*, **89**, 1176 (1967).

(5) E. G. Janzen, J. L. Meyer, Jr., and C. L. Ayers, *J. Phys. Chem.*, **71**, 3108 (1967).

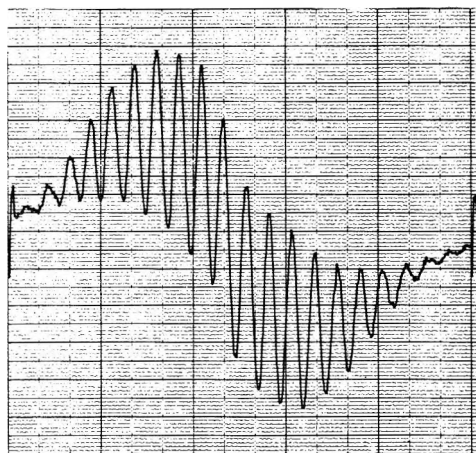
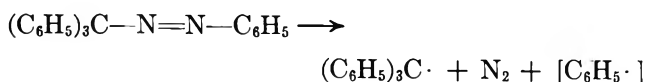


Figure 1. ESR spectrum of signal obtained in heating dry sodium triphenylacetate in the absence of oxygen up to 262° (by progressively increasing the temperature in 10–20° intervals over a period of approximately 3 hr). The spacing between the spikes on the extreme sides is 25 G.

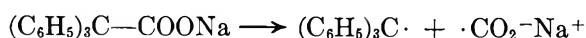
perature (mp 271°). When the heated sample is cooled and opened to air a second signal at lower field appears. These signals are attributed to triphenylmethyl and triphenylmethylperoxy radicals.⁴

When dry sodium triphenylacetate is heated in the absence of oxygen a weak signal is detected at temperatures as low as 55°. The signal intensity increases with increase in temperature. At 240–260° the sample is a brown viscous semisolid. At these temperatures a moderately well-resolved spectrum of triphenylmethyl radical shown in Figure 1 is obtained. About 19–20 broad lines are discernible with a spacing of 1.18 G, the total spectrum width apparently exceeding 25 G. The 1.18 G spacing corresponds to the meta hydrogen splitting, and approximately twice this value is due to the ortho and para hydrogen splitting.⁶

The thermal decomposition of sodium triphenylacetate also produces triphenylmethyl radical in quinoline at 65° (the first signal is detected at 47°), in nitrobenzene at 75–95°, in 1,3-dimethyl-1-aminobutane at 77–116°, and in bis(2-ethoxyethyl) ether at 119°. In quinoline, for example, 19 groups of lines totaling 76 in number are resolved giving the following coupling constants: $A_{\text{para}}^{\text{H}} = 2.75$, $A_{\text{ortho}}^{\text{H}} = 2.50$, and $A_{\text{meta}}^{\text{H}} = 1.12$ G in excellent agreement with previously published values.⁶ Further verification was obtained by comparing this spectrum with one obtained in the thermal decomposition of triphenylazomethane

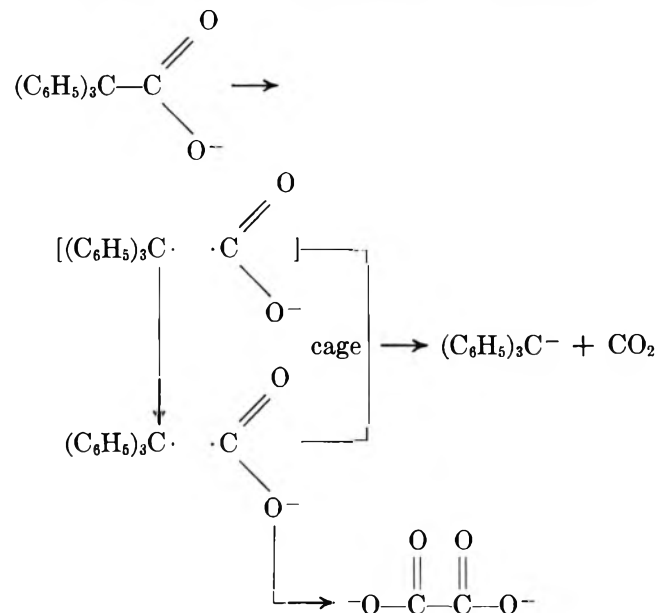


The reaction which produces triphenylmethyl radical most directly should also produce the carbon dioxide radical anion



However, no signals were detected at higher field than triphenylmethyl.⁷ The only other signal detected at any time appeared at lower field than triphenylmethyl and was assigned to the triphenylmethylperoxy radical presumably produced in reactions with incompletely removed oxygen.

Our detection of triphenylmethyl radical in the thermal decomposition of triphenylacetate indicates that the decarboxylation in this case may be homolytic



This mechanism could be tested by comparing the yield of CO_2 and triphenylmethane produced to the amount of oxalate and trityl radical detected.

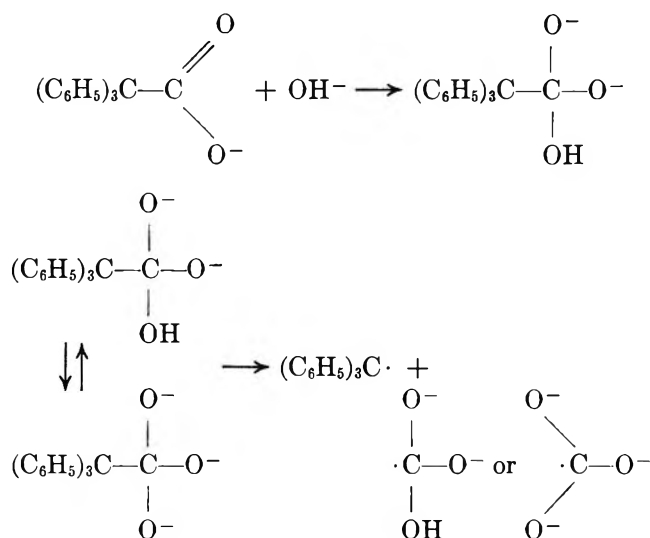
The action of strong bases had a strong effect on the ease of triphenylmethyl radical production from sodium triphenylacetate. Thus, with solid potassium hydroxide the triphenylmethyl signal was present in the sample at room temperature and increased sharply in intensity with increase in temperature to 54° then decreased in intensity at temperatures up to 102°. With *n*-butyllithium a well-resolved solution spectrum of

(6) D. B. Clement and G. J. Sloan, *J. Chem. Phys.*, **33**, 637 (1960); $A_{\text{para}}^{\text{H}} = 2.77$, $A_{\text{ortho}}^{\text{H}} = 2.53$, $A_{\text{meta}}^{\text{H}} = 1.11$ G; in the spectrum shown in this reference, 17 groups of lines are very well resolved. The total spectrum width is 16 G as compared to the theoretical total width of 30.15 G.

(7) (a) The g value for $\text{CO}_2\cdot^-$ is 2.0007 in sodium bicarbonate: P. W. Atkins and M. C. R. Symons, "The Structure of Inorganic Radicals," Elsevier Publishing Company, New York, N. Y., 1967, p 133. (b) A reviewer questions whether the microwave power was varied in the search for the $\text{CO}_2\cdot^-$ signal and states that from his experience $\text{CO}_2\cdot^-$ "can only be detected at high microwave power" when studied in "various matrices." This work was done with a Varian 4502 epr spectrometer with the waveguide and cavity attached to the high power port of the Varian 4500-41A bridge normally used for solution spectra. The microwave power was not varied substantially for these experiments. It should be noted that previous workers have not reported difficulty in detecting the $\text{CO}_2\cdot^-$ signal either in powders or single crystals of various hosts: D. W. Ovenall and D. H. Whiffen, *Proc. Chem. Soc.*, 420 (1960); J. A. Brivati, N. Keen, M. C. R. Symons, and P. A. Trevalion, *Proc. Chem. Soc.*, 66 (1961); P. W. Atkins, N. Keen, and M. C. R. Symons, *J. Chem. Soc.*, 2873 (1962). The radical appears to be stable to 80° in KHCO_3 : J. H. Sharp and M. C. R. Symons, *J. Chem. Soc.*, A, 3075 (1970).

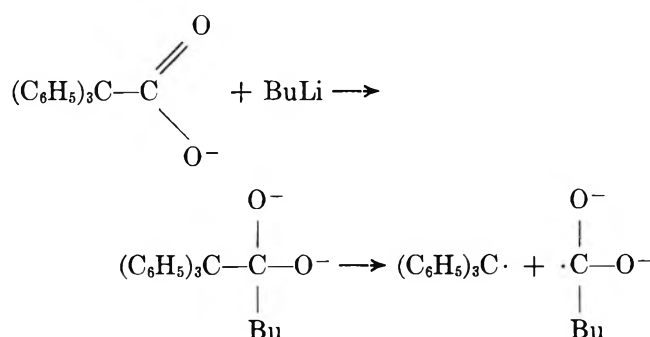
triphenylmethyl was obtained from sodium triphenylacetate at room temperature.

The strong effect of base on the apparent cleavage reaction may be due to nucleophilic attack on the carboxyl group followed by homolytic cleavage to give the one electron reduction product of the carbonate or bicarbonate ion

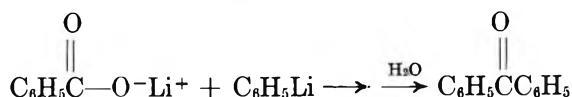


The one electron reduction product of carbonate ion ($\cdot\text{CO}_3^{3-}$) has been observed by esr in the solid state,⁸ but its stability under these conditions is unknown.

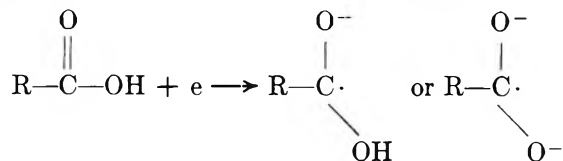
With *n*-butyllithium a similar reaction can occur



The addition of *n*-butyllithium to triphenylacetate ion is similar to known reactions of organolithium compounds to aryl carboxylic acids, *e.g.*⁹



The subsequent cleavage to triphenylmethyl radical and the radical anion of pentanoic acid is not unreasonable, given the known stability of triphenylmethyl radical. The one electron reduction products of alkyl carboxylic acids have been detected by adding sodium atoms to the acids in a rotating cryostat¹⁰



These radical ions are very unstable and have not been observed in solution.

The use of bases or basic solvents to increase decarboxylation rates is well known.¹¹ However, no decarboxylation reactions of diamagnetic compounds have to our knowledge been shown to proceed *via* radical pathways.

A weak signal was detected at 210–215° when dry sodium diphenylacetate ($(\text{C}_6\text{H}_5)_2\text{CHCOONa}$) was heated in the absence of air. Nothing significant was found in a similar trial with sodium 2,2-diphenylpropanoate ($\text{CH}_3(\text{C}_6\text{H}_5)_2\text{CCOONa}$).

The uv photolysis (low pressure mercury lamp) at room temperature under vacuum produced a signal which was too weak for assignment. In a KBr pellet containing sodium triphenylacetate, photolysis produced two signals unless great care was taken to remove all air during pressing by extended evacuation. A carefully prepared pellet gave only one signal if irradiated under vacuum but immediately produced two signals when air was admitted to the pellet. These signals are due to triphenylmethyl radical and triphenylmethylperoxy radical.⁴ The signal due to triphenylmethyl radical was stronger when prepared in a KBr pellet than in pure sodium triphenylacetate.

(8) R. A. Serway and S. A. Marshall, *J. Chem. Phys.*, **46**, 1949 (1967); J. Cunningham, *J. Phys. Chem.*, **71**, 1967 (1967); R. S. Eachus and M. C. R. Symons, *J. Chem. Soc. A*, 790 (1968).

(9) K. D. Berlin, B. S. Pathore, and M. Peterson, *J. Org. Chem.*, **30**, 226 (1965); H. Gilman and P. R. Van Ess, *J. Amer. Chem. Soc.*, **55**, 1258 (1933); D. S. Cram and F. L. Harris, Jr., *ibid.*, **89**, 4642 (1967), see Experimental Section.

(10) J. E. Bennett, B. Mile, A. Thomas, and B. Ward, *Advan. Phys. Org. Chem.*, **8**, 27 (1970); J. E. Bennett and L. H. Gale, *Trans. Faraday Soc.*, **64**, 1174 (1968).

(11) B. R. Brown, *Quart. Rev., Chem. Soc.*, **5**, 131 (1951); G. E. Dunn, E. G. Janzen, and W. Rodewald, *Can. J. Chem.*, **46**, 2905 (1968), and references therein.

The Infrared Spectra of the Oxides and Carbonates of Silver¹

by T. L. Slager,* B. J. Lindgren, A. James Mallmann, and Robert G. Greenler

Department of Physics and Laboratory for Surface Studies, University of Wisconsin-Milwaukee, Milwaukee, Wisconsin 53201 (Received August 17, 1971)

Publication costs assisted by the University of Wisconsin-Milwaukee

Silver(I) oxide was prepared in a controlled atmosphere by heating a pure, clean silver film in O₂ and by reaction with O₃. The infrared spectrum consists of one band at 535 cm⁻¹ in the 400–4000-cm⁻¹ region. From this Ag₂O film, simple silver carbonate was formed by reaction with CO₂. It shows four bands at 1410, 1020, 880, and 690 cm⁻¹. The further reaction with water vapor resulted in the formation of basic silver carbonate having peaks at 880, 705, 1060, 1380, and 1460 cm⁻¹, and a broad weak band in the 3200–3400-cm⁻¹ region. The stability of these species with respect to evacuation and heat treatment is also discussed.

Introduction

Although the preparation of Ag₂O in the bulk phase has been well established in the literature,² the infrared transmission spectrum is not firmly established, because Ag₂O reacts readily with air. Published spectra of powder or bulk phase samples show one or more bands in the 400–4000-cm⁻¹ region.^{3–5} When thin films of silver placed on various supports were oxidized an even more complex picture evolved.^{6,7} Allen and Scaife⁸ reached the conclusion that all previously published spectra were of contaminated material. They claimed only one band appearing at about 530 cm⁻¹ represented the spectrum of Ag₂O.

The question of what happened to silver oxide when exposed to air was also answered by Allen and Scaife.⁸ By comparison with the infrared spectrum of silver carbonates, they ascribe all bands, other than the one at 530 cm⁻¹, which showed up in the literature to normal, basic, and complex carbonates and surface hydroxyl groups.

The purpose of the present study is to prepare silver oxide in a controlled atmosphere starting with pure, clean silver and identify its infrared spectrum. Once spectroscopically pure oxide films have been prepared, their properties are examined by exposing them to CO₂ and H₂O. In this manner we show the sequence of events that occurs when silver oxide films are exposed to air and what compounds are formed, identifying them by their infrared spectra.

Experimental Section

Apparatus. All spectra were taken with a Beckman IR-9 spectrophotometer using a slit program of twice standard width.

In various stages of this project we used two different infrared cells and vacuum systems. The first cell is similar to one previously described.⁹ It has KBr windows and two KBr disks placed at the ends of the heating chamber, with two more electrical leads for a rhenium evaporation filament.

The vacuum system used with this cell (I) is not baked and operates typically in the 10⁻⁵ to 10⁻⁶ Torr range. The second system is an ultrahigh vacuum system used with a cell which is similar to that of Peri and Hannan.¹⁰ The cell is attached to the system through a Kovar-to-Pyrex seal, welded to a 6-in. Varian Conflat flange. Graded seals allow us to make the furnace section out of quartz. Using a modification of a technique developed by Kottke and Greenler,¹¹ KBr windows are sealed to the T-shaped cell. A magnet allows us to place the KBr support plate in position for evaporation of silver from a rhenium filament. Further manipulation with the magnet enables us to move the plate to the quartz section for heat treatment and uv irradiation. The spectra are run with the sample lowered into the T section of the cell. This system (II) was baked to 150° with the sample at 400° and it operated typically in the 10⁻⁸ to 10⁻⁹ Torr range.

Techniques. Once the system has been baked out at 150° and the support plate baked at 400° overnight, silver of 99.999% purity is evaporated from a rhenium filament onto KBr or CdTe plates. The pressure is maintained below 10⁻⁶ Torr throughout the evapora-

(1) The work was supported by a grant from the National Science Foundation.

(2) J. W. Laist, "Comprehensive Inorganic Chemistry," Vol. II, M. C. Sneed, J. L. Maynard, and R. C. Brosted, Ed., D. Van Nostrand Co., Inc., New York, N. Y., 1954, pp 140–150.

(3) E. F. Gross and F. I. Kreingold, *Opt. Spektrosk.*, **10**, 417 (1961).

(4) E. Fortin and F. L. Weichman, *Phys. Status. Solidi.*, **5**, 515 (1964).

(5) N. T. McDevitt and A. D. Davidson, *J. Opt. Soc. Amer.*, **55**, 209 (1965).

(6) N. T. McDevitt and W. L. Baun, *Spectrochem. Acta*, **20**, 799 (1964).

(7) F. I. Kreingold, *Opt. Spektrosk.*, **20**, 336 (1966).

(8) J. A. Allen and P. H. Scaife, *Aust. J. Chem.*, **19**, 715 (1966).

(9) R. G. Greenler, *J. Chem. Phys.*, **37**, 2094 (1962).

(10) J. B. Peri and R. B. Hannan, *J. Phys. Chem.*, **64**, 1526 (1960).

(11) M. Kottke and R. G. Greenler, *Rev. Sci. Instrum.*, **41**, 1235 (1971).

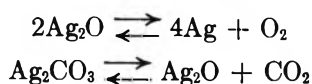
tion. The silver film is calculated to be about 1400 Å thick.

Oxidation of the silver film can be accomplished by two methods. The first is oxidation by heating in oxygen. Both systems I and II are utilized; only results from system I are presented since a double pass of the silver film is possible with this system. The desired amount of O₂ is placed in the cell, and the heater turned on. Temperature equilibrium is established and maintained for specific periods of time. In the other preparation ultraviolet light from low pressure mercury lamps¹² is transmitted through the quartz section of system II causing the formation of O₃. The ozone then oxidized the silver film. This reaction is carried out until oxidation is completed as evidenced by the infrared spectrum.

After the film is oxidized carbon dioxide is added to the system and the infrared spectrum taken. Once the carbonate forms, water is added which transforms the simple carbonate into the basic carbonate. Evacuation and heat treatment are used to examine the properties of these films.

Results and Discussion

Silver Oxide. The preparation of Ag₂O from solution is relatively straightforward and well documented.² Some difficulty arises when one tries to prepare it by direct reaction of silver with oxygen. A plot of equilibrium pressure^{2,8} against the temperature in degrees Kelvin for the reactions



is given in Figure 1. Although we are aware of the deviation from the standard state inherent in thin films, the data serve a useful purpose as an approximation. Consider, using the data as a guide, the preparation of Ag₂O from a silver film using O₂ as the oxidizing agent. Our vacuum system and pressure gauges limit us to pressures of about 450 Torr (0.6 atm). At this pressure, equilibrium is established at 460°K. Thus for Ag₂O to be formed by heating in O₂ the temperature must be somewhat lower. It is also obvious that this reaction has an activation energy since the atmospheric concentration of oxygen is much greater than 1.9×10^{-4} Torr, the equilibrium pressure of O₂ at room temperature, and silver is not oxidized by contact with the air.¹³

A problem encountered in the attempts to prepare Ag₂O from a thin film deposited on KBr was the disappearance of the silver film with no appearance of an infrared spectrum. This reaction occurred when the system had been baked at 400° with a background pressure of 1×10^{-8} Torr. Subsequently, as the evaporated silver film in this well-baked system was heated to temperatures of greater than 375°K the film would disappear. This reaction took place either in vacuum

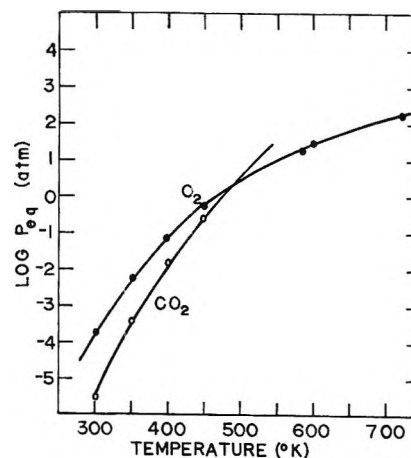


Figure 1. Equilibrium pressure of O₂ for the reaction $2\text{Ag}_2\text{O} \rightleftharpoons 4\text{Ag} + \text{O}_2$ and CO₂ for $\text{Ag}_2\text{CO}_3 \rightleftharpoons \text{Ag}_2\text{O} + \text{CO}_2$.

or in O₂. However, during the preliminary experiments where no bakeout was attempted, this problem was not encountered. The water adsorbed on or dissolved in the KBr was apparently sufficient to inhibit the disappearance of the silver film. To check this hypothesis, we baked the system, deposited the silver film, and added 0.8 Torr of water vapor along with 410 Torr O₂. Under these conditions the silver film did not disappear. With the disappearance of the silver film the KBr plate acquired a yellow tinge but showed no absorption bands in the 4000–400-cm⁻¹ region. We theorize that AgBr was formed when the silver film on a KBr substrate was heated in the well-baked system.

The infrared spectrum of Ag₂O formed by heating a silver film in oxygen for various time periods is shown in Figure 2. The only absorption band in the range 4000–400 cm⁻¹ occurs at 535 cm⁻¹. The oxidation was carried out at 400°K with a pressure of 410 Torr, producing a black film. Complete oxidation occurred in 4 hr as demonstrated by the absence of further growth in the 535 cm⁻¹ band. The same spectrum was obtained when a silver film was exposed to ozone produced by ultraviolet radiation through the quartz section of the apparatus under a pressure of 150 Torr of O₂. In our experiment, the ozone oxidation reaction was slow at room temperature, with complete oxidation only occurring after 40 hr of exposure. The slowness was probably due to the inefficiency of the method of producing ozone. The formation of Ag₂O by reaction with ozone was carried out in system (II). The background pressure of water vapor after bakeout was less than 5×10^{-9} Torr as measured with a Veeco MS II mass spectrometer. We therefore disagree with Laist,² who reports that ozone has no effect on silver in the absence of moisture.

Thus, in disagreement with previous attempts to ox-

(12) Three General Electric G4511 lamps.

(13) W. R. MacDonald and K. E. Hayes, *J. Catal.*, **18**, 115 (1970).

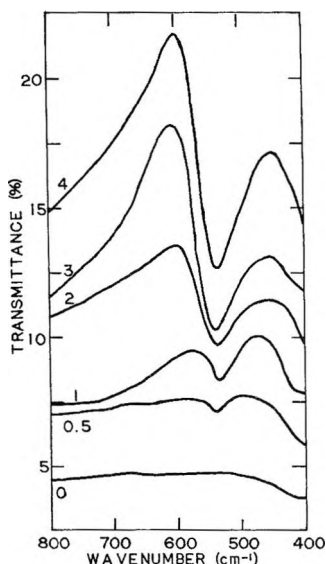


Figure 2. The infrared spectrum of Ag_2O produced by heating a silver film for various time intervals (hr) at 127° in 410 Torr of oxygen.

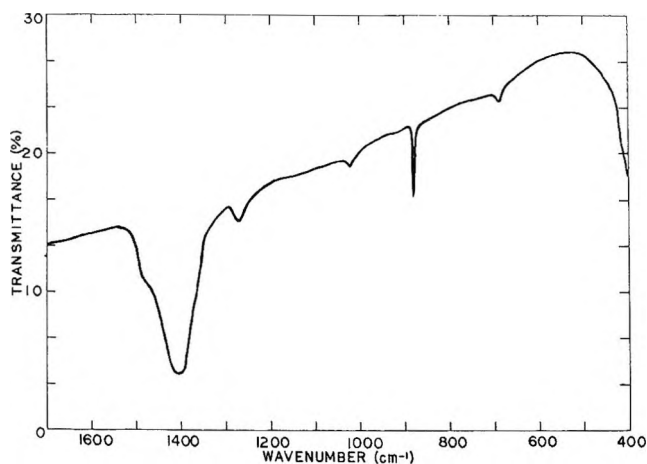


Figure 3. The infrared spectrum of Ag_2CO_3 prepared by exposing Ag_2O to 380 Torr of CO_2 at room temperature.

idize thin films of silver^{3,4,6,7} and in agreement with Allen and Scaife⁸ who worked with bulk materials, we conclude that the spectrum of Ag_2O in the $4000\text{--}400\text{-cm}^{-1}$ region consists of only one strong band appearing at 535 cm^{-1} . Under vacuum the Ag_2O begins to decompose at about 500°K and complete decomposition occurs by about 525°K .

Silver Carbonates. A thin film of Ag_2O was exposed to 380 Torr pressure of CO_2 . The spectrum shown in Figure 3 was recorded after 1 hr. No further change occurred in the spectrum after this time. The 535 cm^{-1} peak of Ag_2O disappeared immediately upon addition of CO_2 with the formation of new bands at 1020 cm^{-1} , 880 cm^{-1} , 1410 cm^{-1} , and 690 cm^{-1} . These bands correspond to the ν_1 , ν_2 , ν_3 , ν_4 vibrations of carbonate species as reported by Gatehouse, *et al.*¹⁴ A comparison between the spectrum of our silver carbo-

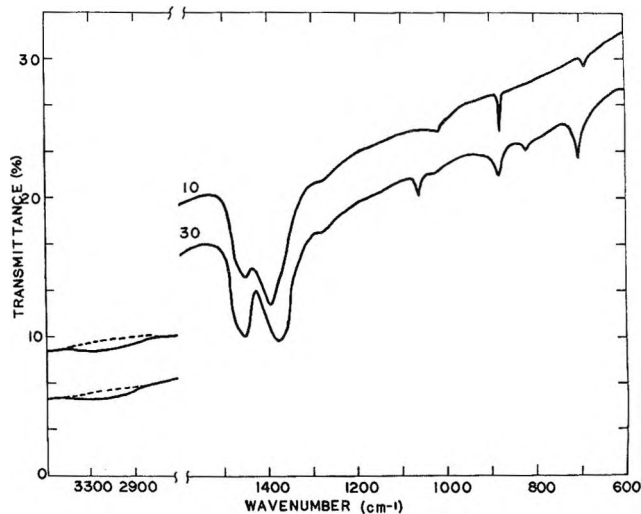


Figure 4. The infrared spectrum of $\text{AgOHAg}_2\text{CO}_3$ formed after various times (min) of exposure of Ag_2CO_3 to 5 Torr of water vapor. (The upper curve is raised 3.33% to separate it from the lower curve.)

nate and that of bulk silver carbonate run as mulls and as a pressed disk are shown in Table I. All of the absorbances appear somewhat shifted from those of the bulk material. Also note that only one band appears in the 1400-cm^{-1} region. These shifts in position and shape can be rationalized in one of two ways. Either a thin film has a different structure than bulk Ag_2CO_3 or the bulk material was altered due to contact with the atmosphere. The band appearing at 1290 cm^{-1} and the shoulder at 1480 cm^{-1} are evidence that a small amount of a complex carbonate was also formed.

The addition of 5 Torr of water vapor to the system caused a further change to occur in the system as seen in Figure 4. A very broad, weak band appears in the $3200\text{--}3400\text{-cm}^{-1}$ region, and the 1410-cm^{-1} band has become a doublet at 1460 and 1380 cm^{-1} . The 1020-cm^{-1} absorbance shifted to 1060 cm^{-1} , the one at 690 cm^{-1} shifted to 705 cm^{-1} , and a new one appeared at 820 cm^{-1} . Allen and Scaife⁸ assigned the two bands in the 1400-cm^{-1} region to a splitting of the asymmetric CO_3^{2-} stretching vibration. They interpreted this splitting as evidence for the aragonite structure of Ag_2CO_3 . However, our stepwise preparation leads us to the conclusion that simple silver carbonate is formed initially and that a reaction with atmospheric water vapor to produce the basic carbonate has clouded the issue. It appears that the splitting of the 1410-cm^{-1} band is characteristic of basic carbonates¹⁴ and the band in the $3200\text{--}3400\text{-cm}^{-1}$ region is characteristic of the formation of hydrogen bonded hydroxyl groups on the carbonate.¹⁵ This then is consistent with the formation of basic silver carbonate ($\text{AgOHAg}_2\text{CO}_3$).

(14) B. M. Gatehouse, S. E. Livingstone, and R. S. Nyholm, *J. Chem. Soc.*, 3137 (1958).

(15) L. H. Little, "Infrared Spectra of Adsorbed Species," Academic Press, Inc., New York, N. Y., 1967.

Table I: A Summary of the Infrared Bands Attributed to Silver Carbonates (cm^{-1})

	ν_1	ν_2	ν_3	ν_4	$\nu_1 + \nu_4$
Self-supporting disk	1070	800, 785	1200–1630	720, 710	1790
Nujol mull	1070	800, 785	...	720, 710	1785
Fluorolube mull	...	800, ...	1400
Allen and Scaife ⁸	1072	802, 785	1430, 1350	720, 705	1790
Thin film preparation	1020	880	1410	690	
Water addition	1060	880, 820	1460, 1350	705	

In our thin films the basic silver carbonate can be decomposed to Ag_2CO_3 by evacuating to a pressure of less than 10^{-3} Torr for 2 hr. The Ag_2CO_3 cannot be decomposed to Ag_2O by heating in vacuum. It decomposes to silver metal at about 350° in a pressure of 10^{-7} Torr or less.

Conclusion

We have demonstrated that silver oxide can be prepared from a thin silver film by two different methods: by heating in O_2 , and by reaction with O_3 . Some of the literature discrepancies have been cleared up. The infrared spectrum of Ag_2O consists of only one band at 535 cm^{-1} . The reaction of the silver oxide film with

CO_2 produced AgCO_3 which has four characteristic bands at 1410, 1020, 880, and 690 cm^{-1} . Contact of Ag_2CO_3 with H_2O produced a splitting of the 1410-cm^{-1} band into two, at 1460 and 1480 cm^{-1} . This is characteristic of the formation of the basic silver carbonate ($\text{AgOHAg}_2\text{CO}_3$).

One of the important features of this work is the utilization of a controlled atmosphere to duplicate the results of others. Atmospheric contamination of thin silver oxide films has caused much of the confusion in the literature.

Acknowledgment. We wish to thank George W. Keulks and Roger R. Ford for their helpful discussions

COMMUNICATIONS TO THE EDITOR

Catalytic Hydrogenation of Propylene:

Verification of Maximum Rate

Publication costs borne completely by The Journal of Physical Chemistry

Sir: Experimental studies of the catalytic hydrogenation of propylene over metal and metal oxide catalysts have been performed by a number of investigators.^{1–12} Reaction rates have been measured at temperatures from -60 to 260° . Both mechanistic and power function kinetic models have been used to correlate the reaction rate data obtained in these studies. Most of the mechanistic models are of the Langmuir–Hinshelwood type and predict a maximum rate if the hydrogen pressure (or the total pressure) is kept constant and the pressure of propylene varied.^{1,6,8–10} Although several investigators have reported an increase in the initial reaction rate with decreasing propylene pressure, to date no experimental verification of the maximum rate has been obtained.

It has been well recognized that the study of initial reaction rates provides essential information regarding

the mechanistic steps of solid-catalyzed gaseous reactions. Thus, we measured the initial hydrogenation rates on a 0.3% platinum–alumina catalyst (Engelhard) and pinpointed the region of propylene partial pressure wherein the maximum rate exists. Experiments were conducted using a single pass differential reactor at a

- (1) O. Toyama, *Rev. Phys. Chem. Jap.*, **14**, 86 (1940).
- (2) P. H. Emmett and J. B. Gray, *J. Amer. Chem. Soc.*, **66**, 1338 (1944).
- (3) L. L. Baker and R. B. Bernstein, *ibid.*, **73**, 4434 (1951).
- (4) G. C. Bond and J. Turkevich, *Trans. Faraday Soc.*, **49**, 281 (1953).
- (5) R. F. Kayser and H. E. Hoelscher, *Chem. Eng. Progr., Symp. Ser.*, **50**, 10 (1954).
- (6) G. B. Rogers, Ph.D. Thesis, University of Wisconsin, Madison, Wis., 1961.
- (7) K. Hirota and Y. Hironaka, *J. Catal.*, **4**, 602 (1965).
- (8) R. H. Shabaker, Ph.D. Thesis, University of Wisconsin, Madison, Wis., 1965.
- (9) G. B. Rogers, M. M. Lih, and O. A. Hougen, *AIChE J.*, **12**, 369 (1966).
- (10) R. Mezaki, *J. Catal.*, **10**, 238 (1968).
- (11) V. Ya. Stetsenko, K. V. Topchieva, and K. Kh. Nguyen, *Kinet. Katal.*, **9**, 55 (1968).
- (12) R. S. Mann and T. R. Lien, *J. Catal.*, **15**, 1 (1969).

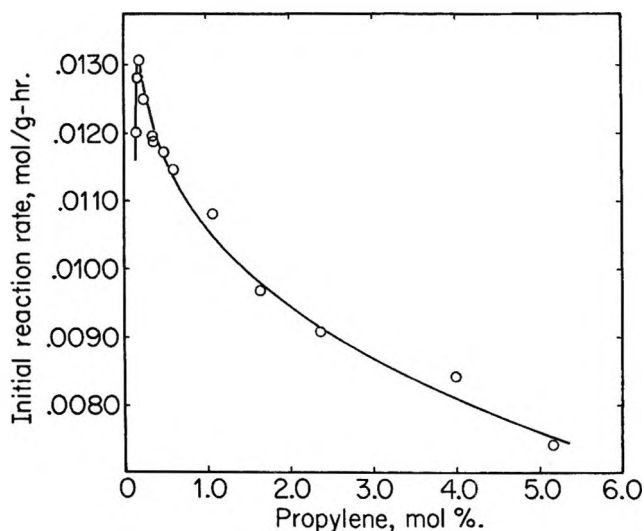


Figure 1. Reaction rate vs. reactant concentration at 1.6° and 1.09 atm.

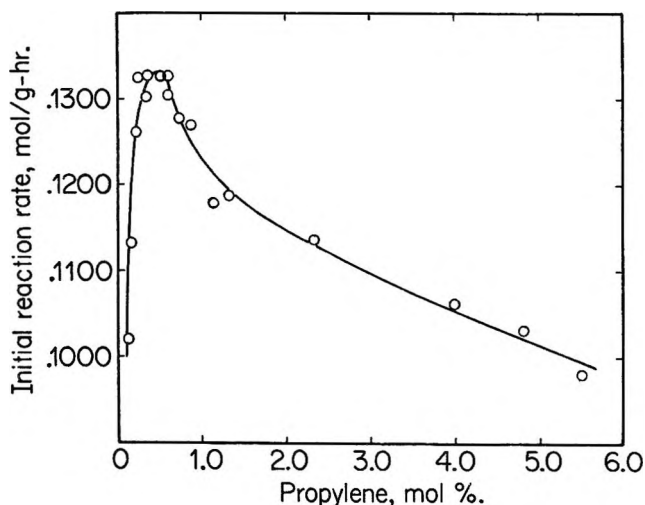


Figure 2. Reaction rate vs. reactant concentration at 38.1° and 1.09 atm.

total pressure of 1.09 atm and reaction temperatures between 1.6 and 38.1°. The weight of catalyst ranged from 0.025 to 0.300 g. The total flow rate of the reactant gas mixture (hydrogen and propylene) was varied from 4000 to 8585 cm³/min at STP. The analyses of the reactants and products were performed by gas chromatography. The experimental conditions utilized in this investigation are presented in detail elsewhere.¹³ Figures 1 and 2 show initial reaction rates as a function of propylene concentration. The curves represent an arbitrary fit to the experimental data. It can be seen from these figures that reaction rate maxima occur at less than 1 mol % propylene.

It should also be noted from the figures that an increase in the reaction temperature at a given total pressure shifts the location of the rate maximum to a higher propylene concentration. It is likely that the shift is due to a change in the equilibrium constants for each

adsorption process involved in the reaction. This shift of the rate maximum can be expected on the basis of mechanistic rate models such as the competitive-non-competitive⁹ and the half-hydrogenated⁸ rate models. The precise prediction of the shift in the rate maximum can be made if and only if the precise estimate of the rate parameters within the models can be obtained from experimental data.

We are performing modeling studies for the purpose of determining the reaction mechanism and developing a mathematical rate expression that will be consistent with the observed rate behavior.

Acknowledgments. The guidance of the late Harding Bliss is gratefully acknowledged. This work was supported by the National Science Foundation and the Allied Chemical Foundation.

(13) S. C. Weiner, Ph.D. Thesis, Yale University, New Haven, Conn., 1971.

(14) To whom correspondence should be sent at Esso Research and Engineering Co., P.O. Box 101, Florham Park, N. J. 07932.

(15) Department of Chemical Engineering, New York University, Bronx, N. Y. 10453.

DEPARTMENT OF ENGINEERING AND
APPLIED SCIENCE
YALE UNIVERSITY
NEW HAVEN, CONNECTICUT 06520

STEVEN C. WEINER*¹⁴
REIJI MEZAKI¹⁵
GARY L. HALLER

RECEIVED NOVEMBER 8, 1971

Free Ion Yields in γ -Irradiated Mixed Solvents

Publication costs assisted by the University of Alberta

Sir: Free ion yields in ethanol-*n*-hexane mixtures have recently been measured¹ and it was noted that the yields were greater than those in pure liquids² that had dielectric constants equal to the bulk dielectric constants of the mixtures. It should be pointed out that the model that was developed to explain the yields in pure liquids² does not apply to such mixtures for two main reasons. (1) The bulk dielectric constant of the mixture¹ is lower than the average microscopic dielectric constant. (2) Some of the electrons and ions generated in the hydrocarbon are probably scavenged by clusters of alcohol molecules, thereby increasing the average dielectric constant in the vicinity of the geminate ion-electron pairs.

The values of the bulk dielectric constants reported in ref 1 are intermediate between the net values that would be obtained if the ethanol and *n*-hexane were in unmixed layers parallel to the electrodes and those that

(1) B. J. Brown, N. T. Barker, and D. F. Sangster, *J. Phys. Chem.*, **75**, 3639 (1971).

(2) G. R. Freeman and J. M. Fayadh, *J. Chem. Phys.*, **43**, 4245 (1967).

would be obtained if the compounds were in unmixed layers perpendicular to the plane parallel electrodes (Table I). The measured dielectric constants are a further indication that the alcohol forms clusters in the nonpolar hexane. The average microscopic values in the unirradiated liquids are probably similar to those in column four of Table I; the average values in the vicinity of geminate ion-electron pairs are probably greater than these.

Table I: Dielectric Constants of Ethanol-*n*-Hexane Systems at 22°

Ethanol		Ref 1	Average dielectric constant	
Mole %	Vol %		Layers parallel to electrodes ^b	Layers perp. to electrodes
100	100	24.7	24.7	24.7
60	40	8.5	11.0	3.0
31	17	3.2	5.7	2.3
5	2.3	1.8 (2.0 ^a)	2.4	2.0
0	0	(1.9 ^a)	1.9	1.9

^a Measured by K. N. Jha in this laboratory. ^b Calculated by assuming that the liquid-liquid interface served as an intermediary electrode in a pair of condensers connected in series.

The free ion yields reported for the ethanol-*n*-hexane mixtures¹ would be more appropriately interpreted in terms of a charge-scavenging process³ than in terms of the free ion yield model for pure liquids.² Treatment of the data requires the use of both microscopic dielectric constants and the scavenging concept. The same interpretation would apply to the results of Kemp and coworkers,⁴ obtained from mixtures of methanol with cyclohexane and with tetrahydrofuran.

The reverse effect, *i.e.*, yields of e_{sol^-} that were lower than "expected," have recently been reported for water-formamide mixtures.⁵ Electrons do not become solvated in the usual manner in formamide but rather react to form negative ions that do not absorb light in the solvated electron region.⁵ In irradiated water-formamide mixtures some of the electrons are solvated by water and have absorption spectra nearly the same as those in pure water.⁵ However, the observed yields are lower than "expected" on a mole fraction basis. The dipole moment of formamide is 3.73 D,⁶ and the dielectric constant of the pure liquid is 109⁷ at 20°; the corresponding quantities for water are 1.85 D⁶ and 80.⁷ Electrons in the irradiated mixtures are preferentially captured by the formamide. A plausible interpretation is one similar to that offered above for the ethanol-hexane mixtures.

To interpret the free ion yields in mixed solvents the model in ref 3 should be used, not that in ref 2. Consideration should be given to the probability that the dielectric constant in the vicinity of the scavenged

electron and ion is greater than the average value for the solution.

- (3) G. R. Freeman, *J. Chem. Phys.*, **46**, 2822 (1967).
- (4) T. J. Kemp, G. A. Salmon, and P. Wardman in "Pulse Radiolysis," M. Ebert, J. P. Keene, A. J. Swallow, and J. H. Baxendale, Ed., Academic Press, London, 1965, p 247.
- (5) D. C. Walker and S. C. Wallace, *Can. J. Chem.*, **49**, 3398 (1971).
- (6) R. D. Nelson, Jr., "Selected Values of Electric Dipole Moments for Molecules in the Gas Phase," NSRDS-NBS 10, 1967.
- (7) A. A. Maryott and E. R. Smith, *Nat. Bur. Stand. (U. S.) Circ.*, **No. 514**, 1, 5 (1951).

CHEMISTRY DEPARTMENT
UNIVERSITY OF ALBERTA
EDMONTON 7, ALBERTA, CANADA

GORDON R. FREEMAN

RECEIVED DECEMBER 2, 1971

Infrared Spectra of Nitrous Oxide Adsorbed on Sodium Type A Synthetic Zeolite

Publication costs assisted by Laboratoire de Recherches Physiques

Sir: In the course of a study of molecular motions in condensed phases by means of the profiles of ir absorption bands, we have obtained the spectra of the two fundamental parallel vibrations ν_1 and ν_3 of N_2O adsorbed on NaA pellets, after dehydration of the zeolite. The spectra are run with an "*in situ*" infrared cell, the gas having been introduced into the cell at low pressure (0.5–20 Torr).

Figure 1 shows the ν_3 band at 2260 cm^{-1} , shifted to higher frequencies by 36 cm^{-1} with respect to the gas phase; it is a broad asymmetrical band at 40° which becomes much narrower when the temperature decreases to -50° . The ν_1 vibration appears as a doublet: the more intense component, at 1303 cm^{-1} , is shifted to higher frequencies relative to the gas phase; the second component, at 1264 cm^{-1} , is shifted to lower frequencies than in the gas phase. At low temperature, the interval between these two ν_1 bands increases (1305 and 1255 cm^{-1} , respectively).

These aspects of the adsorbed N_2O spectrum can be explained by assuming that the N_2O molecule, whose length is almost half the diameter of the zeolitic cavity, is able to move in the whole cage at room temperature and that it remains close to the cations at -50° . The ν_3 vibration is essentially the motion of the central nitrogen with respect to its neighbors, and ν_1 corresponds to the vibration of the end atoms N and O. Furthermore, we can assume that either O or N can be attracted by the positive poles, Na^+ , on the surface of the cavity since N_2O is described by two structures in resonance. The two bands of ν_1 would then correspond to these two modes of adsorption (the molecule can jump from one position to the other by its translational

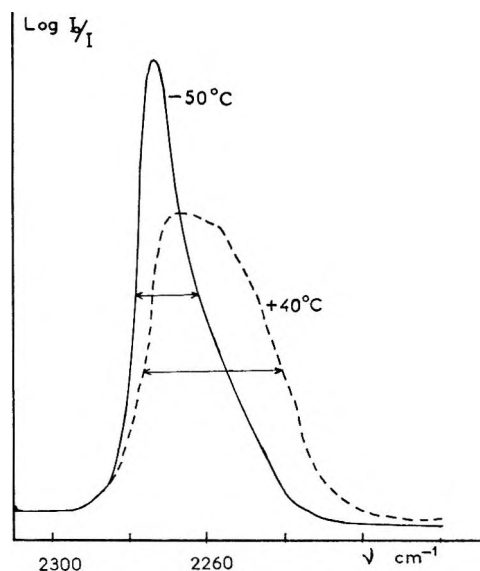


Figure 1.

motion), while the ν_3 vibration would not be sensitive to the difference. A splitting of ν_1 is also observed for N_2O adsorbed on NaCl films¹ but is explained by the existence of two different energy sites, as both shifts are directed toward lower frequencies than in the gas phase. In our case, however, the two components are located on either side of the gas frequency.

Let us now try to explain the width and profile of ν_3 : the field in a zeolitic cavity is very strong² and varies rapidly with distance from the Na^+ ions. During the translation of the molecule, the potential acting on it

changes; if the lifetime of this motion is large with respect to the period of the vibrational motion, then, for each position of the molecule, there will be a vibrational frequency for ν_3 corresponding to the potential in this position. The profile of the band can thus be related to the potential distribution inside the cavity. In the center of the cage, the field is very weak and the frequency of the ν_3 vibration is nearly the gas frequency; inversely, when the molecule is close to the surface, the frequency shift is significant. When the temperature decreases, the translational energy of N_2O decreases and the molecules remain close to the cations; the ν_3 band is displaced to higher frequencies and becomes narrower.

In addition to translation, many other mechanisms may be responsible for the profile of the spectrum, the most important of these being rotation and libration. The latter apparently remain at low temperature, since the observed ν_3 band still shows a significant width ($\sim 17 \text{ cm}^{-1}$). At room temperature this effect would be masked by the distribution of frequency caused by the translational motion inside the cavity.

(1) Y. Kozirovski and M. Folman, *Trans. Faraday Soc.*, **65**, 244 (1969).

(2) J. A. Rabo, C. L. Angell, P. H. Kasai, and V. Shomaker, *Discuss. Faraday Soc.*, **41**, 328 (1966).

GROUPE INFRAROUGE
LABORATOIRE DE RECHERCHES PHYSIQUES
11 QUAI ST. BERNARD
PARIS V^e, FRANCE

E. COHEN DE LARA
J. VINCENT-GEISSE*

RECEIVED DECEMBER 13, 1971

THE NUCLEAR OVERHAUSER EFFECT

CHEMICAL APPLICATIONS

by **JOSEPH H. NOGGLE**, Department of Chemistry, Univ. of Delaware, Newark, Del. and **ROGER E. SCHIRMER**, Eli Lilly and Co., Indianapolis, Indiana.

CONTENTS: Introduction. Nuclear Spin-Lattice Relaxation. Mechanisms of Spin-Lattice Relaxation. The Nuclear Overhauser Effect in Rigid Molecules. The Effects of Internal Motions. Experimental Methods. Transient Methods. The Effects of Chemical Exchange. Applications of the Nuclear Overhauser Effect: A Review of the Literature. Appendix I. Tightly Coupled Spins. Appendix II. Mathematical Methods. Author Index—Subject Index.

1971, 266 pp., \$14.50

THE RADIATION CHEMISTRY OF WATER

by **IVAN G. DRAGANIĆ** and **ZORICA D. DRAGANIĆ**, both at Radiation Chemistry Laboratory, Boris Kidrič Inst. of Nuclear Sciences, Vinča, Yugoslavia

CONTENTS: Brief Historical Survey of the Radiation Chemistry of Water. Interaction of Ionizing Radiation with Water and the Origin of Short-Lived Species which Cause Chemical Changes in Irradiated Water. Primary Products of Water Radiolysis: Short-Lived Reducing Species, the Hydrated Electron, the Hydrogen Atom and Molecular Hydrogen. Primary Products of Water Radiolysis: Oxidizing Species, the Hydroxyl Radical and Hydrogen Peroxide. Radiation-Chemical Yields of the Primary Products of Water Radiolysis and Their Dependence on Various Factors. Diffusion-Kinetic Model. Radiation Sources and Irradiation Techniques. Aqueous Chemical Dosimeters. Author Index—Subject Index.

1971, 256 pp., \$14.00

ADVANCES IN MAGNETIC RESONANCE

VOLUME 5

edited by **JOHN S. WAUGH**, Department of Chemistry, Mass. Institute of Technology, Cambridge, Mass.

CONTENTS: ANDREW HUDSON and KEITH D. J. ROOT, Halogen Hyperfine Interactions. A. G. REDFIELD and R. K. GUPTA, Pulsed-Fourier Transform Nuclear Magnetic Resonance Spectrometer. J. D. ELLETT, Jr., M. G. GIBBY, U. HAEBERLEN, L. M. HUBER, M. MEHRING, A. PINES, and J. S. WAUGH, Spectrometers for Multiple-Pulse NMR. DAVID C. ALLION, NMR and Ultraslow Motions. HORACIO A. FARACH and CHARLES P. POOLE, Jr., Solving the Spin Hamiltonian for the Electron Spin Resonance of Irradiated Organic Single Crystals. M. G. RICHARDS, NMR in Helium Three. Author Index—Subject Index.

1971, 378 pp., \$18.50

RELAXATION IN MAGNETIC RESONANCE: DIELECTRIC AND MOSSBAUER APPLICATIONS

DIELECTRIC AND MOSSBAUER APPLICATIONS

by **CHARLES P. POOLE, Jr.** and **HORACIO A. FARACH**, Department of Physics and Astronomy, Univ. of S. C., Columbia

CONTENTS: The Bloch Equations. Saturation Methods for Determining Relaxation Times. Transient Resonant Absorption. Line Broadening in Solids. Relaxation in Liquids. The Kubo-Tomita Theory. The Redfield Theories. Inhomogeneously Broadened Lines. Spin-Lattice Relaxation in Ionic Solids. Orbach Processes in Rare Earths. Phonon Bottleneck. Cross Relaxation. Exchange Reservoir. Diffusion. Ultrasonic Resonance. High Resolution Nuclear Magnetic Resonance. Paramagnetic Relaxation. The Mossbauer Effect. Dielectric Relaxation. Experimental Determination of Dielectric Constants. Appendix. Author Index-Subject Index.

1971, 410 pp., \$19.50

TRANSFER COEFFICIENTS IN ELECTROCHEMICAL KINETICS

by **J. P. BRENET** and **K. TRAORE**, Electrochemical Laboratory, Louis Pasteur Univ., Strasbourg, France

CONTENTS: The Fundamental Concepts of Electrochemistry. The Theories of Erdey-Gruz, Volmer and Audubert. The Generalized Form of Transfer Overpotential in Electrochemical Kinetics. Attempts at a Theoretical Interpretation of the Transfer Coefficient. Marcus and Levitch's General Theory of Electron Transfer Reactions. Conclusions. Author index. Subject index.

1971, 158 pp., \$11.00

HIGH RESOLUTION NMR OF MACROMOLECULES

by **FRANK A. BOVEY**, Bell Laboratories, Murray Hill, N. J.

CONTENTS: Fundamentals of Nuclear Magnetic Resonance. Isomerism in Polymer Chains. Configurational Sequences and Their Observation: Polymers of α,α' -Disubstituted Vinyl Monomers. Polyacrylates, Polyacrylonitrile, and Polyvinyl Alcohol and Its Derivatives. Haloethylene Polymers. Polystyrene and Related Polymers. Polyolefins and Related Polymers. NMR Investigations of the Mechanism of Propagation in Vinyl Polymerization. The Study of the Conformations of Vinyl Polymer Chains and Model Compounds by NMR. Vinyl Copolymers. Diene Polymers and Copolymers. Ring-Opening Polymers, Polyamides, Polyesters, and Miscellaneous Polymers. Polypeptides. Proteins. Nucleic Acids. Author Index—Subject Index.

1972, 473 pp., \$19.50

STATISTICAL PHYSICS

by **A. ISIHARA**, State Univ. of New York, Buffalo, N. Y.

CONTENTS: PRINCIPLES AND ELEMENTARY APPLICATIONS: Kinetic Theory. Principles of Statistical Mechanics. Partition Functions. Ideal Bosons and Fermions. CLASSICAL INTERACTING SYSTEMS: Linked Cluster Expansion. Distribution Functions. Brownian Motion. Lattice Statistics. Phenomena Near the Critical Temperature. QUANTUM INTERACTING SYSTEMS: Propagator Methods for the Partition Functions. Propagator Methods for Distribution Functions. Transport Phenomena in Degenerate Systems. Irreversibility and Transport Coefficients. Second Quantization. Green's Functions. Subject Index.

1971, 453 pp., \$18.50

ADVANCES IN QUANTUM CHEMISTRY

VOLUME 6

edited by **PER-OLOV LOWDIN**, Dept. of Quantum Chemistry, Uppsala Univ., Uppsala, Sweden, and Quantum Theory Project, Univ. of Florida, Gainesville.

CONTENTS: JOHN C. SLATER: Statistical Exchange-Correlation in the Self-Consistent Field. CLAUDE ASLANGUL, RAYMOND CONSTANCIEL, RAYMOND DAUDEL, and PHILEMON KOTTIS: Aspects of the Localizability of Electrons in Atoms and Molecules: Loge Theory and Related Methods. DENNIS J. CALDWELL and HENRY EYRING: Magnetic Circular Dichroism and Diamagnetic Molecules. SADHAN BASU and PURNENDRANATH SEN: Collective Electron Oscillation in Pi-Electron Systems. HIROSHI FUJIMOTO and KENICHI FUKUI: Molecular Orbital Theory of Chemical Reactions. BRUNO LINDER and DAVID A. RABENOLD: Unified Treatment of Van Der Waals Forces Between Two Molecules of Arbitrary Sizes and Electron Delocalizations. ERNEST R. DAVIDSON: Natural Orbitals. KLAUS RUEDENBERG and RONALD D. POSHLSTA: Matrix Elements and Density Matrices for Many-Electron Spin Eigenstates Built from Orthonormal Orbitals. F. WEINHOLD: Upper and Lower Bounds to Quantum-Mechanical Properties. RALPH E. CHRISTOFFERSEN: *Ab Initio* Calculations on Large Molecules. Author Index-Subject Index

April 1972, about 475 pp., \$24.50

CHEMISORPTION AND REACTIONS ON METALLIC FILMS

edited by **J. R. ANDERSON**, Div. of Tribophysics CSIRO, Univ. of Melbourne, Parkville, Victoria, Australia

VOLUME 1:

CONTENTS: J. V. Sanders: Structure of Evaporated Metal films. D. F. Klemperer: Experimental Techniques. J. W. Geus: Fundamental Concepts in Film Formation. D. O. Hayward: Gas Adsorption. J. W. Geus: The Influence of Adsorption on Electrical and Magnetic Properties of Thin Metal Films. L. H. Little: Infrared Spectra of Surface Species. Author Index. Subject index.

1971, 556 pp., \$32.00

VOLUME 2:

CONTENTS: J. R. Anderson and B. G. Baker: Adsorption, kinetics and surface structure in catalysis. J. R. Anderson and B. G. Baker: Catalytic reactions on metal films. D. R. Rossington: Properties and reactions of alloy films. I. M. Ritchie: The oxidation of evaporated metal films. Author Index. Subject Index.

1971, 324 pp., \$21.00

Need to know about...

The most advanced theory?

Then read such articles as: "Relation between Structure and Retention Time of Sterols in Gas Chromatography" and "Ion Association between Indicators and Indifferent Electrolytes".

The latest applications?

Then read such articles as: "Gas Chromatography of Volatiles from Breath and Urine" and "Identification of Dangerous Drugs by Isobutane Chemical Ionization Mass Spectrometry".

Newest chemicals and reagents?

Then read such articles as: "Clinical Test Kits for Enzymes, Phosphorus and Calcium Determinations, Narcotics Detection, Mercury and Lead Determinations" and "Ultrapure Chemicals: Enzymes, Refractory Metals, Organics, Other Metals".

All are found in ANALYTICAL CHEMISTRY.

Each month you receive information that is fresh, current and relevant to your needs. Brand new ideas are introduced. One of them might be the answer to one of your problems.

Two other good reasons for starting your ANALYTICAL CHEMISTRY subscription now are the 1971-72 LABORATORY GUIDE to Instruments, Equipment and Chemicals and the valuable ANNUAL REVIEWS issue.

The 500-page LABORATORY GUIDE gives you 20,000 separate entries with more than 1000 manufacturers selling over 600 products.

The special ANNUAL REVIEWS issue presents authoritative researchers reviewing the latest methodology and applications of analytical chemistry.

ANALYTICAL CHEMISTRY

American Chemical Society / 1155 Sixteenth Street, N.W., Washington, D.C. 20036

Please send me ANALYTICAL CHEMISTRY at the following subscription rate:

ACS members: U.S. \$5.00 Canada \$ 9.00 PUAS \$ 9.00 Other Nations \$10.00
Nonmembers: U.S. \$7.00 Canada \$11.00 PUAS \$19.00 Other Nations \$20.00

Note: Subscriptions at ACS Member Rates are for personal use only.

NAME _____ POSITION _____

ADDRESS _____

CITY _____ STATE/COUNTRY _____ ZIP _____

YOUR COMPANY _____ NATURE OF COMPANY'S BUSINESS _____

I am an ACS member I am not an ACS member Bill me for \$ _____
 Payment enclosed in the amount of \$ _____ (payable to American Chemical Society)